Master Thesis in Geosciences

On the dynamics of debris flows

Case study Fjærland, Western Norway - a debris flow triggered by a natural dam breach

Hedda Breien

UNIVERSITY OF OSLO

FACULTY OF MATHEMATICS AND NATURAL SCIENCES

On the dynamics of debris flows

Case study Fjærland, Western Norway – a debris flow triggered by a natural dam breach

Hedda Breien

Master Thesis in Geosciences

Discipline: Environmental Geology and Geohazards

Department of Geosciences

Faculty of Mathematics and Natural Sciences

UNIVERSITY OF OSLO

June 2005

Advisers: Dr. Anders Elverhøi (UiO) and Dr. Kaare Høeg (UiO)

This work is published digitally through DUO – Digitale Utgivelser ved UiO

http://www.duo.uio.no

It is also catalogued in BIBSYS (http://www.bibsys.no/english)

Cover photo: C. Harbitz.

Acknowledgements

First of all, I would like to take the opportunity to thank my two supervisors Professor Anders Elverhøi and Professor Kaare Høeg. Anders; you have provided irreplaceable help and inspiration, as well as valuable contact with local residents in Fjærland. And not to forget: your sincere involvement and participation! Special thanks to Kaare for all your advices and your encouraging words. If it was not for you and your fantastic lessons in engineering geology and geomechanics, I would never have found such an interesting field of study. I am lucky to know such a wise and nice person.

This thesis has been part of the Slide dynamics and mechanics of disintegration project at the International Centre for Geohazards (ICG). Many thanks go to all ICG and NGI for letting me stay in such a nice and encouraging research environment and for the help and laughter you all have provided. Special thanks to Dr. Fabio De Blasio at ICG for struggling with the BING-code. You are my guide and hero in rheology and modelling! Beyond that; I would never have got a nicer office-mate. I hope our cooperation will continue.

From the University of Oslo I am particularly grateful to Trond Eiken. The terrain modelling part of my thesis would never have been completed without you! Thank you for your patience and all your help during frustrating hours.

Thanks to all inhabitants of Supphelledalen for your hospitality and the valuable information you all have provided.

I would also like to honour my family for patience and supporting words throughout years of studies. I hope to get more time for visits in the future!

Finally, I wish to thank my boyfriend Geir Ole for unconditional love and support.

Hedda Breien

Oslo, June 2005.

Abstract

Debris flows represent a major threat to human life and property. Due to their ability of entraining material and reaching long run-outs, they have a potential of causing massive damage.

There are many studies on debris flow dynamics. Still, the topic reveals a number of challenges in understanding the forces involved and in representing them numerically. In this respect the recent debris flow in Fjærland, Western Norway, is looked upon as a unique full scale experiment with its 1000 m height drop and 3000 m long run-out.

The Fjærland case includes the breach of a moraine ridge damming a glacial lake, the additional water coming from the glacier, and its resulting flood. The study of this case illustrates how a water flood can evolve into a full debris flow through bulking. Even though the event started out as a flood of water, the study has revealed that the deposited materials and the degree of erosion also result from a significant grain-to-grain contact. It is seen that treating such events as floods is not appropriate where the height drop is large and the bed material erodible.

The primary objective of the thesis has been to provide a thorough documentation and description of the event. Through this work, several eyewitnesses have been interviewed, and detailed pre- and post flow terrain models have been developed through laser scanning and photogrammetry in the purpose of estimating the volume involved in the debris flow. The same terrain data have been employed in a numerical model (BING), trying to simulate the dynamics of the flow. The model uses a Bingham rheology, but is modified to include Coulomb friction and entrainment by Dr. Fabio De Blasio of ICG. The expanded BING-model predicts a run-out, erosion depth and a volume encouragingly similar to what is seen in nature. However, many physical simplifications have had to be introduced, and challenges for further studies are several.

The study reveals the necessity for a dynamical model which, depending on the contents and properties of the material involved, includes both viscous, plastic and frictional forces, allows forces and properties to vary in time and space, as well as taking material entrainment into account.

A most interesting topic for further study is the factor of entrainment. Until now, this phenomenon is not fully understood. The thesis tries to illustrate the phenomenon with the recently accumulated data. One of the findings of the thesis is the recognition of a feedback mechanism, where volume growth increases the entrainment of bed material, which again increases the volume of the flow. For erosion, the volume of the mass flow seems more important than slope angle, at least in slopes steeper than a certain value. This was also recognised in the numerical modelling, shown by an exponential increase in volume. The ability of volume growth can be the explanation for debris flows with very far-reaching run-outs.

There is historical evidence that similar debris flow events have happened in Fjærland twice during the last century. An event like the one that occurred 8 May 2004 is also likely to happen again - in Fjærland as well as any other place where large volumes of water are released at high altitude. This study is therefore important also in the evaluation of hazards related to other glaciers, lakes and dams as well as to landslide-triggered debris flows.

Table of Contents

Appendices

1. Introduction

Mass movements of all kinds threaten human life, and water is often a component either in the triggering and initiation, or in the dynamics of these events. Most research has been dedicated to the initiation process and stability analyses. The study of the dynamics after the landslide is triggered is however essential, especially in the case of debris flows which have the capability of reaching very far and causing great damage. Considering mitigation measures, the study of these processes is crucial.

The debris flow in Fjærland, Western Norway, May 2004 developing from a natural moraine ridge (dam) failure is a unique opportunity for learning more about these processes. This event could be looked upon as a unique full-scale experiment and all its characteristics could be taken advantage of in the search of understanding. Due to the valuable data this event has provided, it is considered an important case for the purpose of studying mass dynamics and the phenomenon of entrainment.

As the Fjærland debris flow developed from a dam breach, water has an especially important role, both in the triggering and the dynamics of the flow. This makes the case applicable to any event where a volume of water is released at high altitude, flowing towards narrow valleys filled with erodible sediments, as well as debris flows developing from slope failures. These extreme events may result from flash floods as well as dam breaches. The latter may involve enormous volumes of water. The Fjærland event is an example of the downstream damage such floods and debris flows may make.

Different names like debris torrents, debris flows, debris avalanches, mud flows and lahars reflect the complex origins and compositions of debris flow mass movements. Of these, the debris torrent (Terzaghi, Peck and Mesri, 1996) probably is the most violent one. The saturated mass of soil, boulders and trees speeds down a confined gully, eroding the channel walls and bed. The flow becomes more self-propagating and more erosive on its way, and finally spreads out in a fan at the mouth of the valley. For convenience, all these mass movements are named debris flows in this thesis.

1.1 Purpose and scope

In this thesis I intend to investigate the physics and behaviour of debris flows in general by investigating the Fjærland case. The main scope is to give a detailed documentation of the event. In addition a numerical model is used in the search for understanding of the physics. Interesting questions are connected to the water and sediment volume involved: Which volumes of sediment and water have been involved? Where has the torrent eroded material, where was material deposited, and what are the controlling factors? How could this happen, and could it happen again – here, or similar places? If any mitigation structure is going to be built, how and where is it most appropriate to build it? The case study is also meant to provide insight to the general phenomenon of entrainment.

To study the phenomenon in Fjærland, knowledge about glacier hydrology, moraine material (till), dam stability, erosion and debris flow mechanics is needed. The continuous change of material properties, rheology and flow characteristics throughout the path is an important aspect. These factors make the event complex and difficult to fully analyse. In this thesis, all the different aspects of the event are touched upon, some topics more thoroughly than others.

After presenting the data, I will treat the different phenomena separately, starting with the storage of water in/under the glacier, and follow up with the dam breach, the sediment volume involved and a description of the debris flow phenomenon, a mixture of water and sediment. A numerical Bingham rheology model will also be used in the discussion of the dynamics.

In this first study of the debris flow in Fjærland, the collection of field data and creation of terrain models are essential, making up a foundation for further studies of the movement mechanisms of the debris. The glacier and its hydrology is important when considering the reason for the flow, but also for the further understanding of the water volume involved, which in turn is an important factor for the debris flow analysis. This is why so much emphasis is put on this aspect. The discussion of what really happened has become a central part of the thesis as it will serve as the basis for further studies of the flow.

1.2 Setting

The dramatic event of Fjærland the 8th of May 2004 developed from a failure of a mountainous glacial moraine ridge, and caused sudden drainage of the lake behind and possibly also a lake trapped within the glacier. The torrent scoured a small river gully through a steep terrain on its way from 1000 m.a.s.l. down to elevation zero, entraining large amounts of material and evolving into a debris flow. The valley affected is mainly overlain by glacial deposits, but also by alluvial material. The torrent started out as a water flood, but after passing a precipice of 300 m height drop (900 to 600 m.a.s.l.), entrainment became significant.

The movement ended in a fan of huge boulders where the valley Tverrdalen meats the main valley Supphelledalen, and fine material and muddy waters inundated the fields of three nearby farms. The total height drop of the debris flow was 1000 m, and the run-out approximately 3000 m. The terrain is relatively steep (average slope 17º), but varies from around 4º at the uppermost stretch to a cliff of around 60º. The flow behaved like a "flood" until it reached the bottom of the cliff where its erosional power developed. The torrent followed the original stream gully, widening and deepening it on its way to dimensions of 50 m width and 8 m depth. It is believed that the water volume involved was larger than the volume of the lake behind the moraine dam itself, and the suggestion is that water has been drained quickly from within the glacier in the process of a jøkulhlaup.

Figure 1.1 Map of Norway. Study area inside red box. Taken from National Geographic.

1.3 Collection of data

The collection of data started in August 2004 (three months after the event) with a thorough walkthrough of the terrain investigating the failure, the debris flow track and the depositional fan. Sediment grain size, deposited stones, boulders in their original positions, as well as the shape of the fan were studied. The observations are illustrated by photos, mostly taken by myself, but supplemented by old photos and photos taken during, and in the days after, the debris flow. Interviews with local residents and eyewitnesses (see Appendix A) have thrown light upon the event of 2004 as well as previous similar events. An old diary written by the now passed-away local inhabitant Eirik Øygard was provided by his grandson Eirik Øygard, and has given documentation to the similar flood and debris flow of 1947 (see Appendix A).

Temperature and discharge measurements every 10 minutes have been collected by the Norwegian Meterological Institute and included in the glaciological analysis of this thesis. From the municipality of Sogndal, documents written in connection with the estimation of the compensation given to the farmers have been made available for the study.

An airborne laser (Light Amplification by Stimulated Emission of Radiation) scanning of the debris flow area was performed September 30, 2004, and a series of aerial photos was taken during the same flight. Blom Geomatics were hired to perform this data collection. Also aerial photos by Fotonor dating back to August 2001 were used in the analysis. Together the laser scanning and the aerial photos have made up the foundation of ortophotos and the generation of 3D models representing the terrain before and after the failure of the dam. This has again provided data for volume estimations and analysis of erosion and sedimentation. In addition an economical map 1:5000 of the fan area has been used.

The software used for the photogrammetry was:

- ZI Image Station Digital Mensuration – for orientation of the photos.
- ZI Image Station Stereo Display – for stereo view and construction of collection boundary.
- ZI Image Station Automatic Elevation – for generation of terrain models.
- ZI Image Station Base Rectifier – for orthophoto generation.

- Micro Station – for combining the different models.
- IRAS/C – for linking the different parts of the orthophotos.

The terrain models were later reworked in Golden Software's Surfer and Global Mapper. The volume estimations have been performed using Surfer. The results are discussed in Chapters 6 and 8, and the gridding report data are presented in Appendix E.

Together, the widely ranging data constitute the basis for the interpretation of the Fjærland torrent event and the understanding of debris flow dynamics. The data from the event is employed to the numerical model BING, which is run in Fortran.

2. Observations

The first two sections of this chapter present the eyewitness data and the field data from Fjærland, which will be used and discussed in the description of the 2004-event (Section 2.3) as well as the recognition of previous, similar events (Chapter 3).

2.1 Eyewitness observations

Witness observations have offered important contributions in the attempt to reconstruct the torrent event of Fjærland, 8 May 2004. The event started out as a breach of the moraine ridge damming a lake, the water flow entraining bed material on its way through the valleys (Figure 2.1 and Figure 2.2). In the end the flow reached the populated Supphelledalen valley. The flow was witnessed from at least four geographically different places, giving observations from different angles and during different stages of the debris flow. The observations are not entirely consistent, and their reliability is to be discussed in later chapters. Detailed interviews and statements can be found in Appendix A.

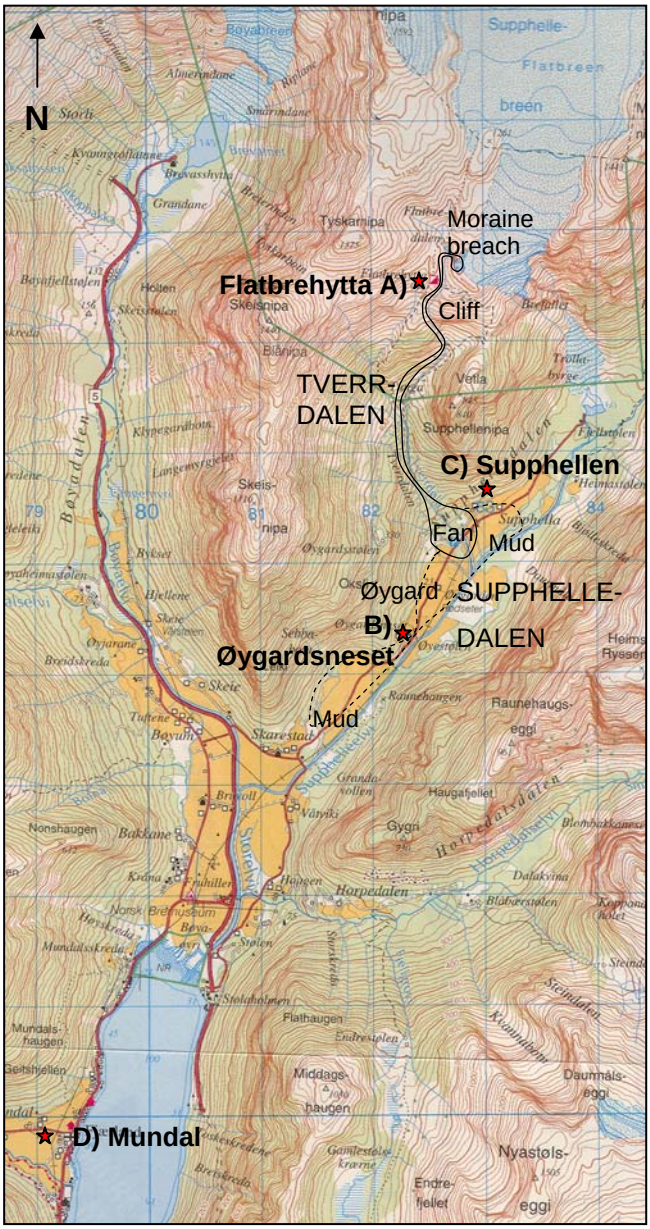

Figure 2.1 Map of Fjærland. The debris flow track and fan area are marked, and the witness observation spots plotted as red stars with letters from A to D. Map: Statens Kartverk, 1:50000, Topografisk hovedkartserie M 711, blad 13171.

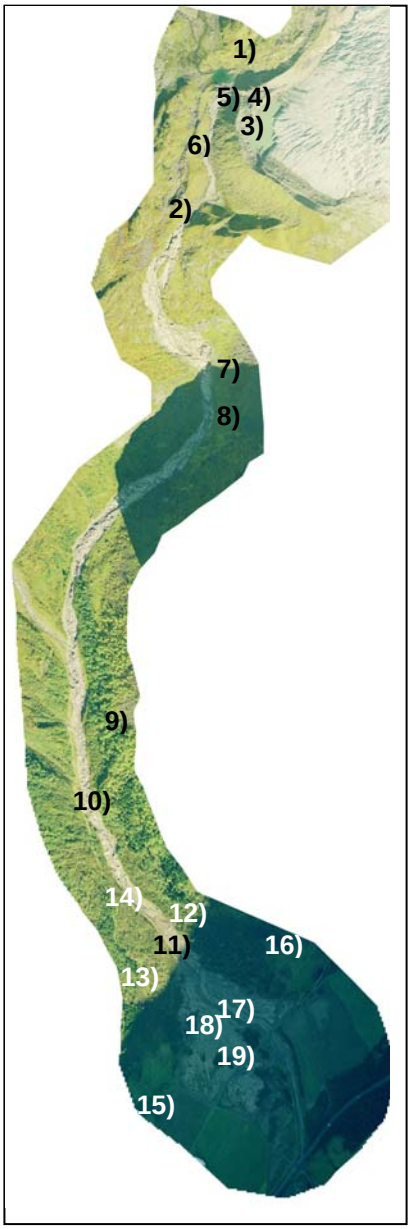

Figure 2.2 Aerial photo of the debris flow track. Numbers represent positions where photos shown in the following text are taken. Photo: Blom Geomatics.

2.1.1 A) From the cabin Flatbrehytta, 994 m.a.s.l.

Figure 2.3

Overview of the dam failure area and the upper 350 meters of the track. The cabin Flatbrehytta is seen at the precipice on the right as a red dot. Photo taken from helicopter in summer 2004, by H. Elvehøy, NVE. See map and air photo in Figure 2.1 and Figure 2.2.

Flatbrehytta is an unguarded tourist cabin situated at the cliffs around 350 m from the moraine ridge. The cliffs have a height drop of 300 meters. Eirik Øygard was at the cabin Flatbrehytta when the failure occurred (see Appendix A). Around 13:00 hours Øygard heard a dump sound; rising and lowering with intervals. From the moraine hill between the cabin and the originally small brook gully he watched the torrent fall over the precipice.

Pictures taken from the cabin by Eirik Øygard show a saturated brownish slush containing stones of up to 15 cm diameter (Figure 2.4). Stones were thrown up in the air implicating a high velocity as the flow approached the precipice. From the moraine hill where the pictures are taken, Øygard could see his farmland at 20 m.a.s.l.. Within around 15 minutes after his first observation, his farmland was inundated.

Figure 2.4 Photos taken by Øygard at the precipice near Flatbrehytta during the debris flow, showing the mass of water and suspended particles. The height of the flow is probably around 10 m, and the size of the particles in suspension up to around 15 cm. The right photo also shows the debris flow in the valley Tverrdalen, but is taken before the debris has reached the flat farmland in the lower valley Supphelledalen. Photos: Øygard, 2004.

2.1.2 B) From Øygardsneset, 25 m.a.s.l.

Øygardsneset is a farm in outer Supphelledalen approximately 1 km downstream the depositional fan area. Ingebrigt Supphellen, living in Supphella (upstream side of fan) observed the torrent from this spot (see Appendix A). His son Ingvar living at Øygardsneset is also one of the eyewitnesses here. The view towards the cabin Flatbrehytta, the valley

Tverrdalen and the farm Øygard is good from his son's house; therefore Ingebrigt Supphellen observed large parts of the event.

As the masses were thrown over the cliffs close to Flatbrehytta, the torrent became visible both from outer Supphelledalen (Øygardsneset) and in the village of Mundal. Ingebrigt Supphellen's first observation of the event was the roaring sound from the torrent and what he describes as a black, horizontal fountain from the precipice. He reports the time of the event accurately as he had paid for petrol for his car in Fjærland at 12:47. This makes it possible to set the time when he first noticed the flow to 12:50. As Ingebrigt stepped out of the car at Øygardsneset he heard a roaring sound and felt the ground shake.

Figure 2.5 The debris flow track at the precipice a few hours after the peak flow shows that the masses spread over a wide area in this section. Water is still flowing. Photo: G. Eithun.

Ingebrigt Supphellen reports a time lag of almost half an hour from this first observation until the debris flow front approached the alluvial fan area in Supphelledalen. He hoped that the masses would not reach the valley as he experienced a similar dramatic happening in

1947, when the bridge and the flood mitigation structures in Supphelledalen were damaged by the stones and the water.

His son Ingvar's explanation is not exactly consistent with respect to time. Ingvar was on the phone talking to the police when he saw the front coming down in the Supphelledalen valley. Therefore the exact time of debris flow front arrival can be set to 13:02, meaning that the time difference between the observations can be maximum 15 minutes. This is to be discussed in Section 2.3.

Ingebrigt Supphellen describes the debris flow front as 10-20 meters high, visible over the trees, and moving with an estimated velocity of around 50 km/h. The large stones seemed to arrive first as a wall of boulders, the water coming later. The front was initially steeper than 45º, but became gentler as it approached the fan area. Also Ingvar Supphellen supports this idea. He adds that the front was steep and stable until it reached the fan area where it suddenly collapsed and stopped. He also tells that the mud inundating the farmland reached their houses (almost 1 km downstream the fan area) at 13:14, around 15 minutes after the first observation of the flood at the precipice. This is consistent with what Øygard observed from his cabin. The whole event is by the two men at Øygardsneset described to last for 2 hours, before all movement stopped.

Figure 2.6 Fan and inundated fields at the farm Øygard. The nearest houses of Supphella are seen in the background. Øygardsneset could be found some hundred meters from the lower left corner. Photo: E. Øygard.

2.1.3 C) From Supphella 30 m.a.s.l.

Two clusters of houses are found in Supphella, those closest to the debris flow situated only 50-100 m from the flanks of the depositional fan. Per Christian Liseter living here first noticed the shaking of the ground as he sat outside reading (see Appendix A). Thereafter stones were thrown through the air over the electric wires (5 m), before any debris flow front was visible. After a flow of water, the debris front arrived, most of the torrent rushing down the valley as a layered mass with the water as a floating layer on top of the stones.

The eyewitnesses do not agree on the timing and composition of the masses as they first approached the valley. From outer Supphella a flow of water was seen to arrive *before* the debris flow front.

Both Ingvar Supphellen and Per Christian Liseter report that the torrent came in pulses. According to Ingvar Supphellen the first one was the biggest. Liseter tells that the torrent changed direction approximately every 15 minutes, and came in 4 or 5 pulses, together constituting 1 hour.

2.1.4 D) From Mundal

Several inhabitants of the village Mundal some 5 km away, observed the torrent at the precipice near Flatbrehytta. The statements about duration of the event vary from 45 minutes to two hours.

2.2 Field observations

A thorough walkthrough of the debris flow area was made by the author three months after the event. The lowest lying areas had then been cleaned for mud deposits and a new river gully had been started using excavators in the bouldery fan deposit. During the days of field investigation the debris flow path was followed from the fan to the moraine ridge failure, and post-flow observations along the path were made. An analysis of the flow features observed is important in the reconstruction of the flow event.

2.2.1 The moraine ridge breach

The debris flow started out as a dam failure causing a flood. The drained lake is dammed between the glacier Supphellebreen and the arch-shaped moraine ridge, and is situated at 1000 m.a.s.l.. The failure occurred at the west end of the lake, and is visible as a v-shaped scar in the moraine with a maximum width of 35 m and a maximum depth of 15 m. As illustrated in Figure 2.8 an ice structure is found in the inner scar area. Whether this is ice transported from the glacier or part of the moraine is not known.

There has been a brook due to overtopping at the place of the scar also before the event, as this has been the lowest point of the moraine ridge since at least 1906 (see Figure 5.2). The pre-flow 3D-model (Figure 2.7) also shows a scar in the moraine ridge.

As the water breached the dam, it took a sharp turn (90º) and did not completely damage the small lake immediately downstream the moraine ridge (Figure 2.7). Most of the masses from the scar (around 25 000 m^3, see Chapter 8) were deposited immediately downstream the ridge. Especially large boulders (meters in diameter) are found just outside the scar.

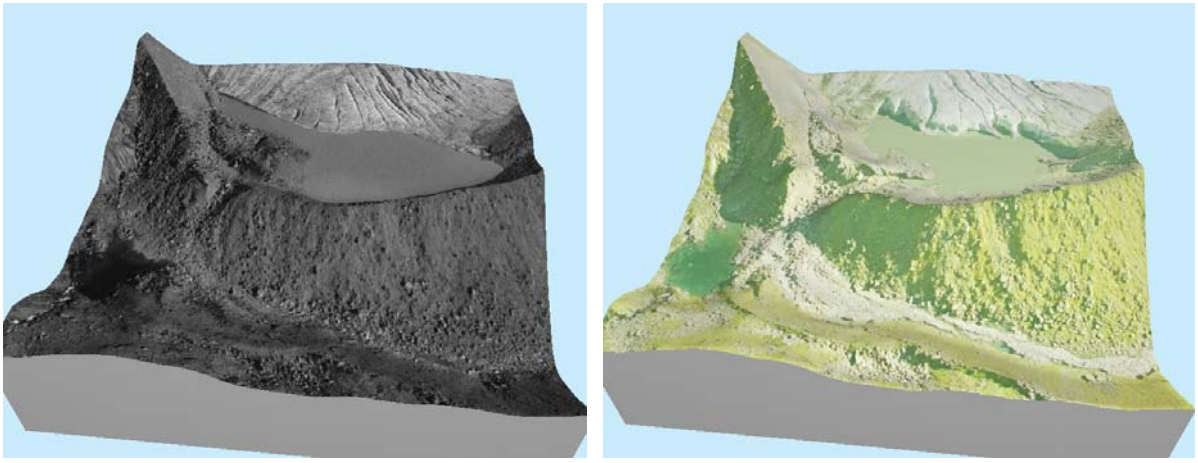

Figure 2.7 3D view of the moraine and its lowest point in 2001 (left) and 2004 (right), generated in GlobalMapper from orthophotos and terrain models. Notice the small scar also visible in 2001.

Figure 2.8 Failure seen from upstream side of dam. The ice structure in the middle of the picture may be ice transported from the glacier and covered by sediments, or an inner part of the moraine. Part of the lake is visible in the right corner.

Figure 2.9 The moraine failure scar seen from downstream toe. Three persons are visible at the crest on the opposite side of the lake, and one person is in the middle of the breach.

Figure 2.10 Most material from the dam breach is deposited immediately downstream the scar.

2.2.2 Debris flow path

The first stretch (300 m) of the flow path has a very gentle slope, around 4º. The area includes an active sandur delta downstream the moraine, where progressively finer sediments are deposited by glacier water. In August 2004 (three months after the event) there was little evidence of the torrent in this upper section (Figure 2.11). This area was covered with snow at the time of the event, and the debris masses ran on top of this snowpack, at least in the early phase. Deposition has occurred, but the stream gully also seems to be somewhat widened in the area, since some erosion has occurred on the flanks.

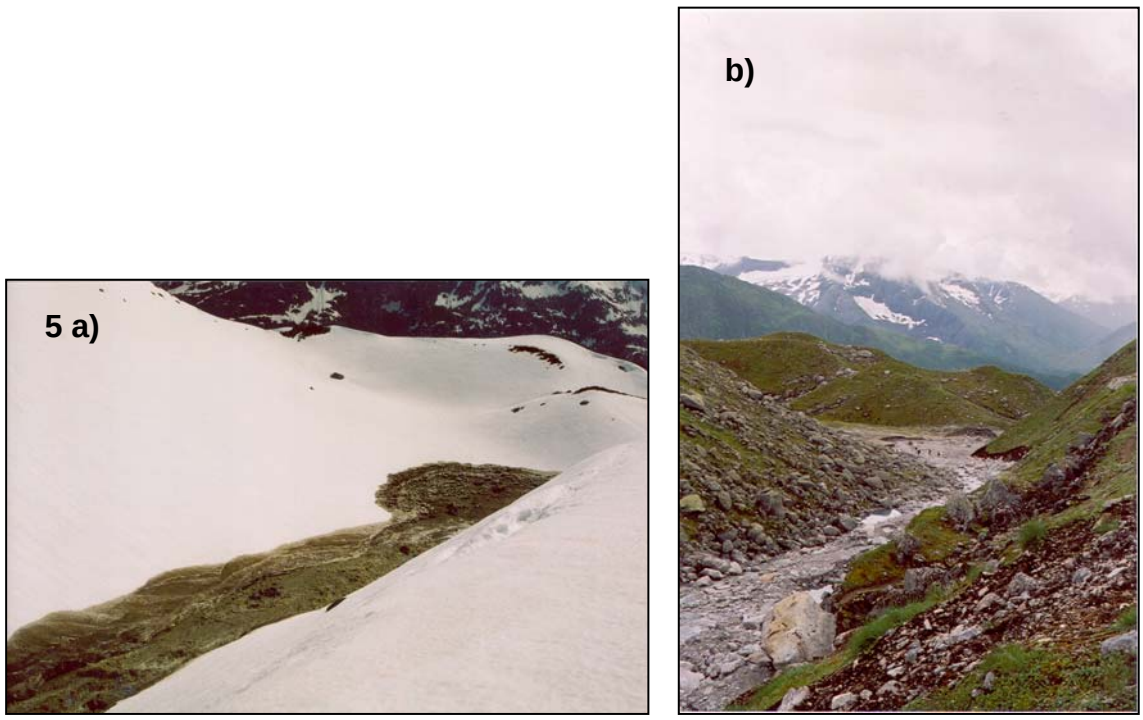

Figure 2.11 a) Along the first 300 m of the path the masses ran on snow. Photo: E. Øygard. b) The same area shows little evidence of the debris flow three months after the event. Lower part of moraine ridge is seen to the left.

At the precipice 300 m down the path, the masses fell from 900 to 600 m.a.s.l., in a slope of around 60º. The area was originally very sparse in sediments due to the steepness of the terrain and the high altitude. The masses however scoured the precipice, removing all vegetation and leaving the bedrock bare in an up to 100 m wide area, as no confining gully for the masses exists here (see Figure 2.12).

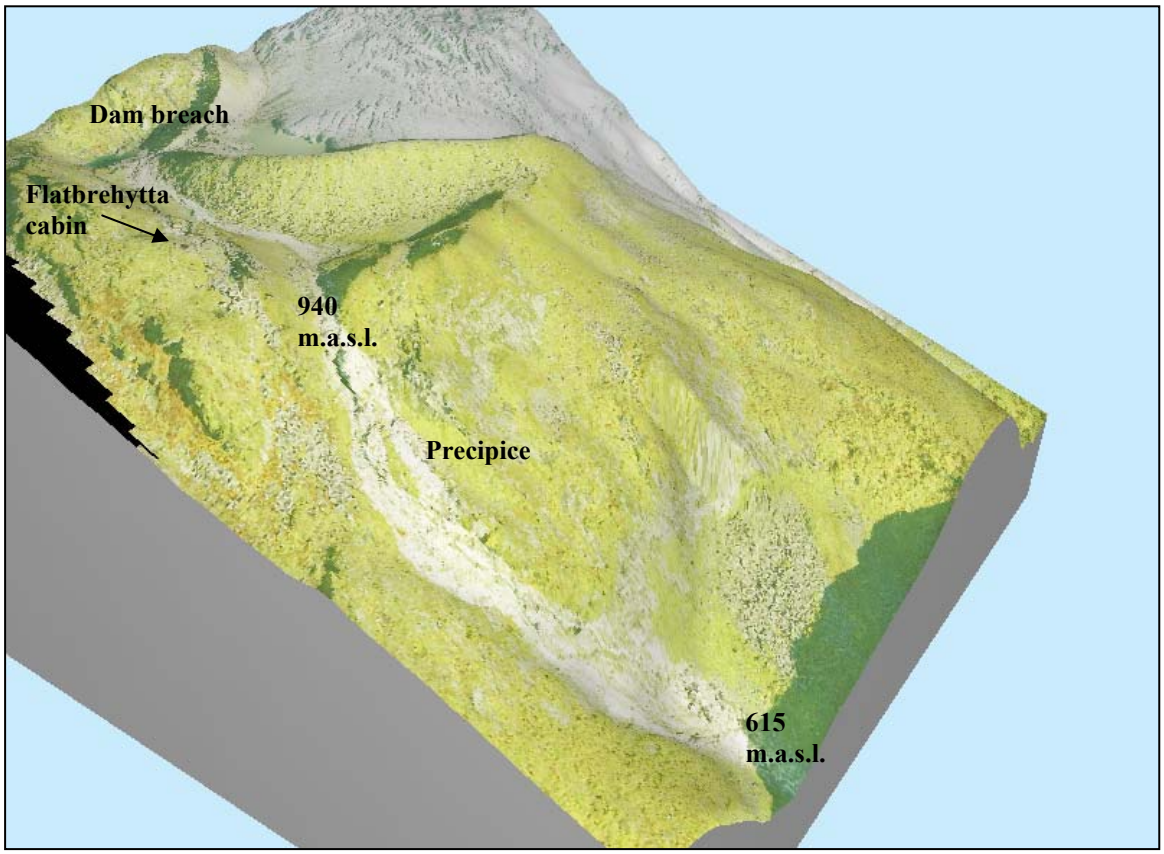

Figure 2.12 3D terrain model from 1000 to 600 m.a.s.l., showing the upper flat part and the precipice. Generated in Global Mapper using orthophoto and terrain model based on aerial photos from 2004.

Figure 2.13 Lower part of the precipice and depression where the water hit the ground.

From the point when the water reached the bottom of the precipice at around 615 m.a.s.l., the loose bed of moraine material starts to thicken, making the erosion potential grow. The large height drop added momentum and erosive power to the mass. Together this resulted in deeper erosion where the flow hit the valley, and the gradual formation of a debris flow as sediment was entrained. The flow can be described as confined all the way to its depositional fan, as it followed a stream gully. Erosion is obvious from this point on.

The first stretch of Tverrdalen beneath the precipice has a slope of around 23º, but decreases to approximately 13º after only 150 m. The erosion due to the torrent of water, boulders and fine sediments produces an average track of around 20 m width and around 1-2 m depth in this 150 m upper part of the valley. However, this section is characterised by a narrow, deep erosion channel in the middle of the track. Boulders around 5 m^3 observed in the track have not been moved at all, as only one or two sides of the stones are scoured. Moss and lichen still growing tell that the stone is the outer limit of the flow (see Figure 2.14). The erosion is light compared to areas further down the track.

Figure 2.14 The debris flow has run on top of the stone as this part is bare, whilst its side against the camera is unaffected and covered by lichen.

The 13º slope soon gets steeper, and approaches 25º for a short stretch. This part also has experienced deep erosion (around 8 m).

The erosion belt winds down the valley, following the stream gully, but widening it severely. The width of the track varies considerably throughout the path, widening to up to 53 m and scouring to a depth of around 8 m. The deepest scour appears in the lower parts of the track,

after passing the exit of a smaller tributary stream (see Figure 2.15). The lower parts of the path are also characterised by being totally scoured, whilst the upper parts are only depleted in fine material, the coarser seeming to remain in the path.

Figure 2.15 The erosion starts to get severe after passing the small tributary stream in the left of the picture. Photo: H. Elvehøy.

The scoured gully is changed from a classic v-shaped river gully, to a rectangular depression with almost vertical sides due to the debris flow. The tourist path on the west side of the gully has been destroyed by the torrent in some areas, and in others it is in danger of being washed out in a later rainstorm as it has been undercut by the debris flow and is mainly hanging on the dipping bedrock. Some places the scour has reached bedrock. The till deposit in the valley prior to the event seems to have been of varying thickness (up to around 10 m).

The debris flow track tends to be the widest in this upper part of the valley Tverrdalen. After the gully meets the small tributary stream in Figure 2.15, the path tends to narrow for a short stretch, but grow deeper. This can be due to the geometry of the terrain, the erodibility of the soil, and also due to a possibly higher velocity of the torrent.

2.2.3 Soil material

Figure 2.16 The vertical sides of the erosion track are up to 8 m high. The upper red part of the material is the weathered soil.

The soil material as far down the valley as shown in Figure 2.16 seems to be finer grained till than at higher altitudes, but a high content of large boulders is evident. The deposit is characterised by a weathered, upper layer up to a few meters thick, and a more coarse-grained lower layer. Blocks are found throughout the whole profile but seem to be more concentrated in some areas. The weathered part is seen as the reddish upper few meters of the profile shown in Figure 2.16. The almost vertical sides of the gully were still standing when the field investigation was done, three months after the event.

Just before the start of the depositional fan the terrain flattens to 5º (100-150 m.a.s.l.). The material in this area consists of slide deposits from earlier events. The eroded gully has revealed layers of such old slide material just above the current fan area (Figure 2.17). Local residents tell that most of the masses from the latest corresponding debris flow in 1947 stopped in this area.

Figure 2.17 Old slide deposit in eroded gully sides, elevation 150 m.a.s.l., most probably being the 1947-event. The erosion depth is here more than 5 meters.

2.2.4 Deposits along the track

Far down the track, large boulders with diameter of around 1-2 m, are found on intact parts of the tourist path just on the west flank of the gully. It is positively known that these stones were never in the path before. It is also seen in the photo, taken just after the event (Figure 2.20) that mud was flowing on the flank during the flow. The depth of the debris flow must have been large and filled the gully.

Some of the boulders fractured during collisions with other boulders ("exploded") are found up to 25 m outside the main track near the fan area (Figure 2.19). The position of the rocks as well as its fractures, are very young, pointing towards recent cracking. Other boulders considerably larger (diameter up to 3 m) have been shown to be moved, if not in such a dramatic way, as they are lying over trees just outside the torrent track (see Figure 2.18).

Figure 2.18 A large boulder has crushed a tree just outside the torrent track. For scale, a camera bag can be seen on the left of the large boulder. Debris flow has passed in the left part of the picture.

Figure 2.19 Recently fractured stone found 20-25 m from main track at elevation 100 m.

Figure 2.20 Boulders have been thrown up on the shoulder of the gully from the debris flow. The upper photo is taken a few days after event (photo: E. Loe), the lower three months later. The middle right 3D-figure is made by draping an orthophoto over a terrain model. The letters mark the corresponding boulders in the three pictures.

2.2.5 Depositional fan

As the valley opens up and the slope gradually decreases to around 12º, deposition seems to start.

The depositional fan is drop shaped, 420 m long and 300 m maximum width, with an area of around 80 000 m^2. It consists of boulders, coarse pebble and trunks of trees (Figure 2.22).

The area was covered by 5-10 m high trees before the event. After entraining the trees, the debris flow filled the lower lying road and parking lot with large boulders of the size of small cars. The outermost boulder has stopped at the flat farmland almost 450 m from the beginning of the fan, at 20 m.a.s.l.. One of the largest boulders found ran almost 90 degrees off the main flow direction and stopped 50 meters from the main fan (see Figure 2.21).

When knowing that the total height drop was 1000 m and the horizontal travel distance 3000 m, the height/travel distance is 0.33. The fan-shaped sedimentation area ranges from approximately 80-90 m.a.s.l. and ends at around 20 m.a.s.l.. The average slope of the fan surface is around 8-10 degrees, and the outer flanks approach 4 degrees. The depth of the deposit has not been measured, but seems to vary from 0.5 m to approximately 5 meters. Some compaction has occurred. Trees still standing have marks showing that during the flow the masses were up to 1.5 m thicker than the deposit today (Figure 2.23).

Figure 2.21 Dimensions of largest boulder found. Deposited outside the main fan area.

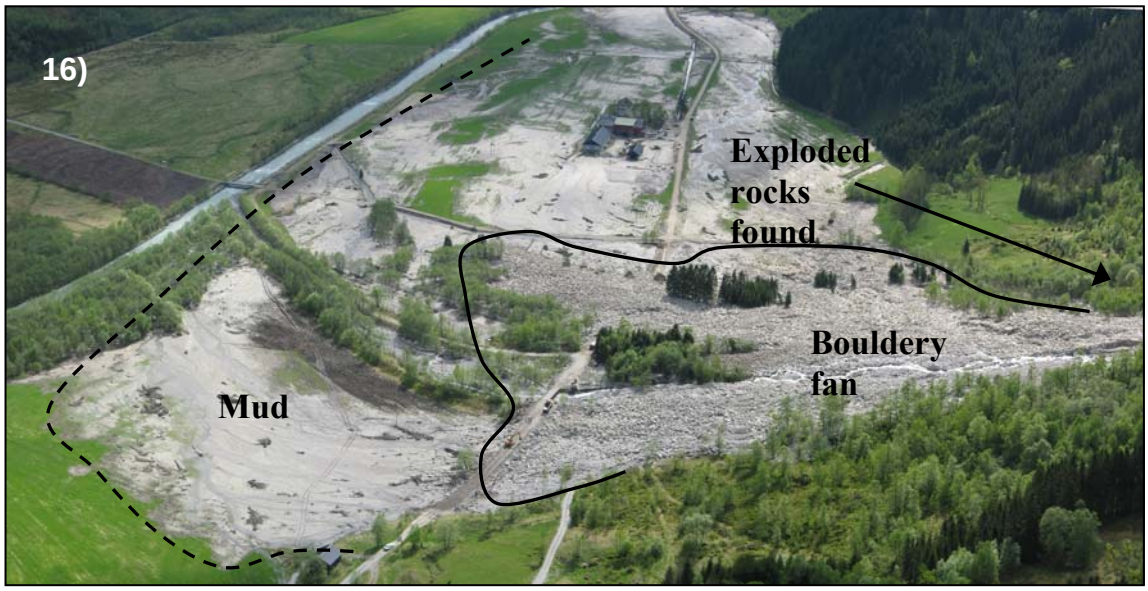

Figure 2.22 The fan area and the farm Øygard seen from the hills on the upstream side of the fan. The barn of outer Supphella in lower part of the picture. Full line represents the outer limits of the bouldery fan, stapled line shows the area covered by mud. Photo: K. Kristensen.

There seems to be a distinct grain size distribution pattern with slope change. All boulders are deposited in the fan, in a slope of 12º to 4º. The finer material is sedimented on the flat farmland or transported to sea. Within the fan itself, the most pronounced pattern is vertical inverse layering (Figure 2.23) where the largest stones are on top (Brazil nut) (see Section 2.4). Where erosion of the fan deposit has exposed profiles, double Brazil nuts (two layers) are observed, which may indicate two debris pulses (advances) (Figure 2.23). There is however nothing that indicates a pattern of different sized boulders in high elevation parts of the fan (80 m.a.s.l.) compared to at the lower parts (20 m.a.s.l.).

There is also a bridging pattern in the deposit. Each bridge ends in a large boulder, producing a force chain backwards. Five main spurs make up the fan.

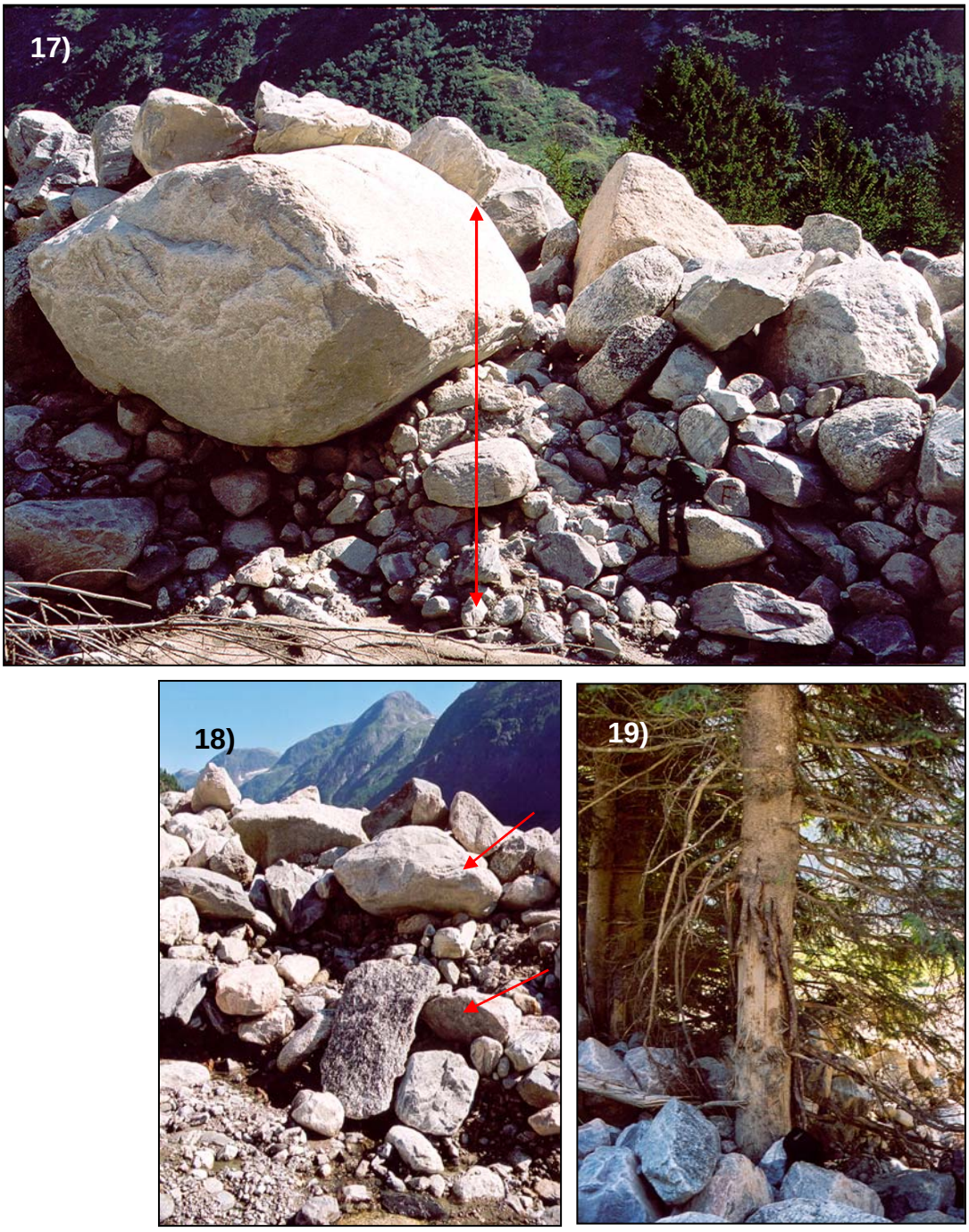

Figure 2.23 Fan deposits in Fjærland. 16) Brazil nut effect. Size of largest boulder in the picture is around 1 m. 17) Brazil nut in two layers may indicate two pulses in the debris flow. 18) The few trees left in the fan are scoured 1.5 m higher than the current deposit.

2.2.6 Mud deposit

The finer fragments sized from sand, silt and clay, were deposited over an area of around 250 000 m^2, and had a thickness of up to 50 cm (see Figure 2.24 and Figure 2.1). According to the farmers, the material turned into a liquid when disturbed even for days after the event.

On the farmland where the finest material was deposited, some 5 cm was purposely left when removing the mud, because of its fertility. Mudlines on the post boxes at Øygardsneset 1 km downstream the fan show the maximum thickness of the mud to be around 50 cm.

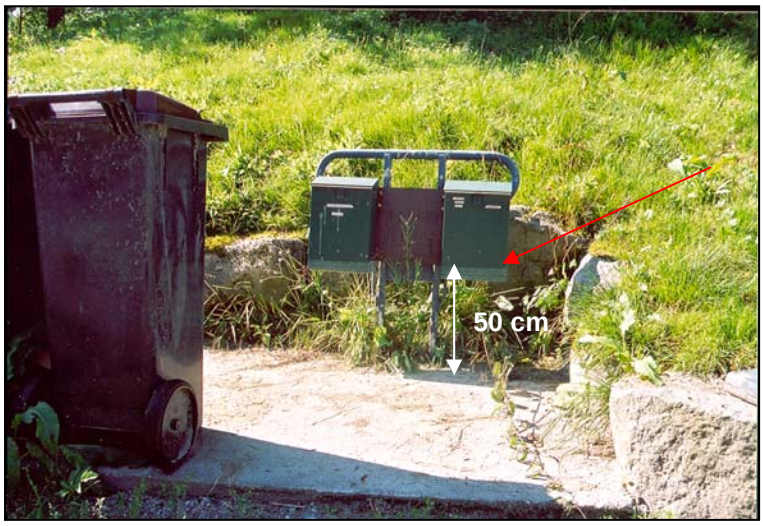

Figure 2.24 Mudmarks on the postboxes at Øygardsneset show thickness of the mud deposit 1 km downstream the fan. For location see Figure 2.1.

2.3 Description of the Fjærland torrent event using eyewitness statements and field observations

When considering witness observations and degree of erosion, the volume of water released is suggested to be larger than the volume of the lake behind the moraine dam itself, and additional water is believed to originate from within the glacier as described in Chapters 5 and 6. As the dam failed and the lake was emptied, water drained from within the glacier.

It is not likely that the flow has had a very high velocity in the beginning of the event, as it took a sharp turn (90º) and did not damage the small lake immediately downstream the moraine ridge (see Figure 2.3). Most of the masses from the scar (25 000 m^3, see Chapter 8) were deposited immediately downstream the ridge. This is not consistent with a high flow velocity. Especially large boulders are found just downstream the scar.

Over this first flat stretch of the track, the masses flowed on top of the snow pack. This, in combination with the gentle slope reduced the erosive power of the masses. The pictures taken by E. Øygard (Figure 2.4) show a flow with numerous particles, but the main part of

the material originating from the moraine breach had been deposited prior to this. The torrent seen in the photos is highly turbulent and carries stones of up to 15 cm diameter, but the masses mainly acted like a very fluid flood. The 300-m height drop and the accumulation of momentum when passing the precipice increased the erosive power of the torrent. Therefore the erosive process is believed to have started at around 600 m.a.s.l.. The erosional power is believed to increase with time and travel distance, due to the propagating accumulation of momentum and increasing concentration of sediments entrained.

The growing debris flow left behind a deep channel ending in a fan of big boulders in the bottom of the valley. The initial volume of the dam failure is very small compared to the total volume of the deposit.

As the flow propagated and entrained material, the density of the flow is considered high (around 1.8 g/cm^3) in the lower parts of the track due to the boulders found on the nearby tourist path at around 200 m.a.s.l. (Figure 2.20). Sediment and water volumes are further discussed in Chapters 6 and 8. The split stones found 20 m from the track indicate that blocks of this size and larger were in turbulent suspension or thrown up from the torrent passing by due to grain collisions, and settling on the flank.

As the drainage from the dam breach decreased towards the end of the event, the water lost erosional power, resulting then in lower sediment concentration again.

Just above the deposition area, the flatter section (approximately 5º) has depleted the energy of the masses, but due to high velocity and/or large volume the masses still flowed. This low slope area is made of old slide deposits, the most recent layers from the event in 1947. As the flow reached slopes of 12º, the loss of energy has become higher than the input from the driving forces, resulting in deposition.

As described by witnesses, the debris flow front was 45º steep and composed by boulders. The front was around 10 m high as it exited the erosion gully and entered the fan area. The front was stable until it suddenly collapsed and stopped, building the fan (Figure 2.25).

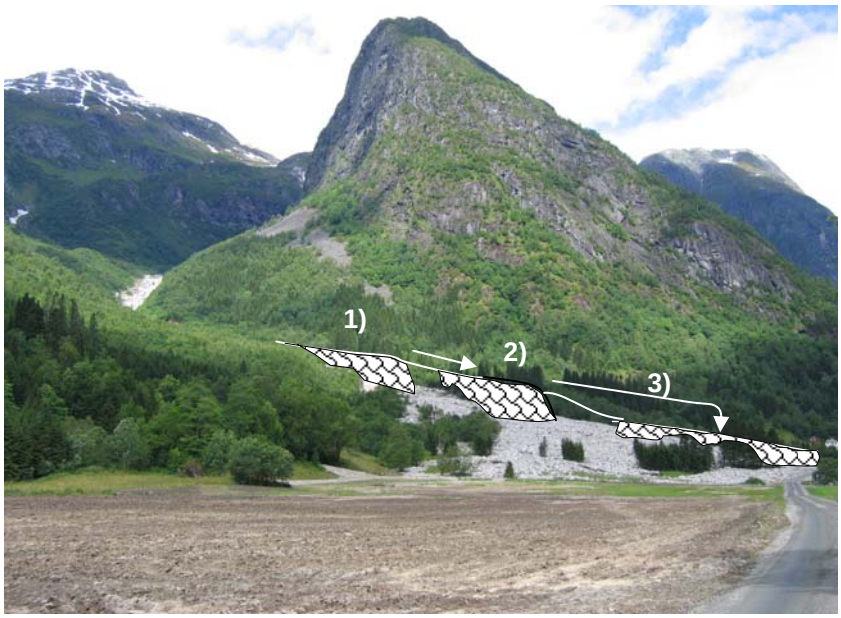

Figure 2.25 Illustration of how the front arrived in Supphelledalen valley and collapsed like a punctured balloon as it reached the lower parts of the fan area. After a sketch by eyewitness Ingvar Supphellen. Photo: C. Harbitz.

2.4 The deposit – Brazil nut effect and bridging

The larger particles in the debris flow of Fjærland ended in a huge fan deposit where the gully flattens out in the valley of Supphelledalen. The fan shows a pronounced inverse grading, as is also observed in debris flow deposits by other authors (Remaître et al., 2003 a; Takahashi, 1991).

The phenomenon has earned much attention in science, as it is important for example in industry, pharmacy and chemistry (Shinbrot, 2004), and can be seen in simple and daily examples like in a bag of potatoes - it need not be the seller that on purpose puts the biggest ones on top. The effect is called the Brazil nut, and refers to the fact that in a box of nuts of different size and type, the large Brazil nuts rise to the top when shaken. Such granular segregation was first reported in 1939, and was given the name “Brazil nut problem” in 1987 (Huerta and Ruiz-Súarez, 2004).

There have been several suggestions why this segregation occurs. These include convection, void filling, arching, inertia and buoyancy. For a further explanation of these terms see Knight, Jaeger and Nagel (1993) and Huerta and Ruiz-Súarez (2004).

It is agreed that the larger the block, the faster it ascends. It is however also observed that there is a critical diameter above which particles *descend*, resulting in the reversed Brazil nut effect.

A certain bridging effect is also found in the fan deposit. Bridging or force chains in a deposit is a sign of unequal force distribution. Force chains are generated between the grains in contact, and may evolve in a debris flow containing large clasts like the one in Fjærland. Stresses are transmitted through this network of particle contacts, and only a fraction of the particles bear a large proportion of the total load (Mueth, Jaeger and Nagel, 1998). This pattern is also found behind the largest blocks, with a chain of coarse particles stacked and locked behind it. Topography and remaining trees may also be a factor in the formation of bridges. Bridging can also be a result of pulse movement, where the different waves flow in different directions due to the deposit of the previous waves.

The double Brazil nuts observed are probably formed due to pulsing behaviour and repeated changes in direction of flow. The deposit shows very high content of boulders, suggesting that grain-to-grain contact has been an important factor in the dynamics. Bridging pattern is probably due to this, in combination with the topography and resulting settling of large boulders in front of each bridge. The force chains are results of contact between grains, showing that at least a part of the debris was not fully liquefied at all times.

These topics are not treated any further in this thesis, but can be studied in the papers by among others the above mentioned authors. Both phenomena point towards a strong grain-to-grain contact working in the dynamics of the flow in Fjærland.

2.5 Total duration

The witness opinion of the total duration of the flow varies from 45 minutes to 2 hours. For example, Ingebrigt Supphellen says that the fountain of black water at the precipice was visible for about 2 hours, but with uneven intensity. Ingvar, his son, says that the duration of the whole event was about one and a half hour, and that as the volume started to reduce, it reduced quickly. For Eirik Øygard, who was at the cabin Flatbrehytta, the event seemed faster, and it did not take a long time before he could see the mud at his TV-antenna in his

fields. He reports that he heard the slide five minutes to one, and went out to watch the event 10 minutes later. After half an hour there was almost no flow in the river (i.e. 45 minutes).

It has been reported that half an hour passed from the masses first were visible at the precipice until they reached Supphelledalen. Half an hour for the masses to travel 2 km seems unlikely, and there is no sign of a temporary basin damming the masses. The most probable reason is that Ingebrigt Supphellen observed the very beginning of the flow at the precipice. The first water wave probably had little erosional power, meaning that water transporting sediment in suspension and by bed-load transport reached Supphelledalen. A small river would not be visible from Øygardsneset due to the forested fan area. As the torrent gradually entrained more and more material the front of the debris flow developed, explaining the time-lag between the first observation of water and the arrival of the debris flow front.

A scary and dramatic event can seem never to end, but it can also seem to be over in seconds because people tend not to get time to think. In this case it seems that 45 minutes is the most appropriate estimate of the main part of the debris flow. It is difficult to determine when the water flow stopped, since the river was large and sediment-rich for days after the event. This is seen in pictures taken hours and days later.

3. Previous debris flow events in Fjærland

When examining the fan deposit, scoured areas on the flanks have revealed sediments that probably are old landslide or debris flow deposits (Figure 3.1). Under a layer of soil, stones and boulders can be found, resembling the deposit of the new fan. According to Eirik Øygard all the hills in the opening of Tverrdalen (100-150 m.a.s.l.) towards Supphelledalen are landslide deposits. Also the presence of alders, which are the fastest to recover after a landslide, indicates unstable times. It should however be noted that snow avalanches are common in the area.

Figure 3.1

On the flanks of the fan cuts exposing old slide material are found. The boulders on top of the soil are fresh and originate from the 2004 debris flow, whilst the boulders seen beneath one m of mould were deposited here in the past.

Nearest neighbour upstream the fan area, Per Christian Liseter, has cleaned his fields for stones and buried the biggest boulders, covering them with soil. During this work fertile mould has been found, buried under meters of coarser sediment resembling slide material. When he earlier has reworked other sections of his farmland due to frequent stones and boulders, similar mould was found.

Ingvar Supphellen living at Øygardsneset 1 km downstream the fan has had large areas inundated by mud due to the 2004-debris flow. No stones or coarse particles are found in

this area, since the stretch from the fan to the farm is almost flat. When digging a trench in his fields, similar layers of mud were found under a meter of soil. These findings suggest that similar events may have occurred in the same area before. The mud at Ingvar Supphellen's fields has been shown to be very fertile. According to him, it is a fact that there "always" has been a big difference in the fertility between his farm and Supphella further up in the valley, an area the debris flow from Tverrdalen does not reach. This may suggest that something happens here from time to time.

There is historical evidence that similar events have happened twice during the 20th century, one in 1947 and one in 1924. According to his father Ingebrigt Supphellen, still living in Supphella, the event dating back to 1947 damaged the bridge over Tverrdøla (near the fan) and divided the river into two parts. The road was damaged by the flow, but the stones carried were not as large as in 2004. However, they were big enough that local residents had to use a stump puller to remove them. Most material was deposited just before the start of the 2004-fan at elevation 100 m. Ingebrigt Supphellen knows that the reason for the event in 1947 was a moraine ridge failure.

Photos taken before the 2004 debris flow event show a small breach scar in the ridge, probably dating back to 1947. As seen from Figure 3.2 this was evident in a photo taken around 1980, but not in the photo from 1906. It seems however that in 1906 this area was lower than the rest of the ridge, and it almost looks like the glacier had grown in the direction of the breach area, almost damaging the ridge here.

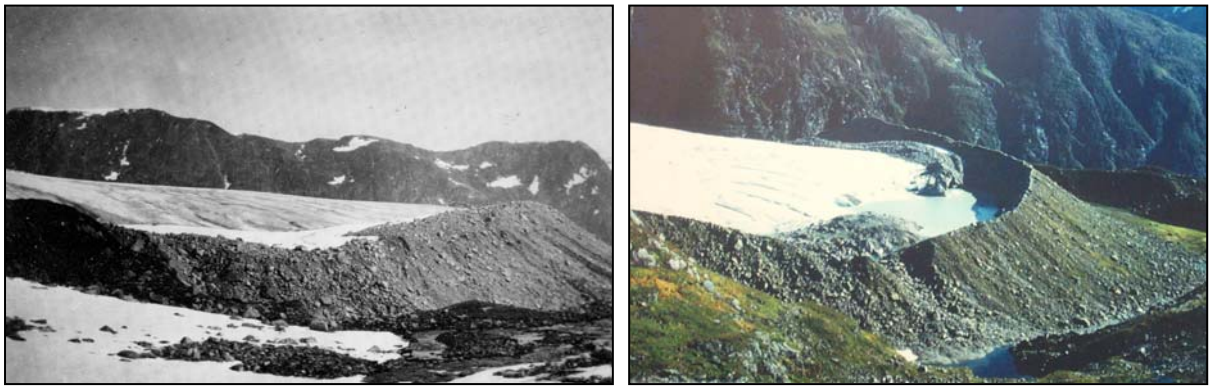

Figure 3.2 Left: The lowest point of the ridge is seen even in photos from 1906 Photo: Monchton, NGU photo archive. Right: A significant breach is seen. Photo is taken approximately around 1980. Photo: Norsk Bremuseum.

A diary written by his neighbour and Eirik Øygard's grandfather, also called Eirik Øygard, November 11, 1947, describes this event (see Appendix A). He compares the flow of the river Tverrdøla to a snow avalanche. The masses were described as black and saturated with sediments. The diary also tells that the 3 m high flood mitigation structure in Supphelledalen was overtopped and damaged by the flow. Also the pulsating nature of the debris flow and the change of direction are described, as well as the ground shaking and the masses cascading down the precipice at around 900 m.a.s.l..

The locals in Fjærland also report a big slide in the 18th century, and the tale says that the farm Øygard was abandoned due to this event. It is not known if this was due to fear of new slides or floods or because the boulders were too big and the volume too large to be removed, as they had no machines to help them. The name Øygard (which means abandoned farm) could result from this happening. Old maps show the farm with the name Rødsete. The name Øygard can however also have its origin from the Black Death as is very common for farms in Norway. Another explanation to the name can be the meandering glacial river, forming islands in the landscape, where the farm was built. This is the case in the nearby valley Jostedalen. Øy means both island and abandoned in Norwegian.

It can be read in the local history book "Fjærland Bygdebok" that Øygard was left "abandoned during the Black Death *or in a later event"*. Trygve Mundal, local resident of Fjærland and the owner of the book, has however his own complete record of the people living at Øygard dating back to 1616.

In 1900, the houses of the farm Øygard were moved approximately 300 m, from near the forest down to the flat fields where they are presently located. According to the inhabitants this was done either due to the fear for snow avalanches or because they were able to "control the river better than before". A millhouse on the downstream side of the fan is also reported to have been rebuilt three times due to avalanches or floods over the last centuries (Figure 3.3).

Figure 3.3 The millhouse has been rebuilt three times due to avalache activity. Photo: E. Loe.

All this indicates that mass flows regularly occur in this valley, and that some of them originate from the moraine ridge and glacial lake is probable. The events 57 and 80 years ago were probably not as large as the one in 2004. If a debris flow was the cause of an abandoning of Øygard, a size of the event similar (or larger) to the 2004-flow may have occurred. This could mean that a flow of this size or larger has a recurrence interval of 300 years. To get a further understanding of this, dating (C-14 or corresponding) of the deposits in the area could be carried out.

3.1 Future events

A new debris flow in the future is not unlikely. The scar in the moraine has not reached bedrock, and sliding from the sides will also gradually fill the scar. If the climate continues to warm up, melting will fill the lake rapidly, and a new dam failure will probably occur. The cut-off of drainage channels under/in the glacier (see Chapter 5) is also likely to occur from time to time. The question is how large a future event will be. Availability of erodible bed material is often a limiting factor for returning debris flows, and in the Fjærland case erosion has reached bedrock only a few places. The magnitude of a new event cannot be determined accurately, but it seems from earlier events that the size of the 2004-event is in the upper range, and that the present scour of the gully will limit new flows from growing to the same magnitude. See also Chapter 12.

4. Terrain modelling

This section describes the methods used in the photogrammetry process as well as in the laser scanning, and discusses their reliability. These techniques allow the reconstruction of 3D geometry of post- and pre-flow terrain and 3D change in topography. Multi-temporal air photos allow for elevation change estimations which can result in debris flow volume estimates.

4.1 Aerial photos and photogrammetry

The use of vertical aerial photos as a stereo model in terrain modelling requires overlapping sets of photos. It is necessary that the photos are positioned correctly relative to each other, and also to the real world. This means that the position of the airplane is required.

First an *interior orientation* where the pixel coordinates are recalculated into the camera-coordinate system is performed. There are approximately 20 000 x 20 000 pixels in each picture, and the camera-coordinate system is in mm. The transformation used is an Affine transformation, meaning that also form or scale is changed during the transformation.

Second, a *relative orientation* is needed. This determines how the two pictures are positioned relative to each other. If at least five points in the two pictures are found to be the same, there is only one possible relative position. In this case, 10 points were used to increase accuracy

Third, *absolute orientation* must be performed. This is done to determine how the pictures are positioned relative to the actual terrain coordinate system.

4.1.1 Stereo model

This work resulted in pre- and post-event stereo models of the area, the 2001 aerial photos representing the pre-flow terrain and both the 2004 photos and the laser data represent post-flow terrain. The stereo models can be used for visualisation and direct measuring, but also to manually check the terrain models.

Problems

Given parameters in the photos should match the GPS data from the airplane. It seems that in this case there are some meters in offset between the coordinate system on the ground and the one in the GPS data set. The height difference between the GPS data and the control points in, for instance, corners of houses are large in some places (7.8 m). An offset is normal, especially when the distance to the GPS reference station is large. This will however not affect the absolute precision of the coordinates or heights. This can be due to control point quality and/or that the reference station for the GPS was situated far away. The control points were taken from coordinate lists and maps.

4.1.2 Orthophotos

An orthophoto can be generated if aerial photos, with known absolute orientation, and a terrain model are available. The aerial photo is projected on to the terrain, and the result is a map of x- and y-coordinates with a photo draped on it. This is an image in an orthogonal (map) projection, and can be used to for example to measure the widening of the gully, but not the vertical erosion (i.e. 2D). Two orthophoto versions are made in this case, one based on the photos from 2001, and the second on the 2004 photos.

When making the orthophotos, the terrain elevation from the laser scanning was used both in combination with the pictures from 2001 and 2004. This is a simplification, but the elevation error for a point in the picture will be small, as the height to the plane is large (2450 and 3900 m). An orthophoto is two-dimensional (elevation not included) and the horizontal difference will be minimal.

As this decision was made, it was not known that the laser scanning missed control heights, which makes these errors larger. The problem of uncertain control heights is further discussed in Sections 4.2.1.

4.1.3 Digital terrain models

The computation of a terrain model is based on a procedure which identifies and measures common points in a stereo model by image correlation. The photos are taken from different directions, and in steep terrain the photos from different angles will look different. Some

features may be visible only in one of the pictures, or a boulder may seem not to have the same form as the angle changes. Visualisation of the terrain models are shown in Figure 4.1 and Figure 4.2.

In this case terrain models from 2004 were to be compared to terrain models from 2001. Some difficulties related to this comparison were:

- movement of objects in the meantime (stones etc)
- vegetation change and growth
- 2004 photos in colour to be compared to 2001 photos in greyscale.
- shadow in parts of the track and in the moraine breach area. Especially colour photos (2004) turned out to be unclear in these parts.
- 2001 photos taken at inappropriate time of year (summer)
- 2001 photos not especially made for the purpose (shooting angle not optimal)
- 2001 photos taken from higher altitude (3900 m) than the 2004 photos (2450 m).

The laser data however can be used directly to form grids and terrain models. Also length profiles and cross sections can be extracted without much effort. This is a main gain using this method.

The interpolation method used in Surfer to develop grids from the data, was in all cases linear triangulation. The DTMs produced from photogrammetry are regular grids (with 3.3x3.3 m cells) which favour this interpolation method.

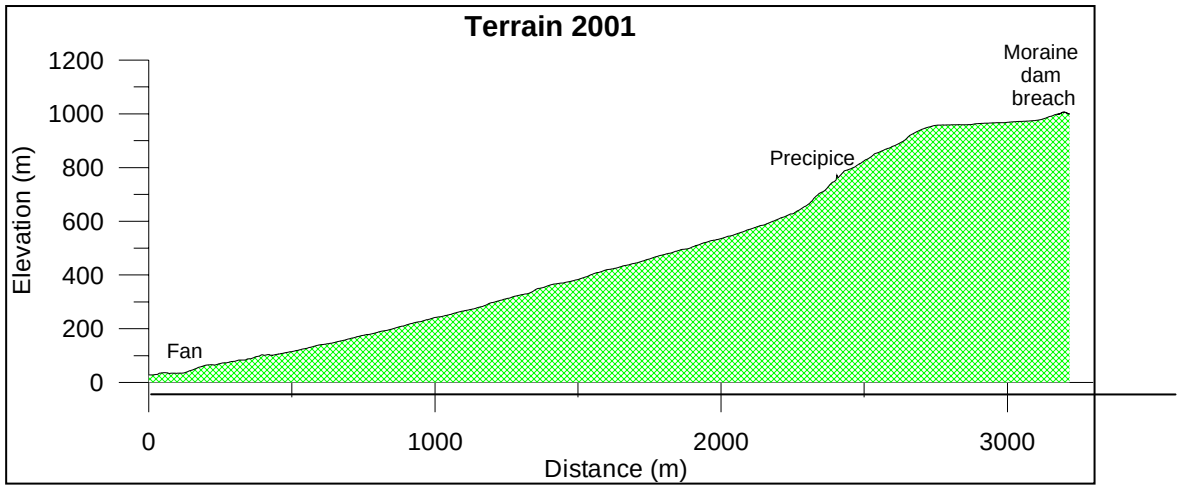

Figure 4.1 Length profile of debris flow track, generated from terrain model.

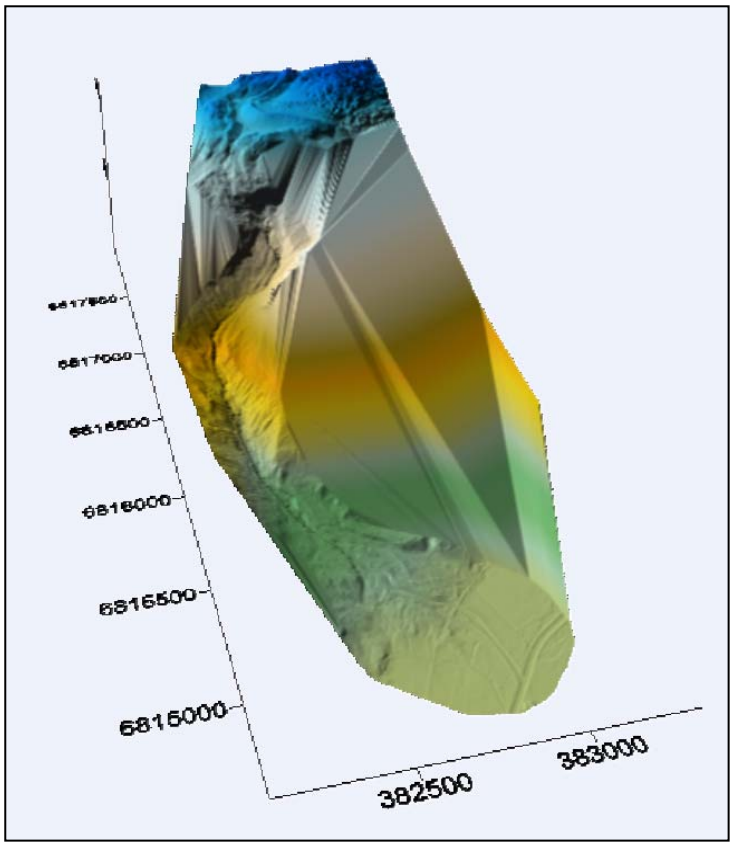

Figure 4.2 Surface terrain model generated in Surfer.

4.1.4 Resolution

The standard deviation for the stereo models is 6.4 µm, which for the 2004 model corresponds to approximately 10 cm when using an average scale of 1:15 000. This is found by:

$0{,}0064\,mm \cdot 15000 = 96\,mm \approx 10\,cm$ in horizontal direction.

The scale is mostly larger than this, 1:10 000 at the glacier but 1:16 000 in the Supphelledalen valley.

Corresponding standard deviation for the 2001-model will vary from 12.8 to 16 cm, dependent on the scale varying from 1:20 000 to 1:25 000.

The pixel resolution is 12 µm in both series from 2004 and 2001; that is, the pixels are 18 on a 1:15 000 scale and 30 cm on a 1:25 000 scale (at 0 m.a.s.l.), but this will vary with the terrain altitude. The 2004 pictures have been taken from a lower altitude (2450 – 2480

m.a.s.l.) than the pictures taken in 2001 (3900 m.a.s.l.). This means that each pixel is smaller in the 2004-pictures. The terrain model based on the pictures from 2001 will therefore be less accurate than the one using the 2004-pictures. Since the flying altitude is more or less constant above sea level, the biggest uncertainty will occur in the lowest areas (farmland and fan). Here the height from ground to the airplane is the largest. The variations in resolution will be relatively large as the elevation variations within the area are pronounced (1000 m).

The vertical precision (height precision) is believed to be 0.06-0.15 ‰ of the flying altitude in flat terrain, whilst in steep terrain it can drop to 0.9 ‰ (Barstad, 1998). The precision will be considerably reduced by a higher flying altitude. This means that the precision of all terrain models must be determined by the pictures taken in 2001 (altitude 3900 m.a.s.l.). The distance between the plane and ground decreases in higher altitudes, and this must be taken into account when estimating the uncertainty. This means that the heights are within a range of 23 cm (0.06 ‰ of (3900-25) m) for the lowest flat areas in Supphelledalen. In the precipice area the uncertainty may reach 0.9 ‰ of (3900-700) m, which is 2.88 m, and the flatter areas near the moraine get an uncertainty of around 0.006 ‰ of (3900-1000) m, which means 17.4 cm. This means an average of around 20 cm.

There is also a minimum limit for cell size in photogrammetry, which is a function of resolution, camera and flying altitude. The 2001 photos determine the cell size of the grids generated. In this case the minimum cell size was 3.24 m, and a cell size of 3.333 m was chosen for all grids, as for comparison the same cell sizes are needed in all the grids. Each cell gets an averaged value of several pixels. In the generation the points are given different colours indicating whether the pixels have almost the same value (orange), strongly differing values (red), or few values (blue). Typically, very steep terrain or hummocky surfaces with many blocks, get red colour. Especially the precipice from 900 to 600 m.a.s.l. turned out to be difficult to represent accurately.

As photos from different angles are needed in photogrammetry, steep terrain commonly creates problems. This is especially the case in the precipice area but also on the east flank of the stream Tverrdøla due to the steep terrain towards the mountain Vetle Supphellenipa.

4.2 LIDAR laser scanning

The laser used was of the type ALTM 2300, a LIDAR (Light Detection and Ranging) laser scanner. The method is based on distance measurements between the scanning device and the reflecting object, and precise orientation of the measuring device (Figure 4.3). The laser sends pulses of beams at regular intervals towards ground, and an oscillating mirror sweeps the beams in a Z-pattern across the flight path. The ground reflects the laser pulse, and the time interval between the transmission and the return of the pulse is measured and transferred into distance. Also the angle of the beam hitting ground is measured. The strength of the reflected signal varies with the properties of the ground.

The method requires accurate determination of the airplane's position and orientation (direct georeference). This is done by GPS and an integrated Inertial Navigations System (INS). The laser's position at each pulse admission can be determined, and by observed angles and distances, positions on ground are found. The GPS reference receiver should be within 20-50 km for accuracy (Turton and Jonas, 2005, Barstad, 2002)). The result is measured points characterised by x, y, z coordinates.

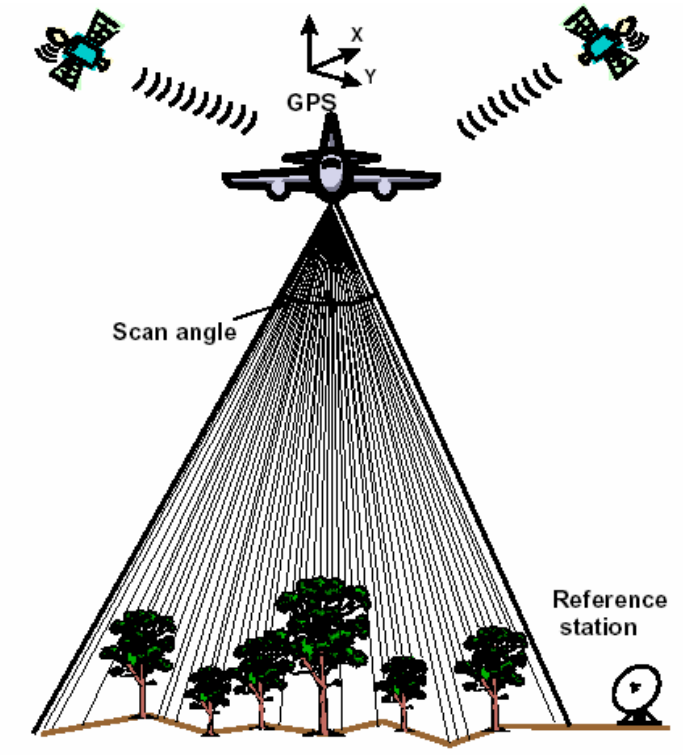

Figure 4.3 Airborne laser scanning. Taken from Hyyppä et al., 2000.

Table 4.1 Technical parameters for laser scanning flight in Fjærland

Parameter	Performance
Operating altitude	700 m
Speed	75 m/s
Scanner frequency	32 Hz
Laser pulse frequency	33 kHz
Scanning angle	18º

System calibration can be extensive. One common calibration method is to use control areas of known height and compare these with measured heights. This is believed to remove bias and systematic errors by moving or tilting the model to fit the control points. This has not been done in the Fjærland case as discussed in Section 4.2.1 below.

Laser scanning is especially useful in areas covered by forest and in areas of low contrast or low solar radiation. A laser is not dependent upon daylight or solar radiation, as the laser itself generates the beams. Compared to classical photogrammetry this is a big advantage. The laser scanner also has the opportunity to register two or more returns from the same pulse. This means that in a forest it is possible to measure the elevation of the ground as well as the elevation of the tree tops, displayed as first and second pulse return. In the Fjærland project the second pulse represents ground.

4.2.1 Errors

A laser scanning is vulnerable to disturbance. Errors in the GPS measurements (Barstad, 2002) contribute to a large part of the inaccuracy. Variations in the GPS measurements after initialisation may occur if the airplane is not smooth enough in its turns. The varying reflecting properties of the ground together with varying angle of the beam will result in variations in accuracy throughout the area. Also air contamination and humidity may affect the reflection.

The laser “cloud” is dense, but the point density varies along the path, both due to the variations in terrain and angle, and also because of the variability in overlapping between the different stretches.

The GPS in the plane can cause absolute offsets in height in the resulting terrain model. As mentioned, control points with known height can be measured in flat terrain in both ends of the wanted area. The laser scanning executed in Tverrdalen lacks such calibration, meaning that although the relative height differences in the model are correct, the model may have to be tilted or a parallel displacement may have to be made for the heights to be true elevations above sea level. But, as mentioned, the terrain representation and the relative heights within the model are correct. The problem arises when the model is to be compared to models generated from other techniques or at other times, as is the objective in this case. It could be possible to manually measure several control points (5-6) which are known not to have moved in both the laser data sets as well as in the 2001 model, and in this way orientate the laser terrain model correctly for the future.

It turned out that the terrain generated from the laser scanning had lower elevation than if using aerial photos. That is, laser elevation lines lay above 2004-photo lines in the generated maps. This offset becomes larger the further down the valley you get. It is small at high elevations near the moraine ridge.

It seems however that the laser is more correct than the photo generated terrain in the precipice area. The error is probably due to the steepness of the terrain. The direction or angle, from which the 2001 photos are shot, may not be ideal for this terrain.

As seen in Figure 4.4, the laser scanning (blue line), which ideally should fit exactly the red line (aerial photos from 2004) is consequently situated higher. When studying the contours carefully, it was found that the laser scanning data are not reliable. They are too low in altitude. In the figure, the blue and the red lines should exactly match and lie above the green one in the gully due to erosion.

The offset between the control points and the aeroplane GPS data set in the photogrammetry could be a factor when considering why the laser-generated terrain model does not match the one generated from aerial photos, as absolute coordinates are used in this comparison.

However, the heights do not match when comparing the laser data with the old map, indicating that this is not the case.

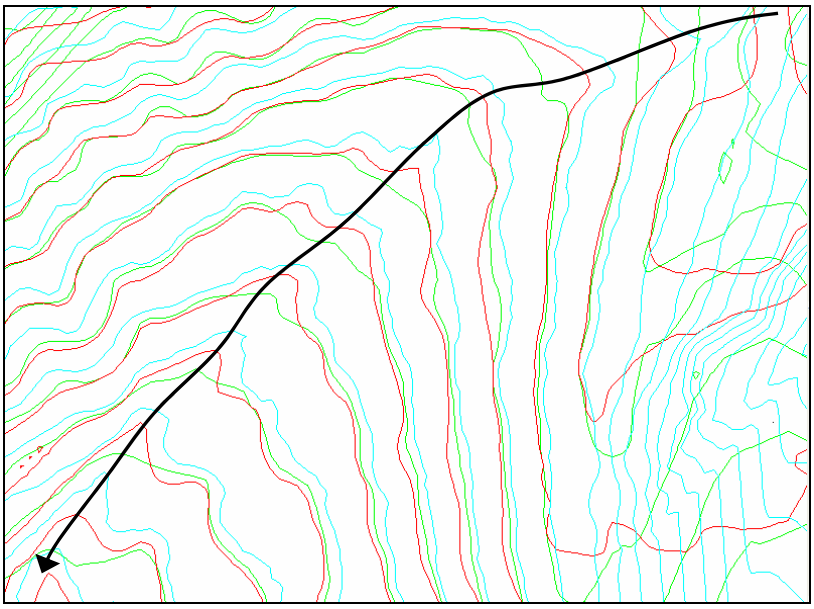

Figure 4.4 Example of contours. Green lines show 2001-contours generated from air photo, red lines 2004-contours from air photo, and blue lines show laser-based contours from 2004. Black arrow indicates direction of debris flow.

The orthophotos have been used to determine profiles (coordinates) along the track to carefully examine and analyse. The profiles shown in the terrain models from 2004 are compared to the same profiles from 2001. In this way erosion along the track becomes visible. As discussed, steep terrain is difficult to represent correctly using both photogrammetry and laser scanning.

The terrain models do not only offer a visualisation of the event, but when subtracting the model representing the 2001 terrain from the one representing 2004, using Surfer, negative values will display erosion, and positive values sedimentation. In this way it is possible to determine the total volume involved in the debris flow as well as any pattern of erosion or sedimentation related to physical parameters like slope angle.

4.3 Laser vs. aerial photos

4.3.1 Volume estimate

Since it seems that the absolute heights of the model generated by the laser scanning are lower than the actual terrain, it is most appropriate to use the aerial photos from 2001 in combination with the aerial photos from 2004, and not the laser scanning, in the volume estimation. This is discussed in more detail in Chapter 8. Another advantage in relying only on the aerial photos in the estimation is that two comparable techniques are used in the generation of the heights. The problems of steep terrain are the same in the two air photo-models, and the accuracy estimation technique is also the same in both. Since no laser scanning exists pre-flow, if the 2004-laser scanning was going to be used, it had to be compared with the model generated from the 2001 aerial photos. The accuracy is of course not optimal in the models as they are now used, and could be improved by manual effort, using breaklines along ridges and streams etc.

A height precision of +/- 20 cm and a change in elevation of 2 m will give an anticipated volume estimate accuracy of 10 % (Chapter 8).

4.3.2 Visualisation using profiles and 3D models

The laser data is suggested to represent the terrain in a better way than the photogrammetry. The laser data includes more elevation points, and the elevation precision of these points is better than what the aerial photos give. In addition, the laser has the advantage of looking vertically downwards. No two positions are required, excluding the problem of view behind steep terrain.

According to Blom Geomatics, the accuracy expected from a laser scanning is 5 cm; whilst Hyyppä et al. (2000) claims that this is the accuracy between the data points, and not real world vertical accuracy. Their experience suggests a standard error of vertical accuracy of 15 cm on flat ground, increasing to 40 cm for slopes of 40º.

After considering this, the laser data are being used when generating profiles and representing the terrain, because the relative height differences are correct within the model.

5. Glaciology and the Supphellebreen glacier

As the debris flow in Fjærland had its origin in a flood from the glacier Supphellebreen, glaciology and glaciohydrology are important factors in the search for understanding of the phenomenon. An important task is to determine the water volume released from the lake and glacier. This can be approached by following glaciological traces, trying to reconstruct the way of water transport, as well as considering field and eyewitness observations.

The most probable reason for the moraine ridge breach and the additional water volume from the glacier is a blockage of the glacier's normal drainage route, and that due to high melting rates prior to the event self-enlarging channels at the base of the glacier supplied the lake with water. This chapter attempts to explain the glacier's capacity to store water and then suddenly release it. This also highlights the probability of similar happenings in the future.

5.1 Glaciers in Norway

Norway is among the countries with the largest glaciated areas in Europe (Liestøl, 1989, Andreassen, Elvehøy and Kjøllmoen, 2004). 2 750 km^2 of glaciers constitute around 1 % of mainland Norway. The Norwegian landscape of mountains and narrow fjords is mainly formed by glaciers and ice ages, but also the flatter areas of eastern Norway are formed by glaciers. Today most of mainland Norway's glaciers are situated in Western Norway.

The peak of the glacier extent during the last ice age (Weichsel) occurred 18 000-20 000 years ago (Nesje, 1995). After Weichsel ice age the climate warmed and the ice retreated. The Holocene period dates from 9000 years ago until present. In the beginning of Holocene, most or all of the ice disappeared. New glaciers were formed in higher mountainous areas when the climate cooled approximately 5000 years ago (Nesje, 1995), and most of today's glaciers are remnants from this period. These glaciers experienced their maximum extent in 1750 (Jørgensen et al., 1997).

Until 1930, the climate remained relatively cold. End moraines from 1930 are found several places, also near the upper and the lower Supphellebreen glaciers. After 1930, the overall

trend has been withdrawal of the ice in Norway, although coastal glaciers have experienced advancement since 1960. As shown in Figure 5.1 below, the growth of Supphellebreen has been pronounced. Since 2001 most glaciers have experienced a mass deficit (NVE, 2005). This may be a result of both low winter precipitation during 2001 and 2003, and high degree of summer melting in 2002 and 2003.

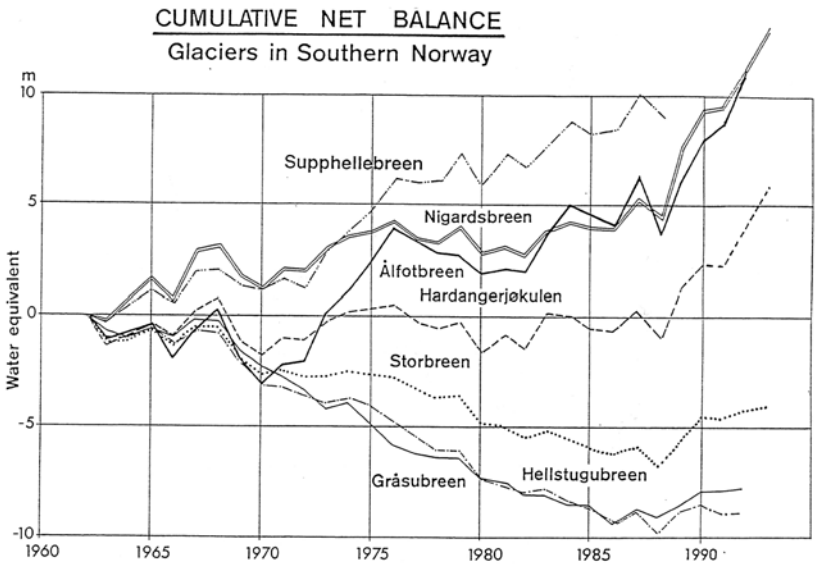

Figure 5.1

Cumulative net balance for some Norwegian glaciers showing that coastal glaciers have been growing whilst inland glaciers have retreated. Taken from Liestøl, 1995.

5.2 The glacier Supphellebreen

The glacier Supphellebreen is an arm of Jostedalsbreen, the largest glacier in mainland Europe (487 km^2 (Østrem, 1989)), and is situated in the county of Sogn and Fjordane in Western Norway. Supphellebreen has an approximate area of 11.8 km^2, and its elevation varies from 1730 to 720 m.a.s.l.. There is also a regenerated glacier part named Trollabyrgje below this elevation, as a result of ice falling from the snout. This is the lowest glacier in the hemisphere south of the Arctic circle (Aarseth et al., 1988), ranging from approximately 55 to 600 m.a.s.l..

5.2.1 Characteristics

Supphellebreen has an aspect towards the south, and the main part of the glacier has a length of 8.4 km in the glacier flow direction. According to NVE (Østrem, 1989), the glacier is cascading, meaning that it has a rough and steep surface. The danger of icefalls in the snout

area is characterised as very large (Østrem, 1989), and the ice has a movement of around 2 meters per day in the ice fall area, which is among the highest velocities in Norway (Norsk Bremuseum, 2005). 2 million tons of ice break off every year and cascades down to the lower glacier. Other areas of the glacier are flat; hence the name Flatbreen is used in this area. This main part (above 1200 m.a.s.l.) is an over-deepened basin, flat or bowl-like in shape. If the glacier should retreat, a lake could form in this area. The exact topography of the bed is however not investigated.

Figure 5.2

Supphellebreen anno 1906. Photo taken towards the moraine and the Fjærland fjord. No lake is evident. Photo: Monchton, NGU photo archive.

Figure 5.3

Supphellebreen anno 2004. A lake has formed between the glacier and the moraine. Failure of moraine in right end of the ridge. Normal drainage route is towards the left.

5.2.2 History

Supphellebreen reached its maximum around 1750 (Orheim, 1968), during the Little Ice Age. The moraine ridge damming the present lake probably dates back to this period. When studying the photos from 1906 and 2004 shown above (Figure 5.2 and Figure 5.3), the withdrawal of the glacier is evident, although periods of growth have been experienced. It is also clear that the shape of the moraine ridge has not changed much in the last 100 years. Only the smaller, inner moraine shown in the picture from 2004 could be of newer origin, probably from around 1930 when the ice had been advancing for some years and started retreating. The pictures show that already in 1906 the moraine had a lowest point where the breach is today (lower right corner in the photo).

5.3 Glacier hydrology

Running water in glaciers has mainly two origins (Hambrey, 1994). Surface melting is the most important one, but additional contribution comes from the snow along the valley sides.

The main transportation route is through channels. Water in temperate glaciers also runs under the glacier as sheetflow.

Under the surface of the glacier, there are principally two types (Hambrey, 1994). The Röthlisberger (R-) channels that run entirely through ice can be several meters in diameter and transport large volumes of water in a short time. The smaller Nye (N-) channels are eroded into bedrock beneath the glacier, but can also be combined with a R-channel above. The flood in Fjærland is probably related to flow in R-channels, as it seems to have developed during a short time. N-channels need more time to form. However, water may also be transported as a sheetflow under the glacier. This may especially be the case if few drainage channels have had time to develop.

5.3.1 Formation of a channel

Channels in glaciers are kept open and the size enlarged by the flow of water itself. The transition of heat from water to ice and the frictional heat generated are responsible for this process (Nesje, 1995, Paterson, 1994 and Liestøl, 1989). When the pressure from overlying

ice exceeds the water pressure the drainage channel will be reduced, proportional to the third power of the difference.

When the flux increases, the melting of the side walls will also increase. At the same time the water pressure rises. The result is enlargement of the channel. The size is adjusted to an average discharge, as the processes are not fast enough to follow rapid variations.

During the winter season small amounts of melt water is produced, resulting in low rates of flow through the ice. The small degree of water flowing, in combination with deformation of the ice, closes most of the drainage channels during the winter (Nesje, 1995). As the spring comes, the drainage passways need time to develop, resulting in storage of melt water and high water pressure within the ice or at the base of the glacier (Hambrey, 1994).

The time needed for a sufficient R-channel to develop, ranges from a few days to several weeks (Paterson, 1994), but the larger the channel, the faster the growth due to higher degree of heat dissipation relative to the area of the walls. Water pressure is commonly less in big channels, making the water drain from the smaller to the larger ones (Liestøl, 1989), again enhancing the rate of flow. The water flow gradually opens and widens the channels throughout the summer (Paterson, 1994), resulting in lowering of the basal water pressure again.

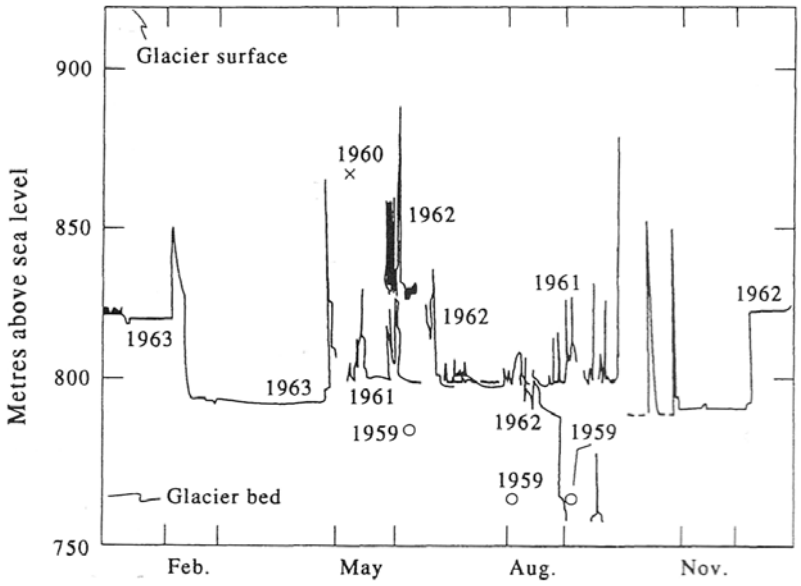

Figure 5.4

Water pressure in the glacier South Leduc, Canada, showing higher average water pressure during winter than during summer. The peaks are associated with storms or high melting. Taken from Paterson, 1994.

As mentioned, when a drainage system is cut off (Paterson, 1994), water pressure builds up beneath the ice, partly counteracting the glacier weight and resulting in enhanced glacial motion. This means that melt water and water pressure determines the rate of basal sliding. A few millimetres thick layer of water under the ice can increase the glaciers movement with 100 % (Hambrey, 1994). As discussed, Supphellebreen has a rapid movement.

In the days before May 8, 2004, Supphellebreen was observed to be especially active. Calving and ice falls are results of glacier movement. This movement supports the idea of high water pressure in and under the ice because of high melting rates and change in drainage pattern.

5.3.2 Discharge variations

Floods are not uncommon in glacier rivers. These rivers have a discharge pattern (Hambrey, 1994) characterised by extreme diurnal variations and maximum flood during summer.

Figure 5.5 shows how discharge is related to temperature in glacier rivers. They show pronounced floods every 24 hours where the discharge can be twice the minimum of that same day. This diurnal pattern is related to the weather condition and the sun's intensity during the day, melting water rapidly transported through moulins. Also the base-flow component influences river flow. Base flow is slow in its response and results from water transported through snow (Paterson, 1994).

This means that water transport through snow is slow, and drainage through ice channels more rapid. A rapid flood like the Fjærland is likely to be due to a sort of channel drainage, most probably at the base of the glacier.

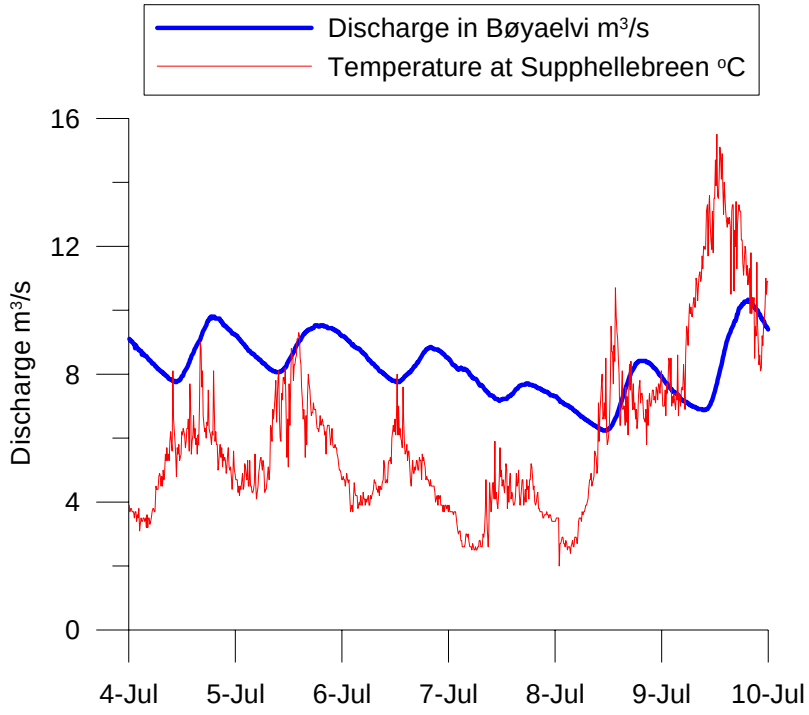

Figure 5.5

Glacier rivers follow diurnal variations, especially in summertime, displaying floods every 24 hours. This is an example from July 2004 in Fjærland.

The glaciers Bøyabreen and Supphellebreen are neighbouring arms of Jostedalsbreen and situated at almost the same elevation (see Figure 2.1). They are also of approximately the same size, so that the discharge measurements in the river of Bøyaelvi can be correlated to the temperature data from the station at the moraine ridge near Supphellebreen. Also the Bøyaelvi river shows a high discharge on May 8, meaning that there was a natural flood this day, probably also from Supphellebreen. A blockage of the drainage channels may have stopped this flood and forced the water towards the lake. There is no measured data available from the Supphelleelvi river, nor temperature measurements from Bøyabreen. The Supphelleelvi river is believed to have a daily discharge slightly smaller than Bøyaelvi.

5.3.3 Storage of water

In the beginning of the melting season there is a time lag (Paterson, 1994) between discharge peaks and melting peaks in glaciers. This period diminishes throughout the melting season; probably as a result of the development of drainage channels and the reduction in snow cover; meaning that the drainage rate rises. Normally, from July to August, which is the period of maximum runoff in glacier rivers, the discharge is higher than the melting. This means that water must have been stored in the glacier during the early months of summer

and later released. Other evidences of a glacier's capacity of storing water are found in the literature. Paterson (1994) mentions examples of glaciers releasing up to 38 % more water during the entire summer than the measured ablation during the same period.

Sudden floods unrelated to weather conditions have been observed by Mathews on the Athabasca glacier (Paterson, 1994), where there are no visible ice-dammed lakes. This means that the water must have come from within the ice. Also drilling and tunnelling in glaciers have uncovered cavities at great depths. According to Paterson (1994) these holes must be filled with water in order not to be closed by the ice. Some glaciers have also been observed to heave half a meter in the beginning of the melting season, believed to be a result of higher water pressure and water-filled cavities at the bed of the ice.

Together with sudden floods and glacial movement, all this supports the idea that water may be stored in cavities or lakes under or within the ice of a glacier.

5.4 Glacial lakes and Jøkulhlaups

Lakes can be dammed by glaciers in several ways (Hambrey, 1994);

- at the surface of the glacier (supraglacial)
- within the ice (englacial)
- under the glacier (subglacial)
- at the end of the glacier (proglacial)

The latter is the case at the glacier Supphellebreen in Fjærland, the lake growing as the glacier retreats.

Such ice-dammed lakes are often filled during the melting season of the glacier, and in many cases more or less regularly emptied by outburst floods, so called jøkulhlaups or Glacial Lake Outburst Floods (GLOF) through channels or under the ice.

Jøkulhlaups may occur regularly or be more unexpected. The frequency of the floods is often regulated by the variations in glacier thickness, retreat or growth. According to Paterson (1994), most jøkulhlaups occur at the end of summer or early autumn (July and August), as a result of the melt-water filling of the lake, but there are examples of late outbursts, like the

jøkulhlaup from Østerdalsisen in October, 1945 (Liestøl, 1956). The last similar flood from Supphellebreen through Tverrdalen valley occured in November, 1947.

Jøkulhlaup hydrographs show pronounced peaks. These sudden outburst floods can be extreme, and discharges of 50 000 m^3/s have been recorded in outburst floods from Grimsvötn in Iceland (Paterson, 1994). Grimsvötn is one of the best known lakes experiencing regular outburst floods. Another famous glacier dammed lake was the ice-age lake Lake Agazi in Canada, with a size of over 200 000 km^2.

5.5 History of Supphellebreen lake drainage

According to Aarseth et al. (1988) the moraine- and glacier dammed lake at Supphellebreen fills each spring, and drains through drainage channels beneath the ice towards Supphellen during summer/autumn (Figure 5.6 and Figure 6.5). The drainage used to occur in August or September in the 1960s, but when the report was written (1988) this time had changed to July, probably as a result of thinning of the glacier (Aarseth et al., 1988). This can have two origins; the melting rate causing faster filling of the lake, as well as the lower pressure of a thinner glacier making it easier to develop drainage tunnels under the ice or uplift it. Aarseth et al. (1988) stated that the normal drainage pattern of the lake is a jøkulhlaup (glacial lake outburst flood (GLOF)), the drainage occurring over a time period of hours. The jøkulhlaup normally has direction towards Supphellen, through the icefall. The flood of 2004 took the opposite direction, through the moraine (Figure 5.6).

Also Orheim (1968) writes that the glacier dammed lake is regularly drained each autumn under the regenerated glacier and down to Supphellen. As seen from Figure 5.6, the lake can be completely emptied by these jøkulhlaups.

These drainage tunnels are cut off before each spring. According to Orheim one can determine the start of the melting season by the water level in the lake. He states that as a rule there is very little ablation before the end of May, and that the melting water generated before this typically refreeze in the snow. According to Nesje (1995), the ablation season in Norway usually ranges from May 1 to September 30.

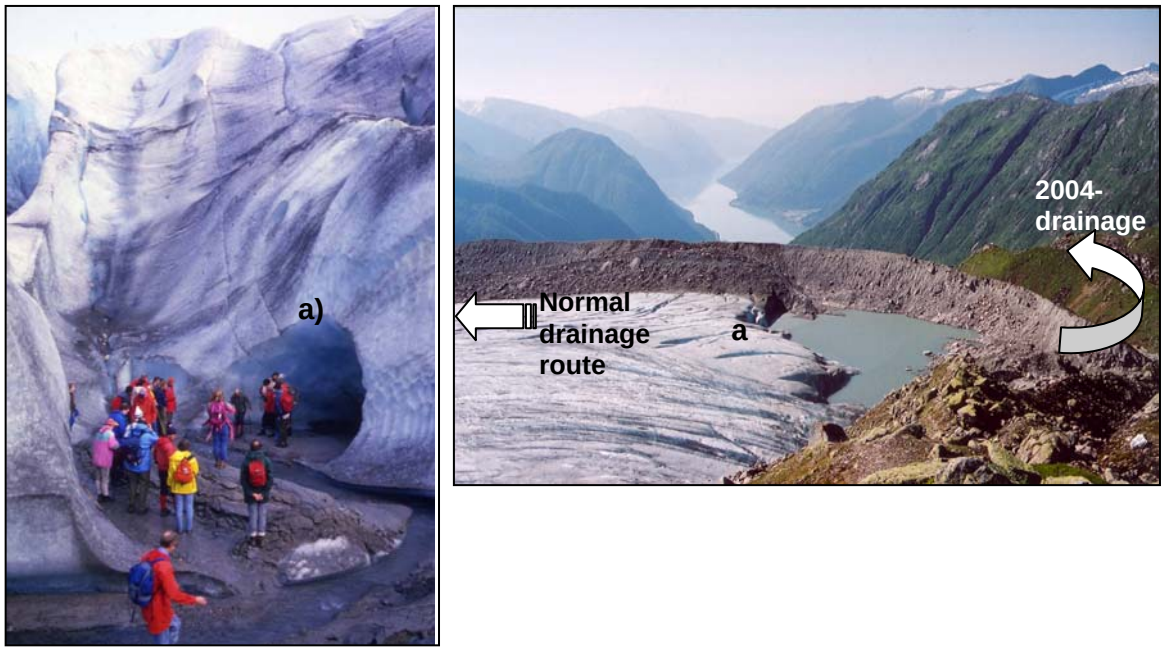

Figure 5.6 The moraine- and glacier-dammed lake usually drains through the ice towards the icefall in Supphellen every summer/autumn. The drainage channel of 1988 is here seen from the inside of the lake, and the letter a marks the position of the channel. The lake is completely emptied. Photo: J. O. Hagen.

This shows that the ice near the lake and the icefall towards Supphella is in continuous change, and that drainage channels are opened and closed each year. The opening of a drainage channel towards the icefall is necessary to empty the lake. If the melting rate is high and no such drainage channel develops, a breach of the moraine may be the outcome. According to locals, this happened both in 1947 and around 1920, and the tale tells about similar and very severe flow in the 1700's making the inhabitants leave Øygard.

There is also a possibility that the lake was not drained during the summer/autumn of 2003 (suggested by locals), meaning that the lake already stored unusual large amounts of water before the melting season of 2004 started.

It should be noted that only parts of the glacial melt-water usually enters the lake. The river Supphelleelvi has its origin at the glacier tongue in Supphella and flows all season in accordance to the discharge variations of glacial rivers described earlier.

6. Estimated water volume involved in the flow

The water volume involved in the debris flow is not known, but has a crucial role in the dynamics of the torrent since it influences mass flow parameters like yield strength, viscosity, density, velocity and thereby the erosional power and the run-out length. An estimation of the water volume involved is made considering the glacial lake area, total drainage area, temperature, witness observations and cross sections throughout the erosion track. Sediment volume is treated in Chapter 8.

6.1 Glacial lake area

The glacial lake area was measured to 8750 m^2 in the 2001-photos. When compared to the aerial photos taken after the event in 2004, it is seen that the shape of the lake has changed, and that the lake level has decreased (refer to Figure 6.1 and Figure 6.2). This is partly due to the fact that the glacier has retreated between 5 and 15 m over the three years, releasing new area to be covered by melt-water. The retreat of the glacier is also evident along the moraine ridge southeast of the lake. It must be noted that the 2004-aerial photos were shot late September, almost 5 months after the water release, and should not be taken as accurately representing the actual lake immediately after the breach.

The existence of the lake itself is a result of glacier retreat. A further withdrawal will change the shape of the lake, as well as the larger area available would decrease the water level if the water volume stayed constant. A retreat of the glacier however means a higher degree of melting.

The 2001 picture seems not to show a totally filled-up lake, and there is no significant stream over the moraine ridge. The orthophoto combined with the terrain model from 2001 indicates that the lake level could increase with 2 to 3 meters before any overflow would occur. From the aerial photos taken in September 2004, it is seen that the lake area was 7280 m^2. This means that the area of the lake has decreased from August 2001 to September 2004.

An additional lake area could possibly be found beneath the glacier snout, meaning that the thin snout could be floating, and hide parts of the lake.

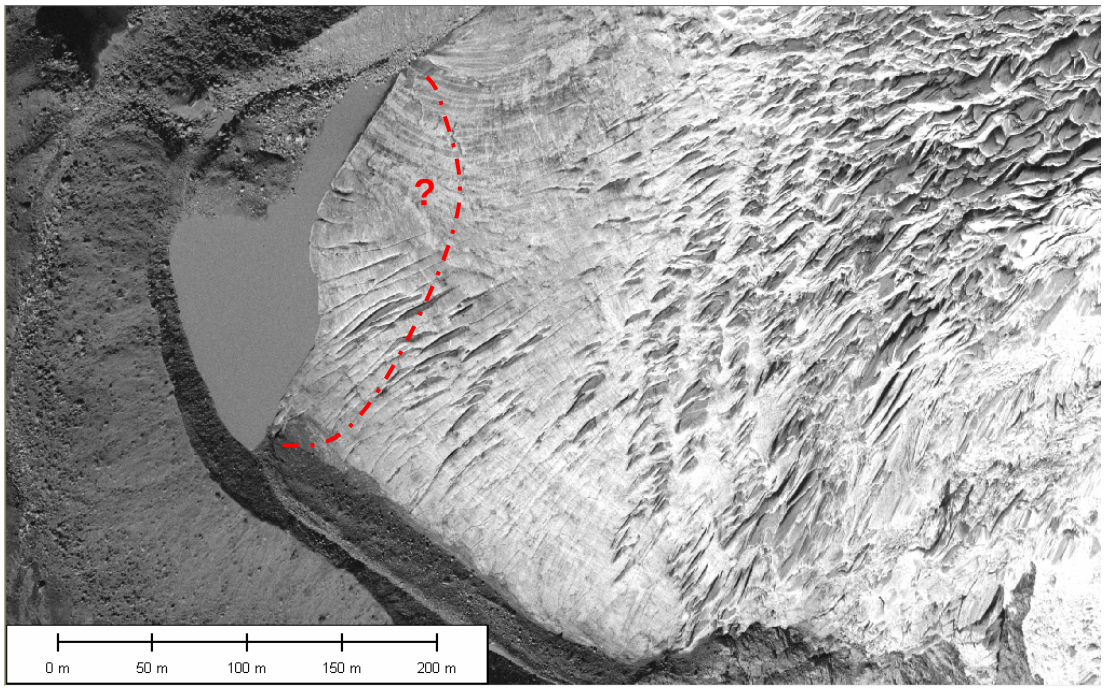

Figure 6.1 The moraine, glacial lake and glacier snout seen from the air in 2001. Red stapled line illustrates the possibility of the lake having larger area than seen from the air. Photo: Fotonor.

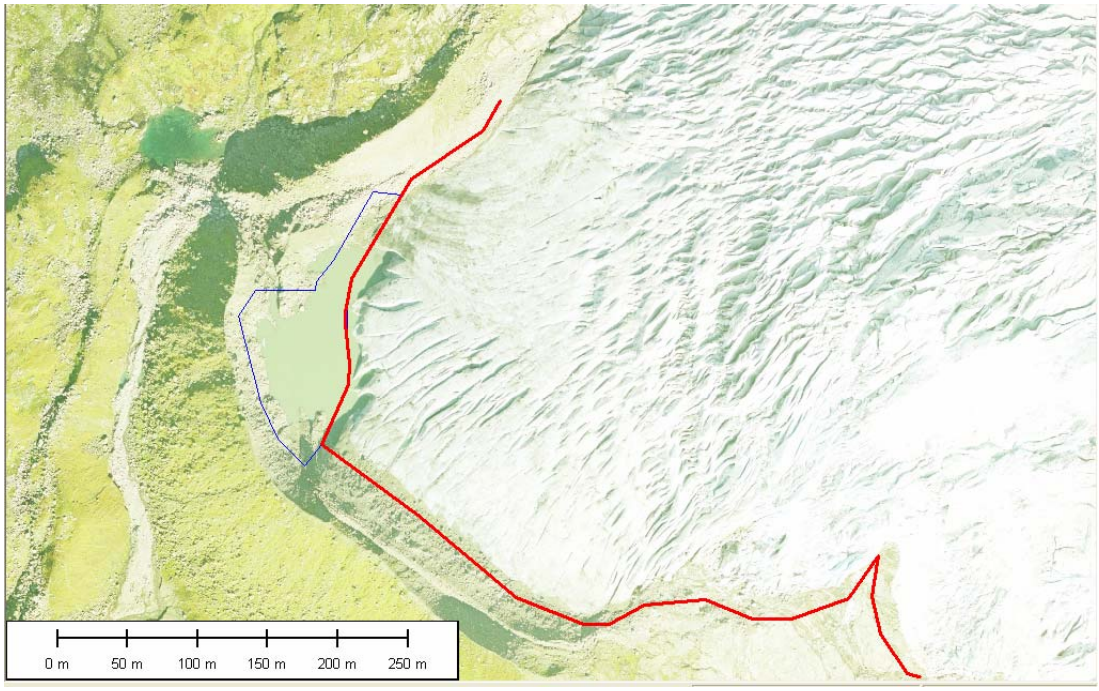

Figure 6.2 After the emptying of the lake, 30 September, 2004. Red line indicates glacier snout in 2001 and blue line indicates extent of glacial lake in August 2001. Photo: Blom Geomatics.

The glacial lake probably had a surface of approximately 10 000 m^2 when the moraine failure occurred, due to the filling of the lake. Possible additional lake area beneath the snout is not taken into account in this estimate. According to NVE the water level sank around 5 m during the event 8 May, 2004 (Elvehøy, 2005). A shoreline in the snow was recognised a few days after the event, showing the original lake level approximately 5 m above the surface of the lake (refer to Figure 6.3 and Figure 6.4). The drained volume of the lake is then estimated to 50 000 m^2.

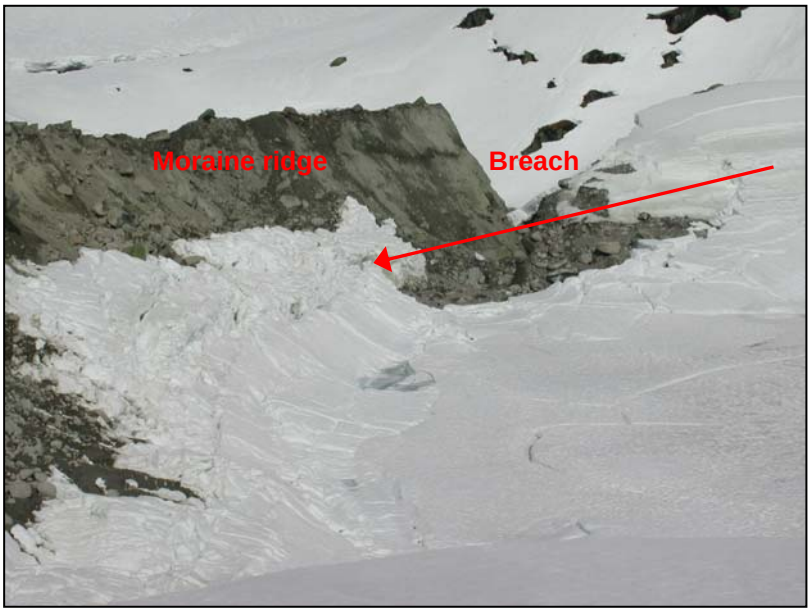

Figure 6.3

The moraine ridge from its inside, the arrow showing the former water level of the ice covered lake. Photo: Elvehøy, NVE.

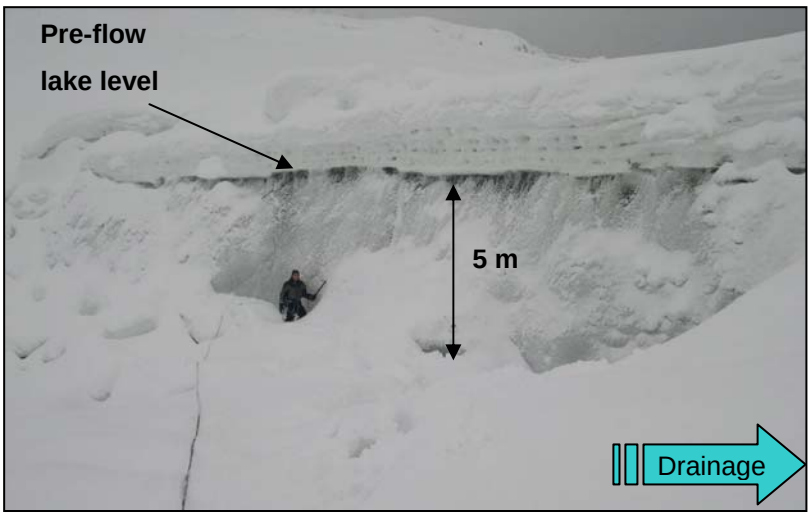

Figure 6.4

Lake level line seen a few days after the drainage. Photo: E. Loe.

6.2 Additional water from the glacier

Due to the fact that the moraine failed and the amount of sediment eroded in Tverrdalen, more than the 50 000 m^3 of lake water may have escaped through the scar in the moraine. The additional water must have come from a sub- or englacial lake formed due to early melting and cut-off of the normal drainage channels, or due to opening of new channels emptying a usually closed sub-/englacial lake. The normal route for most of the glacial meltwater is through the icefall and the regenerated glacier down to the river Supphelleelvi. This is also the route for the regular jøkulhlaups from the lake. In addition to the fast motion of the glacier, the observed glacier retreat could possibly be a factor in a change of the canal system, as the ice is relatively thin in the passage area over to Supphellen.

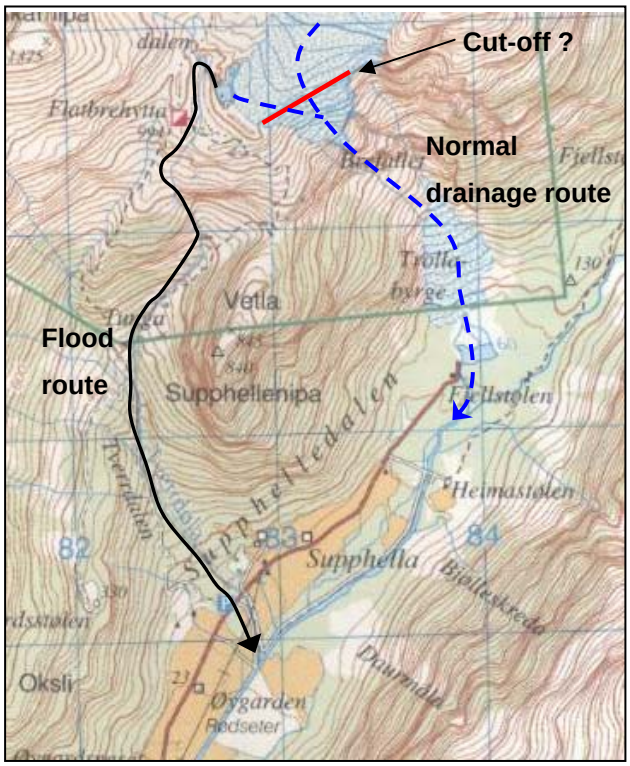

Figure 6.5

Map of the area. Stapled blue arrow indicates normal drainage route, red line indicates cut-off of drainage channels and full black arrow indicates debris flow route.

The idea is supported by the observation of scars and sediment rich ice in the upper end of the lake just after the flood 8 May, 2004 (see Figure 6.6). This is interpreted as the outlet of a glacial tunnel that suddenly drained stored water from the glacier towards the lake due to the high pressure developed at the base of the glacier. It seems that the water has entered the lake under its ice cover (maybe at the base of the glacier), vertically lifting the ice sheet, as the ice on the lake was still intact after the event. This is seen in pictures taken by NVE from a helicopter three days after the flow. If the water drained through the breach with the same

speed as the additional water was supplied from the glacier, an uplift of the ice was not necessary. Another possibility could be that the lake extended under the glacier, and that a collapse of the glacier ice in the above mentioned scar region (for example due to thinning) caused a flood wave.

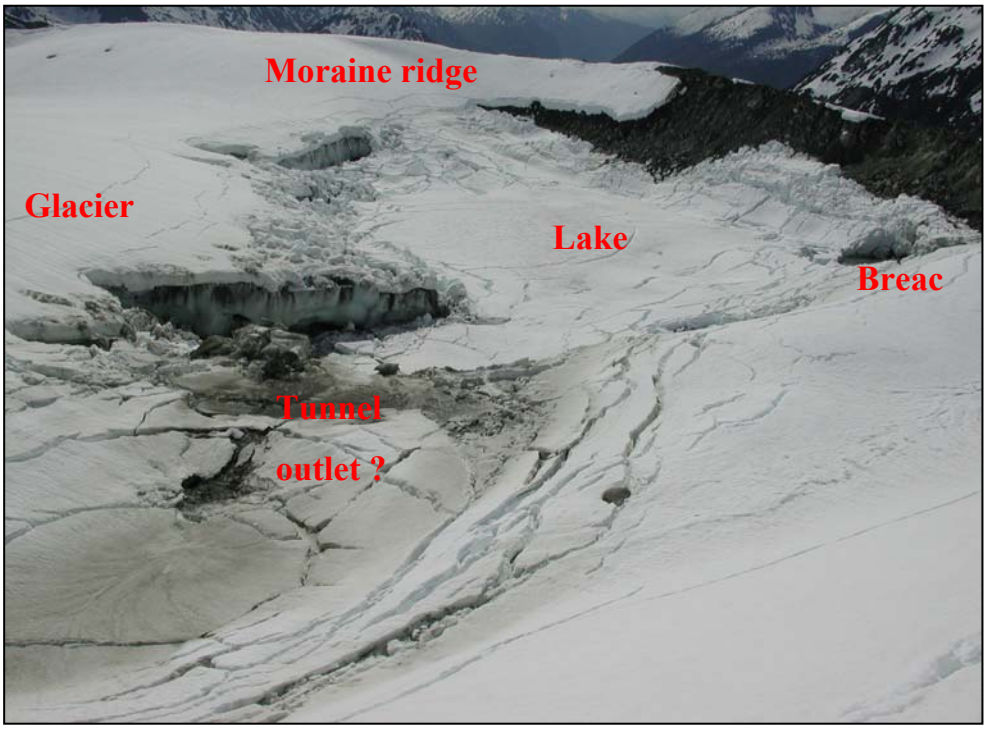

Figure 6.6 Outlet of glacial tunnel is seen as dark sinkholes and scars in the glacier. Photo: Elvehøy, 2004.

6.2.1 Temperature and melting

The weather was relatively warm during the days before the event, with a sharp temperature peak starting May 5, approaching the highest temperature May 7, the day before the moraine breach. This also coincides with a significant peak in discharge in the river Bøyaelvi, originating from the neighbouring glacier Bøyabreen (see Chapter 5.3.2). If the drainage route through Trollabyrgje was blocked, this melt-water from Supphellebreen had to be stored in the glacier or the lake.

It was not noticed by the local residents whether the discharge in Supphelleelvi was abnormal in the period prior to May 8. If the drainage path was blocked, the river would have been smaller than normal, but possibly not noticeable as far down the valley as where the farms are situated. Supphelleelvi also gets water input from smaller creeks draining

towards it (Figure 6.5). As this happened in early May, a high temperature would cause melting also in nearby snow covered areas, resulting in high river discharge. In that way the absence of drainage from the glacier may not be noticable. Ingebrigt Supphellen living at the innermost farm in Supphelledalen reports that in November 1947, when a similar but smaller event occurred, an unusual low level of Supphelleelvi river was observed. This could possibly be explained by the late date of the event. The drainage path could have been blocked off for the whole summer, but the lack of discharge was not noticed before the melting period from other areas was over.

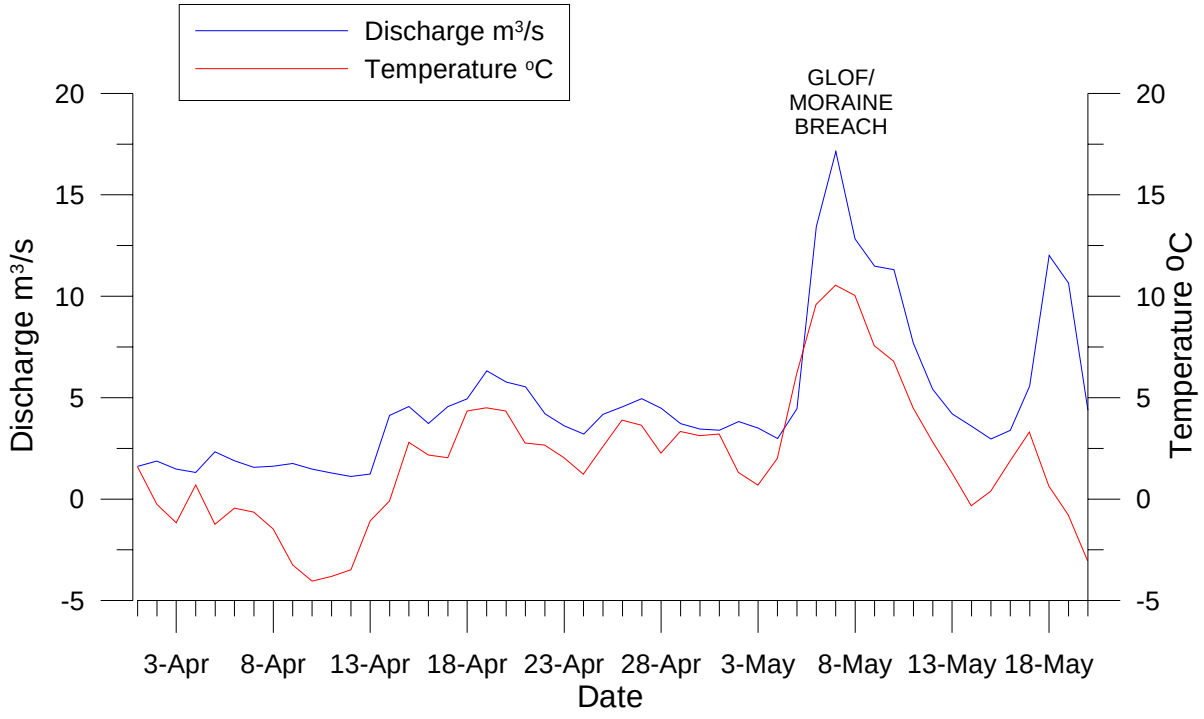

Figure 6.7 Correlation between temperature at Supphellebreen 1000 m.a.s.l. and discharge in Bøyaelvi.

The amount of water coming from the glacier is unknown. The warm weather, approaching 10º C at the weather station on the moraine ridge (1000 m.a.s.l.), has melted snow and ice on the glacier estimated to be 250 mm at 1200 m.a.s.l., 125 mm at 1400 m, and 50 mm at 1600 m (Elvehøy/NVE, 2005) during the few warm days before the event. To use this in an estimate of added volume of water, the drainage area of the glacier Supphellebreen must be known.

The terrain above 1200 m.a.s.l. is flat or bowl-like (Østrem, 1989). This makes a natural isolation or cut-off of the drainage, encouraging the theory of blockage of meltwater from a large area, possibly the whole part of the glacier situated above 1200 m.a.s.l. (approximately 10 km^2). According to calculations done by NVE, this makes the maximum water volume stored in the glacier to be 500 000 m^3 at the date of the flood. How much of this (if any) has been blocked off and released to the lake is unknown. The area could be varied with a factor of 10 or possibly more, from around 1 to 11.8 km^2, which is the total drainage area of Supphellebreen (NVE, 1988). Also precipitation may have contributed with additional water.

The theory of the channel-opening process and the movement of the glacier described in Chapter 5 could mean that the Fjærland flood started during the days or hours before the breach of the moraine dam, as a small channel started to fill the lake with melt-water, exponentially increasing the size of the tunnel and the volume of water draining through.

Blockage of tunnels could be due to the fact that spring came early this year, causing higher degree of melting earlier in the season, *before* the tunnels were sufficiently opened to transport the required amounts of water towards the ice fall. Another possibility is that the lake level was unusually high already before the melting process started.

6.3 Estimated water volume considering cross sections

In an attempt to estimate the maximum cross sectional area available for water flow, profiles of the eroded gully were studied. The laser scanning has been used when creating the cross sections. The systematic error due to the lack of control heights does not influence the result in this case as no comparison is made with the 2001-data (see Section 4.2). All cross sections can be found in Appendix B.

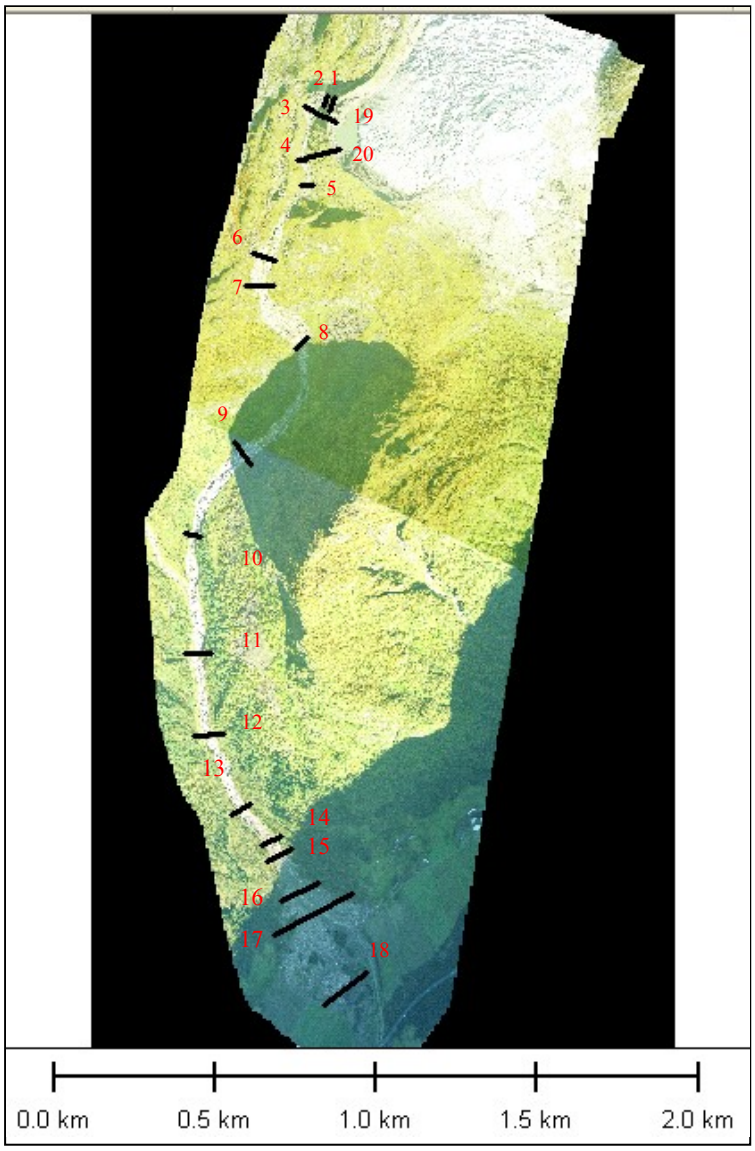

Figure 6.8

Cross sections 1-20 shown on aerial photos from 2004.

It must be remembered that only towards the very end of the event, the cross sections approached the depths suggested in the figures. As the path most probably was continuously eroded, the scenarios evaluated are artificial.

The investigation indicates that the water volume was not evenly distributed throughout the event. Both jøkulhlaup- and dam breach hydrographs commonly show a pronounced peak. The reader is directed to the work of Courivaud et al. (2004) for further information on dam breach hydrographs. Eyewitnesses in the valley Supphelledalen observed highest intensity in the beginning and also that the masses came in pulses. Water probably also flowed for some time before any significant amount of sediment was eroded. Therefore, the average velocities and the discharge obtained are probably not very representative for the event, but some estimates are presented below.

6.3.1 Scenarios

As the uncertainties are large, different scenarios have been assumed in the search for the most likely sediment/water ratio; the water volume ranging from 50 000 m^3 (only lake volume) to 550 000 m^3 (lake + max. additional water) and a sediment volume from around 100 000 m^3 to 450 000 m^3 (see Chapter 8).

The first cross section evaluated is the scar in the moraine. The area available is estimated to 394 m^2. As the lake level could not approach 1000 m.a.s.l. (level of moraine crest) due to the existence of a depression in the ridge (997 m.a.s.l.), the water could not fill the whole cross section. The lake level seemed to decrease 5 m during the event. The bottom of the scar is eroded down to 992 m. As the surface of a water table is horizontal, the cross section available is calculated to 90 m^2. This is tried illustrated in the sketch in Figure 6.9. The smallest cross section available is however the one that could limit the water volume.

A time of 45 minutes is chosen in the below calculations, based on judgement of witness statements.

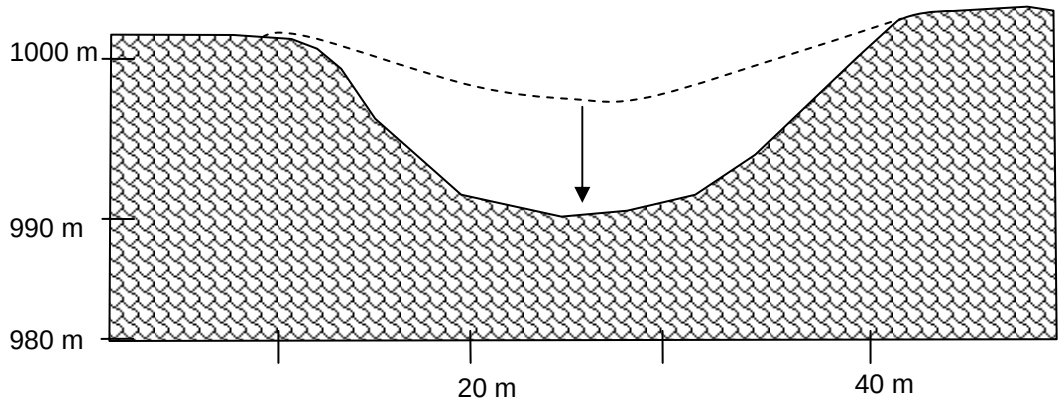

Figure 6.9 Illustration of scar, stapled line represents pre-flow terrain.

For the smallest water volume considered (50 000 m^3), if the water flow was continuous throughout 45 minutes, the average velocity of the water through the scar in the moraine (profile 1) can be calculated as follows:

$$\frac{water\ volume\left(m^3\right)/area\left(m^2\right)}{time\left(s\right)} = velocity\left(m/s\right) \qquad (6.1)$$

$$\frac{50000m^3/91.5m^2}{2700s} = 0.2\ m/s = 0.72\ km/h$$

The 50 000 m^3 does not include the solid masses from the moraine scar material itself. This could illustrate the case if the masses slid out fast, leaving only water flowing through.

$$\frac{volume\left(m^3\right)}{time\left(s\right)} = \frac{50000m^3}{2700s} = 18.5m^3/s \qquad (6.2)$$

A volume of 50 000 m^3 over 45 minutes gives an average discharge of 18.5 m^3/s. Distributed over 2 hours however, this volume produces an average discharge of 7 m^3/s.

The largest water volume considered is 500 000 m^3, which would give 200 m^3/s discharge throughout 45 minutes and 70 m^3/s throughout 2 hours. The water flow did most likely last for a longer time than the debris flow and peak discharge, as reported by locals and photographers. This also means that the peak discharge most probably has been larger than suggested above.

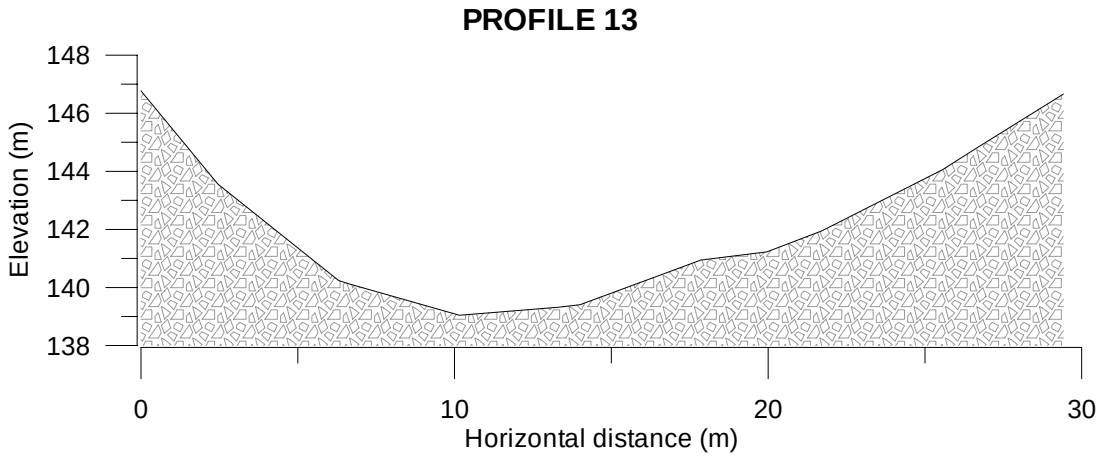

Figure 6.10 Cross section 13.

The measurements show that some of the largest cross sectional areas, far down the track, are around 140 m^2. Since these are cross sections near the fan, also almost all the volume of eroded material should be added to the flow. The largest volume expected to flow through this cross section is therefore 500 000 m^3 of water + 450 000 m^3 soil (see Chapter 6) making up 950 000 m^3 wet debris. Making the same assumptions as in the previous example, the average discharge through this maximal cross section is calculated to 350 m^3/s throughout 45 minutes.

Different volume scenarios and velocities are shown in Appendix C and the 20 profiles can be found in Appendix B. The sediment estimates are presented in Chapter 8.

These considerations show that there is space enough for all scenarios (from 50 000 to 500 000) to occur if the channel bed had been eroded *before* the masses started to flow – which did not happen. This means that there was probably much less space than assumed above, if not the erosion was in proportion to the masses flowing, so that it all the time would be room enough for the masses. The low velocities obtained, compared to witness observations of 50 km/h, are average velocities calculated assuming that the bed was maximally eroded before the event. The actual velocities were most probably higher.

The volume of 950 000 m^3 is much more than expected volume, the chapter on sediment volume discusses this and limits the range of volumes. The water volume is difficult to determine, but when also considering the geometry of the scar, the degree of erosion and the expected density of the debris flow, it will be shown that the most probable water volume involved is set to 100 000 m^3 (Chapters 7 and 8).

7. The moraine ridge breach

Floods due to failure of moraine ridges may evolve into debris flows relatively fast because of entrainment of material downstream. These debris flows often run for tens of kilometres due to the large water volume. Himalaya is probably the area most prone to this type of events. United Nations Environment Programme (UNEP, 2002) has recently reported that 24 glacial lakes in Bhutan and 20 in Nepal are potential sources of GLOFs and resulting far-reaching debris flows. But also man-made dams may fail, making the problem of a large water volume release and subsequent erosion an important problem in all kinds of environment.

Moraine ridges are commonly steep (up to 40º) and high, and comparable to constructed dams. Most natural moraine ridges have been stable for hundreds and thousands of years, but the probability of failure may grow as a result of climate change. This is due to ice avalanches into the dam, high overflow during storms and melting of ice cores (Clague and Evans, 2000).

Generally, there are different mechanisms that can cause a ridge failure (Clague and Evans, 2000):

- Overtopping due to ice or rock avalanche into lake, earthquake or extreme meteorological conditions, causing severe erosion of moraine unless it is armoured by coarse material. The cohesion of moraine sediments is often low.
- Internal erosion (piping) gradually weakens the dam. The actual sediment in the dam determines the internal erosion factor. These vary between 3 and 10, and a value above 5 indicates susceptibility for piping
- Melting of ice core or interstitial ice
- Earthquake causing collapse of dam

7.1 Ridge failure

The failure of the moraine ridge damming the glacial lake is the cause of the debris flow in Fjærland. The reason for the dam breach is however not so clear.

As suggested in Chapter 5 on glaciohydrology, early melting may be the background of the flood. A gradual rise in the water table of the moraine dammed lake may have overtopped the moraine and led to erosion, or internal piping may have become enhanced. Another possibility is that the ridge for some reason simply could not stand the pressure of the water due to high water level combined with weakening of the moraine.

7.1.1 Failure mechanisms

The failure of the ridge may have started out as a small lowering of the ridge, rapidly growing with time. This is seen in a series of large scale dam failure experiments done by Høeg, Løvoll and Vaskinn (2004). An *overtopping* of a man-made embankment dam of rockfill with a moraine core resulted in a total dam failure, the breach developing in 2 hours. They conclude that overtopping first leads to slow dam toe erosion, but as soon as the scour reaches the upstream crest of the dam, the damage of the dam is rapid.

Internal erosion may also fail a dam. The top flow line through an earthen dam may, due to a developed leak, emerge at the downstream surface, and gradually erode the face in a channel-like structure. This process is called piping and was tested by Høeg et al. (2004). They found that it took a long time to develop a total failure by piping. First when the tunnel widening reached the crest of the dam, breaching took place.

In the headcut process as described by Høeg et al. (2004) erosion grows upwards towards the crest, eventually causing failure. As erosion is largest in the lowest parts of the dam, undercutting leads to faster opening of the breach. Headcutting is most common in cohesive materials (Courivaud, Lempérière and Fry, 2004), due to the capillary forces and the characteristic steep slopes of such materials. A noncohesive material would most probably slide out, and a headcutting process would not occur. Erosion starting at the crest working its way to the ground foundation is a common failure mechanism due to overtopping in noncohesive materials (Courivaud, Lempérière and Fry (2004)).

For dam failures removal of lateral and/or underlying support are also important in creating increased shear stress. This results in periodical failures of the side slopes, for instance in a failure scar that is developing. At the time of side slope failure, tests have shown significant drop in soil-moisture tension, and therefore loss of shear strength.

7.1.2 The breaching process

Two separate stages may be recognised in a failure process (CD, 2004; Courivaud et al., 2004, Høeg et al., 2004)). The process starts out with a deepening of the breach until ground, or equivalent, is reached, shaping the scar more or less into a V-form. The following widening stage laterally enlarges the scar to a trapezoidal form with almost vertical sides (Figure 7.1). Rockfill dams, clayfill, gravel and moraine dams all produced almost vertical scar sides in the tests by Høeg et al. (2004).

Franca, Braunschweig and Almeida (2004) have experienced that the initial width of the scar is the same as the dam height, the final average width around 1.7 times this, and the final breach depth 80 % of the dam height. In Fjærland the height from the crest to the ground in this section of the dam is around 25 m. According to the theory of Franca et al., the final breach width should be 1.7 times 25 m, which means 42.5 m. The breach width in Fjærland is around 35 m, which could indicate that the process stopped (Figure 7.1).

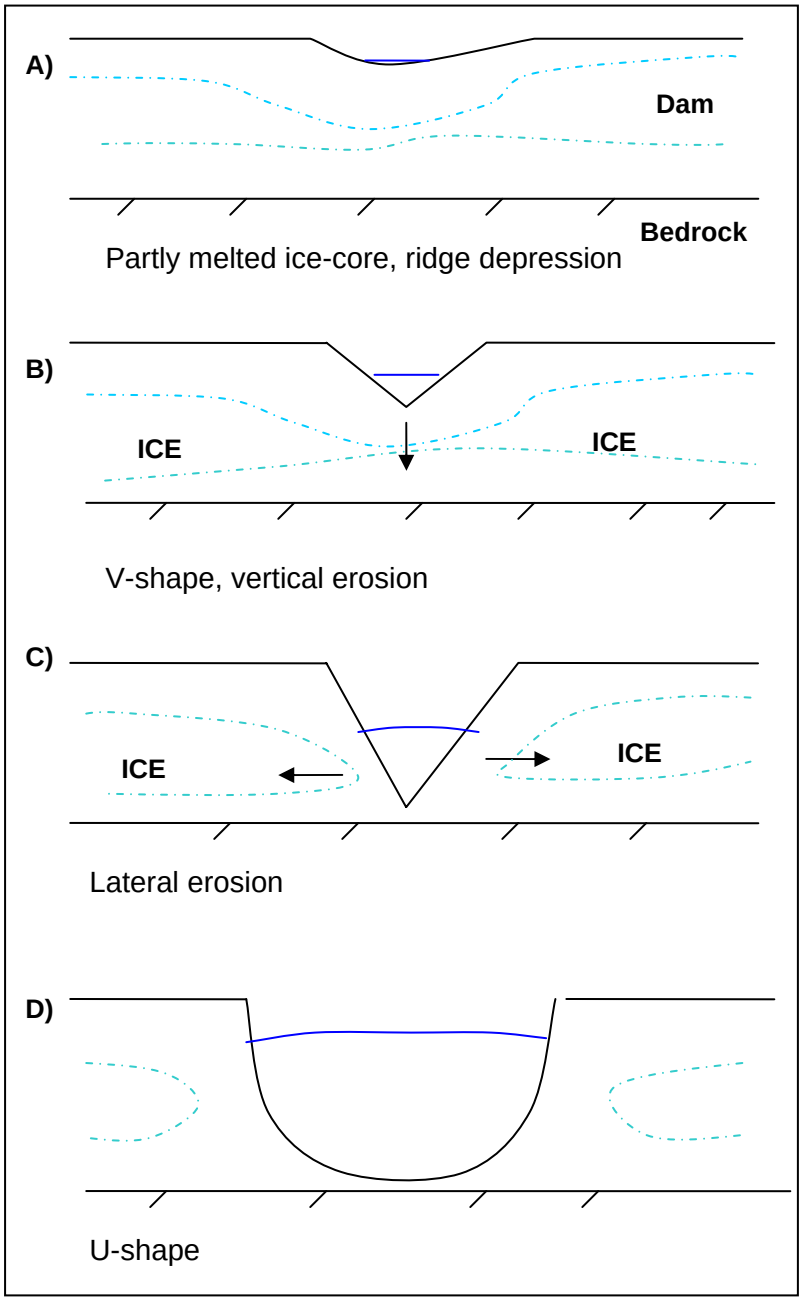

Figure 7.1

Illustration of stages of a breaching process.

Breach deepening and widening mainly depends on (Courivaud, Lempérière and Fry, 2004):

- The reduction rate of the reservoir level during the breaching process. If the water level decreases rapidly, the deepening may stop before it reaches ground level. Also widening stops. If the water level is high for a long time due to high inflow rate, the widening may result in very large breaches (a breach of 800 m developed in the Machhu II dam failure).

- Soil properties: grain size, cohesion, compaction, permeability.

In a dam constructed by cohesive material, the widening of the breach will be slow. The progression (Courivaud, Lempérière, Fry, 2004) may be considerably faster and the breach may get wider, if the material is cohesionless and the reservoir level stays high for a long time.

It seems that the widening process in Fjærland has been stopped before the breach has reached a full trapezoidal form. Very similar breaches have been observed in enormous GLOFs from Himalaya (Figure 7.2). This could mean that moraine material dams may exhibit a larger resistance to breach widening than many other dam types, due to existence of cohesive clay material and/or ice.

Figure 7.2

Breach of moraine causing glacial lake outburst flood and debris flow in high altitude Nepal. Photo: Øystein Lund.

Pickert et al. (2004) state that breach widening strongly depends on the soil/water interactions in the soil matrix. Suction in partly saturated soil increases the strength of the soil, and may for example influence erodibility and stability of the slope. A material of high cohesion will be stable also in an almost vertical position due to capillarity. The stabilising force is based on soil-moisture tension and increases the effective stress and the apparent cohesion.

Suction changes with rainfall intensity, slope geometry, porosity, degree of saturation, strain rate and soil properties (Chen, Lee and Shen, 2000). A Coulomb failure criterion will look like this when suction is taken into account (Lambe, 1996):

$$\tau = (\sigma - p_a)\tan\varphi' + (p_a - p_w)\tan\varphi^b + c' \qquad (7.1)$$

where

p_a = pore air pressure

p_w = pore water pressure

φ^b = friction angle relative to matric suction

The increase in shear strength caused by an increase in matric suction is described by φ^b. The resulting increase in strength can be significant. φ^b normally varies between ½ φ' and φ' (Høeg, 2004). When the soil is saturated, we get the classical shear strength relationship as modified by Terzaghi in 1936. In Fjærland the water content of the dam is believed to be high due to a melting ice core and/or snow, and moraine material flows easily when exposed to too much water.

The fact that the breach scar still is quite small is also an indication that the water volume was in the lower end of the range (50 000 – 500 000 m^3) suggested.

7.2 Possible ice core in Fjærland

Whether the moraine ridge in Fjærland is ice-cored is important in the evaluation of the dam stability, and is not known at this time. A further investigation of the moraine is planned in June 2005, unfortunately after this thesis work has been terminated. Seismic reflection and refraction, Ground Penetrating Radar (GPR) and electrical resistivity methods will be used.

The melting of an ice core would strongly reduce the safety factor of the dam. Not only would the porosity grow larger, but the material would get wet and unstable. The moraine at Supphellebreen is situated at 1000 m.a.s.l., and this is well below the normal permafrost limit (1450 m.a.s.l.) in mountain ranges like Jotunheimen in Norway (Meteorological Institute, 2003). Sporadic permafrost can however be found 300-400 m below this limit, and according to Norwegian Meteorological Institute very little research has been done in the western part of Norway on permafrost limits.

As the moraine is in contact with the glacier all year round, as well as with the icy water in the lake, there is a good chance the moraine is ice cored. The topography makes the moraine

exposed to cold winds, and for a thick moraine ridge like this, it would also take a considerable amount of energy to fully melt an ice core during a short summer.

Internal erosion (piping) may continuously have weakened the moraine in Fjærland if an ice core has started to melt. This would also enhance the melting process. If the moraine is or has been partly ice cored, an incipient melting process will start internal erosion. The water flow will cause ever more ice to melt, which again will force erosion growth. The lower part of the crest could possibly be a result of such melting, internal erosion causing settlement. In experiments, and in the field, sinkholes have been observed due to piping. The sinkholes usually occur on the upstream side of the crest and leads to overtopping (Figure 7.3).

The most probable cause of the local lowering of the crest in Fjærland seems to be erosion due to previous overtopping. Piping may be the direct cause of the failure, but may also weaken the material so that erosion due to overtopping gets more efficient. The area downstream the moraine is wet all year round, indicating such piping.

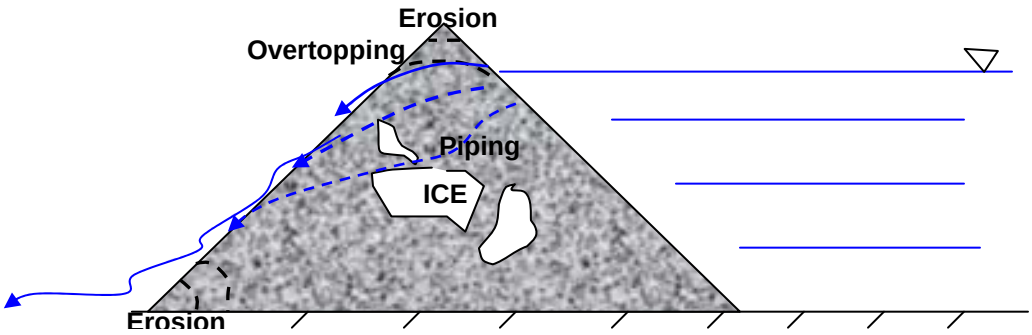

Figure 7.3 Illustration of different mechanisms possible in a dam with partly melted ice core. Both overtopping and piping may lead to breaching.

8. Estimated sediment volume involved in the flow

Ice ages usually remove evidence and sediments of earlier times, therefore the main part of Norwegian soils and moraines were formed during the last glaciation (Weichsel, 118 000-9000 years ago) or in the following warmer Holocene (Jørgensen, Sørensen and Haldorsen, 1997). As the soil in Fjærland, like in most parts of Norway, is produced by glaciers, glaciology has a key role also in the study of the sediments involved in the debris flow. The material incorporated in the debris flow is mainly glacial sediment: in addition to the moraine ridge studied, the valley scoured by the torrent is covered by this sediment type. Some of the material in the lower parts of the valley is however resedimented slide material as discussed in Section 2.2.3. The first section of this chapter treats the characteristics of till.

8.1 Characteristics of the till

Repeated cycles of moving ice, melting, freezing and incorporation of material result in a till deposit. Normally, the formations (for example a ridge) is called moraine, whilst the soil material is called till.

The till cover (Haldorsen, 1983) is thin and discontinuous over large areas of Norway, especially in the western part, due to glacial net erosion in the steep terrain. This part of Norway is also mainly covered by erosion resistant bedrock types like Precambrian rocks (>650 mill. years).

Average till cover in Norway does seldom exceed 5 m. Most of the moraine sediment has been transported relatively short distances (Jørgensen et al., 1997; Haldorsen, 1983), often less than 5 km. Leeside valleys often has thicker till, in for example Gudbrandsdalen up to 50 m in thickness. Commonly, tills in mountainous areas are composed by local material, whilst the cover in valley bottoms is more far-travelled (Haldorsen, 1983).

Till is characterised by poor sorting (Jørgensen et al., 1997, Hambrey, 1994), and is composed of fragments of all sizes; from clay to boulders due to the different formation processes like abrasion, melt-freeze and plucking. The various particles can have completely different rock type origin and can be sharp as well as rounded. Tills in Norway are normally

coarse grained tills where clay constitutes less than 10 % of the fine material (< 16 mm) and gravel between 2 and 16 mm makes up 20-40 %. The boulder fraction is between 30 and 70 % of the total till (Haldorsen, 1983). Grain size distribution data from 3000 Norwegian moraines show high content of gravel, sand and silt relative to clay (see Figure 8.1) (Jørgensen et al. (1997). The Fjærland till seems to include very large amounts of boulders, making a grain size analysis difficult to perform.

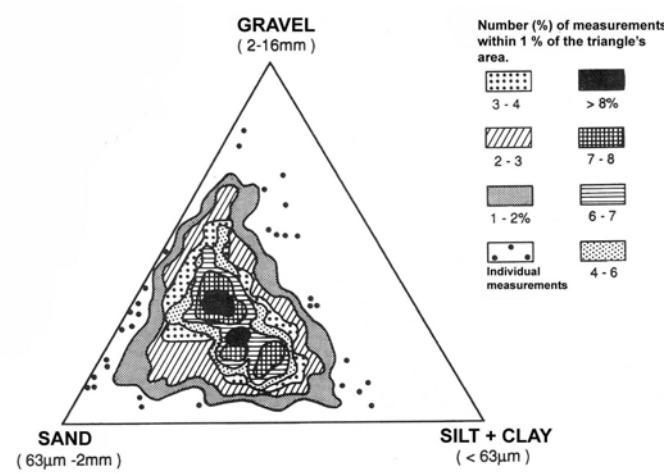

Figure 8.1

Grain size distribution of 3000 Norwegian tills. The left maximum in the figure corresponds to tills generated from coarse sedimentary bedrock, whilst the right maximum displays tills generated from finer rocks like clayey slates. Boulders are not included in the figure. Modified from Jørgensen et al., 1997.

The till composition depends on:

1) Transport:
    - sediment transported at the base is crushed into fine, round material.
    - sediment transported on top or within remains coarse and sharp.
2) Sediment origin:
    - rock type, characterised by shear strength, hardness and degree of fracturing (Jørgensen et al., 1997). A gabbro is difficult to pluck for the glacier, whilst granite and sandstone produces huge amounts of blocks and coarse material. A clayey slate gives clayey till. In general, coarse sedimentary rocks, sandstones and gneisses give rise to sandy tills (clay content is genereally less than 5 %), whilst Cambro-Silurian rocks are crushed to a sediment of more than 10 % clay (Jørgensen, 1997)

- steep terrain and fractured bedrock (common in Western Norway) produces coarse material (Haldorsen, 1983)
- lowland fields produce fine grained sediment (Haldorsen, 1983)
- leeside till is coarser than pushside till

Moraines are seldom homogenous (Jørgensen, 1997). Although the overall pattern is unsorted material, sorted lenses often occur. The amount of sorted material reflects the degree of water present in the sedimentation period.

8.2 The till of Fjærland

The Precambrian rocks of Norway are generally composed of gneisses, granites, deformed sedimentary rocks and volcanic rocks (Aschehoug og Gyldendals Store Norske, 2004). The Fjærland deposit is therefore suggested to contain a large fraction of sand due to these rock types, a considerable amount of boulders due to the steep terrain, and little clay. Depending on whether the material is far-travelled and the direction of ice motion, clay originating from a belt of Cambro-silurian rocks (545-417 mill. years) south-west of Fjærland (Aschehoug og Gyldendals Store Norske, 2004) may be found in the deposit. The material at low elevations is considered more far travelled than the material at higher elevations. The discussion in Chapter 7 however indicates that a certain amount of clay exists.

The material in Tverrdalen and lower lying Supphelledalen is believed to be basal till and composed of material deposited under the ice due to pressure-melting and basal shear (Nesje, 1995, Jørgensen, 1997). This type of sediment (Haldorsen, 1983) is typically compact, fine-grained and has a smooth surface. The thickness of the deposit in Fjærland varies with steepness of terrain and altitude.

As discussed, some of the material involved in the 2004-flow are old slide deposits. The area is also prone to snow avalanches and rock falls supplying the valley with sediments.

8.2.1 Supphellebreen moraine

An advancing glacier pushes material in front of it, resulting in a terminal moraine ridge. Such a moraine ridge displays the maximum extent of the glacier. Even a glacier that is

retreating may push up small ridges in the winter season. These proglacial tills usually consist of coarse material if they are situated above the marine limit (Haldorsen, 1983).

The moraine ridge at Supphellebreen is a perfectly shaped end moraine. It is approximately 650 m long, shaped like an arch and is around 25-50 m high. The slope is up to 33º on the downstream side, and 34.5º on the upstream side.

The material of an end moraine is usually coarse and field investigations and photos from Fjærland support this view. Large boulders are visible, especially on the upstream side since this side lacks vegetation. Fine material is found between the blocks.

Some water is usually overflowing the lowest ridge point (Figure 2.7) in the melting season, making up a small stream. There are also indications that more dramatic floods have occurred here from time to time (see Chapter 3). The reason that the failure became more severe in May 2004 may be due to the larger amount of water, advanced internal erosion, or a partly melted ice core.

8.3 Sediment volume estimate

The sediment volume incorporated in the debris flow of Fjærland was estimated using Golden Software's Surfer, generating grids of the developed terrain models (see Chapter 2) and subtracting the pre-flow from the post-flow grids (Figure 8.2). To minimise the error only the area affected by the torrent plus some meters on each side, were taken into account. The area outside the track should display zero change. This is however not the case throughout the whole path, due to inaccuracy of the models and change in vegetation from 2001 to 2004.

For control, the track was divided into 7 sections (Figure 8.3). The smaller the area studied, and the more homogeneous each area is, the easier it is to figure out the result. For close-up of all parts and details on calculated sediment change resulting from the aerial photos, laser and economical map, see Appendix D.

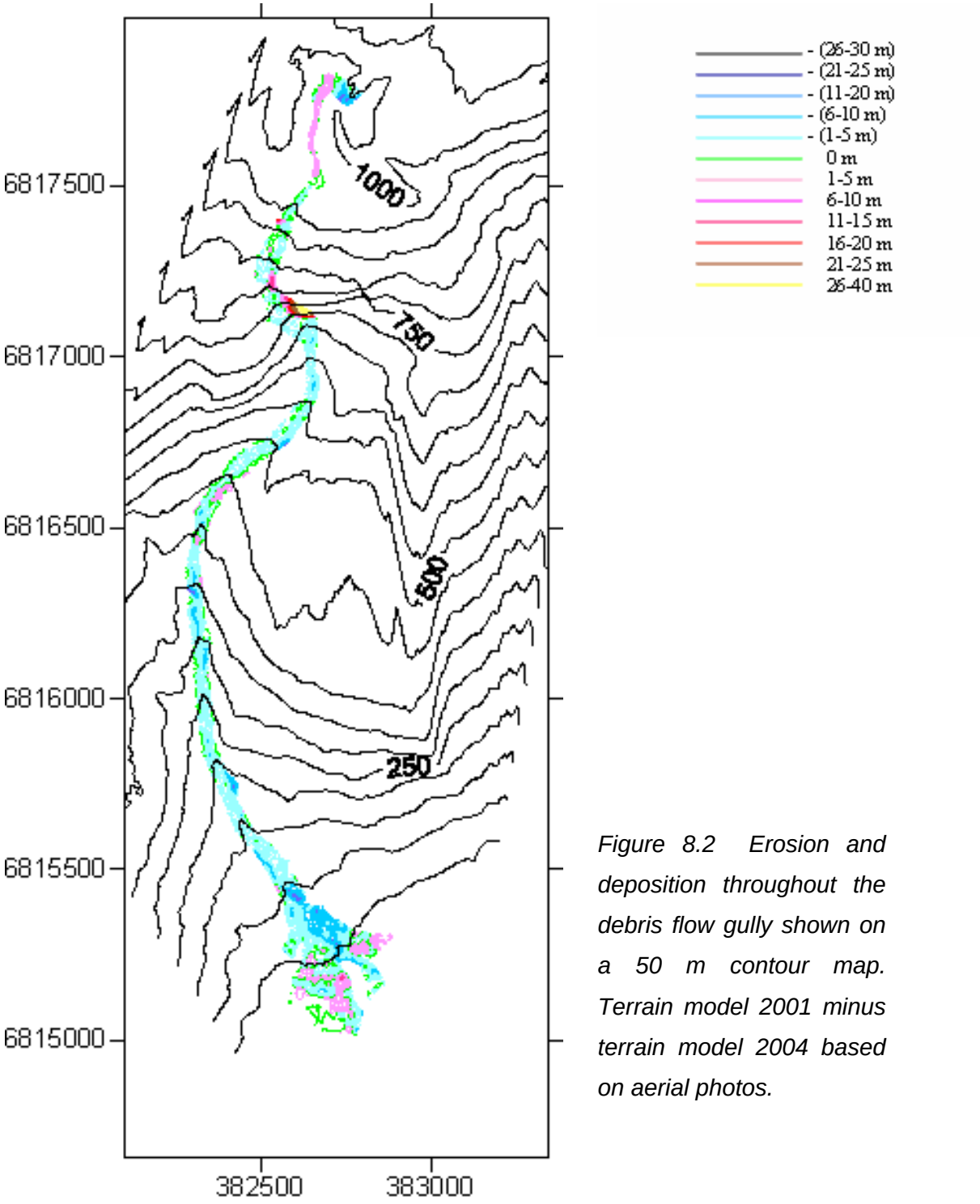

Figure 8.2 Erosion and deposition throughout the debris flow gully shown on a 50 m contour map. Terrain model 2001 minus terrain model 2004 based on aerial photos.

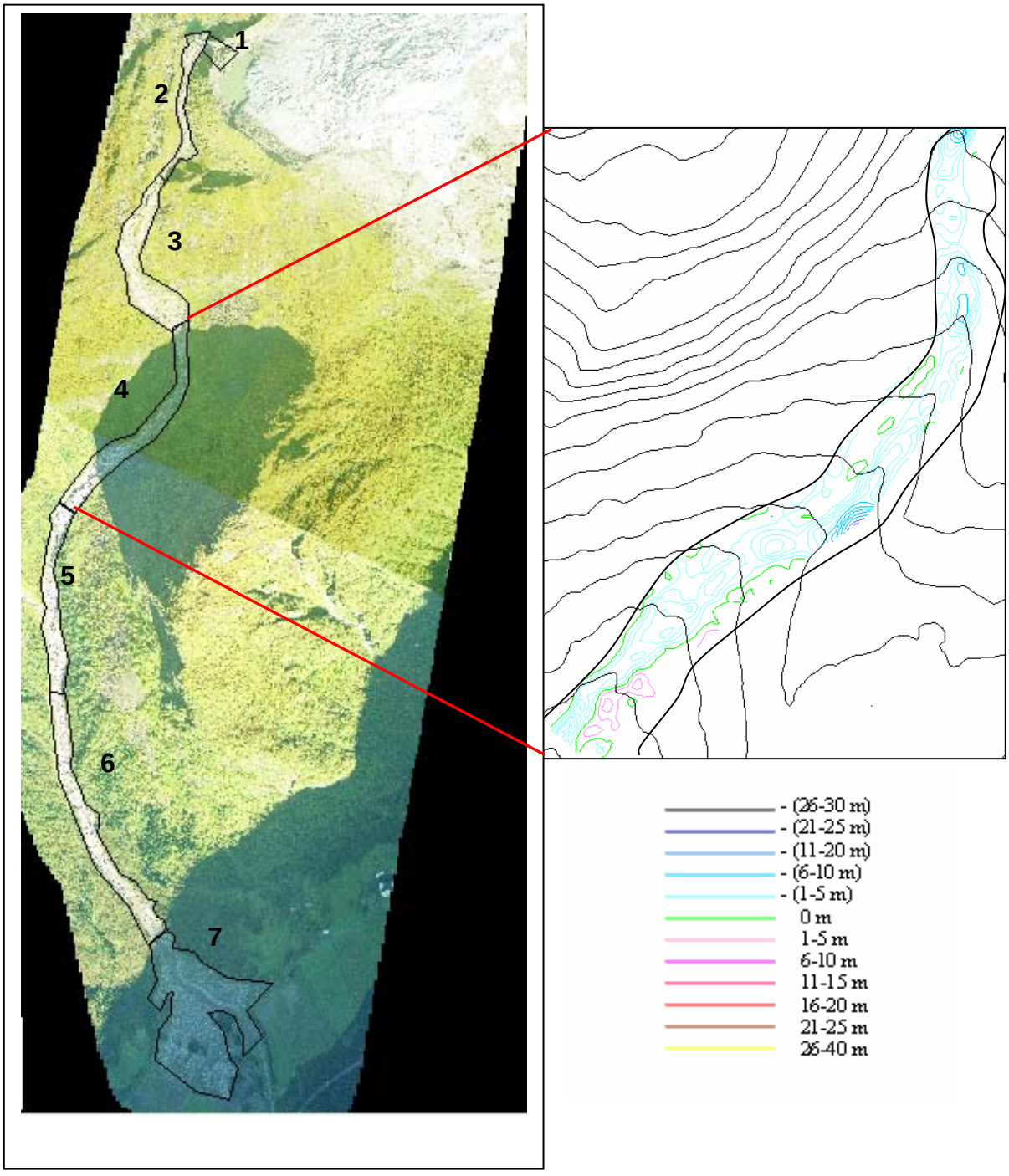

Figure 8.3 The division of the debris flow track into 7 sections. Right: example of contours, section 4, showing net sedimentation and net erosion. Sedimentation in lower left corner is due to boulders settled or moved a few meters.

Table 8.1 Overview of calculated volumes using different terrain models. Section number can be found in Figure 8.3. Numbers in bold are used in later considerations. Numbers in italics represent erroneous numbers.

Section		Aerial photos 2004-2001	Laser scanning Laser 2004-air photo 2001	Ec. map 1:5000 Air photo 2001 - ec.map
	Area (m^2)	Volume (m^3)	Volume (m^3)	Volume (m^3)
1 Moraine scar	4 345	**-23 041**	-25 778	
2 Flat area	11 473	**8 526**	-11 334	
3 (Precipice)	29 308	*(22 926)*	*(-62 446)*	-
4 Beneath precipice	29 043	**-48 067**	-118 875	
5 Tunga	21 879	**-70 157**	-130 092	
6 Tverrdalen	33 018	**-103 714**	-176 948	
7 (Fan)	75 094	*(-156 284)*	*(-309 975)*	**105 532**
Total	204 160	*(-369 811)*	*(-835 448)*	
Total (-3 and 7)	129 066	**-236 453**	-463 027	

The areas used in the calculations are somewhat larger than the actual size of the track; this is seen in the item for total area in the table above (129 066 m^2), which is larger than the measured area of the track (99 900 m^2) for the reasons noted above.

8.3.1 Accuracy of the estimate

The terrain modelling method is expected to give a volume accuracy of around +/-10 % in this case. On the other hand, the lacking control points for the laser data results in terrain models that are not suitable for multi-temporal comparison (see Section 4.3). For the photogrammetry-based estimates, considerations about the difficulty of representing steep terrain must be taken into account. This is especially true for the lower parts of the track, where the terrain is very steep on one of the sides. This area is also the section with the most severe erosion. Almost vertical gully sides are observed in lower parts of the track. A potentially large volume may here be lost (both using photogrammetry and laser) as shown in Figure 8.4. Where negative values dominate also the flanks of the track, it is suggested that erosion estimate may be too large (see Appendix D).

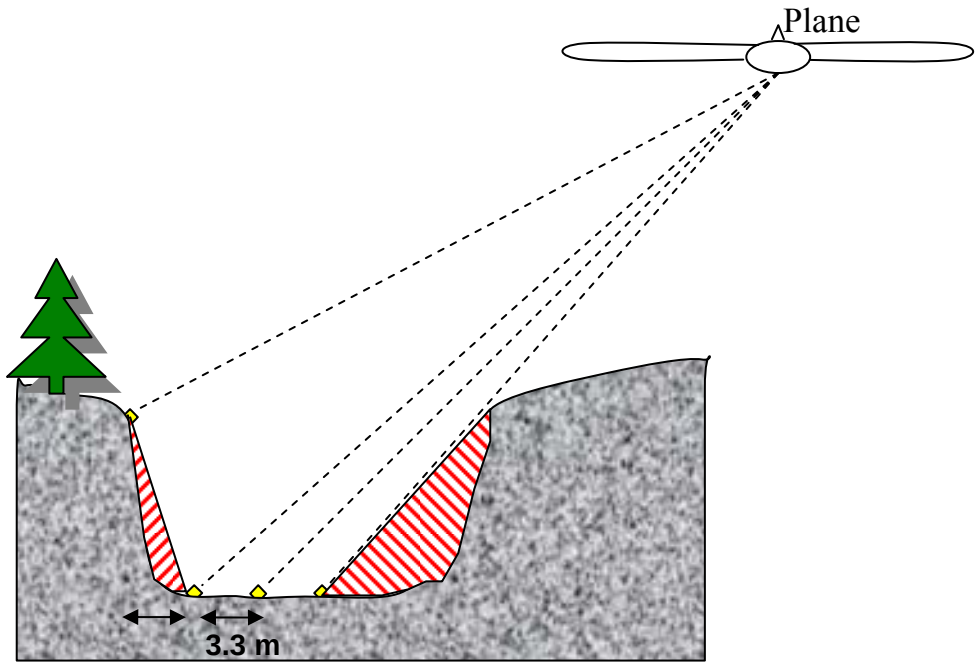

Figure 8.4 A potentially large area (volume) may be lost in steep terrain. Example of losses in a gully of vertical sides are here shown in red.

The eroded volume should roughly correspond to the volume of the depositional fan. In addition, a part of the eroded material travelled further and was deposited on the flat farmland, whilst some of the finest material was transported to sea and thereby lost.

The disturbed and remoulded sediment will not have the same properties and the same densities as the undisturbed soil. Therefore the volume of the deposit may not correspond to the volume eroded, and the generation of a volume budget is therefore difficult. The packing is most likely less dense in the debris flow deposit than it was originally. As the volume estimate of the fan is not accurate, I base my discussion on the eroded volume.

8.3.2 Areas not included in the estimate

In the following I will use the volumes estimated through terrain modelling without taking into account the following areas (and Table 8.1):

- the cliff from 900 to 600 m.a.s.l. (Section 3)
- the fan area (Section 7)

Both sections include errors. The cliff section displays thick deposition (see Table 8.1), while field investigations and air photos however show erosion of the soil layer and vegetation leaving the bedrock bare. I consider the exclusion not to affect the result in an unacceptable way, as there was very little loose sediment in the area.

Due to the fact that the fan area was almost completely covered by trees when the aerial photos were taken in 2001 (see Figure 8.5), the estimation relying on these photos does not represent the correct ground elevation change. Due to this forest, the 2001-terrain therefore seems to lie higher than the 2004-terrain, displaying severe erosion also in the depositional area (see Table 8.1). Since the erosion process is considered finished as the mass flow enters the fan area, not to include the fan gives a better approximation of the totally eroded volume.

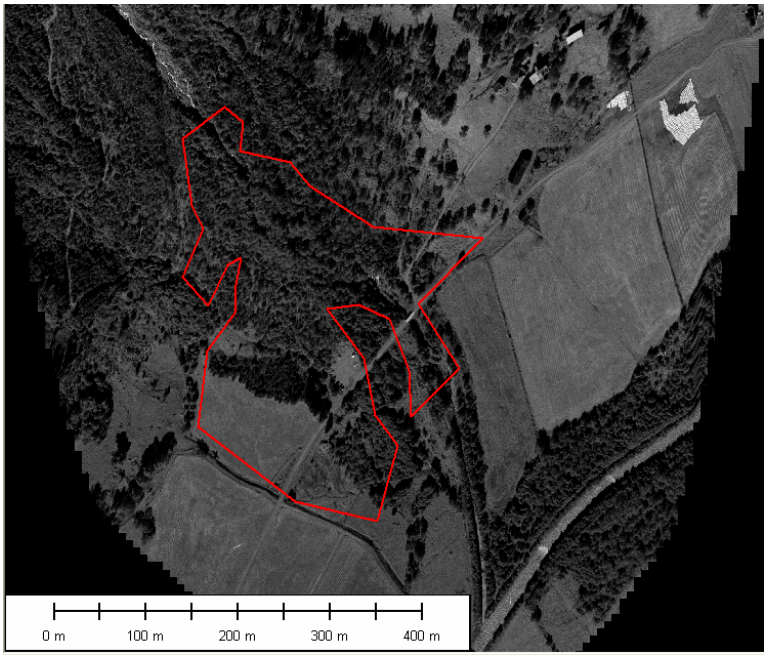

Figure 8.5 Part of aerial photo displaying the fan area in 2001. Red line indicates the limits of the 2004-fan. The dense forest in the 2001-photo has caused problems in calculating the fan volume. Air photo: Fotonor.

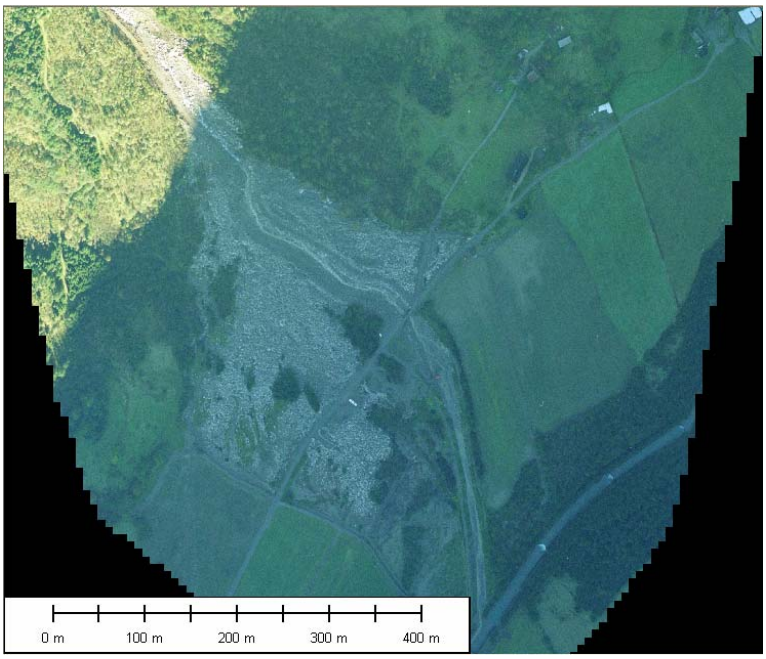

Figure 8.6 Part of aerial photo showing the fan in September 2004. Mud inundating the fields is removed. Air photo: Blom Geomatics.

8.3.3 Photogrammetry vs. laser

As previously described, two methods of generating a pre-flow terrain model have been used. The lack of measured control areas in the laser scanning made this method generate a lower terrain than expected. This resulted in a large erosion volume estimate (-460 000 m^3), as the extra meter(s) of erosion accumulates through the 3 km long track. When examining the contours and profiles from 2001, 2004 and the laser scanning (Figure 8.7 and Figure 8.8), there seems to be a systematic error in the laser estimate, largest at low elevations, lowest at high elevations (see Section 4.2). The error is not necessarily constant over the whole model, and this makes it difficult to compensate for. Profile 12 shows that the photogrammetry gave a 2004-terrain that matches well with the 2001-terrain, as the surfaces approach each other on the sides where no erosion has occurred, whilst the laser scanning displays lower elevations. For further details about the laser scanning or the photogrammetry, see Chapter 2.

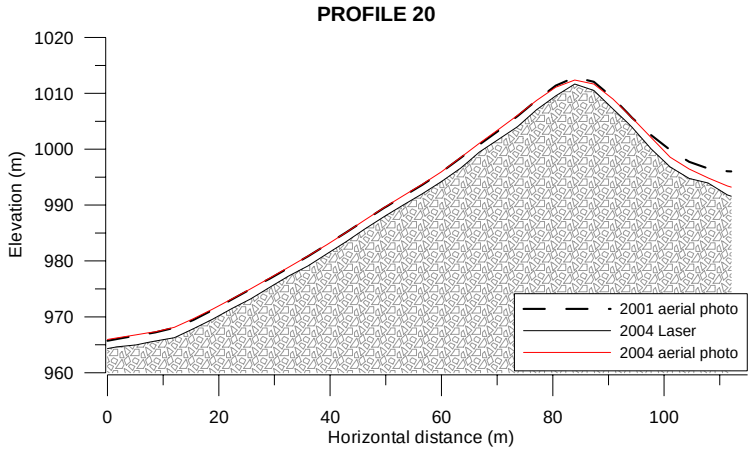

Figure 8.7

Intact moraine ridge at 1000 m.a.s.l.. The offset between the laser and the aerial photo is lowest at high altitudes.

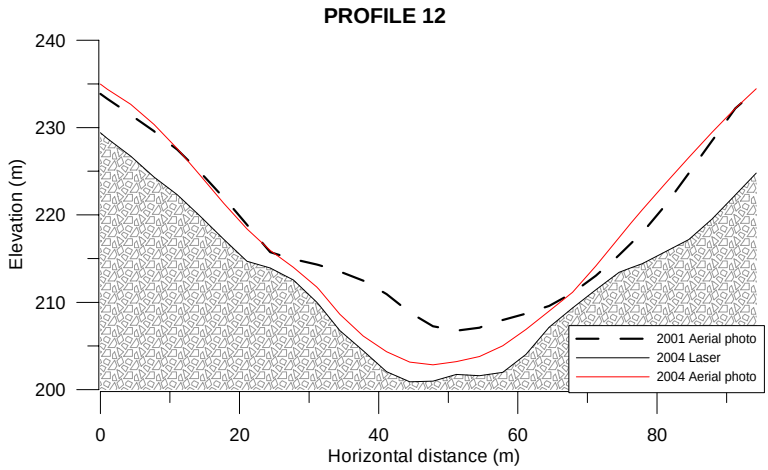

Figure 8.8

The offset is larger at 200 m.a.s.l. The laser terrain line should meet the stapled line on the sides of the gully where no erosion has occurred. The red line satisfies this condition.

Preliminary conclusion

Based on the foregoing discussion, for volume estimations the laser scanning is not applicable. Using the aerial photos alone resulted in a total eroded volume of $\approx 240\ 000\ m^3$.

8.4 Estimated sediment volume considering profiles and field observations

8.4.1 Erosion depth

For a check of the volume estimate from Surfer, the erosion depth observed during field work is considered. The area of the visibly eroded debris flow track, from the moraine scar at 1000 m.a.s.l. to the upper end of the fan (at 90 m.a.s.l.) is measured to 99 900 ≈ 100 000 m^2 in the orthophoto, using Global Mapper. The length of the track is 2 770 ≈ 2 800 m, and the average width of the track can be calculated to 36 m. Area and length estimations are of high quality (horizontal accuracy is very good). To check the estimates, manual measurements of the erosion depth should be done at intervals throughout the track.

When knowing the area of the track, an average erosion may be computed. Average erosion throughout the track of 1 m would result in an eroded volume of 100 000 m^3, whilst 4 m erosion gives 400 000 m^3. The Surfer estimate of ≈ 240 000 m^3 corresponds to an average vertical erosion of 2.4 m over the 100 000 m^2. The upper parts (down to approximately 600 m.a.s.l.) did not experience much erosion, partly due to snow cover, partly due to low sediment concentration in the water, lower velocity and partly because there was little loose material to scour. The area below the precipice is measured to ≈ 62 200 m^2. The volume estimate of 240 000 m^3 distributed only over this area would then give almost 4 m of average erosion. In addition some material originated from the cliff and the area above, meaning that average erosion is somewhere between 4 and 2.4 m. Considering the field estimates of erosion, an average gully deepening of a bit less than 3-4 m seems correct.

All 20 profiles showing erosion may be found in Appendix B. These are derived through the terrain modelling methods also used for the volume estimation (aerial photos and laser scanning), and are thus not suitable for cross validation of the erosion depth and volume estimate. The profiles show eroded cross sections of up to 130 m^2. If all cross sections from beneath the cliff were around 100 m^2, the eroded volume would constitute 280 000 m^3.

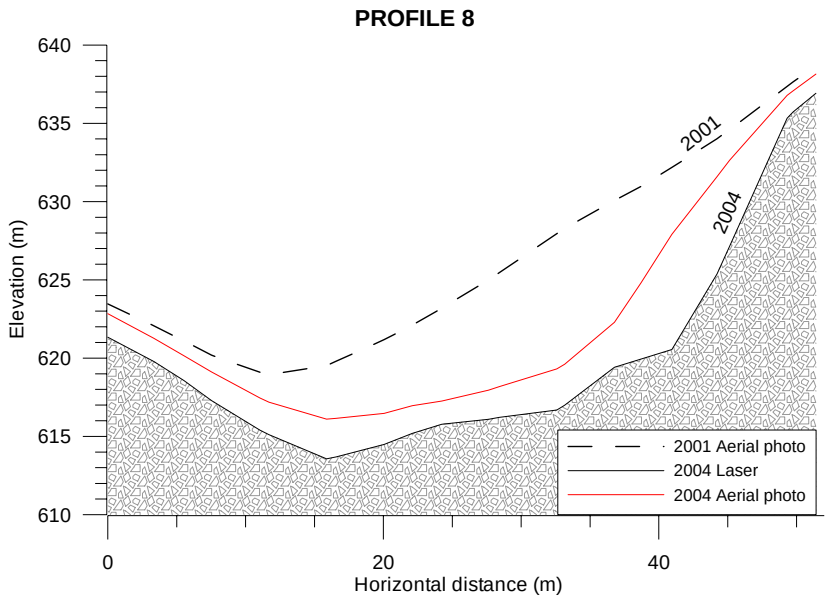

Figure 8.9

Profile 8.

8.4.2 Deposit depth

The deposited masses should roughly match the eroded masses, although it must be considered that some sediment is lost. An estimation of the deposited volume could throw light upon the discussion on eroded volume, assuming the relationship between in-situ and remoulded densities are known. In this case they are not, therefore a comparison between eroded and deposited volume does not provide reliable help in the estimate of involved volume.

Fan deposit

As an economical map 1:5000 exists for the valley Supphelledalen, this was used instead of the model generated from the 2001 aerial photos in an attempt to calculate the volume of the fan. When using the map and the 2004 model, a positive volume, indicating deposition, was found in the fan area. The total deposited volume in the fan was estimated to ≈ 105 000 m^3 using this method.

The fan area is measured to cover ≈ 75 000 m^2 using Global Mapper. The estimate found (105 000 m^3) by subtracting the terrain model based on the economical map 1:5000 from the 2004-model corresponds to an average deposit thickness of 1.4 m, which seems small. One of the local farmers, Eirik Øygard, has been reworking parts of the fan area. He suggests a

fan thickness of approximately 5 to 6 m. This is in the central area of the fan. Towards the flanks, the thickness clearly decreases.

The fan area has probably been covered by trees for a long time, therefore there may be errors in the economical map. Due to this, a few attempts to estimate the fan volume are shown in Table 8.2. The fan is divided into a central area and flank area according to the figure, and the thicknesses used are average thicknesses of each part.

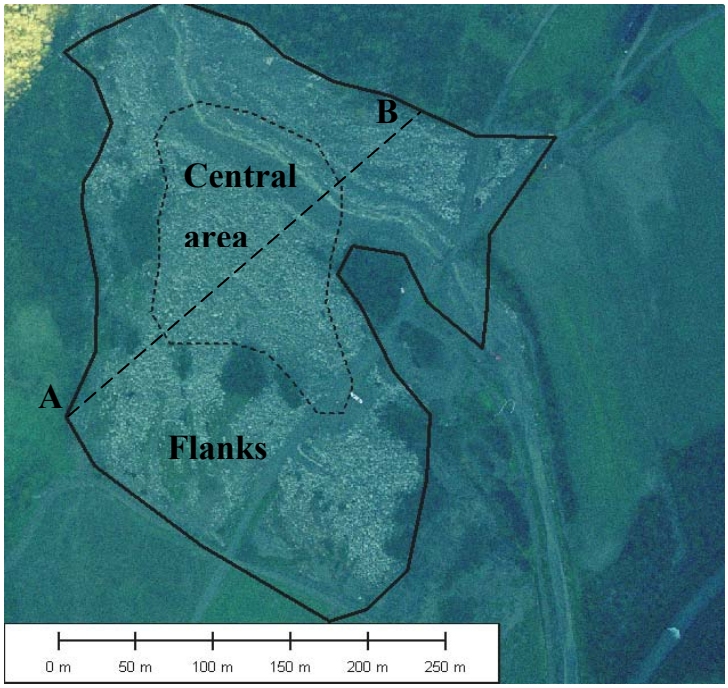

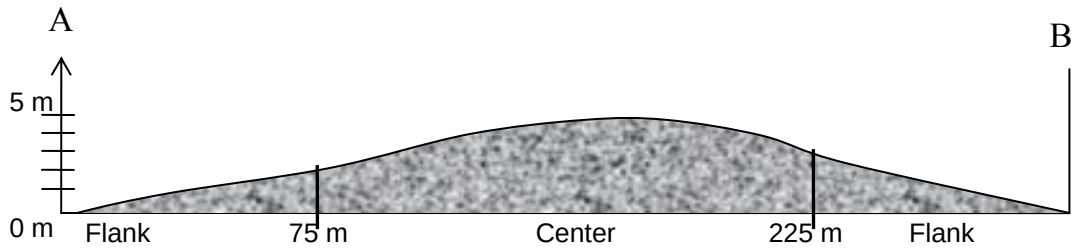

Figure 8.10 Illustrations of fan divisions and geometry. Length profile from A to B seen in aerial photo above. The river is not taken into account. Estimates of fan thickness are varied in Table 8.2 below. Note: when the air photo was taken some of the deposit had been removed.

Table 8.2 Fan volume estimates.

Fan volume estimates					
Scenario	**Central area (m^2)**	**Flank area (m^2)**	**Central thickness (m)**	**Flank thickness (m)**	**Total volume (m^3)**
Maximum 1	20 000	55 000	6	1	175 000
2	20 000	55 000	5	1	155 000
3	20 000	55 000	4	1	135 000
4	20 000	55 000	3	1	115 000
5	20 000	55 000	2	1	95 000
Minimum 6	20 000	55 000	1	1	75 000

Probable fan volume

As seen from Table 8.2 a fan of 75 000 m^3 is found as the minimum fan volume (1m). When considering field observations, witness statements and volume calculations using the economical map, this is too little. The fan is thicker in its central area (possibly around 5-6 m) than at the flanks. This makes a fan volume of around *160 000 m^3* likely.

Mud deposit

Some material is deposited as mud over the nearby farmland, with an area of around 250 000 m^2. The area is shared by several farmers. When an average thickness of 20 cm is considered, this constitutes *50 000 m^3*. This number coincides with the farmers' observations. The appraisers have in total made 43 400 m^3 of mud the basis of the compensation offered the farmers.

Lost to sea

The volume lost to sea is unknown, but due to the high content of water involved in the flow, this volume could be considerable. Observations of the sediments are made also out in the main arm of the fjord Sognefjorden. A minimum of 10 000 m^3 and a maximum of 50 000 m^3 is assumed deposited in the sea.

8.5 Comparison to similar happenings

A glacial lake outburst flood in Nepal, Himalaya, released five million m^3 of water and three million m^3 of sediments were eroded and transported 40 km (Watanabe et al., 1994). It was also estimated that around 10-15 % of the material left the region as suspended load. This means that the volume of water had eroded a sediment volume corresponding to 60 % of the water volume itself. If this is representative also for a case like Fjærland, one could expect 10-15 % of the eroded material to be transported to sea.

This could mean that if the estimate of an eroded volume of 240 000 m^3 is relatively correct, a water volume of around 384 000 m^3 would be needed to mobilise the volume. The moraine material in Fjærland is however easily eroded, which could suggest less water volume for the same erosion. Of a total of 240 000 m^3 between 24 000 and 36 000 m^3 fine material should then be transported to sea. On the other hand, erosion depends on among other factors volume, velocity of the masses and slope angle. See also Chapter 9.

Based on empirical data, Huggel et al. (2004) state that a glacial lake outburst volume of 50 000 m^3 could trigger a debris flow of 100 000 – 150 000 m^3. This gives support to the idea of water estimate in the lower end of the range. A solid mass volume of 240 000 m^3 would according to Huggel et al. (2004) require a water volume of around 100 000 m^3. It is assumed that the sediment eroded is moraine material in Huggel's case.

8.6 Sediment concentration

In the first scenario discussed in section 8.5 (Watanabe et al., 1994), the sediment volume of 240 000 m^3 constitutes 38.5 % of a total volume of 624 000 m^3, giving a total density of 1.5 g/cm^3. Based on Huggel et al. (2004), a density of 1.8 g/cm^3 is computed. An overview of different possibilities is given in Table 8.3 below. The concentrations range from 23 to 86 %, giving densities of the mass flow from 1.3 to 2 g/cm^3.

Table 8.3 Sediment concentration scenarios. A dry till density of 2.2 g/cm^3 is assumed.

Sediment volume (m^3)	Water volume (m^3)	% solids in debris flow	Density of flow (g/cm^3)
150 000	50 000	75	1,9
150 000	100 000	60	1,7
150 000	200 000	43	1,5
150 000	300 000	33	1,4
150 000	400 000	27	1,3
150 000	500 000	23	1,3
240 000	50 000	83	2
240 000	100 000	71	1,8
240 000	200 000	55	1,7
240 000	300 000	45	1,6
240 000	400 000	38	1,5
240 000	500 000	32	1,4
300 000	50 000	86	2
300 000	100 000	75	1,9
300 000	200 000	60	1,7
300 000	300 000	50	1,6
300 000	400 000	43	1,6
300 000	500 000	38	1,5

8.7 Uncertainties

The area estimates are reliable. The uncertainties in the vertical direction of the models are larger. As mentioned, the vertical accuracy is believed to be 20 cm. For a large area like the one in Fjærland, the error will accumulate and grow. The worst case scenario implies that both the pre-flow and the post-flow model exhibit the maximal inaccuracy, but in different directions. By this I mean that if the 2001-model is 20 cm too high in elevation and the 2004-model is 20 cm too low, an error of 40 cm would develop. Over an area of 100 000 m^2, the error could grow to 40 000 m^3. This must be considered in addition to the uncertainties previously mentioned (see Section 8.3.1). This is around 17 % of the estimate. However, the photogrammetry method is reliable and should give a +/- 10 % estimate of the correct volume.

8.8 Conclusion

When considering the above factors, a maximum of 300 000 m^3 (5 m vertical erosion from the precipice) and a minimum of 150 000 m^3 (2,4 m vertical erosion from the precipice) are set. The minimum estimate is however suggested to be unrealistically low.

Table 8.4 Maximum and minimum values of eroded volume.

	Total volume (m3)	Average vertical erosion, whole track(m)	Average vertical erosion, beneath precipice (m)
Minimum	150 000	1,5	2,4
Maximum	300 000	3,0	5

In the following I will use an estimate of *240 000 m^3* as the total volume eroded. This is considered correct +/- 10 %. This is based on the volume estimated using photogrammetry (236 453), but due to the fact that the terrain models show less steep erosion walls (more like a v than a u), and also for convenience, the volume is risen to 240 000 m^3. A water volume of *100 000 m^3* will be used. This gives a flow density of *1.8 g/cm^3*. If remoulded and in-situ material had the same properties, distributions like the one shown in Table 8.5 could seem likely.

Table 8.5 Solid volume distributions.

Sediment volume (m^3)	Fan volume (m^3)	Average fan depth (m)	Field deposit (m^3)	Lost to sea (m^3)
240 000	160 000	2,26	50 000	30 000

Table 8.6 Water volume distributions.

Total water volume (m^3)	Lake volume (m^3)	Additional water from the glacier (m^3)
100 000	50 000	50 000

9. Erosion, entrainment and deposition

Commonly debris flows generated from erosion by water (Scott, 2000) are granular, with a low content of fine particles. They often also follow streams, and such river channels are already sorted and depleted in fine material, as in Fjærland. A flood of water incorporates bed material, but a flow of saturated debris may impose even higher degree of drag forces and erosion. The formation of surges due to longitudinal sorting and boulder fronts (see Chapter 10) may also enhance the entrainment capacity of a debris flow (Hungr et al., 2005). Erosion and destabilisation of bed material due to drag, strength loss or liquefaction again results in instability of the gully flanks. Undercutting due to lowering of the bed and steepening of the sides may lead to massive failure of the flanks along the flow channel, supplying more material to the debris flow or favouring later debris flows.

Channel scour has been somewhat overlooked in debris flow literature (Remaître et al., 2003 a), although it has a great effect on volume and rheology. From initiation to deposition, debris flows can grow 10-15 times. Other authors claim even higher degree of entrainment along the path. Remaître et al. (2003 b) reports a dam breach in Faucon Stream in 1996, similar to the case of Fjærland. An intense thunderstorm caused failure of the dam, resulting in an outburst flood with a height drop of 1000 m, channel scour and entrainment. The mobilised volume was 5000 m^3, whilst the total deposit had a volume of approximately 100 000 m^3. The lobe deposit was 150 m wide, 200 m long and 1.5 m thick. Estimated channel scour (S), after Jakob et al 2000:

$$S = \frac{(V_{tot} - V_{ini})}{L_C} \tag{9.1}$$

where

L_C = channel length from fan apex to breached dam

V_{tot} = total volume

V_{ini} = initial volume

Using this relation, the scour rate between initiation area and fan in Faucon Stream became 29 m^3/m. Erosion however varies throughout the track.

No good dynamical model simulating debris erosion and entrainment has yet been successfully completed, although attempts of models determining where entrainment is likely to begin (Hungr et al., 2005) have been produced. Some of the most difficult problems in this work are the uncertainties concerning pore pressures and material properties of the flowing debris. Other factors believed to influence both erosion and deposition are summarised below:

- bed material
- slope angle
- geometry of gully channel (undercutting and unstable flanks)
- material of debris flow
- formation of bouldery front
- velocity
- concentration of sediments in the debris flow
- total volume or magnitude of the flow

It would be worthwhile to make an attempt to determine an erosion constant. In this search, the study of naturally occurred events is crucial, supplemented by laboratory experiments.

9.1 Fjærland case

9.1.1 Erosion and entrainment

The volume of the moraine breach in Fjærland is considered small compared to the volume of the debris flow and the volume of the fan. The estimate of around 25 000 m^3 from the ridge itself compared to the total volume of 240 000 m^3 gives an average scour rate of around 72 m^3/m for a length of 3000 m.

The main part of the eroded volume in the Fjærland torrent has its origin in the area from beneath the precipice (625 m.a.s.l.) to the start of the fan (96 m.a.s.l.). This is an area of 62 200 m^2, with a length of 1820 m, width 34 m and average slope 16.5º. The three sections of the track beneath the precipice generated for the purpose of volume estimation (see Table 8.1 and Figure 8.3), have been further divided into 10 reaches (i), for the purpose of studying erosion (Figure 9.1). The fan is further divided into 4 reaches. Characteristics for each reach are found in Table 9.1 and Table 9.2.

$$V = \sum_{i=1}^{n} L_i \cdot B_i \cdot C_i \qquad (9.2)$$

where V = volume, B = width, L = length, C = erosion depth, i = reach number

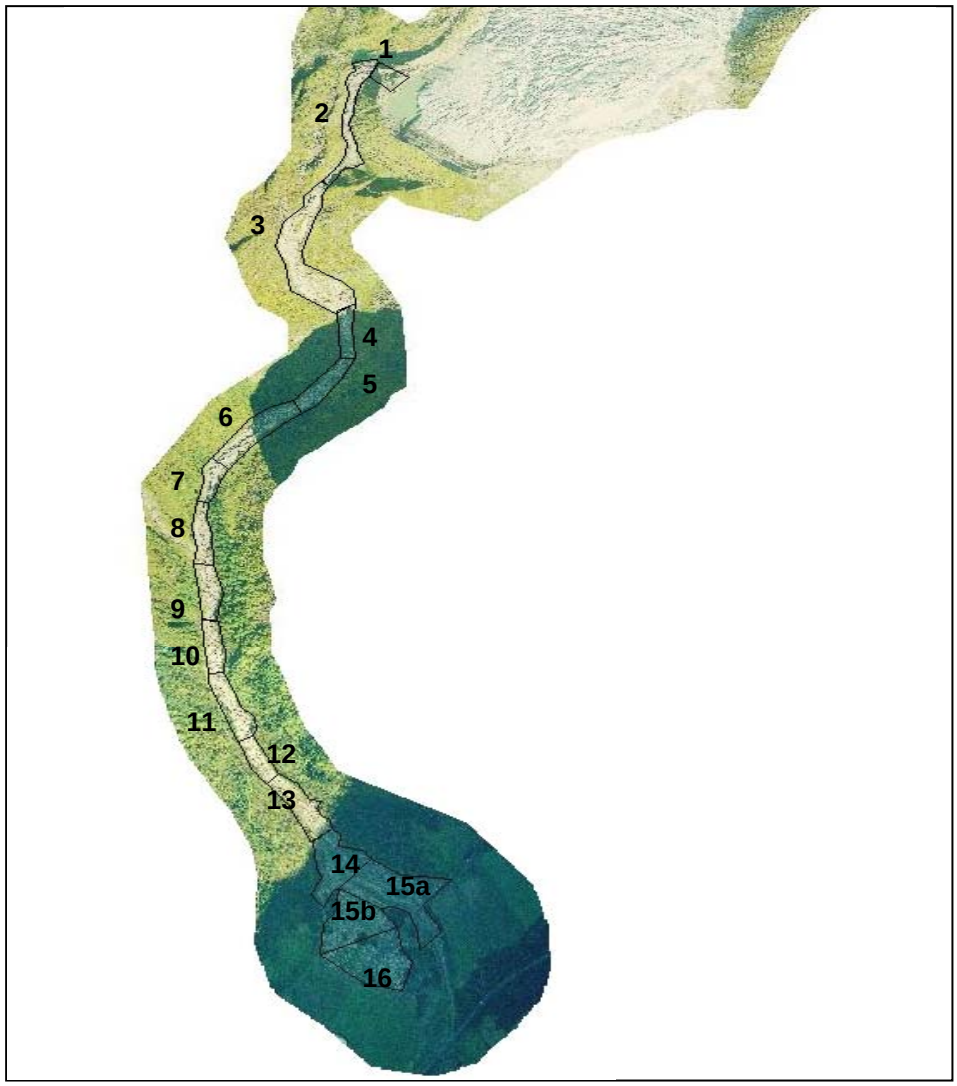

Figure 9.1 The debris flow track divided into different reaches.

Table 9.1 Overview of erosion and characteristics of different sections. For position of reaches, see Figure 9.1.

Section	Eroded volume (m^3)	Cumulative volume (m^3)	Area (m^2)	Length (m)	Width (m)	Slope (º)	Vertical erosion per m (m/m)	Vol. eroded per m (m^3/m)
4	15 349	29 864	4098	159	25,8	25	3,75	96
5	17 918	47782	6188	196	31,6	15,5	2,89	91
6	14 800	62582	11077	260	42,6	16,5	1,33	57
7	11 392	73974	4236	124	34,2	21	2,69	92
8	28 490	102464	5988	193	31	15,5	4,76	147
9	30 260	132724	6552	176	37,2	17	4,62	170
10	17 463	150187	5736	199	28,8	15	3,04	87,8
11	30 880	181067	6480	194	33,4	13,38	4,77	159
12	14 556	195623	3900	128	30,47	13,72	3,73	114
13	40 816	236439	7970	192	41,51	12,6	5,12	213
Total	**221924**	**236439**	**62225**	**1821**	**34,17**	**16,5**	**3,67**	**123**

Table 9.2 Characteristics of the fan sections and distribution of deposits.

Section	Deposited volume (m^3)	Area (m^2)	Length (m)	Slope (º)	Vertical deposition per m (m/m)
14	16671	14259	137	11,41	1,77
15a	41875	23214	(196) (260)	9,65	1,81
15b	32854	16365	146	10,73	2,02
16	14132	21256	169	3,51	0,67
Total	**105532**	**75094**	**452**	**8,8**	**1,57**

The flat area near the moraine ridge has, according to the calculations in Surfer, experienced net deposition. The slope is around 5º in the area, and the average deposition per meter is 1.3 m, when the area enclosed is 6558 m^2. The precipice has not experienced much erosion, mainly due to limitations in amount of erodible material and the flat area above (resulting in deposition and lower velocity).

If the total volume eroded (≈ 220 000 m^3) over the areas beneath the cliffs are distributed throughout the 62 200 m^2, an average vertical erosion of 3.5 m is obtained, which seems reasonable when considering field observations.

The first part beneath the precipice, is relatively steep; around 25º, and encloses an area of 4100 m^2. The erosion in the area was calculated to be around 15 000 m^3. This corresponds to average vertical erosion per travel distance (m) of almost 4 m. Such deep erosion is also seen from field investigations where the flow hit the ground beneath the precipice. This is however not representative for the upper reaches. They are commonly steep, but the erosion is shallower and the width less than further down the track (see Figure 9.2).

Figure 9.2 The debris flow track in Tverrdalen seen from the air in the direction of the flow a few days after the event. The fan is located where the two valleys meet. Mud is seen to inundate the fields in the flat lowland. Photo H. Elvehøy.

For each meter travelled, the debris flow can be imagined to grow with 57 m^3 in one of the upper reaches and up to 170 m^3 in one of the lower reaches. The estimated results are summed up in Table 9.1. For similar characteristics of the three areas from the breach to the cliffs, see Table 8.1. These areas are not included here since they contribute very little to the eroded volume.

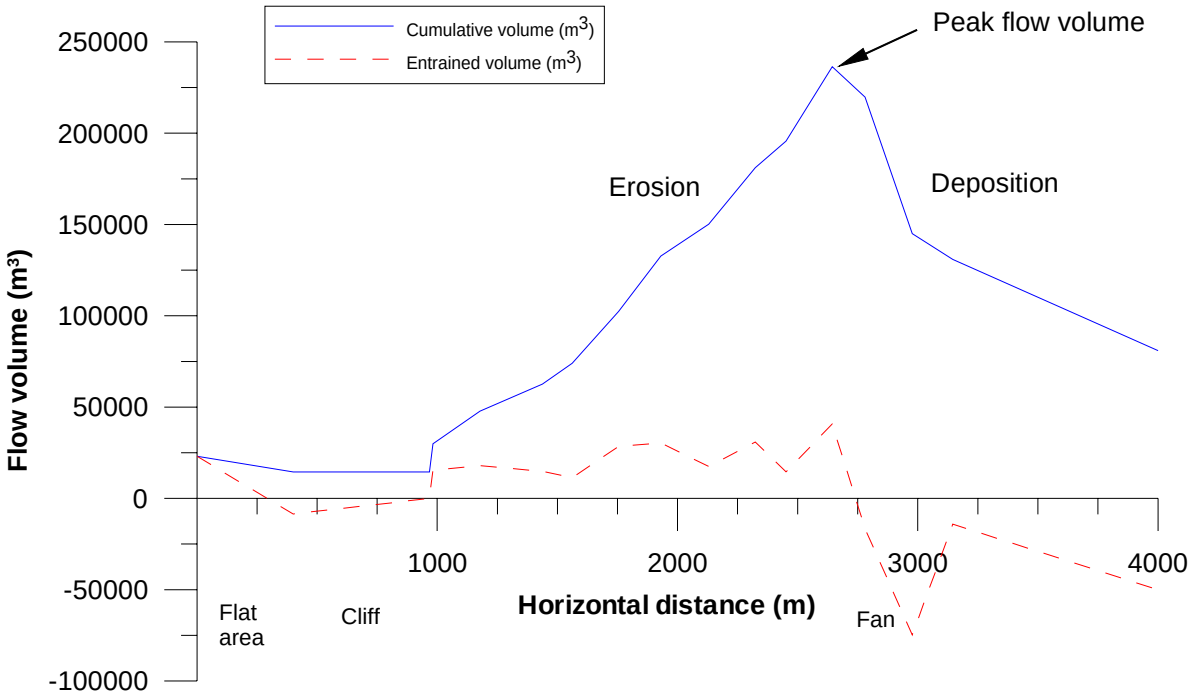

Figure 9.3 Volumetric change of derbis flow throughout path.

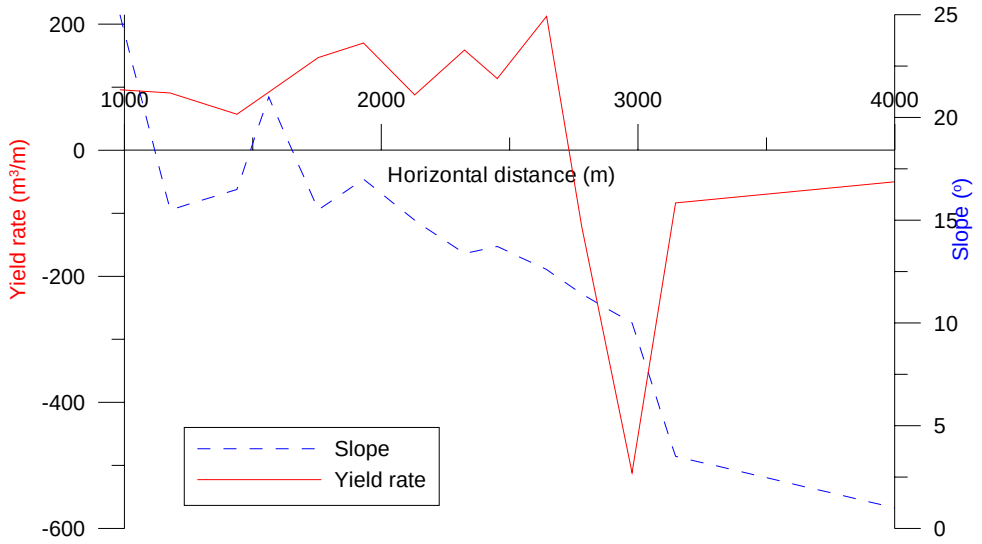

Figure 9.4 Slope and yield rate from below the cliffs to end of deposition area.

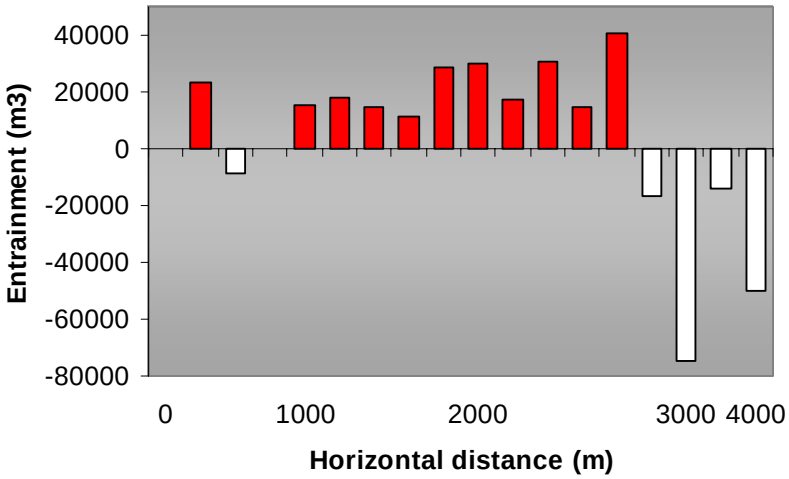

Figure 9.5 Bar representation of entrainment in every reach, starting from the breach, ending at the end of the mud deposition on the farmland. Red displays entrainment, white represents deposition. Note: the reaches do not have the same length (see Table 9.1 - Table 9.2).

As seen from Table 9.1 and Figure 9.3, the volume grows with a factor of ten from the start at the moraine breach (0 m) to the beginning of the fan (2644 m). At distance 2644 m from the breach the volume of the flow is at its peak. Deposited volume does notseem to equal eroded volume. This may be due both to lack of good deposition data, the loss of sediment to sea and the differences in density.

The volume eroded in the ten reaches studied is around 220 000 m^3. When also the around 25 000 m^3 from the moraine scar is taken into account, the value grows to almost 250 000 m^3. Some material is also eroded from the flat area at around 1000 m.a.s.l. and from the cliffs. The sides of the eroded gully are probably somewhat steeper than estimated, meaning that the volume is slightly underestimated. The total eroded volume is suggested to be approximately 250 000 m^3. Some of the material from the upper part is however sedimented before the precipice, and some deposition occurs at the same time as erosion. This is the reason for the slightly lower earlier calculated eroded volume (240 000 m^3, see Section 8.8).

Eroded volume per travel distance is by several authors called channel debris yield rate, and is by Huggel et al. (2004) reported to be up to several hundreds of m^3/m where lake outbursts have been the triggering factor. Such high yield rates seem to be linked to happenings where water is not a limiting factor. This is also considered to be the case in Fjærland. The yield rates vary from 57 to 212 m^3, the largest values typically occurring in the lower parts of the track. The yield rate of 212 m^3/m occurs in an area of average slope 12.6º whilst a higher altitude slope of 25º has a yield rate of only 96 m^3/m.

Conclusion

These data, supported by field investigations, suggest that flow volume, more than the slope angle, determines erosion, although they both are important factors. One would expect that steeper paths produce larger erosion and entrainment (up to a critical slope too steep to create erosion). It is not expected that the critical slope is as gentle as around 18º. As the volume of the torrent grows with distance travelled, the potential to erode increases. This is also dependent on velocity and acceleration, which is believed to increase with distance due to the entrainment of material and height drop. Entrainment affects the velocity in two ways, as a slurry of too high sediment concentration will eventually stop in a gentle slope, both due to viscosity and friction. It is also likely that the debris flow in Fjærland was especially erosive due the too high content of boulders in the front. The high boulder content increased with distance due to the higher degree of erosion, the higher yield strength, and the nature of the bouldery till in the gully. The author considers a flow of moderate to high sediment concentration to be very erosive. On the other hand, a low sediment flow would produce a higher velocity, and according to Hungr et al. (2005), debris flows with low sediment concentration is believed to be more erosive than more sediment rich flows.

9.1.2 Deposition

Slope angle seems to be especially important for deposition. Huggel et al. (2004) use an average slope angle in the determination of debris flow run-out based on empirical data. Their model is programmed to stop the debris flow when an average angle between initiation point and end point of 11º is reached. In cases tested this always gave conservative estimates, which means higher degree of safety for the inhabitants to be protected. In the case of Fjærland, the average slope angle between the moraine ridge breach and the end of the fan is around 18º. The mud travelled even further, decreasing the average slope angle.

Hungr et al. (1984) were of the early researchers focusing on entrainment and introducing the concept of yield rate. They found that deposition starts at between 10 and 14º slope for unconfined and between 8 and 12º for confined flows. Other researchers have also found slopes around 10º to result in deposition. However, there is probably no such thing as a magical slope angle stopping all flows. Topography is also an important factor. The point of incipient deposition has in all cases studied been found to coincide with the exit of a channel and an opening of a valley (Hungr et al., 1984). It seemed that the exit from a channel to a wider area was more important than the slope angle.

This coincides well with the Fjærland case, where main deposition started at 12º, and where also the valley Tverrdalen, which the debris flow followed, meets Supphelledalen, meaning that the area available for flow widened.

Conclusion

It seems that the boulders deposited within a range of a few degrees (i.e. over a short terminal distance) whilst finer material may deposit over a large area. Also the exit of a gully to a wider area is an important factor in deposition. In addition to this, it is likely that flow volume and velocity would influence the deposition rate and slope. It is generally agreed that lower sediment concentration (lower yield strength) results in longer run-out and lower deposition angles. This issue is further treated in Chapter 11.

For a more detailed study of erosion and yield rate, also a velocity profile along the debris flow path would be interesting for the study of erosion dependence on velocity.

10. Debris flows – a literature review

On the basis of field observations and eyewitness reports it can be stated that the Fjærland flow changed considerably throughout its path. Factors influencing the nature of the flow are considered to be

- changing water content
- increase in scouring and bulking with time and travel distance,
- change in terrain and vegetation throughout the path
- flow material (concentration, grain size distribution etc.)
- bed material
- deposition of large blocks along the path and in the fan as well as final deposition of fine material.

Due to this, factors like friction, grain collision, viscosity, density and yield strength may have had varying importance throughout the event. This chapter presents a discussion of debris flow mechanics and dynamics based on a literature review and relates earlier findings to the Fjærland debris flow.

10.1 Flow type related to grain size distribution and maturity

Debris flow material is commonly of variable size. One flow can contain solids of all sizes, as well as trees and cars. Yet it is common to divide such flows into types according to the sediment concentration or grain size distribution, because these are parameters influencing the flow behaviour and the type of force dominating. According to Iverson (1997 a) silt and clay commonly constitute less than 10 % of the mass. Bulk densities normally range from 1800 to 2300 kg/m^3, and volume fraction of grains from 0.5 to 0.8. Experiments have shown that when the volumetric grain concentration of a mixture is larger than 0.4, the fluid acts almost like a rigid-plastic solid, but flows like a liquid when pore pressure or agitation is

high enough (Iverson & Vallance, 2001). A mixture of 240 000 m^3 sediment and 100 000 m^3 of water will give a density of 1850 kg/m^3 and grain concentration of 0.7.

Solid friction, liquid viscosity and particle collisions play important roles in the mechanics of a debris flow (Chau et al., 2000). Some dimensionless numbers (like friction number, Savage number and Bagnolds number) can be useful when dividing debris flows into groups. It is for example shown that stress due to grain collisions dominate over viscous fluid stresses if Bagnolds number is above 40 (dispersive stress dominates over viscous stress) (see below), and that grain collision stresses dominate over grain friction stresses if Savage number is above 0.1 (Iverson and LaHusen, 1993).

→ Bagnold number $B = \frac{\dot{\gamma}\,\rho\delta^2\lambda^{1/2}}{\mu}$ (10.1)

where

$\dot{\gamma}$ = average shear strain rate

δ = typical grain diameter

λ = linear grain concentration

ρ = density of liquid

μ = viscosity

When using a shear strain rate of 2, a grain diameter of 0.1 m, sediment concentration of 0.7 and a viscosity of 300 gives a Bagnold number as low as $5{,}6*10^{-5}$, and a Savage number of $5{,}7*10^{-4}$. This means that viscous stresses should dominate over dispersive and friction dominates over collision.

Following Coussot (1992) cited in Laigle (1997), debris flows can be divided into two groups:

- Granular debris flows. Less than 1 % of the solid mass is fine particles smaller than 40 μm.
- Muddy debris flows. Fine-material fraction is higher than 10 % of the solid mass.

Takahashi (1991) uses the terms stony debris flow, immature debris flow, muddy debris flow and hybrid debris flow. Later he defines different types of debris flows as follows (Takahashi, 2000):

- Stony debris flows: collision of grains dominates the stress. In such a flow the concentration of large grains is high, the relative depth (depth/size distribution) is small, and the Bagnold number is large (typically ≥ 20). Particle collisions and dynamic sieving concentrate the biggest boulders in the front of the flow, building a head.
- Viscous debris flows: stress due to viscosity dominates. The viscosity of the mass is very large, and the flow is only turbulent in the front. Both Reynolds and Bagnold numbers are small.
- Muddy debris flows: stress due to turbulent mixing dominates. Here the particles are small, but not as small as in a viscous flow, and the motion is very turbulent. This typically happens when relative depth is large, and Reynolds number is large. Concentration of large blocks in a head is not common.
- Immature flows: the concentration of coarse particles is under 0.3. Immature flows are characterised by two separate layers, where the sediment is carried only by the deepest layer, pure water flowing on top. In contrast, a stony flow is a flow with only one layer; a collision layer.
- Hybrid flow: develops if the upper layer of water is a turbulent suspension layer.

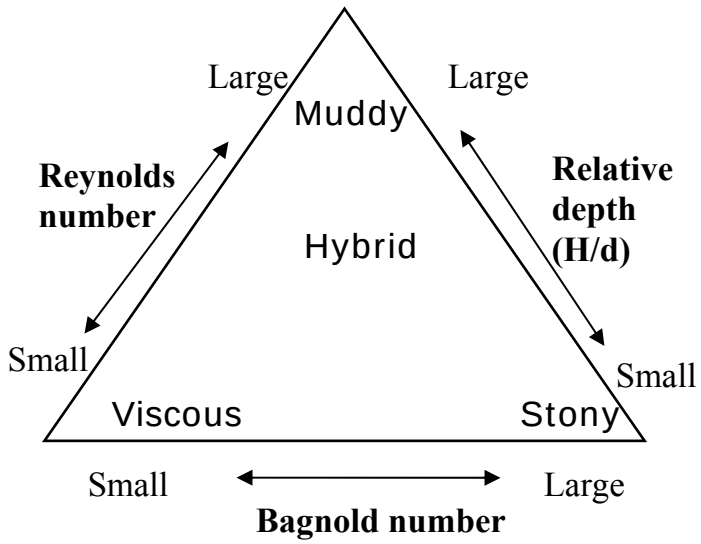

Figure 10.1

Debris flow regimes and their dependence on Re, Ba and H/d. Modified from Takahashi (2000).

Armanini et al. (2000) describe some of the same flow regimes in a little bit different way: They talk about mature slurries, and mean a mass with a liquid content just filling the pores, while an immature flow has a higher liquid content, with the extra water flowing in a layer on top, as in Takahashi (2000). They also mention a state of undersaturation, where a basal shear layer moves a rigid plug. This means that the grains are in the top layer of the flow, whilst they in an immature flow are at the bottom (see Figure 10.2). The authors claim that the mature condition can occur only in a very limited range of slope angles (θ), the so-called "θ-mature". The flow will be undersaturated if the slope is steeper, and immature in a gentler slope. In addition, transport capacity is an important concept. The authors also connect concentration to velocity, and state that the lower the concentration the higher the velocity. This means that a mature debris flow moves relatively slowly, whilst an immature flow moves fast. When the particles are not in contact (Takahashi, 2000) the mass will flow more easily. That is; the lower the sediment concentration, the lower the resistance. Particles settling to the bottom will also enlarge the resistance. Iverson (1997 a) states that the debris flow solids are made up of grains larger than silt, whereas grains below this limit act as part of the fluid.

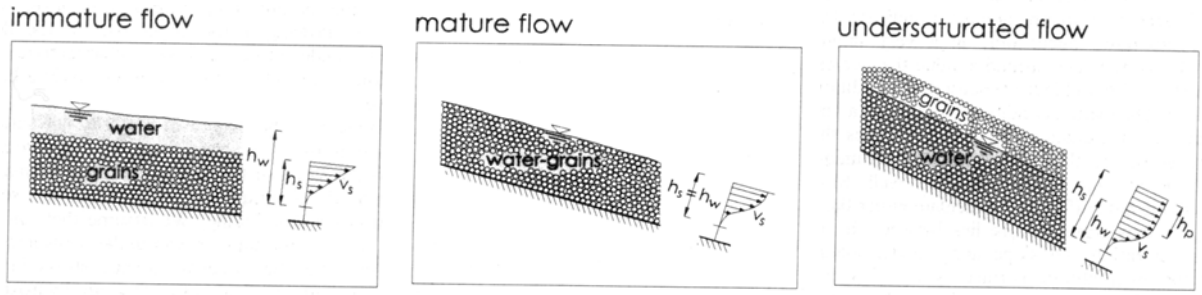

Figure 10.2 Flow figurations depending on water content. Taken from Armanini et al., 2000.

The eyewitnesses of Fjærland report inconsistently about the layering and order of ingredients in the torrent. This makes it unclear whether a complete mixture, a layered flow or separated components approached the fan area. This can be due to the different geographical positions of the witnesses. As previously explained, the physics of the flow also changed considerably throughout the event. The flow started out as a water flood and developed into debris flow after entrainment of bed material. The pictures taken by Eirik

Øygard from the cabin Flatbrehytta shows a turbulent flow of high velocity, throwing stones through the air. This can probably be characterised as a *fluidised flow*. In such a flow there is a relative movement between grains and water, meaning that the water is flowing between the grains, and faster than the grains. The smaller particles move with the speed of the water. The flow could maybe be characterised as *undersaturated* (grains on top of moving water) in the steep slope beneath the cabin, or even *hyperconcentrated*. The term hyperconcentrated flow is often used for flows intermediate between floods and debris flows and is more like a debris flood. Viscosity is the parameter controlling these flows' rheology the most. A normal flood has sediment concentration below 4 % (by volume), whilst a debris flow often has concentration over 60 %. Some authors define the limits of a hyperconcentrated flow as 20-60 % sediment, others the transition between Newtonian and non-Newtonian fluid as the lower limit and the yield strength capable to suspend gravel the upper limit (60 Pa) (Pierson, 2005). The latter indicate that the masses shown in Figure 2.4 taken at the precipice can be characterised as a debris flow, due to the size of the stones seen. It is however not known if these grains settled rapidly. The upward forces making the particle stay suspended are turbulence, convection and momentum transfer from grain collisions.

It is unclear whether the flow ended in a mature debris flow. Only a limited range of slope angles is thought to produce a mature flow. The further down the track the torrent flowed, the more solids were entrained, resulting in higher sediment concentration. The degree of erosion, and most importantly the eyewitness observations of a front resembling a wall of large boulders, proposes that the torrent developed into a *mature stony* flow.

Most probably only water ran through the valley during the first period of the event. In the Supphelledalen valley this could only be seen from the upstream side of the fan area as the river Tverrdøla (which the flow followed) runs on this side. First as the erosional power increased with growing entrainment (and vice versa), a debris flow front, steep and higher than the trees, consisting of a mixture of all kinds of sediments, approached the valley. One witness however reports that the torrent was divided into layers (water on top of granular material), as described by Armanini et al (2000) as *immature* debris flow. This type of flow has a higher liquid content than a mature flow and moves considerably faster. Immature flows are observed to occur in gentle slopes, which is also a factor indicating that this type of flow could occur in the depositional area.

The same witness tells about stones thrown through the air, indicating a high degree of collisions in the flow. The blocks found in the path on the track's flank as well as fractured stones found up to 25 m from the main track, also points towards grain-grain contact (collisions).

Turbulence, very high density of the flow, and high pore pressure, fully or nearly liquefying the mass may also be factors contributing to the transport of large stones, but stones thrown far out of the main flow indicate grain collisions. This does not support a theory of immature flow and a layer of water on top, but rather points towards a mature flow. A *hybrid flow*, where the upper layer is a turbulent suspension layer, is not a good alternative, as it is not probable that blocks of the size found on the path can be suspended in a water layer. An immature flow is also described to have a concentration of coarse particles under 0.3. This is not probable (see Section 8.6). However, an immature flow may have developed where the slope is very gentle and deposition has started.

The witnesses on the downstream side of the fan report that the boulders came first and the water afterwards. This is probably due to the fact that the stony front entrained the forest in the fan area and deposited, whilst the more liquid fine grained masses flowed further. As the torrent decreased in size, also the size of the stones entrained decreased, meaning that it later looked like only water was flowing.

The deposit is also important in determining the type of flow. It is clear that the flood developed into a debris flow, both due to the size of the boulders, but also due to the inverse layering described in Section 2.4.

The importance of all this lies in the fact that the stresses and forces change with sediment concentration and size distribution, and are therefore crucial in any attempt to develop a set of equations describing the motion of the debris flow. The deposits, as well as witness statements, are evidence of the high content of coarse, frictional material, meaning that any equations representing the dynamics must include friction and collision.

10.2 The form of a debris flow

Despite the variability in composition and its unsteady and nonuniform behaviour, debris flows typically approach a steady state condition, with a drop-shaped longitudinal profile, and constant maximum depth and length (Hungr, 2000; Tognacca, Bezzola and Minor, 2000). This drop is characterized by a steep bouldery front, followed by finer grained, saturated debris, eventually decaying into a dilute tail (Genevois et.al., 2000, Hungr, 2000; Iverson, 1997 a; Johnson, 1984; Takahashi, 1991). Coarse debris accumulates at the head of the debris flow as a result of grain-size segregation and migration within the flow, or entrainment at the front itself (Iverson, 1997 a; 2003). The high permeability of the coarse material makes the pore pressure dissipate to near zero at the head. The body behind the front has a pore pressure close to the weight of the overburden, fully or nearly liquefying the mass, due to high compressibility and moderate permeability (Iverson, 2003; Iverson et al, 2000). This shows that different forces dominate in different parts of the flow, from a high resistance front of solid forces to a low resistance tail of fluid forces. The head serves like a dam, the body pushing on it from behind (Iverson, 2003). This behaviour also results in the formation of side levees, which retard lateral spreading, concentrate the flow and increase run-out length (Iverson, 2003). Other explanations of these levees have been proposed by Johnson (1984), suggesting that dead regions are formed at the sides when the fluid flows in a channel. Many authors have showed velocity profiles of debris flows, the highest velocity being in the middle of the flow, decreasing towards the sides. Another explanation can be waterloss from the mass at lateral margins, making the material on the sides stop earlier than in the middle.

The motion of debris flows mimics that of wet concrete (Iverson 1997 a), and surges down its path in waves like water on asphalt. Each surge typically has the coarse front, evincing the maximum depth of the surge. This behaviour and form of the flow is also observed in experiments (Genevois et al., 2000), and the interviews with local eyewitnesses in Fjærland support this theory (see Section 2.1).

A debris flow often starts from rigid masses, transforms during flow to a liquid and ends up in a rigid deposit (Iverson, 1997 a). This means that both pore fluid pressure and concentration vary in time and space, and mediate friction and flow resistance (Savage and Iverson, 2003). Bozhinskiy and Nazarov (2000) describe the process of debris flow in three

phases. In the early phase the density of the flow is almost like for water, and the solids incorporated are not interacting. The next stage occurs soon after initiation. Here density is very high, and the solids interact in the flow. This stage has longer durability, and eventually ends in a third stage where the flow decelerates and deposits. The flow density is here close to limiting, and the water is flowing through a rigid skeleton of grains.

For the Fjærland case, the variations in water and sediment content with time and space is especially important for the modelling of the flow. The variations are very large, as the flow has much higher sediment concentration the further down the valley it comes due to ever increasing entrainment. The flow acted almost like a flood the first 400 m of height drop. Also time is an important aspect. The sediment first present in the flow was limited (dam material), and the water flow continued after the removal of this first material. The sediment concentration at the high flat part before the precipice decreased with time, whilst it increased at the downstream side of the precipice.

As the debris flow entered the alluvial fan area, it reduced its momentum, spread out and suddenly stopped. Witnesses describe the settling process as a balloon being punctured. The shape of a debris flow fan has been shown to resemble the half of an ellipse (Shieh and Tsai, 1997), and this is also recognised in Fjærland. At this point all the kinetic energy has degraded to irrecoverable forms, and the granular temperature (see Section 10.4) is reduced to zero (Iverson, 1997 a). Pore pressures in the deposit remain high for a long time after deposition, but are gradually decreasing with time and consolidation. The maintenance of pore pressure was also observed in the fine deposits in Fjærland. According to Iverson (1997 b), typical consolidation time (T) varies between 20 minutes and 100 days. The variables are viscosity (μ), depth of deposit (h), compressibility (C) and hydraulic permeability (k). For a thicker deposit consolidation time is longer.

$$T = \frac{h^2 \mu C}{k} \qquad \text{(Iverson, 1997 b)} \qquad (10.2\text{ a})$$

This corresponds to the one-dimensional consolidation relation in soil mechanics:

$$T \propto \frac{H^2}{Cv} \qquad (10.2\text{ b})$$

where H is the longest drainage path and Cv is the coefficient of consolidation depending on permeability, M-modulus and unit weight of water ($Cv = kM/\gamma_w$) (Lambe and Whitman, 1979).

10.3 Mobilisation

Most mobilisation hypotheses rely on the assumption that debris flows initiate due to liquefaction, partial or full, caused by elevated pore pressure, and not by shear stress growth. In addition the increased water content adds weight to the soil. Iverson et al. (1997) describe three processes mobilising debris flows: Coulomb failure, liquefaction by high pore pressure, production of granular temperature by grain agitation. A short description of basic soil mechanics is given in Appendix F.

In the case of Fjærland, erosion is the main mobilisation factor throughout the path. Lin and Chang (2003) made experiments showing that in debris flows triggered by surface runoff, it is the erosion of the bed surface that is important in the formation of the flow, not the increase in pore pressure. According to Tognacca and Bezzola (1997), surface flow is the most common debris flow trigger in the European Alps. The main processes in the evolution of such a debris flow are suggested to be:

- water infiltration
- surface runoff
- erosion
- bedload transport
- granular flow of dry material.

Readers are referred to Chen, Lee and Shen (2000), Tarantino and Bosco (2000), Lin and Chang (2003) and Iverson et al, (1997) among others for a more complete treatment of mobilisation.

10.4 Forces acting in a debris flow

One of the most significant challenges in debris flow modelling is the fact that debris flows are multiphase flows. The forces acting in the flow are not only due to the different components, but rather to the interactions *between* phases and components. The factors influencing the motion can be summed up to:

- Gravity (body forces)
- Pressure forces
- Viscous stress
- Buoyancy
- Friction grain-bed and grain-grain
- Collisions grain-bed and grain-grain

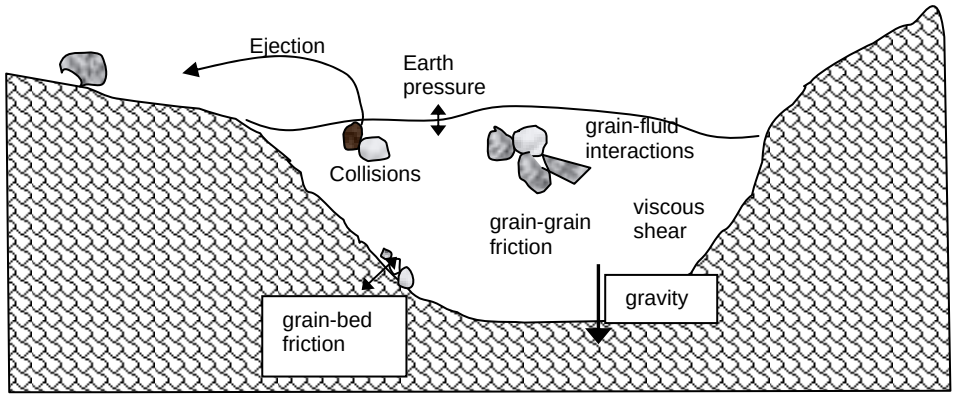

Figure 10.3 Illustration of forces acting in a debris flow.

Granular temperature is an important phenomenon in soil deformation and motion. It is a measure of grain agitation (Iverson et al., 1997), and can be defined as the mean square root of the grain velocity. Higher granular temperature reduces the bulk density and increases the fluidity of debris (Iverson, 1997 a). It can be generated and maintained by continual conversion of bulk translational energy to grain fluctuation energy, and can in this way mobilise a flow from a landslide. Grain agitation can also occur in dry granular materials, probably being the reason for the rapidness and flowing nature of dry rock fall avalanches

like the famous Elm avalanche of 1881. The motion of such sturzstroms (Cruden and Varnes, 1996) is due to the dispersive stresses created by the momentum exchange between the colliding particles. No liquid is needed for the material to flow. Such grain agitation is also a main factor in lifting large boulders and throwing them out of the flow.

10.5 Dynamics and Models

The dynamics of debris flows are less well understood than the initiation and triggering mechanisms, and different views exist. The most obvious way to study a flow is to treat it as a fluid and make use of fluid dynamics. Yet, debris exhibit resistance to flow larger than that of pure water. In addition other forces due to grains may influence the dynamics.

There are several models of momentum transport in debris flows, some relying on rheology, others on two-phase flow/Coulomb mixture theory. Most models are two dimensional, but several 3D-models have also been presented. Newton's second law, conservation of momentum; $F = m \cdot a$ (assuming mass is constant) is the basic relation of the models. Here F is force, m is mass and a is acceleration (dv/dt). The different models vary mostly in the forces included and how they are represented.

10.5.1 Rheological models

Traditional rheological models have long been the most used, like Johnson's viscoplastic or Bingham model, Hershel-Bulkley models and later Takahashi's Bagnold model. Rheological models combine the relevant relationship between shear stress and shear deformation, with the Navier Stokes equation. This coupling could in principle permit us to calculate velocity, pressure and stress etc. of the fluid. A big problem in this approach is to find the correct rheology. It is most often difficult to measure the parameters needed and the rheological properties do also change radically both in time and space.

The **Navier Stokes** equation in x-direction:

$$\rho\left(\frac{\partial u}{\partial t}+u\frac{\partial u}{\partial x}+v\frac{\partial u}{\partial y}+w\frac{\partial u}{\partial z}\right)=-\rho g_x-\frac{\partial P}{\partial x}+\frac{\partial \tau_{xx}}{\partial x}+\frac{\partial \tau_{xy}}{\partial y}+\frac{\partial \tau_{xz}}{\partial z} \qquad (10.3)$$

where

ρ = density, g = gravity,

t = time, P = pressure,

τ = shear stress, u, v, w = velocity in x, y and z direction,

In most rheological models the material is assumed rigid and do not move until a critical shear stress threshold, the *yield strength*, is overcome. A Newtonian fluid like water is different in that it responds immediately and continuously to any stress, and thus has a linear relationship between shear stress and shear rate. A debris flow is special in that it contains both fluid and solids, and will not have such a linear relationship. This must be taken into account in the dynamics. A viscoplastic or Bingham model combines the viscous deformation and plastic attributes (Iverson, 1997 a) in the representation of τ:

$$\tau=\tau_y+K\left|\frac{\partial u}{\partial y}\right|^{\alpha} \quad \text{in general for a Hershel-Bulkley fluid} \qquad (10.4)$$

α = 1 Bingham fluid

α > 1 shear thickening fluid

α <1 shear thinning fluid

K = flowing coefficient

τ = shear stress

τ_y = yield stress

For a Bingham rheology (viscoplastic) this gives:

$$\tau=\tau_y+\mu_B\frac{\partial u}{\partial y} \qquad (10.5)$$

$\tau = \rho g\left(H - y\right)\sin\beta$ for Bingham fluid structure (10.6)

where

H = thickness of flow

y = height to studied point

μ_B = Bingham viscosity

Basically, the mass does not move until the yield strength, which is treated as static, is exceeded by the shear stress. This corresponds to the Coulomb strength. To exceed the yield stress, an equation for the critical thickness Tc of Coulomb debris needed for the mass to flow is developed by Johnson (1984):

$$T_c = \frac{\left(\frac{c}{\gamma \sin\beta}\right)}{\left(1 - \frac{\tan\varphi}{\tan\beta}\right)} \tag{10.7}$$

where

c = cohesion = τ_y

γ = unit weight = ρg

β = slope angle

This means that the debris will not flow unless it exceeds the critical thickness (or stops when the depth becomes less than this). Johnson also had an explanation how debris flows can transport big boulders. The largest particle (Rm) that a Coulomb debris flow can carry was found to be:

$$R_m = \frac{\frac{c}{\gamma} f(\varphi')}{\frac{\gamma_b}{\gamma} - 1} \tag{10.8}$$

where

γ_b = unit weight of large particle

$f(\varphi')$ = function of friction angle

Both friction angle and cohesion must be considered in a model obeying the Coulomb law. A high φ´ is accompanied with a greater critical thickness than a lower φ´, and failure cannot occur if friction angle is greater than the slope angle. The fact that debris flows are observed flowing on very gentle slopes, could mean that the friction angle for debris flows is very low (Johnson, 1984) or that pore pressure is very high.

Johnson's model had to be adjusted to include both Coulomb friction and a dynamic viscosity part. In this model, a central plug of uniform velocity, and a zone of laminar flow with decreasing velocity to the sides are present. A decrease in slope angle will increase the thickness of the plug. When the plug thickness equals the thickness of the whole flow, the flow will stop. This Coulomb-viscous model is written as follows:

$$\tau = \sigma' \tan\varphi' + c' + \mu_c \left(\frac{\partial u}{\partial y} \right) \tag{10.9}$$

where

μ_c = coefficient of viscosity,

$\frac{\partial u}{\partial y}$ = shear rate,

So, combining the Bingham model with Coulomb friction gives:

$$\tau = \tau_y + \mu \frac{\partial u}{\partial y} + (\sigma_n - u)\cos\beta \tan\varphi \tag{10.10}$$

Other theories

According to Iverson et al (1997 a), Bingham and also Bagnold theories do not take into account the pore pressure effects that cause liquefaction nor granular temperature as factors influencing soil rigidity and motion. Simple rheological models like the Bingham viscoplastic model can be successfully used for the shear resistance of relatively fine grained debris flows including a certain fraction of clay (Ayotte and Hungr, 2000, Iverson, 2003). According to Martino (2003), a Bingham plastic model may overestimate the yield stress due to shear thinning at low shear rates, and underestimate it when the material is shear thickening. He concludes that a Hershel-Bulkley model fits a rheological behaviour over a

wide range of shear rates. Also Coussot (1992), cited in Laigle (1997), means that the behaviour of muddy debris flows is well described by a Hershel-Bulkley model. The rheological parameter K above and yield stress τ_y are generally expected to increase exponentially with volumetric concentration (Martino, 2003).

According to Iverson (1997 a, 2003) and Iverson and Vallance (2001), viscoplastic models do not take into account the interaction between solid grains and viscous fluid. Coarser flows with a smaller concentration of clay particles behave more like frictional material (Ayotte and Hungr, 2000) making a Bingham model inappropriate. Moreover, in unliquefied parts of debris flows, grain to grain contact dominates, and a Coulomb frictional model must be used (Iverson, 2003). Takahashi's model uses Bagnold's findings from 1954 to take the grain interactions into account in his inertial grain model. Alternative approaches include two-phase flow models, a Coulomb mixture approach, suggested by Iverson (1997 a). However, there is more to be done in this field. As mentioned, the rheological models seem to be appropriate for more viscous and fine grained slurries, but for flows with a higher concentration of coarser particles (like in Fjærland) and a new model is needed, combining viscous stress with friction and collision.

Both Iverson (1997 b) and Hungr (2000) have developed 2-D models simulating the surging behaviour of a debris flow, letting the resistance vary linearly throughout the body of the flow. Since only a Bingham model is used in this thesis (Chapter 11), the Iverson and the Hungr models are both briefly presented in Appendix F.

The different types of models proposed seem to have their advantages and disadvantages, and may be applicable to different types of debris flows. For a further study of what type of model is representing the flow in Fjærland most accurately, a comparison of a Bingham rheological model and a model developed by for example Hungr or Iverson would be valuable.

An attempt to model a flow of the type found in Fjærland meets many complexities. The mechanical behaviour ranges from bed-load transport possibly to a mature debris flow. The mechanics alternate both in time and space, thus definition of a common rheology is very complex. However, only a modified Bingham-model is employed for the work in this master thesis (Chapter 11).

11. Numerical Modelling of the Fjærland debris flow

"Saturated till may flow on the gentlest of slopes" (Hambrey, 1994, p. 114). The statement shows this soil type's capability to move, and is commonly seen near glaciers where flow till can be found. But also further from the glacier saturation makes till unstable. This, in combination with high erodibility and steep terrain may be reasons for the magnitude of the dramatic event in Fjærland.

The goals of numerical modelling are:

- To model the run-out
- To study how volume influences erosion and deposition
- To study how slope angle influences erosion and deposition.
- To investigate which type of physics best can illustrate the debris flow in Fjærland.

Run-out modelling is also useful when considering the design of mitigation structures.

Erosion is an extremely important aspect of the Fjærland case. As the main part of the initial masses from the moraine ridge was deposited around 1000 m.a.s.l., the whole volume of the debris flow can be said to be eroded and entrained on the way. A preliminary numerical model is here suggested.

Different types of physics are tested out in the attempt to model the dynamics of the flow in Fjærland. Due to the high content of coarse material, a model combining Bingham and Coulomb friction is being developed by Dr. Fabio De Blasio at the International Center for Geohazards (ICG), Oslo. The model is based on the BING code and is programmed in Fortran. The basic form of BING has been modified to include Coulomb friction as well as sediment entrainment during the debris flow. This 2D-model makes use of the length profile of the debris flow track in an attempt to simulate the flow.

11.1 BING

BING is a simple Lagrangian (reference moves with the flow) dynamical model for the flow of a Bingham material, developed by Imran et al. in 2001. It is based on two-dimensional formulations of the Navier Stokes equation and the conservation equation, as only the flow direction and the direction perpendicular to the bed is taken into account. A length profile from a terrain model is needed.

The model uses the Hershel Bulkley form (here Bingham) of the yield strength and the equations are simplified by depth integration. The flow masses are divided into vertical sections in the flow direction, each node being equally spaced when the model is started. For each time step, acceleration and position is calculated in every node, resulting in a relative difference in both acceleration and spacing between the nodes. Equations for both plug layer and the total mass are developed. The volume per unit width (area) represents the flow volume in the model. At each node the depth of the flow is calculated.

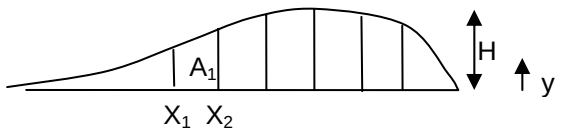

Figure 11.1 Illustration of division of the debris flow into sections in BING.

For a case where both particle-particle and particle-water interactions develop, a model incorporating the two effects should be used. For this purpose, the BING model is tried further developed by Fabio De Blasio to include friction and entrainment, better simulating the Fjærland case.

BING only includes two directions, meaning that the Navier Stokes equation becomes:

$$\frac{\partial u}{\partial t} + u\frac{\partial u}{\partial x} + v\frac{\partial u}{\partial y} = \frac{1}{\rho}\left(-\frac{\partial P}{\partial x} + \frac{\partial \tau_{xx}}{\partial x} + \frac{\partial \tau_{xy}}{\partial y} \right) + g\sin\beta \tag{11.1}$$

$$0 = -\frac{1}{\rho}\frac{\partial P}{\partial y} - g\cos\beta \tag{11.2}$$

When otherwise not noted, all terms are explained in Section 10.5.

The continuity equation used can be written as:

$$\frac{\partial u}{\partial x}+\frac{\partial v}{\partial y}=0 \tag{11.3}$$

This must be combined with a constitutive relation describing the fluid. For a general Hershel Bulkey fluid:

$$\tau_{xy}=\lambda\left[\tau_y+K\left|\frac{\partial u}{\partial y}\right|^{\alpha}\right]+(1-\lambda)\left[\rho g\left(H-y\right)\cos\beta\tan\varphi\right] \tag{11.4}$$

$0\le\lambda\le1$ is a measure of importance of cohesion relative to friction. λ of 1 gives the fluid a cohesive behaviour, whilst a λ of 0 makes it purely frictional. In this way λ is meant to simulate the degree of contact between grains in the fluid. λ is constant in this model, but will in nature vary with both x, y and t due to entrainment, building of a bouldery head, the Brazil nut effect, etc. Assuming a Bingham fluid, α = 1. For the fluid to move,

$$\tau>\tau_y\lambda+(1-\lambda)\left[\rho g\left(H-y\right)\cos\beta\tan\varphi\right] \tag{11.5}$$

A further mathematical description of the BING-model is presented in Imran et al (2001).

11.1.1 Erosion

Several simplifications are made in the simulation of erosion/entrainment of sediment. One of them is the assumption of no-slip condition, meaning that the velocity is zero at the bottom of the flow. The erosion incorporated is based on shear stress at the base, and does not take into account the action of grains.

$$\begin{aligned}\frac{dh}{dt}&=cU^{Y}\left(\tau_{xy}-\overline{\tau}\right)\mathrm{sgn}\left(U\right) \quad for \quad \tau_{xy}>\overline{\tau}\\ &=0 \qquad\qquad\qquad\qquad\quad for \quad \tau_{xy}\le\overline{\tau}\end{aligned} \tag{11.6}$$

where

$\overline{\tau}$ = critical shear rate for erosion, c = erosion constant,

Y = exponent, U = average velocity of the flow,

In the model used, Y is set to zero, meaning that erosion does not depend on velocity in the simulation. This is a simplification. Velocity must however be larger than zero ($\mathrm{sgn}(U)$).The erosion is dependent on sine of slope angle and the height of the flow. It is assumed that erosion starts at elevation 600 m.a.s.l., at the bottom of the cliff.

The acceleration a_j^* of each node j is reduced with respect to the case where the debris flow mass is constant:

$$a_j^* = \frac{acceleration\ without\ entrainment}{1+(eroded\ mass)/(original\ mass\ of\ debris\ flow)} = a\left[1+\frac{dh}{dt}\left(X_{j+1}-X_j\right)\frac{\delta t}{A_j}\right]^{-1} \quad (11.7)$$

where

a = acceleration without entrainment

Aj = area of each section (Figure 11.1)

Xj = each node (Figure 11.1)

11.2 Challenges

As Chapters 6 and 8 show, especially the water volume involved, but also the sediment volume, is uncertain.

Solid/water concentration develops from very low (liquid) near the moraine breach to high as the debris flow approaches the fan area, and does also vary with time. Water continued flowing also after the initial failure of the moraine ridge, and as the erosion was low in the high altitude flat area, the solid/water ratio decreased with time in this area. Since the material from the moraine ridge had very little influence on the masses downstream the precipice (as most of it deposited in near vicinity of the breach), this decrease in sediment concentration did not occur in the lower parts of the track before the event was close to termination.

Problems encountered in the modelling process were:

- Water content influences yield strength, density, viscosity and friction angle. Therefore, these factors should be allowed to vary with the water content. If water content is being varied, this should also be reflected in yield strength, viscosity, density and internal friction angle. The relationship between these parameters is not known. Here the model is run using constant parameters throughout the track.
- The continuous water supply from the glacier. Modelling an abrupt release of a large volume will not represent reality, as the masses were distributed over time.
- The long duration of the flow.

These problems are not solved. Yet, attempts are made and simplifications taken.

11.3 Running the models

Only one parameter has been changed in each computer run. The importance of each parameter on run-out is also easier studied in this way. One way to simulate the variations in water content could be to start out with very low yield strength, increasing with travel length. This is not done here. The extremes of maximum and minimum yield strength are not known on beforehand. Therefore different (but constant) yield strengths are tried, and the effects on run-out and velocity studied.

The parameters used are:

Parameter	**Y**	**λ**	**φ (°)**	**c (m/sPa)**	τ_0 **(kPa)**	**μ (Pa s)**	**γ (g/cm^3)**
Values used	0	0 0.2 0.5 0.7 1	8	$2\cdot10^{-6}$, $5\cdot10^{-6}$, $8\cdot10^{-6}$	1	300	1.8

11.4 Pure Bingham model – BING 1

The first attempts of modelling the physics of the flow included pure Bingham material, neglecting friction (BING 1). It is a simple model, but offers a good opportunity for a parameter study.

11.4.1 Yield strength effects

The simplest case looked at is one with a constant yield strength throughout the track and a constant volume abruptly released. The existence of a yield stress predicts the presence of a rigid plug and a critical thickness of the flow, as developed by Johnson (1984). As the thickness of the debris flow approaches the critical thickness, the velocity gets so low that the flow stops. Low yield strength is expected to produce long run-outs.

When running a pure Bingham model trying to simulate the viscous slurry of the beginning of the event, the yield strength was held low. Increasing the yield strength will simulate debris flows of higher sediment concentration. Low, high and intermediate values were searched. Three different runs are shown in Figure 11.2, using constant yield strengths of 400, 800 and 10 000 Pa. In all figures where terrain is included, thickness of flow is exaggerated.

Table 11.1 BING 1. Run-out varying with yield strength in a Bingham model. Volume 20 000m^3.

	Yield strength (Pa)	Run-out (m)	Elev. at run-out termination (m.a.s.l.)	Max. velocity (m/s)
Scenario A	400	1541	438	22
Scenario B	800	1060	588	24
Scenario C	10 000	180	986	16

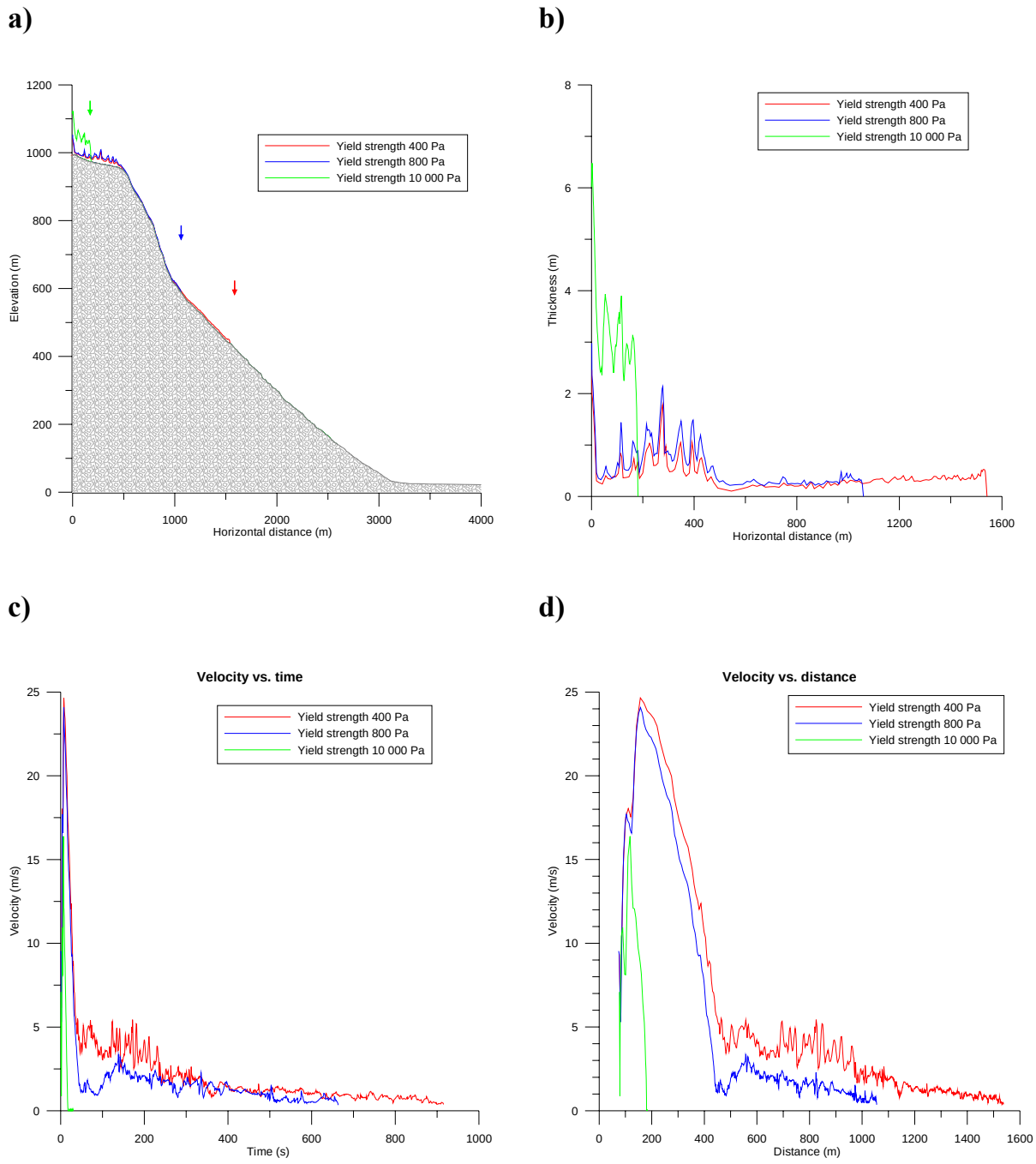

Figure 11.2 BING 1: Results from the pure Bingham model, constant volume 25 000 m^3. Not to scale. a) Effect of yield strength on run-out. b) Deposition of Bingham material, using different yield strengths. c) Effect of yield strength on velocity as a function of time. d) Effect of yield strength on velocity as a function of distance.

The slurry of lowest yield strength flows most easily and has the longest run-out. None of the runs reached the fan, the most mobile ending at elevation approximately 440 m (Figure 11.2 a) and Table 11.1). Due to the low volume included this is not surprising. Only the initial volume of the moraine ridge scar (25 000 m^3) is used (no entrainment).

Most of the material is seen to be deposited on the almost flat plain at elevation around 1000 m.a.s.l. (Figure 11.2 b). This agrees with the field observations. It is also seen that the slurry of highest yield strength has a thicker deposit than the more easy-flowing mixtures. This also means that it must terminate first. The yield strength is otherwise not seen to influence for example form of velocity profile or deposit in any degree. This is seen from Figure 11.2, where the peaks of oscillations occur at the same position and time.

The highest velocity (25 m/s) occurs in a pronounced peak a few seconds after the initiation of the flow (Figure 11.2 c and d). The overall trend in the runs is decreasing velocity with time and distance, possibly due to volume decrease. Effect of volume change is studied later in this section.

The slurry of lowest yield strength has the overall highest velocity. Higher density due to the higher content of particles is not taken into account. This could possibly neutralize or even overrun the yield strength effect.

The masses with the lowest yield strength stopped after 15 minutes.

11.4.2 Volume effects

The effect of volume was studied by increasing the initial flow volume by a factor of 4, i.e. 100 000 m^3. The results are shown in Table 11.2 and Figure 11.3.

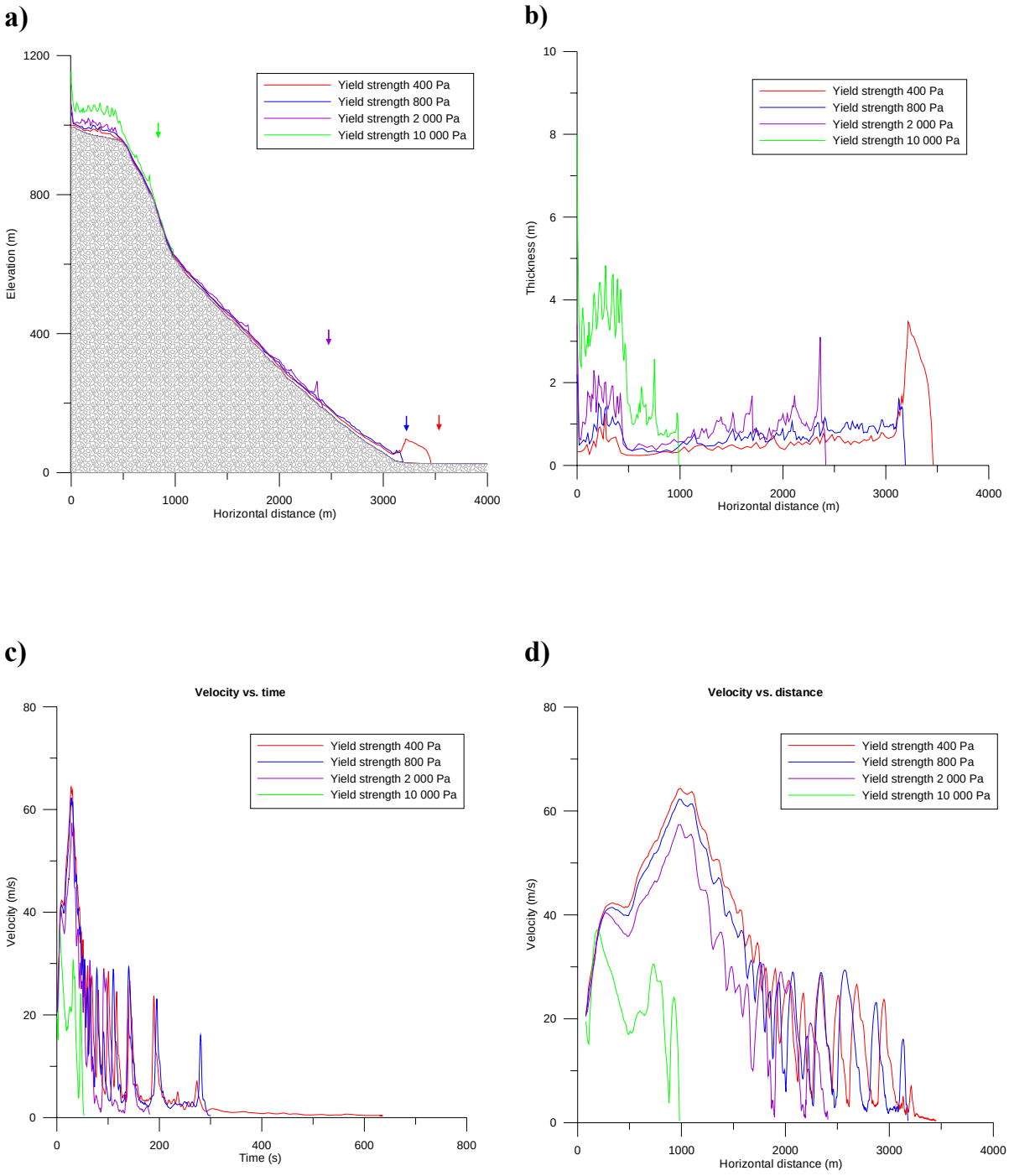

Figure 11.3 BING 1, Volume 80 000m^3. Not to scale. a) Run-out of different yield strength materials of high volume. b)Run-out and profiles of deposit. c) Velocity of the flows as a function of time. d) Velocity of the flows as a function of distance.

Table 11.2 BING 1: Run-out varying with yield strength. Volume 100 000m^3.

	Yield strength (Pa)	Run-out (m)	Elev. at run-out termination (m.a.s.l.)	Max. velocity (m/s)
Scenario A	400	3460	26	65
Scenario B	800	3190	30	62
Scenario C	2 000	2416	186	57
Scenario D	10 000	986	617	37

Extended run-out was found for all yield strength values. Both masses of 400 Pa and 800 Pa yield strength reached the valley Supphelledalen and deposited as a thick fan in the area where the fan is found in the field. Although deposition occurs on the flat high altitude plain, there are enough masses continuing downwards to reach the fan.

Also the velocity is seen to rise with increasing volume; for all flows passing the precipice a velocity around 60 m/s was reached here. From this point on the velocity decreases. The simulated average velocity in Tverrdalen is around 25 m/s, which means 90 km/h, and decreasing to 20 m/s (72 km/h) when approaching the exit of the gully (fan). The velocity is computed to grow with increasing volume, as expected, and also with increasing slope.

11.5 Modified Bingham model – BING 2 and 3

11.5.1 Bingham + erosion - BING 2

As discussed, erosion is an important part of the Fjærland event, meaning that this phenomenon must be accounted for in the numerical model. This is done according to the explanation and equations in Section 11.1.1.

11.5.2 Bingham + erosion + Coulomb friction - BING 3

Due to the high content of granular material, the inclusion of Coulomb friction gives a physics that is believed to illustrate the flow in a better way than pure Bingham rheology.

The BING model has been extended to include viscous erosion. Erosion due to the grains and boulders should however also be incorporated in further studies. No-slip condition is still assumed. Results are shown in and Table 11.4 and Figure 11.4.

First a scenario of Bingham material and erosion was run (BING 2), thereafter Coulomb friction was added to the model, giving a scenario of a Bingham rheology including Coulomb friction as well as erosion (BING 3).

Table 11.3 Overview of models used.

	BING 1	**BING 2**	**BING 3**
Bingham	yes	yes	yes
Erosion/ entrainment	no	yes	yes
Coulomb friction	no	no	yes

It seems that slope angle has a crucial role in erosion and sedimentation processes, and this is also reflected in the modelled velocity. Deposition starts when the slope angle becomes too gentle. In the Fjærland case it seems that a decrease to 12 º is sufficient for deposition to occur. Volume of flowing mass is suggested to be an even more important factor when it comes to erosion (see Chapter 9).

Erosion has been included both when running a pure Bingham model (BING 2), as well as in the Bingham + Coulomb friction model (BING 3). Yield strengths of 400 Pa and 2000 Pa have been used. The results are seen in Figure 11.4 and Table 11.4. When using 2000 Pa yield strength in a BING 3 model, the masses stopped before approaching the cliff. The results of this run are therefore not included in the figures.

a)

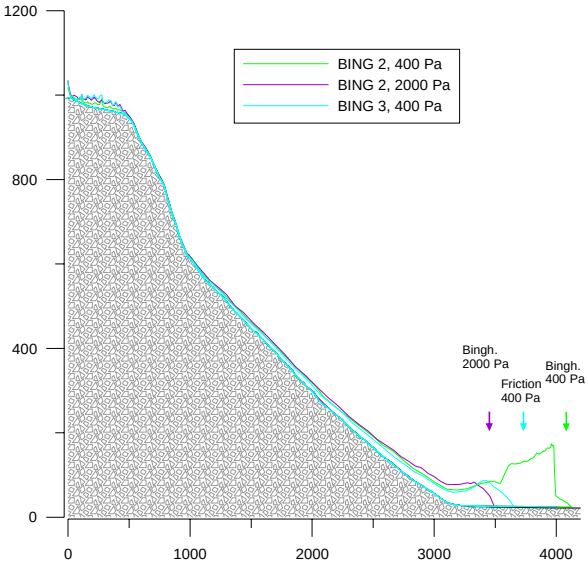
BING 2, 400 Pa
BING 2, 2000 Pa
BING 3, 400 Pa
Bingh. 2000 Pa
Friction 400 Pa
Bingh. 400 Pa
1200
800
400
0
0
1000
2000
3000
4000

b)

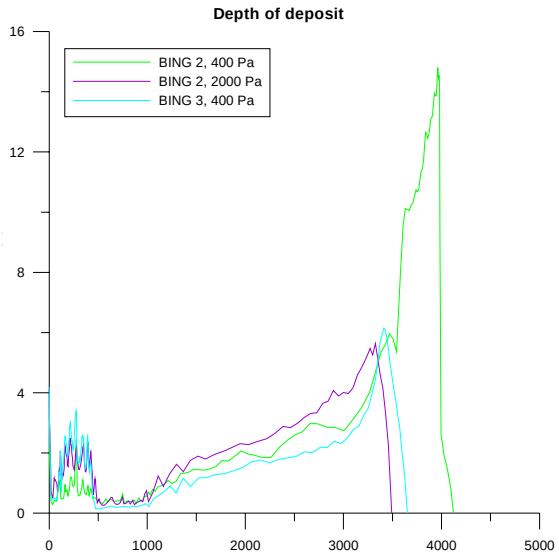
Depth of deposit
BING 2, 400 Pa
BING 2, 2000 Pa
BING 3, 400 Pa
16
12
8
4
0
0
1000
2000
3000
4000
5000

c)

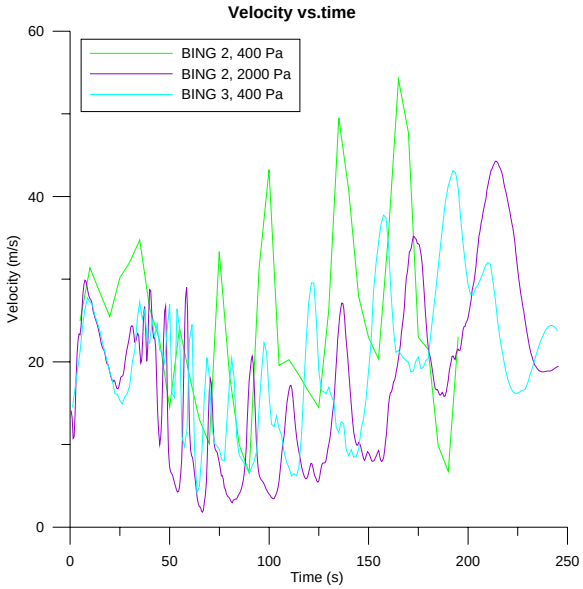
Velocity vs.time
BING 2, 400 Pa
BING 2, 2000 Pa
BING 3, 400 Pa
Velocity (m/s)
60
40
20
0
0
50
100
150
200
250
Time (s)

d)

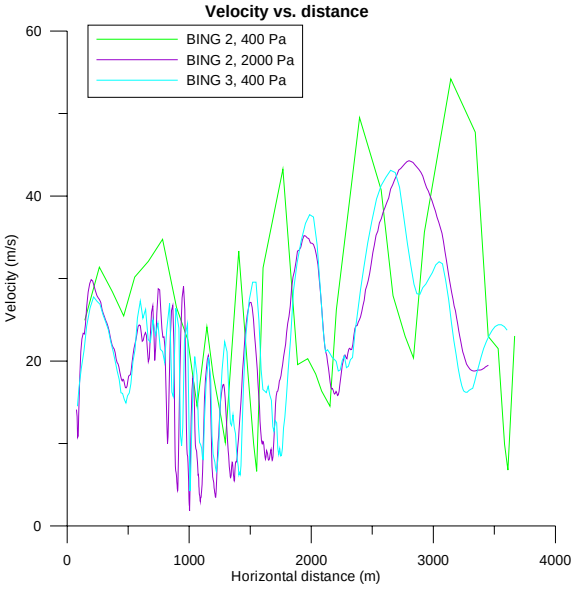
Velocity vs. distance
BING 2, 400 Pa
BING 2, 2000 Pa
BING 3, 400 Pa
Velocity (m/s)
60
40
20
0
0
1000
2000
3000
4000
Horizontal distance (m)

e) **f)**

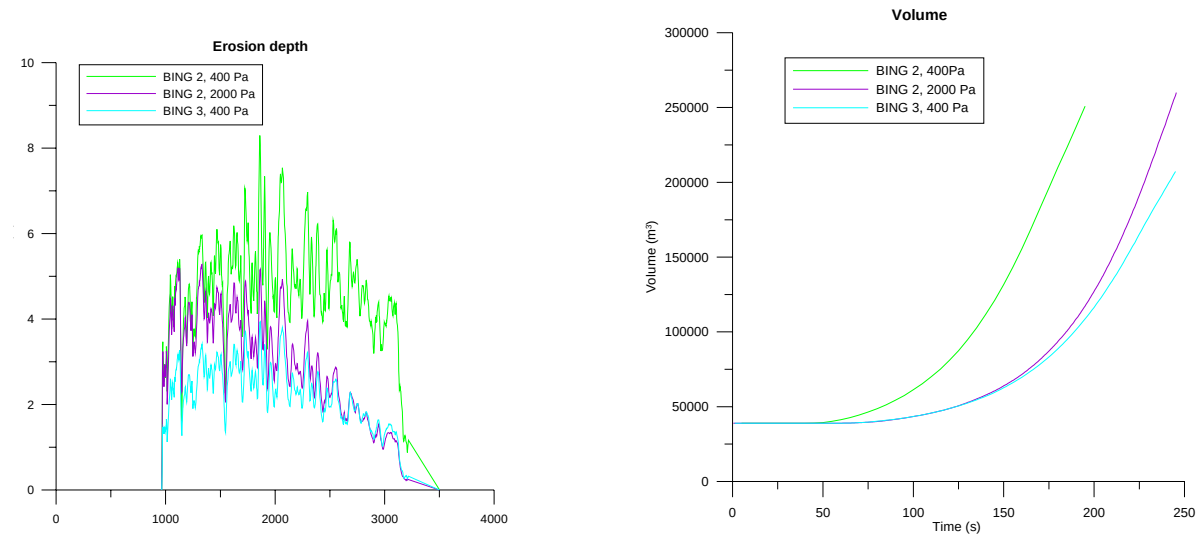

Figure 11.4 BING 2 and BING 3: Results from running the modified BING-model. Comparison of BING 2 (pure Bingham material with entrainment) and BING 3 (Bingham material with Coulomb friction and entrainment). Not to scale. a) Run-out. b) Run-out and profile of deposit. c) Velocity as a function of time. d) Velocity as a function of distance. e) Erosion depth along debris flow path. f) Accumulated volume.

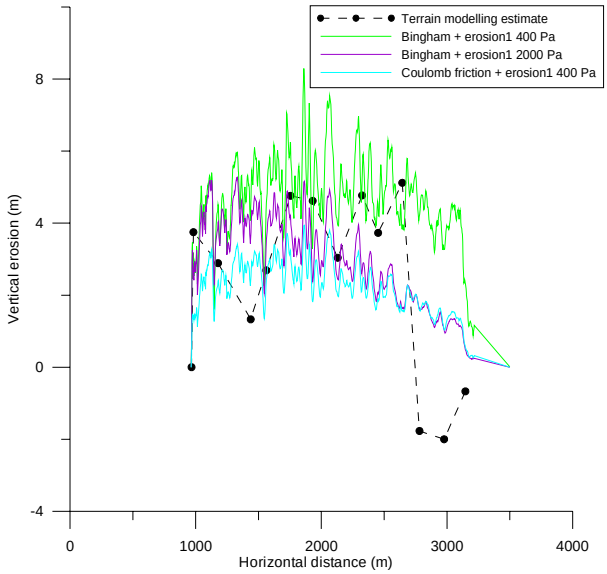

Figure 11.5 Erosion depth estimated using terrain model, as well as with the BING model. Terrain model data are shown as black dots. Not to scale.

Table 11.4 Run-out and depth of deposit for different types of rheology.

	Yield strength (Pa)	Run-out (m)	Depth of deposit in fan (m)	Max. velocity (m/s)
Scenario A	400	4100	15	54
BING 2				
Scenario B	2000	3349	5,5	44
BING 2				
Scenario C	400	3651	6	43
BING 3				

a)

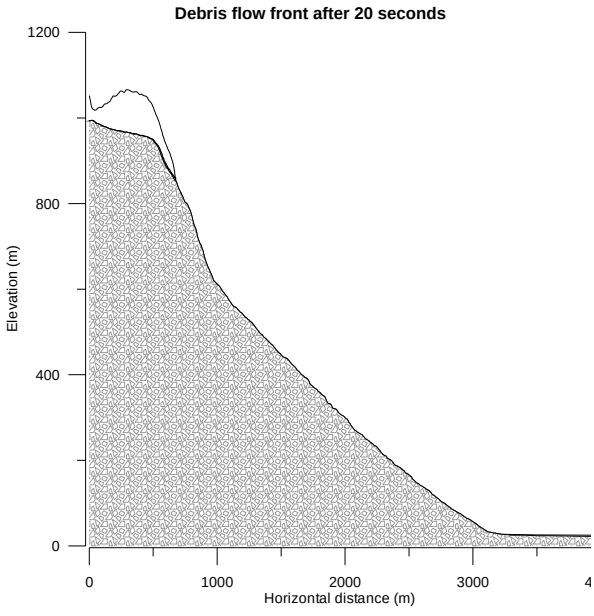

b)

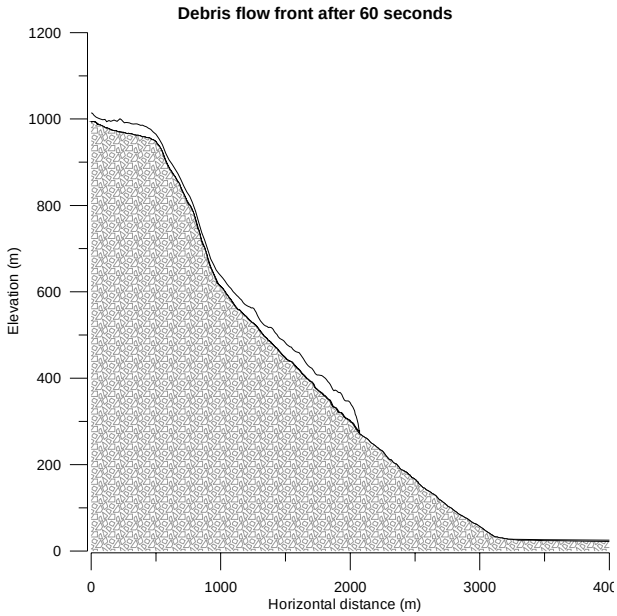

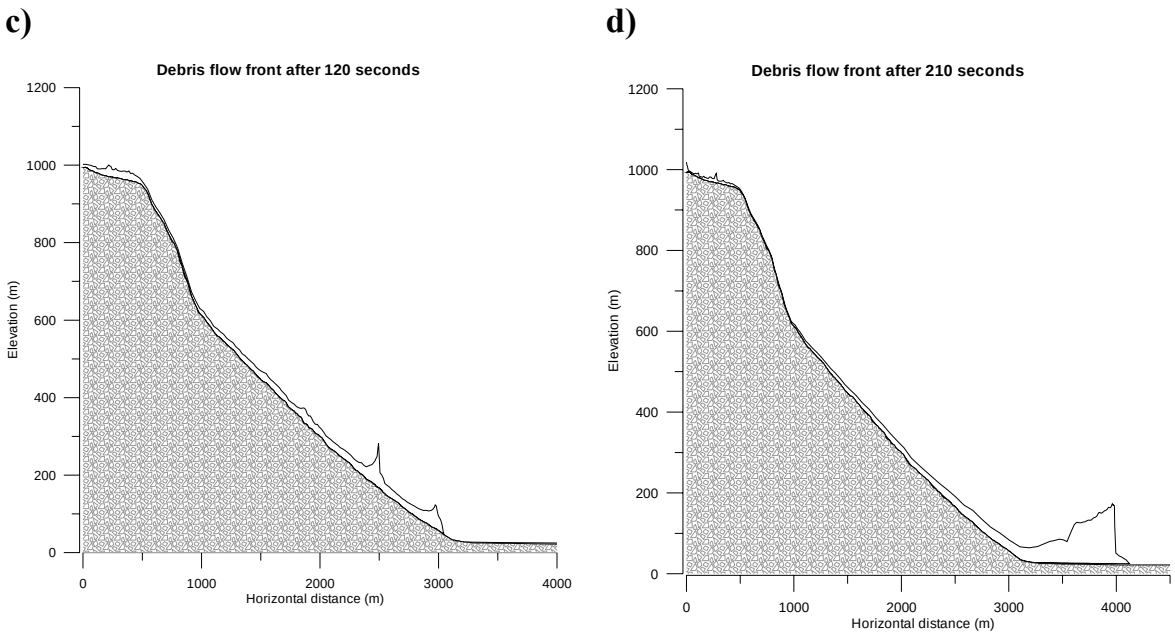

Figure 11.6 Debris flow front at different time steps. BING 2, yield strength 400 Pa. Not to scale. a)=20 s, b)=60 s, c)=120 s, d)=210 s.

11.5.3 Velocity

The figures show large oscillation in the velocity calculations throughout the track. These are to be commented in Section 11.7.

Velocities are generally lower when erosion is included than in a pure Bingham model of large volume (Figure 11.3 c and d and Figure 11.4 c and d). This is expected due to higher resistance. The velocity seems to increase with distance in BING 2 and 3, as opposed to the decrease with distance for runs without entrainment. Entrainment results in larger volume, but also in higher sediment concentration which in turn should slow down the flow.

Velocity is determined by slope angle but also by earth pressure and depth of flow. The velocity seems to be small just beneath the cliff. This may be due to the fact that the model predicts little mass to enter this area (small thickness, see Figure 11.4 b). The effect of this seems to be more important than the increased velocity due to the steep slope. Further down the track the large volume (thickness of flow) results in high velocities. Only one witness observation (guestimate) on velocity exists from the field (at the exit of the gully at elevation

100 m.a.s.l.), therefore a comparison and discussion of relative importance of these factors can not be made.

The average simulated velocity in BING 3 is around 15-20 m/s (54-72 km/h), which is slightly higher than the witness guestimate of 50 km/h. The velocity seems to increase with distance, and reaches a peak of 43 m/s just before the formation of a fan.

An almost immediate stop of the flow seems to occur in the simulation. This matches well with the farmers' descriptions of the event (see Section 2.1.).

11.5.4 Erosion and deposition

As seen from Figure 11.6 b, the modified BING models deposit sediments along the entire path due to the no-slip condition assumed. The debris flow front is high in the beginning (flat terrain) and becomes thinner where the terrain steepens. Due to erosion starting at the bottom of the cliff, the mass gets input of new material so that the flow does not stop due to thinning. A head can be recognised from the figures as the flow seems to be thickest in the front. A debris flow has a pulsating nature, but the background for the two peaks seen in C is unclear and may be due to numerical instabilities.

11.5.5 Depth of deposit

The model uses a width of track of 34 m, meaning that also the deposit area (fan) is 34 m wide. If spread over a larger area (fan is 75 000 m^2), the depth of the deposit and/or the run-out would decrease. The run-out lengths of the runs described in Figure 11.4 are all slightly longer than the actual observed run-out (fan). The yield strength used for BING 3 (friction case) is also very low, resulting in long run-out.

11.5.6 Erosion depth

The erosion depth estimates from BING 3 are close to the dataset presented in Chapter 9. The model is simple, but overall these estimates using Coulomb friction and entrainment (blue line, Figure 11.5) matches very well with the observed data and the data estimated from Surfer (dots, Figure 11.5). The erosion depth is around 3-4 m and decreases towards zero.

However, the distribution of erosion depth throughout the path differs slightly from what is seen in nature. From the Surfer estimates the depth is almost homogeneous from elevation 600 m.a.s.l., increasing slightly with distance, until an abrupt change towards deposition at elevation 90 m.a.s.l. (distance 2600 m). Both BING 2 and 3 however predict increase in erosion depth only for the first 500-1000 m of travel (depending on rheology), followed by an almost constant decrease towards zero erosion. This may be a result of the simulated erosion not depending on velocity. The point where no erosion occurs is also predicted at lower slope and elevation than observed in nature.

The modified BING-models predict erosion depth from the debris flow height and sine of slope angle. The slope angle is known at all times, flow height must however be calculated. The flow height is assumed to increase with travel distance and entrainment, which should give deeper erosion with distance. However, the slope angle decreases (see Figure 9.4). The combination of the two determines the erosion depth. As previously discussed (Chapter 9), the deep erosion observed in the end of the debris flow track can be explained by the volume of flow being of greater importance than the slope angle.

11.5.7 Feedback mechanism

The more erosion is occurring, the larger the volume of the flow gets. As seen above, the volume influences the velocity of the flow. Higher volume is seen to produce more erosion. It is also seen that velocity grows with increasing volume, and this is also expected to make the erosion grow.

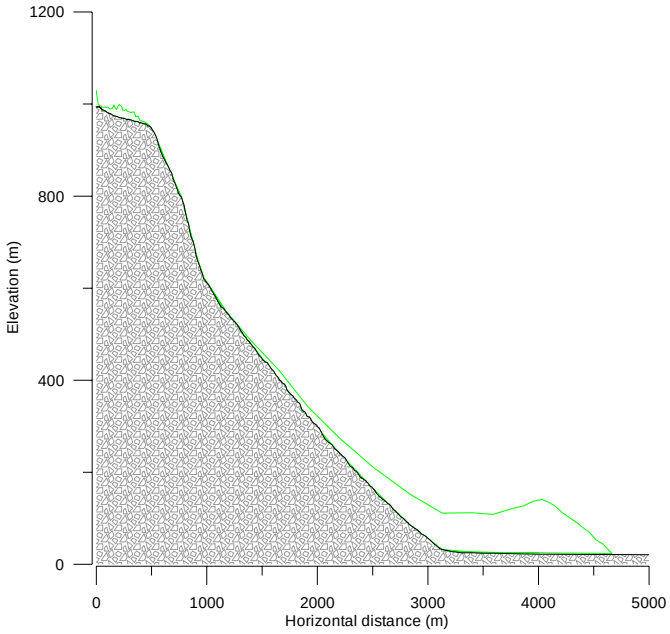

Figure 11.7

A 60 % higher erosion constant (c = 0.000008 instead of 0.000005) gives enormous volumes. This run is stopped after 4 minutes simulated time but will continue to flow and entrain. Not to scale.

An exponential increase in volume is observed in the numerical simulations when the critical shear rate for erosion approaches zero. This is the proposed reason for the extreme growth of debris flow mass reported by several authors (e.g. Hungr, McDougall and Bovis, 2005).

$$\tau = Hg\rho\sin\beta$$
$$\frac{dh}{dt} = c\left(\tau - \overline{\tau}\right) = \frac{dH}{dt} \qquad (11.8)$$

where H = thickness of flow

The behaviour with time:

$$H = \frac{\overline{\tau}}{\rho g \sin\beta}\left[H_0 - \frac{\overline{\tau}}{\rho g \sin\beta}\right]\exp\left[\rho g \sin\beta ct\right] \qquad (11.9)$$

when $\tau > \overline{\tau}$, else H is constant

11.6 Summary of results using different models

The results of the numerical modelling show that a pure Bingham flow of constant volume as small as 25 000 m^3 never will reach the fan area, although the yield strength is held very low. For an initial volume as small as the one found in Fjærland, entrainment is necessary to achieve long run-outs. A higher initial volume (100 000 m^3) would reach the fan area if the yield strength is held low enough (800 Pa). The velocity of a pure Bingham material, neglecting entrainment (BING 1), approaches a peak of 60 m/s in the precipice area, and it is from this point on decreasing due to the combination of loss of material and lowering of slope.

If including entrainment in the pure Bingham model (BING 2) from beneath the precipice (starting with an initial volume of 20 000 m^3), a flow of 2000 Pa will grow to 250 000 m^3 and deposit in the fan area. The velocities are generally lower than if there was no erosion. Lowest velocities are found at the cliff, increasing to 54 m/s with travel distance due to increased volume.

When also including Coulomb friction in the erosion model (BING 3), velocities are lowered even more. The erosion depth is however less than in BING 2. The material of 400 Pa yield strength (Bingham + friction) seems to act similarly to the BING 2 material of 2000 Pa yield strength.

This means that increased yield strength decreases run-out length whilst increased volume generally increases run-out length and velocity. Entrainment is found to be a very important factor for run-out length.

Decrease in slope generally lowers the velocity of flow. When entrainment is included the increase in volume however seems more important for velocity than slope angle does. When it comes to degree of erosion the numerical model predicts that slope angle influences the erosion more than volume does, and also that an eroding, pure Bingham material of low yield strength (BING 2) produces deeper erosion than a material including Coulomb friction (BING 3).

11.7 Uncertainties

Values for density and viscosity, as well as yield strength, must be assumed in the model. As no in situ measurements are done, neither during the debris flow nor during field work, these parameters contain a high degree of uncertainty. The fact that the parameters may change considerably during motion should also be taken into account. The grain size distribution is also not measured, but the soil sediment assumed is till. 1,8 g/cm^3 is used for density, according to the sediment/water distribution found in Section 8.8.

When implementing entrainment in the model, also parameters like yield strength should vary throughout the track (mostly grow with distance). The model however uses constant yield strength.

Another problem is the continuous flood of water coming from behind throughout 45 minutes. The aspect of time is not treated any further in the thesis, but the erosion constant should probably be decreased when considering the long duration of the event.

Modelling deposition is a problem in itself due to the fact that the model is two-dimensional. This means that 3D effects and topography are not taken into account. Especially deposition is influenced by this. As discussed in Chapter 9, the exit of a gully is, in addition to slope and volume, a very important factor for deposition. The spreading of the material can not be simulated in this model. The computed height of the deposit is therefore also incorrect, since the deposit can spread only over the 34 m average width.

The velocity is seen to oscillate a great deal. This may have several explanations, for instance computational instability and the rough topography. The latter means that the sine of β oscillates, giving also an oscillating velocity. It might give a better picture to make a smoothing (average) of the topography. Debris flows are known to have a pulsating flowing behaviour. The oscillations observed in the numerical modelling can most probably not be related to this phenomenon.

As mentioned, this erosion model does not include velocity.

11.8 Velocity estimate based on ballistic stones

Considering that stones have been found 20 m outside the main track (ballistic stones), obviously thrown through the air, an attempt estimating the velocity of the flow at the point of "take-off" has been made. Clearly, some assumptions are necessary. The stone is assumed to be thrown from the flow at an angle of 45 degrees, both upwards and in the direction of flow (see Figure 11.8 and Figure 11.9). The forest in the area is fairly dense and this suggests that the stones are likely to have been thrown upwards over the trees to reach a distance of 20 m.

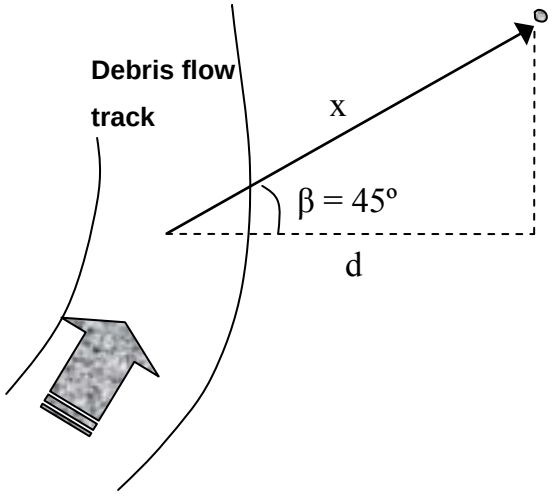

Figure 11.8 Illustration of angle at which stones are thrown from the main flow.

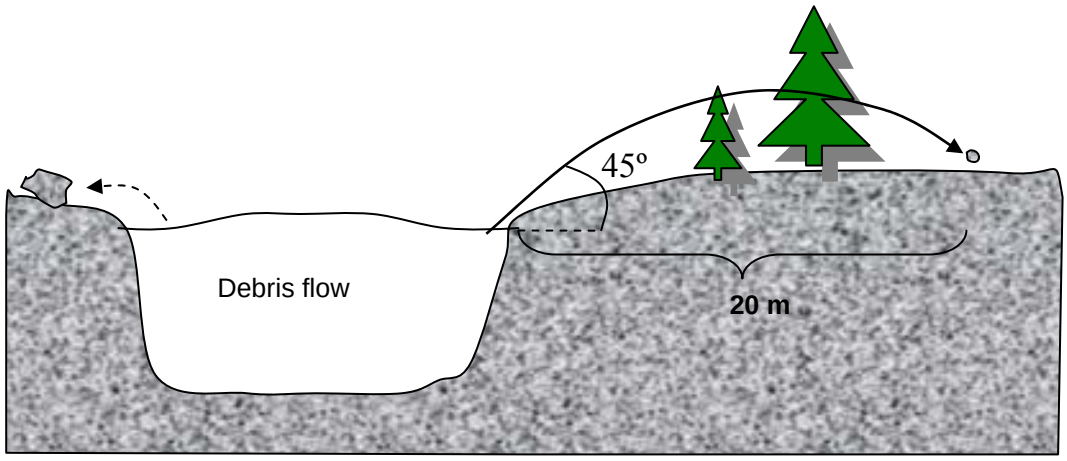

Figure 11.9 Illustration of how ballistic stones may have been thrown 20 m out of track.

Using Newton's equations for the motion of the stone in the gravity field, the velocity is found:

$$v_0 = \sqrt{g \cdot d / \cos\beta}$$
$$v_0 = \sqrt{10 \cdot 20 / \cos 45} = 16,8 \qquad (11.10)$$

This is the velocity of the ejected stone. If the velocity of the stone is comparable to the velocity of the debris flow, we find that the velocity at the point (just before entering the fan) should be 16.8 m/s, or 60 km/h. This fits surprisingly well with the witness guestimate of velocity (50 km/h).

Most probably the stones have been thrown out of the stream due to inelastic collisions and fracturing as discussed in Chapter 2. This may implicate that the velocity of the stone may not have the same velocity as the main flow. This would require a rather different method of analysis to arrive at an estimate of debris flow velocity, and will not be attempted here.

For derivation of equation 11.10, see Appendix F.

12. Mitigation measures

Run-out of a future debris flow in Fjærland of the same size as the 2004-event, will be affected by the present fan as the terrain has been changed by the deposits. Presently, the trees are removed in the fan area, which means that a new flow would move easier. The deposit may lead a new flow further before it starts to deposit, but it could also stop the flow due to the presence of larger boulders and an open grain structure. Whether the present fan itself is enough for catching new debris is not known, but it is probable that events of similar or greater magnitudes will overrun the fan. In that case, mitigation measures should be taken.

To prevent damage from debris flows, there are in general different countermeasure alternatives (Schuster, 2000):

- Avoidance – probably the most effective alternative. Avoid developing and house building in the area at risk.
- Reduction of downstream effects – build retention structures, like check dams that entrap material, and are designed in such a way that water escapes. Build deflecting structures to lead the flow in desired direction. Can be combined with debris basins. A debris basin will trap most of the material (see Figure 12.2).

If an outburst flood from a dam is involved:

- Prevention at dam – many alternatives: Build erosion protection like armouring. Excavation of channel spillway or diversion tunnel. Build check dams on the dam to reduce the velocity of the flow. Install pumps to lower the lake level, as was temporarily chosen in the case of Val Pola until an outlet tunnel was built.

To avoid a rainfall-induced debris flow is not easy, but awareness when building roads and drainage can reduce the probability of occurence. Vegetation can act in a stabilising way. Plant roots increase soil strength (Turner, 1996), acting like reinforcement in the soil and binding unstable soil to more stable layers. However, roots can also act in the opposite direction (Turner, 1996), to enhance instability. Especially succulent plants absorb great quantities of water, adding weight to the soil. Roots can also contribute to further weathering of the soil.

The building of a retention and defelcting wall has been started on the downstream side of the Fjærland fan. This is thought protecting the farm and farmland from flowing water and fine material. Coarser material will be sedimented in the fan area. If a future event is a fully grown and high magnitude debris flow running further than the event of 2004, the structure would most probably fail and the flow pass over.

To catch the high energy coarse masses, a large catchment area would be needed. Another possibility could be to build sedimentations basins, but these are expensive and material sedimented need to be removed from time to time. The field observations also point towards very high energy of the flowing masses.

Figure 12.1 Retention and deflecting dam being built between the fan and the farm Øygard. Photo taken May 2005.

Figure 12.2 Deflecting dam for a debris flow built in Hardanger, Norway. Notice basin and drainage opening.

13. Conclusions and recommendations

This thesis highlights the problems related to the physics involved in a debris flow and attempts to study the factors controlling erosion and entrainment through the recent debris flow in Fjærland, Western Norway, caused by a natural dam breach. The main goal of the study has been to provide a thorough documentation of the event, and for this purpose, field work, interviews with eyewitnesses and terrain modelling have been employed. An attempt of numerical modelling of the case has been performed in cooperation with Dr. DeBlasio of ICG, using an extended version of the rheological model BING, including Coulomb friction and erosion. The results and conclusions of the work are summarised below.

13.1 Conclusions

The study reveals the importance of volume growth through bulking and the development of grain-to-grain contact in originally very water-rich flows.

Erosion and entrainment of bed material is seen to be very important for run-out length and velocity of a debris flow. Among the aspects mostly determining erosion, the volume of the flow has been found to be especially important. In this study a feedback mechanism, poorly treated in previous literature, is recognised. The phenomenon is also seen in the numerical modelling and may be part of the reason why debris flows often grow so much and reach long run-outs. In this case study there is seen little dependence on slope angle (above a certain value), but this may be due to the fact that the slope angles throughout the main part of the erosion track only vary between 15 and 20º.

Deposition however, seems to be determined largely by slope angle. In Fjærland deposition starts at 12º, and all boulders are settled before the slope reaches 4º. Erosion seems not to appear where the slope is below 12º, but also 3D topography plays a role. Channelisation of the flow may increase the run-out and reduce the angle of deposition, as well as the exit of a gully favours spreading and deposition.

Erosion due to the debris flow in Fjærland was extreme; the mass volume growing with a factor of ten, from around 25 000 m^3 to around 240 000 m^3 (+/- 10 %) in less than an hour.

The large amounts of water involved and the huge bouldery deposit, as well as the finer sediments inundating the lower farmland, are evidences of the complex dynamics of this type of mass movement. Large boulders and fractured blocks found 20 m off the main track point towards a significant grain-to-grain contact and collision impact during the flow. However, the ratio of the different forces involved varied with time, distance and depth of the flow.

The BING-model has been modified to include both Coulomb friction and entrainment, but due to the complexity, numerous simplifications had to be introduced. The model predicts a run-out, erosion depth and volume very similar to what is seen in field. The results seem promising, but the velocity estimates may be too high, based on witness accounts. The velocities are also oscillating, maybe due to instability in the numerical computations. The problem of varying material properties of the mass throughout the event also needs further studies.

For mitigation work, an important problem in the use of a model like the modified BING, is to find the right erosion constant. This will depend on several factors, bed material's erodibility being one of them. The application of the model to more case studies would be fruitful in this process.

The debris flow event in Fjærland seems to be a result of the combination of heavy melting on the glacier, insufficient opening of drainage channels, and erodible downstream material. The melting of an ice core in the moraine ridge may also have weakened the dam, facilitating breaching. There is historical evidence that the normal drainage route for the glacial lake is through yearly opening of channels towards the icefall in Supphella. When such channels do not open, a filling of the lake and a breach of the dam is unavoidable. Earlier floods from the lake through Tverrdalen towards Supphelledalen (drainage route of the 2004-event) have happened twice during the last 100 years.

The breach in the moraine ridge will be filled by sliding and instability of the breach walls, making the water level of the lake rise again. Future flooding events will occur, and a possible global warming could accelerate their frequency. A significant withdrawal of the glacier could however reveal possibilities for new drainage routes.

The potential bulking material along the path will be a limiting factor for the magnitude of future events. Large amounts of the till material is taken out by the 2004-flow, but the bed is not depleted. Also the fresh unstable walls of the gully may accelerate erosion if a new flow occurs.

In a human perspective the magnitude of a new flow will probably be less than the 2004-event. Historical evidence also points towards the 2004-event being one of the largest that has occurred at this site. The fan area should however be kept to serve as a catchment area for a possible flow of new coarse material, whilst finer deposits may be led away from the farmland by a deflecting dam.

13.2 Personal experience and further work

Problems encountered during the thesis work were several, and mainly related to the terrain modelling process. A time frame of 5 months has delimited the accuracy of the terrain models used. This accuracy may be increased by manual effort, and field measurements of erosion depth at intervals throughout the gully could provide cross-validation of the volume estimates. Manual field measurements of control points could also make the laser data applicable to a greater extent. When considering what controls debris flow erosion and debris flow growth, a study of the effect of velocity and grain size on erosion, is recommended.

As no adequate model for erosion and entrainment exists, this will be the focus of later work. Experimental studies are planned in this perspective, to provide insight into the physics of mass flows and to serve as the basis for numerical modelling. The Fjærland case may be used to “calibrate” the suitability of the numerical model.

As mentioned, a field investigation of the moraine ridge is planned in June 2005, making use of geophysical measuring techniques for the purpose to discover whether the ridge is ice cored. This may be important in the evaluation of the risk of future events, as well as provide knowledge useful for investigation of similar areas. Dating (for instance C-14) of the discovered old debris flow deposits in the valleys Tverrdalen and Supphelledalen would also be important in the estimation of debris flow frequency.

13.3 Applicability to other sites

Global warming causes glaciers to melt and accelerates the frequency of storms. Especially in the Himalayas and Alps, events similar to the Fjærland event will occur. Steep slopes of many expanding cities worldwide are however very prone to similar debris flows induced by flash floods. These events are expected to represent an even greater threat.

The case of Fjærland may be applied to a variety of other sites where the release of water in elevated areas may be a hazard resulting in massive erosion and impact downstream, and the general findings are applicable to many types of debris flows. This case study will hopefully provide help in the recognition of similar hazards, as well as in the planning of hazard zoning and mitigation measures.

References

Aarseth, I., Bogen, J., Holtedahl, H., Klakegg, O., Nesje, A., Rye, N., Orheim O., and Roland, E., 1988. *Glaciology, hydrology and glacial geology around Jostedalsbreen*. A field guide to excursion 10 September – 13 September 1988 organized in conjunction with symposium on snow and glacier research relating to human living conditions. Ed: Olav Orheim. NVE and Norsk Polarinstitutt, Oslo.

Andreassen, L., Elvehøy, H, Kjøllmoen, B., 2004. *Glaciological investigations in Norway in 2004*. Report no 2 2005, ed: Kjøllmoen, B.. Norwegian Water resources and Energy Diroctorate. p 90.

Armanini, A., Fraccarollo, L., Guarino, L., Martino, R., Bin, Y., 2000. Experimental analysis of the general features of uniform debris flow over a loose bed. In *Proceedings of the second international conference on Debris–flow Hazard Mitigation: Mechanics, Prediction, and Assessment*, pp. 327-334. Eds. Wieczorek, G.F., Naeser, N.D. Balkema, Rotterdam.

Aschehoug og Gyldendals Store Norske Ettbinds Leksikon, 2004. Eds: Smith-Meyer, T., Reisegg. Ø.. Kunnskapsforlaget, Oslo.

Ayotte, D. and Hungr, O., 2000. Calibration of a runout prediction model for debris-flows and avalanches. In *Proceedings of the second international conference on Debris–flow Hazard Mitigation: Mechanics, Prediction, and Assessment*, pp. 505-514. Eds. Wieczorek, G.F., Naeser, N.D. Balkema, Rotterdam.

Barstad, B., 2002. Høgdekartlegging med laserskanning frå fly. Institutt for kartfag, NLH. Kartdagane 2002, Oslo.

Barstad, B., 1998. Datafangst for Terreng modellering med Digital fotogrammetri. Fjellanger Widerøe. Foredrag på Forum for fotogrammetri og fjernmåling, 3. og 4. desember 1998.

Bozhinskiy, A.N., Nazarov, A.N., 2000. Two-phase model of debris-flow. In *Proceedings of the second international conference on Debris–flow Hazard Mitigation: Mechanics, Prediction, and Assessment*, pp. 263-269. Eds. Wieczorek, G.F., Naeser, N.D. Balkema, Rotterdam.

Chau, K.T., Chan, L.C.P., Luk, S.T., Wai, W.H., 2000. Shape of deposition fan and runout distance of debris-flow: Effects of granular and water contents. In *Proceedings of the second international conference on Debris–flow Hazard Mitigation: Mechanics, Prediction, and Assessment*, pp. 387-395. Eds. Wieczorek, G.F., Naeser, N.D. Balkema, Rotterdam.

Chen, H., Lee, C.F., Shen, J.M., 2000. Mechanisms of rainfall-induced landslides in Hong Kong. In *Proceedings of the second international conference on Debris–flow Hazard Mitigation: Mechanics, Prediction, and Assessment,* pp. 53-60. Eds. Wieczorek, G.F., Naeser, N.D. Balkema, Rotterdam, 2000.

Clague, J.J., Evans, S.G., 2000. A review of catastrophic drainage of moraine-dammed lakes in British Columbia. *Quaternary Science Reviews* 19 (2000), pp. 1763-1783.

Courivaud, J-R., Lempérière, F., Fry, J-J., 2004. Modelling of Breach formation and Progression. *Proceedings from the International Seminar on Stability and Breaching of Embankment Dams*, Oslo, Norway, 21-23 October, 2004.

Cruden, D, M., Varnes, D., J., 1996. Landslide types and Processes. In *Landslides – Investigation and Mitigation*, Special Report 247, Tansportation Research Board, National Research Council. National Academy Press, Washington D.C., pp. 36-75.

Elvehøy, H., NVE, 2005. Pers. comm., 16.02.2005.

Franca, M.J, Braunschweig, F., Almeida, A.B., 2004. RoDaB: dam breaching model with different breach simualtion methodologies. *International Seminar on Stability and Breaching of Embankment Dams*, Oslo, Norway, 21-23 October, 2004.

Genevois, R., Tecca, P.R., Berti, M., Simoni, A., 2000. Debris-flows in the Dolomites: Experimental data from a monitoring system. In *Proceedings of the second international conference on Debris–flow Hazard Mitigation: Mechanics, Prediction, and Assessment*, pp. 283-291. Eds. Wieczorek, G.F., Naeser, N.D. Balkema, Rotterdam.

Haldorsen, S., 1983. The characteristics and genesis of Norwegian tills. In *Glacial deposits in North-West Europe*, pp 11-18. Ed. Ehlers, J., A.A. Balkema, Rotterdam.

Hambrey, M.J., 1994. *Glacial environments*, pp. 33-80. UCL Press Limited, London.

Hansson, G., Cook, K., 2004. Determination of material rate parameters for headcut migration of compacted earthen materials. *Proceedings from the International Seminar on Stability and Breaching of Embankment Dams*, Oslo, Norway, 21-23 October, 2004.

Huerta, D.A., Ruiz-Súarez, J.C., 2004. Vibration-Induced Granular Segregation: A Phenomenon Driven by Three Mechanisms. *Physical Review letters*, vol 92, number 11, pp. 114301-1 – 114301-4.

Huggel, C., Kääb, A., Salzmann, N., 2004. GIS-based modeling of glacial hazards and their interactions using Landsat-TM and IKONOS imagery. *Norsk Geografisk tidsskrift – Norwegian Journal of Geography,* Vol. 58, pp. 761-73.

Hungr, O., 2000. Analysis of debris flow surges using the theory of uniformly progressive flow. *Earth Surface Processes and Landforms*, 25 (2000), pp. 483-495.

Hungr, O., McDougall, S., Bovis, M., 2005. Entrainment of material by debris flows. In *Debris-flow Hazards and Related Phenomena*, pp. 135-158. Eds. Jakob, M. and Hungr, O.. Praxis Publishing Ltd, Chichester, UK.

Hungr, O., Morgan, G.C., Kellerhals, R., 1984. Quantitative analysis of debris torrent hazards for design of remedial measures. *Canadian Geotechnical Journal*, 21, pp. 663-677.

Hyyppä, J., Pyysalo, U., Hyyppä, H., Samberg, A., 2000. Elevation Accuracy of Laser scanning-derived digital terrain and target models in forest environment. *Proceedings of EARSeL-SIG-Workshop LIDAR*, Dresden/FRG. EARSSeL eProceedings No. 1, pp. 139-147.

Høeg, K., 2004. Lecture in Landslides and mass transport, GEO 4170, UiO, Norway.

Høeg, K., Løvoll, A., Vaskinn, K.A., 2004. *Stability and breaching of embankment dams: field test on 6 m high dams. The International journal on Hydropower and Dams,* Issue 1, 2004. Aqua –Media International Ltd.

Imran, J, Harff, P., Parker, G., 2001. A numerical model of submarine debris flows with graphical user interface. *Computers and Geosciences*, 27, pp. 717-729.

Iverson, R.M., 1997 a. The physics of debris flows. *Reviews of Geophysics*, 35, 3 / August 1997, Paper number 97RG00426. pp. 245-296. (a)

Iverson, R.M., 1997 b. Hydraulic modelling of unsteady debris-flow surges with solid-fluid interactions. In *Proceedings of first international conference on Debris–flow Hazard Mitigation: Mechanics, Prediction, and Assessment*, pp. 550-560. Ed. Cheng-Iung Chen. American Society of civil Engineers (ASCE), New York. (b)

Iverson, R.M., 2003. The debris-flow rheology myth. In *Proceedings of third international conference on Debris–flow Hazard Mitigation: Mechanics, Prediction, and Assessment*, pp. 303-314. Ed. Dieter Rickenmann and Cheng-Iung Chen. Millpress, Rotterdam.

Iverson, R.M., Denlinger R.P., LaHusen, R.G, Logan, M., 2000. Two-phase debris-flow across 3-D terrain: Model predictions and experimental tests. In *Proceedings of the second international conference on Debris–flow Hazard Mitigation: Mechanics, Prediction, and Assessment*, pp. 521-529. Eds. Wieczorek, G.F., Naeser, N.D. Balkema, Rotterdam.

Iverson, R.M., LaHusen, R.G., 1993. Friction in Debris Flows: Inferences from Large-scale Flume Experiments. In *Hydraulic engineering, Proceedings of the 1993 ASCE Conference*, pp. 1604 – 1609.

Iverson, R.M., Reid, M.E., LaHusen, R.G., 1997. Debris-flow mobilization from landslides. *Annu Rev. Earth Planet. Sci*., 25. pp. 85-138.

Iverson, R.M., Vallance, J.W., 2001. New views of granular mass flow. *Geology*; February 2001; v. 29; pp. 115-118.

Jakob, M., Anderson, D., Fuller, T., Hungr, O., Ayotte, D., 2000. An unusually large debris flow at Hummingbird creek, Mara Lake, British Columbia. *Canadian Geotechnical Journal*, 37, pp. 1109-11025.

Johnson, A.M., 1984. Debris flow, in *Slope Stability*, Eds: D.Brunsden and D.B. Prios, Wilwy, New York, pp. 257-290.

Jørgensen, P., Sørensen, R., Haldorsen, S., 1997. *Kvartærgeologi*, Landbruksforlaget, Otta, 248 p.

Knight, J.B., Jaeger, H.M., Nagel, S.R., 1993. Vibration-Induced Size Separation in Granular Media: The Convection Connection. *Physical Review Letters*, vol 70, number 24, pp. 3728 – 3731.

Laigle, D., 1997. A two-dimensional model for the study of debris-flow spreading on a torrent debris fan. In *Proceedings of first international conference on Debris–flow Hazard Mitigation: Mechanics, Prediction, and Assessment*, pp. 123-132. Ed. Cheng-Iung Chen. American Society of civil Engineers (ASCE), New York.

Some of the original ideas of the above paper found in:

Coussot, P., 1992. Rheologie des laves torrentielles. Thèse de Doctorat de l'Institute National Polytechnique de Grenoble, France, C.E.M.A.G.R.E.F., collection Etude, série Montagne n. 5, 415 p.

Lambe, P.C., 1996. Residual soils. In *Landslides – Investigation and Mitigation*, Special Report 247, Tansportation Research Board, National Research Council. National Academy Press, Washington D.C., pp. 507-524.

Lambe, T.W and Whitman, R.V., 1979. *Soil Mechanics*, Wiley Series in Geotechnical Engineering, pp. 406-412. John Wiley and Sons, New York.

Liestøl, O., 1989. Kompendium i Glasiologi. *Meddelelser fra Geografisk institutt, Universitetet i Oslo. Naturgeografisk serie*. Rapport nr. 15. pp. 79-86.

Liestøl, O., 1995. Kompendium i Glasiologi. *Meddelelser fra Geografisk institutt, Universitetet i Oslo. Naturgeografisk serie*. Rapport nr. 3. 111 p.

Lin, M.L., Chang, B.S., 2003. Triggering of debris flow caused by groundwater upwelling and surface runoff. In *Proceedings of third international conference on Debris–flow Hazard Mitigation: Mechanics, Prediction, and Assessment*, pp. 327-338. Ed. Dieter Rickenmann and Cheng-Iung Chen. Millpress, Rotterdam.

Martino, R., 2003. Experimental analysis on the rheological properties of a debris-flow deposit. In *Proceedings of third international conference on Debris–flow Hazard Mitigation: Mechanics, Prediction, and Assessment*, pp. 363-373. Ed. Dieter Rickenmann and Cheng-Iung Chen. Millpress, Rotterdam.

Meteorological Institute, 2003.

http://met.no/met/klima_2050/forskning/permafrost_norge.html. Visited 15.03.05.

Mueth, D. M., Jaeger, H.M., Nagel, S.R., 1998. Force Distribution in a Granular Medium. *Physical Review* E57, 3164.

National Geographic, 1998. http://www.nationalgeographic.com/xpeditions/atlas/index.html. Visited 09.05.05.

Nesje, A., 1995. *Brelære*. Høyskoleforlaget AS, Kristiansand. 118 p.

Norsk Bremuseum, 2005. http://www.bre.museum.no. Visited 10.02.05

NVE (Norwegian Water resources and Energy Administration), 2005.

http://www.nve.no/modules/module_109/publisher_view_product.asp?iEntityId=5268. Visited 24.02.2005.

Orheim, O, 1968. Store Supphellebre – En glasiologisk undersøkelse. Hovedoppgave i kvartærgeologi og geomorfologi, UiB.

Paterson, W.S.B., 1994. *The Physics of glaciers*, pp. 8-25 and pp.103-131. Butterworth-Heinemann, Elsevier Science, Oxford.

Pickert, G., Jirka, G.H., Bieberstein, A., Brauns, J., 2004. Experiments on overtopped homogeneous embankments: Soil/water interaction and breach development. *Proceedings from the International Seminar on Stability and Breaching of Embankment Dams*, Oslo, Norway, 21-23 October, 2004.

Pierson, T.C., 2005. Hyperconcentrated flow – transitional process between water flow and debris flow. In *Debris-flow Hazard and Related Phenomena*, pp. 159-202. Eds. Jakob, M. and Hungr, O.. Praxis Publishing Ltd, Chichester, UK.

Remaître, A., Malet, J.-P., Maquaire, O., 2003 a. Study of a debris-flow event by coupling a geomorphological and a rheological investigation, example of the Faucon stream (Alpes-de-Haute-Provence, France). In *Proceedings of third international conference on Debris–flow Hazard Mitigation: Mechanics, Prediction, and Assessment*, pp. 375-385. Ed. Dieter Rickenmann and Cheng-Iung Chen. Millpress, Rotterdam. (a)

Remaître, A., Malet, J.-P., Maquaire, O., Laigle, D., Ancey, C., Locat, J., 2003 b. Torrential hazard assessment using a debris-flow runout model. The case of the Faucon stream. In *Fast slope movements – Prediction and Prevention for risk mitigation*, pp. 445-451, ed. Picarelli, L., Patron Editore, Bologna. (b)

Savage, S.B., Iverson, R.M., 2003. Surge dynamics coupled to pore-pressure evolution in debris flows. In *Proceedings of third international conference on Debris–flow Hazard Mitigation: Mechanics, Prediction, and Assessment*, pp. 503-514. Eds. Dieter Rickenmann and Cheng-Iung Chen. Millpress, Rotterdam.

Schieh, C.-L., Tsai, Y.-F., 1997. Experimental study on the configuration of debris flow fan. In *Proceedings of first international conference on Debris–flow Hazard Mitigation: Mechanics, Prediction, and Assessment*, pp. 133-142. Ed. Cheng-Iung Chen. American Society of civil Engineers (ASCE), New York.

Scott, K.M., 2000. Precipitation-triggered debris-flow at Casita Volcano, Nicaragua: Implications for mitigation strategies in volcanic and tectonically active steeplands. In *Proceedings of the second international conference on Debris–flow Hazard Mitigation: Mechanics, Prediction, and Assessment*, pp. 3-13. Eds. Wieczorek, G.F., Naeser, N.D. Balkema, Rotterdam.

Schuster, R.L., 2000. Outburst debris-flows from failure of natural dams. In *Proceedings of the second international conference on Debris–flow Hazard Mitigation: Mechanics, Prediction, and Assessment*, pp. 29-42. Eds. Wieczorek, G.F., Naeser, N.D. Balkema, Rotterdam.

Shinbrot, T., 2004. The brazil nut effect – in reverse. *Nature*, vol 429, 27 May 2004, pp. 352-353.

Statens Kartverk, 1:50000, Topografisk hovedkartserie M 711, blad 13171.

Takahashi, T., 1991. *Debris flow*. IAHR Monograph Series. Rotterdam: Balkema. 152 p.

Takahashi, T., 2000. Initiation and flow of various types of debris-flows. In *Proceedings of the second international conference on Debris –flow Hazard Mitigation: Mechanics, Prediction, and Assessment*, pp. 15-25. Eds. Wieczorek, G.F., Naeser, N.D. Balkema, Rotterdam.

Tarantino, A., Bosco, G., 2000. Role of suction in understanding the triggering mechanisms of flow slides associated with rainfall. In *Proceedings of the second international conference on Debris–flow Hazard Mitigation: Mechanics, Prediction, and Assessment*, pp. 81-88. Eds. Wieczorek, G.F., Naeser, N.D. Balkema, Rotterdam.

Terzaghi, K., Peck, R.B., Mesri, G., 1996. *Soil Mechanics in Engineering Practice*, Third Edition. John Wiley & sons, Inc, New York, p. 375.

Tognacca, C., Bezzola, G.R., 1997. Debris-flow initiation by channel-bed failure. In *Proceedings of first international conference on Debris–flow Hazard Mitigation: Mechanics, Prediction, and Assessment*, pp. 44-53. Ed. Cheng-Iung Chen. American Society of civil Engineers (ASCE), New York.

Tognacca, C., Bezzola, G.R., Minor H.-E., 2000. Threshold criterion for debris-flow initiation due to channel-bed failure. In *Proceedings of the second international conference on Debris –flow Hazard Mitigation: Mechanics, Prediction, and Assessment*, pp. 89-98. Eds. Wieczorek, G.F., Naeser, N.D. Balkema, Rotterdam.

Turner, K., 1996. Colluvium and Talus. In *Landslides – Investigation and Mitigation*, Special Report 247, pp. 525-549. Tansportation Research Board, National Research Council. National Academy Press, Washington D.C.

Turton, D., Jonas, D., 2005. Airborne Laser Scanning – Cost effective spatial data. www.gisdevelopment.net/technology(rs/ma03001pf.htm. Visited 10.03.2005.

UNEP, 2005, United Nations Environmental Programme.

http://www.unep.org/Documents.Multilingual/Default.asp?DocumentID=245&ArticeID=3042&l=en

http://www.grida.no/inf/news/news02/news30.htm. Visited 10.05.05.

Watanabe, T., Ives, J.D., Hammond, J.E., 1994. Rapid growth of a glacial lake in Khumbu Himal, Himalaya: Prospects for a catastrophic flood. *Mountain Research and Development*, Vol. 14, no. 4, pp. 329-340.

Østrem, G., Selvig, K. D., Tandberg, K., 1988. *Atlas over breer i Sør-Norge*. Meddelelse nr 61 fra Hydrologisk avdeling, NVE, p. B-92.

Appendices

Appendix A – Witness observations

A1 – Interviews with eyewitnesses
A2 – Description of debris flow event by Ingebrigt Supphellen
A3 – Diary of Eirik Øygard, 1947 debris flow event

Appendix B – Terrain profiles

B1 – Length profile
B2 – Cross profiles

Appendix C – Water volume estimates

Appendix D – Sediment volume estimates

D1 – Elevation change from 2001 to 2004
D2 – Grid volume computations

Appendix E – Gridding reports

E1 – Aerial photo 2001
E2 – Aerial photo 2004
E3 – Laser 2004
E4 – Economical map 1:5000

Appendix F – Dynamics of debris flows

F1 – Basic mechanics
F2 – Dynamical models
F2 – Velocity estimation based on ballistic stone

Appendix A

Witness observations

Used for the reconstruction of the debris flow event in Fjærland, May 8 2004 and the recognition of earlier events.

A1 – Interviews with eyewitnesses

Ingebrigt Supphellen

- It started around one o'clock in the afternoon, 8 May 2004. I had been to the petrol station down in Fjærland to tank diesel, and drove directly to my son's house at Øygardsneset, one of the outermost farms in the valley of Supphelledalen, located 2 km from the fan area. I have a receipt from the petrol station showing that I paid for the diesel at 12:47. The distance between the station and Øygardsneset is a few kilometres, and I guess it would take me around 3 minutes to drive to the farm.

The view towards the cabin Flatbrehytta, the valley Tverrdala and the farm Øygard is superb from his son's house, so Ingebrigt Supphellen saw everything except the break of the moraine.

- As I stepped out of the car I heard a roaring sound and felt the ground shake. I turned around - immediately I thought it came from the mountainside at the other side of the river, where it slides are common, especially in winter. As I saw nothing I turned towards the inner part of the valley, where the glacier Supphellebreen often calves. The runup can go over the valley towards the opposite mountainside, causing ground motion and a roaring sound. Then, suddenly, I saw the fountain, black as rock, from the precipice at the cabin Flatbrehytta.

His son Ingvar was at the other side of the river, in a tractor with his two children. Ingebrigt tried to signalize and shout. Ingvar heard the sound of the torrent.

- At first he thought it was something wrong with his tractor, because he was at the bridge. If he has a load on his tractor he has to drive it in reverse to get over the bridge. With one kid under each arm he ran towards the house to save himself and the children. Well inside the house he called the police.

- From the time when I saw the fountain it took a little bit less than half an hour before a huge black front, higher than the tree-tops, speeded down. I thought it took such a long time before I saw anything, so I hoped that nothing was going to reach the valley this time. I would say that the front was between 10-20 meters high, but nearer 10 than 20, steeper than 45º, and had a velocity of around 50 km/h. The slope of the front became gentler as it approached the fan area. The fountain of black water at the precipice was visible for about 2 hours, but with uneven intensity.

- The stones came first, the water afterwards. The entire time one could hear the sound of breaking trees through the roar. The river was thick because of the trees, almost as I could walk over it. Luckily, the weather was warm, the snowmelt rapid and the river huge, so that the trees were transported out in the fjord instead of blocking the river. A few days before the event, the glacier had been very active and calved more than usual. The spring was early and sudden.

Ingebrigt remembers a smaller slide in 1947, where the river was divided into two parts and two bridges were built.
- The road was damaged, but the stones that came down were much smaller than was the case now. Anyway, they were big enough for us to need a stump puller. I helped cleaning the road and fields for stones, and also raising the bridge. This was done so that we did not need to

remove all the stones. So the road had to slope steeply upwards to the bridge. I know for sure that it was the moraine ridge that failed this time also. A now dead relative of mine, Mikkel Supphellen, told me that the river from the glacier Supphellebreen was smaller than normal at this moment.

There was also a slide 80 years ago which he has heard about, but do not have any detailed information about.
- In the 1700's though, a huge slide in the same area resulted in the people at the nearest farm Øygard abandoning the area. They left because they feared new slides or because they did not have the equipment to clean up and start farming again. This must be the origin of the name Øygard, as Øygard means abandoned farm. The farm is also called Rødseter in some maps, so that might be the original name.

Ingvar Supphellen, son of Ingebrigt

- I was at the other side of the river, in my tractor and with my two kids. I heard the roaring sound when I was at the bridge, and since it is possible that the tractor can overturn, I thought something was happening to the tractor. I jumped out, and as I turned around I saw the fountain from the precipice. Then mud speeded through the forest and splashed between the trees without damaging them. Here are often a lot of tourists in the area, so I ran inside to call the police. As I was on the phone talking to them, through the window I saw the front coming down in the valley. I know the time was 13:02; I got the time from the police. My father came here approximately ten minutes to one, and the slide started immediately after that. The duration of the whole thing was about one and a half hour. As the volume started to reduce, it reduced quite quickly. The front was high and stable until it approached the fan area, and then suddenly collapsed and stopped. The first wave was the biggest; afterwards smaller pulses came, shifting from one side of the fan to the other. I called the police again when the mud passed our house to tell we were ok.

Hans Jørgen Øygard was in the forest at the time, in the track of the flow, cutting timber.
- He heard the sound and felt the ground shake, through ear guards and helmet! He did not know what or where the sound came from, but he knew he had to run. He found a tractor and drove down to us.

Ingvar got a lot of mud on his fields due to the flow.
- 10000 m^3 I have removed. My fields were inundated by 60 cm (at the cowshed) of mud. There was only mud and no sand on my property. The work was difficult, because it was impossible to walk on the material for several days and it turned liquid as you disturbed it. But as we tested the mass it turned out to be very fertile, so I have used it on my farming land. Now I can say that for me this event has been positive. It is a fact that the farms downstream Tverrdøla and the fan are much more fertile than the farm Supphella further in the valley. That must mean that something is happening here from time to time.

He says that during the event of 1947 no stones reached the valley. Ingvar was not born at the time.
- At least nothing reached my fields. That means that the event must have been smaller than the 2004-event. There are tales that the farm Øygard was abandoned during the 1700's due to a big slide. If their fields were hit they probably could not use the land for years.

Per Christian Liseter

Liseter lives on the opposite side of the slide, on the upstream side of the fan, and owns parts of the river that was damaged in the event.

- I sat outside reading for my exam when the ground started to shake and a roaring sound was heard. My first reaction was to look over the river, to the opposite mountainside, as slides and rock falls are common there. Another possibility was that the glacier was calving. As I turned around I saw a few stones flying through the air, over the house and over the electricity wire further down. I did not know where they came from, so I was a bit afraid. I called my daughters; they were in Fjærland, to tell them to stay until I knew anything more. Then I just ran. I met my neighbour, and we went inside and watched through the window. Suddenly Ivar, my neighbour, shouted out; "we have to run". A huge black front came surging down. It was visible over the trees! Some stones still came flowing through the air. We ran over to the other side of the fields, looking at it from there. The flow cut down the trees, which were transported with its roots first. *Then* the stones came, rushing towards Øygard. The water was floating on top of the stony layer, over the trees.

This means that some stones came through the air before the black front showed up. The large blocks were not in these first masses, but came afterwards. There was a water layer on top of the stones.

- I think a large block settled, and then the pulse changed direction, towards me. After 15 minutes the masses again turned towards Øygard. Totally, it took about one and a half hour. As the flow changed direction towards me and towards Øygard, more and more of the road was chewed up. The only possible connection to other people was at the other side of the river. I tried to calm down, and had fun of the mailbox that was still there, as everything else was damaged.

- The wave effect was the scariest thing. All the masses did not come down at once; I guess it was more like 4 or 5 large pulses. They were high above the house, and it seemed that the wave effect influenced the change of direction.

- The river ran over my fields inundating them for days after the event. 12,5 crop acres (50 mål = 50 000m^2) of good farming land was destroyed. Also the protection structure near the river Storelva, 350 m from the fan was destroyed. During the cleaning up, I digged holes to bury the big blocks, and found fertile soil one and a half meter down, under old slide material like stones and gravel. Also earlier I have found such soil. I have always had a lot of blocks in my fields, and a few years ago I had a man, Kjell Kjøsnes, to dig up the fields with an excavator and clean them. This man found a lot of nice soil deeper down. Tons of good soil was taken up!

- We have always been afraid of all the snow avalanches here, and have given up the cowshed. It gets damaged every winter. In earlier times the people here offered to the mountain Vetle Supphellenipa for it to stay stable!

Eirik Øygard

Eirik was at the cabin Flatbrehytta, between the moraine ridge and the precipice. His father built the hut 50 years ago, and Eirik is running it now. He brought food and prepared it for the summer, and had his wife and daughter with him.
- I heard a dump sound going up and down. I was standing on the moraine near the precipice, watching the event. After maybe ten minutes, I saw that the muddy water had reached my parabola antenna far down my fields. It was terrible to stand there, just watching my fields being destroyed. I was also afraid my mother was taken by the masses. Luckily, she was not home.
At this point he recognised the seriousness of the event and called the alarm central. As the helicopter came to pick them up a few hours later, everything was calm.

After the event he has removed 10000 m^3 of mud from his fields to be able to use them.

A2 - Description of debris flow event in Fjærland, May 8, 2004

Written by eyewitness Ingebrigt Supphellen

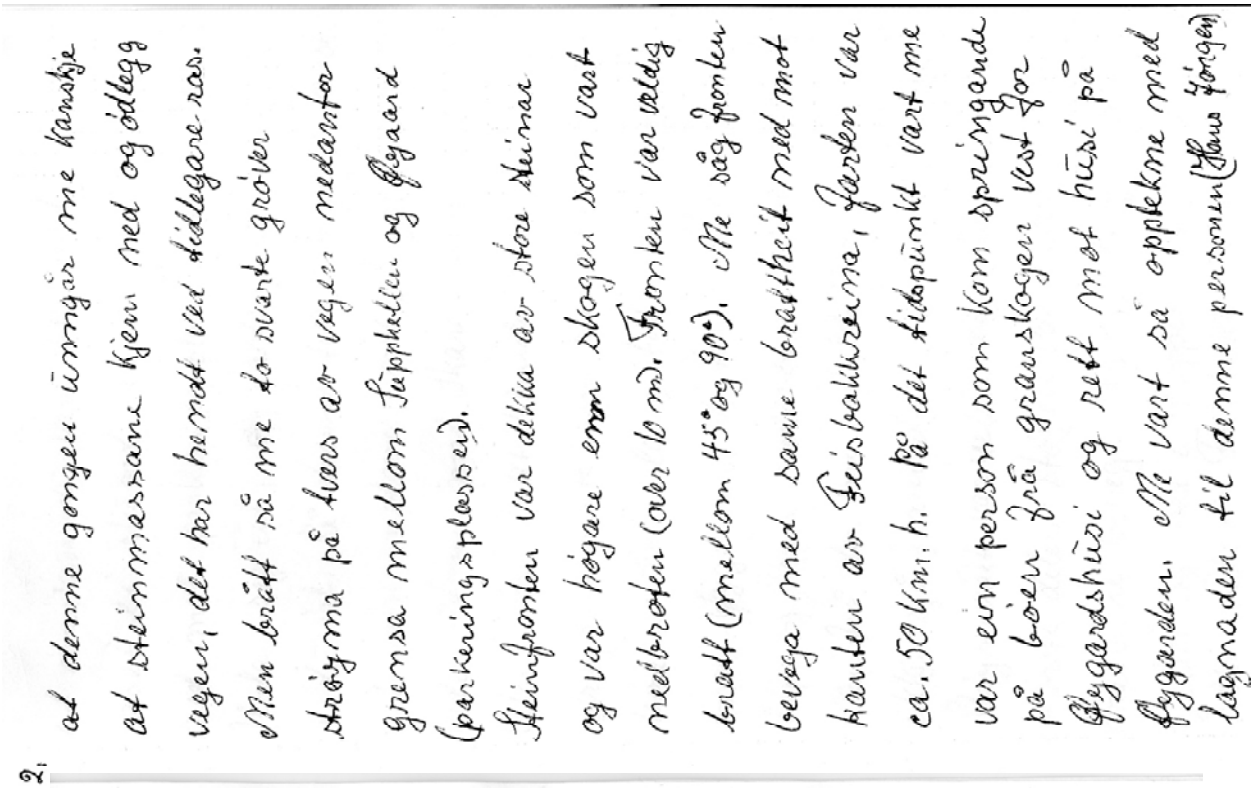

3.

at merksemdi vart teke bort frå raset ei stund. Då raset var kome med mot parkeringsplassen hadde det flata seg út, og farten var mykje redusert. På denne tiden strømde mest alt vatn nedover mot fjygarden og vidare utover mot Skarestadøyane. Vatnet var sterkt blanda med jord, og strøymde saktе som ei supe nedover bøane. Etter lang tid avtok vassmengden mot fjygarden, då tok raset ~~tatnet~~ nytt løp og rann nedover i Tuppheller gnr. 58 bnr. 1. Men frå der me oppheldt oss kunne me ikkje sjå fram der.

Støymevået var veldig høgt, årsaka til største delen støyen var sikkert der massane bevega seg i fritt fall frå fjellet og ned i Hoppelvi. Då raset velta nedover Feisbakkane høyrde

4.

me òg knekka samtidig med den andre støyen, dette kan nermast samanliknast med langvarig maskin-gevereld. Mykje skog vart førd med til Tuppheller elvi, ei stund byrja skogmassane å samlast opp ved bruì som ligg utanfor utløpet for Tverrdalselvi, så me var redde for at bruì kunne verta ødelagd, men desse massane forsvant etter ei tid. Skogen låg som eit teppe på elvi, og flaut nedover elvi med vatnet sin hastigheit. Det var ei lukke at Tuppheller hadde så stor vassføring denne dagen, hadde vassføringi vore liti kunne skogen sett seg fast i elveløpet, og skapt store demningar som kunne ført til store ødeleggelsar. Ca. klokka 15 byrja vassmengden

som rann ut fjellet å arta, men var fremdeles svart. Etter ei tid fann mesteparten av vatnet tilbake til sitt opprinnelege leie på toppen av steinmassane, og med til brui som låg mest uskadd, men løpet under brui var heilt oppfylt. Etter at vatnet seig bort frå bóane låg det att eit tjukt lag jord (bilt). På garden til Reidun og Ólyskein Sørensen berekna takstfolki til Statens defondet at 9600 m³ jord måtte flyttast, mellom 7 og 10 cm skulle liggja eigjen og plóyast med. Steinmassane frå raset dekka kommunevegen frå Kvernagrovi til Veslelógrovi. Vegen til Stupphella vart stengd av raset laurdag og provisorisk veg opna att fyrstkomande onsdag

ut på dagen. Denne vegen vart lagd på sórlege forbyggningen av Tverrdalselvi med mot Stupphellelvi og opp mot kommunevegen langs Kvernagrovi. Kommunen sette inn stor aktivitet for å opna den permanente vegen så fort som mogeleg.

Ingvorigt Stupphellen

Diary of Eirik Øygard, Fjærland, November 11, 1947

Used in the recognition of earlier debris flow events in Fjærland.

11. november 1947

ei stund utpå og las F.S.S. Mythe: "The spirit of the Hills ". Ei bok bakteriologen L.H. Aynsley sende meg. Og so fyre middag var eg tenkt gå upp og måla fallhøgdi på vatsleidningi.

Eg såg ut vindauga og fram at Tverrdala var tom for vatn. Dette tykte eg var underleg då grøvene andre stader var heller store. Ei stund etter høyrde eg duning nett som frå megtigaste snøskredor. Då ringde Kaia og spurde um eg såg kor Tverrdala ræste. Jau, eg såg det.

Vatn, stein og jord kom rullande nedyver i slike mengder lik snøfonn. Heile gilet såg ut til å vera fullt av vatn. Og eg tenkte: " No må me røma husi". Dette er liknande som eit år nede i Hardanger då raset tok ei heil grend. Eg sprang upp på bøen. Då såg eg vatsmassane kor dei fossa utfyre stupi ved rabbane ned Nipesteinsdalen. Kor det såg skræmeleg ut. Og eg tenkte: " No blir det ei springveit alt". Men enno heldt vatnet seg i elvelægjet. Egtvila ikkje på det vilde koma ned på bøen. For vatsmasser myrke av jord og aur heldt ved i aukande mengd.

Eg trudde det snart vilde fylla gilet og så koma sprutande ned yver Feissbakkane. Best det er kjem vatnet ned Storåkeren, beste jordstykket mitt - og då - ja - då er det heller ikkje langt att til springveiti. Alt arbeid hittil hadde altso vore til fånytte. Det var ikkje underleg eg ikkje fekk sova i natt. Noko låg i instinktet og gav eit fyrevarsel.

På Storåkeren gjekk ei mengd sauer - men fyrr elvi kom ned der for dei som jagde av hinmannen der i frå. Dei ana det. Villdyri anar slikt. Instinktet fortel. Sauene liver i fjellet som ville i sumarmånadene. Eg torde ikkje gå upp med same. For i slike høve kann ein lett koma upp nett der elvi slær seg yver og då kastar ho store steinar høgt uppetter trestomnane nett som me kastar småstein. Men eg våga springa yver. No galdt det bægja vatnet med nedhoggen skog so ikkje alt skulde koma heim på dyrka mark. Ho rann so vidt utyver so det var ikkje fårleg. Men alderskogen hadde mist borken langt uppetter stomnane av steinspruten med same ræsingi kasta seg yver den 3 m. høge forbygningi.

Aa stå attmed gilet og kjenna jordi dirra medan kreftene tok med seg stor stein som i brak og dun og dur for nedyver tronge gilet. Det tyktest nifst. Elvi lagar seg eit lægje der ho rann smalt. Men so mykje stein kjem så med so då det blir breidare hiver ho steinane til eine sida. Når der blir høgt so velter ho seg burt på hi - grev undan steinurdane og fyller til det blir høgt, so velter ho um att. Slik held ho på inntil store haugar ligg att der ho for nokre timar sidan gjekk i djupt lægje. Supphellsbrui var nedøyrd med stein og stor haug som ein kjøl der elvi hadde djupt lægje. No gjeng heile elvi nokre meter heimanfor brui, der ho hev skore i gjennom vegen. Likeeins hadde ho skore djupt lægje gjennom vegen i Trona. Supphellagardane er fråstengde i kveld. Dei kann ikkje koma ned i bygdi.

Og no - natt regnar det fælt att - no grev ho villare og villare.

Kor vil det bli i morgo ?

Avskrift etter notat av Eirik Øygard.

Appendix B

Terrain profiles
Generated in Golden Software's Surfer

B1 - Length profile

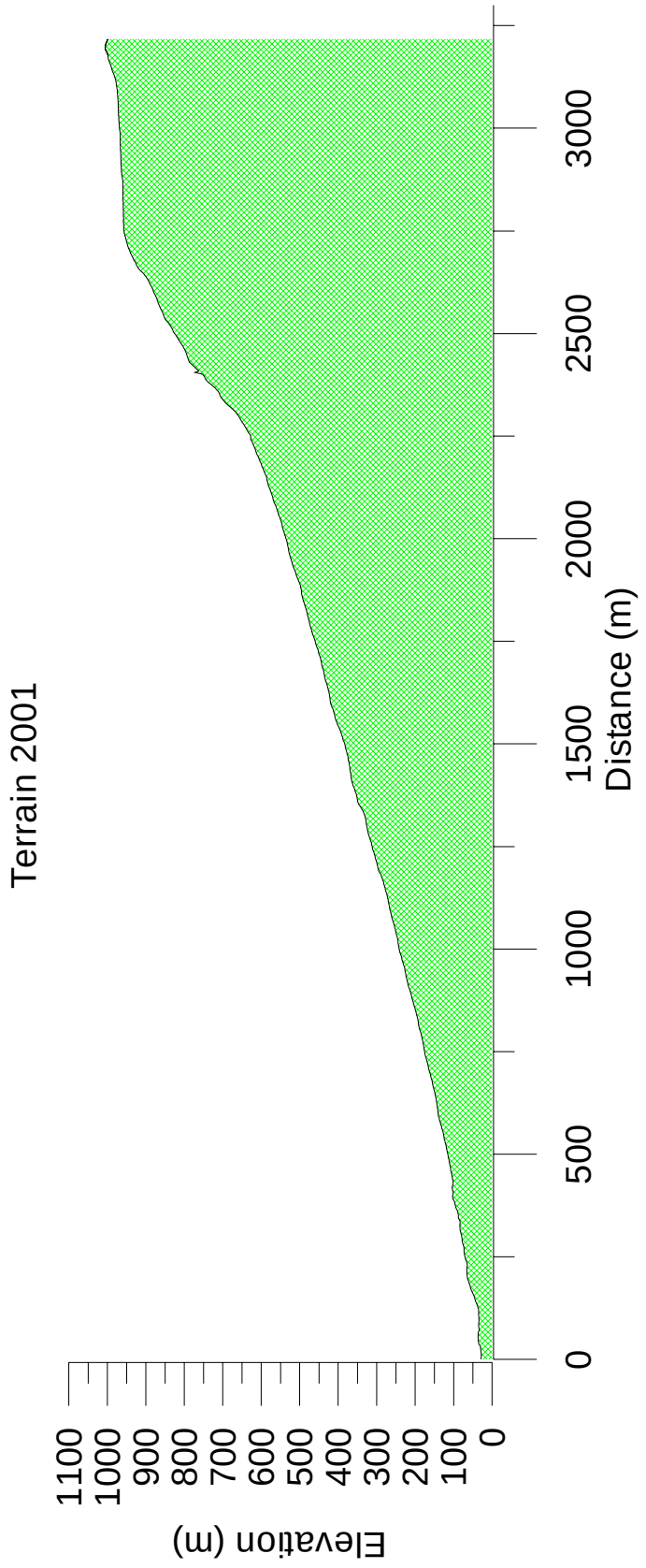

Figure B1-1 Length profile along debris flow track, 2001 terrain.

B2 - Cross profiles

PROFILE 1: Moraine scar

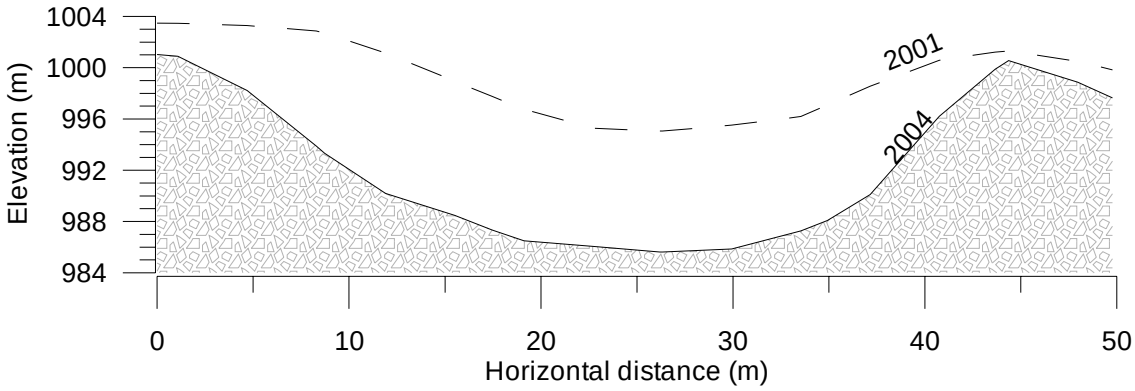

PROFILE 2: Moraine scar

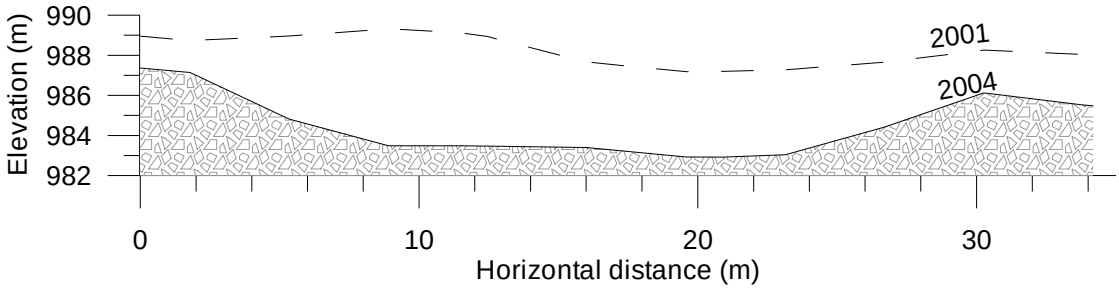

PROFILE 3

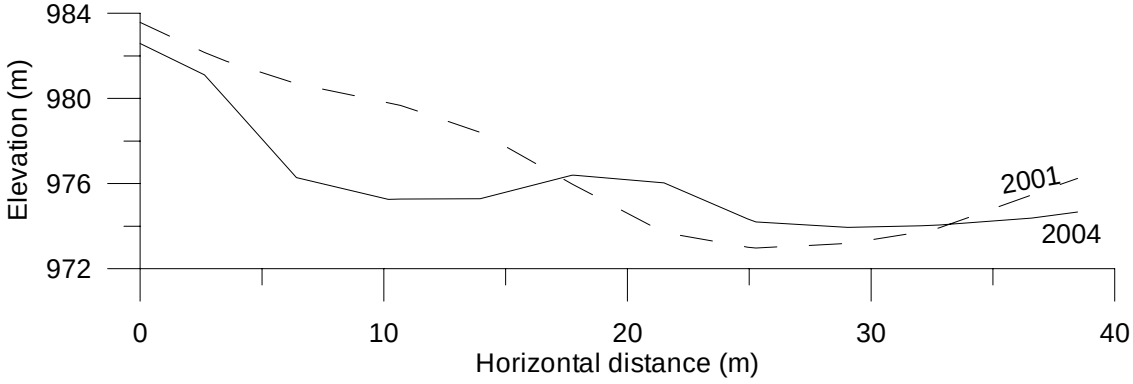

Appendix B

PROFILE 4

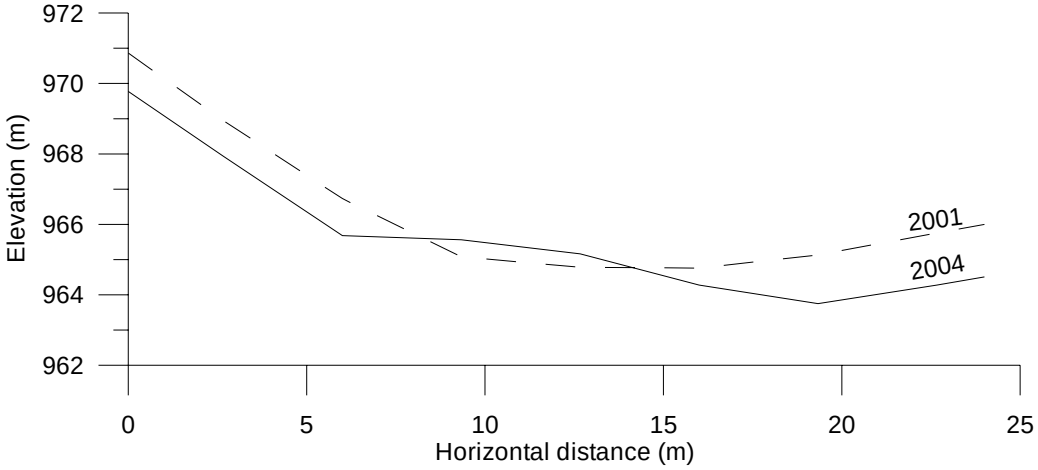

PROFILE 5

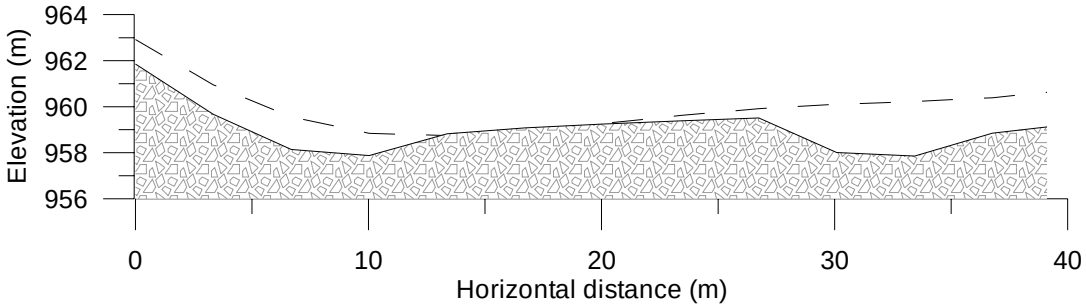

PROFILE 6

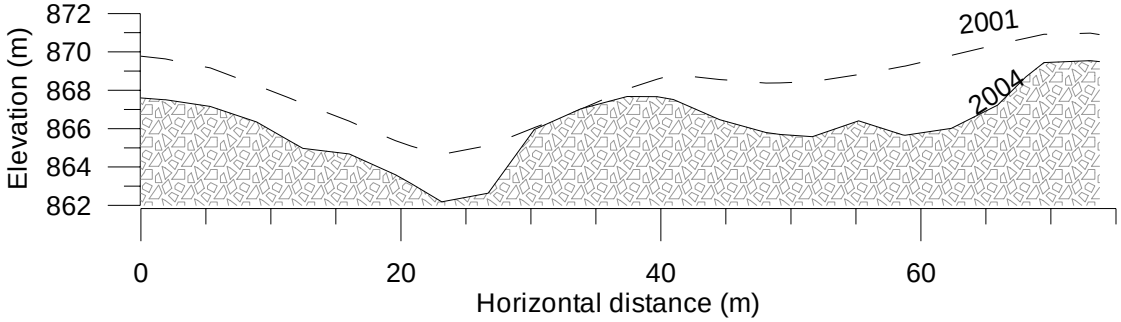

Appendix B

PROFILE 7

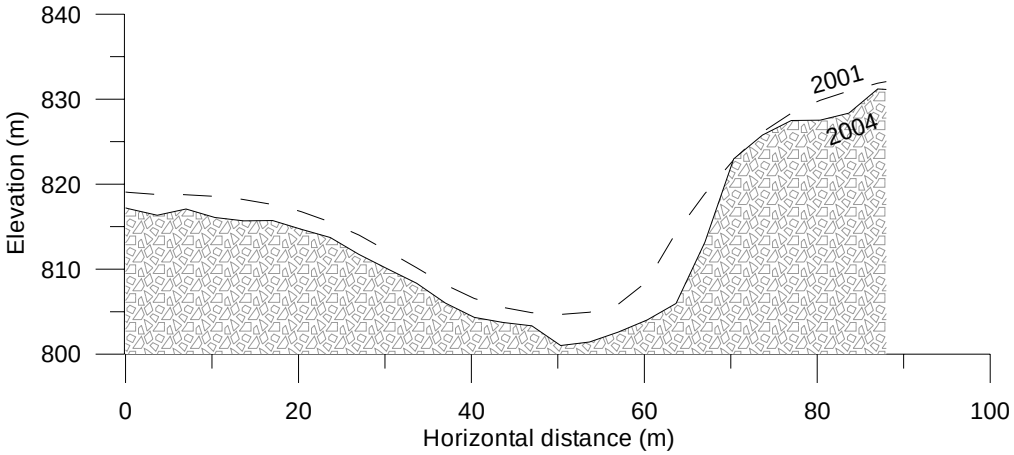

PROFILE 8

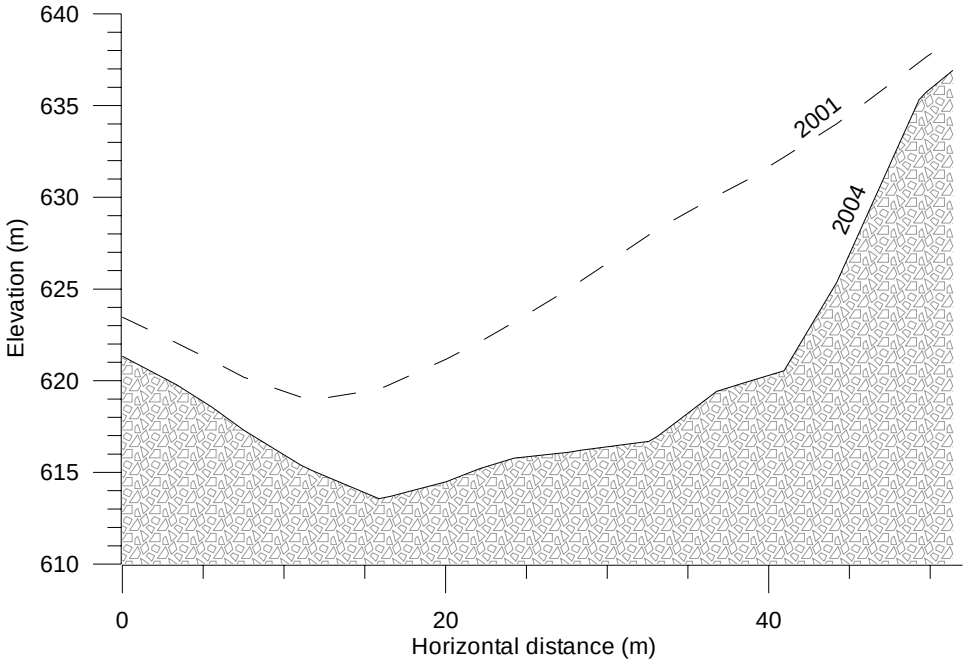

PROFILE 9

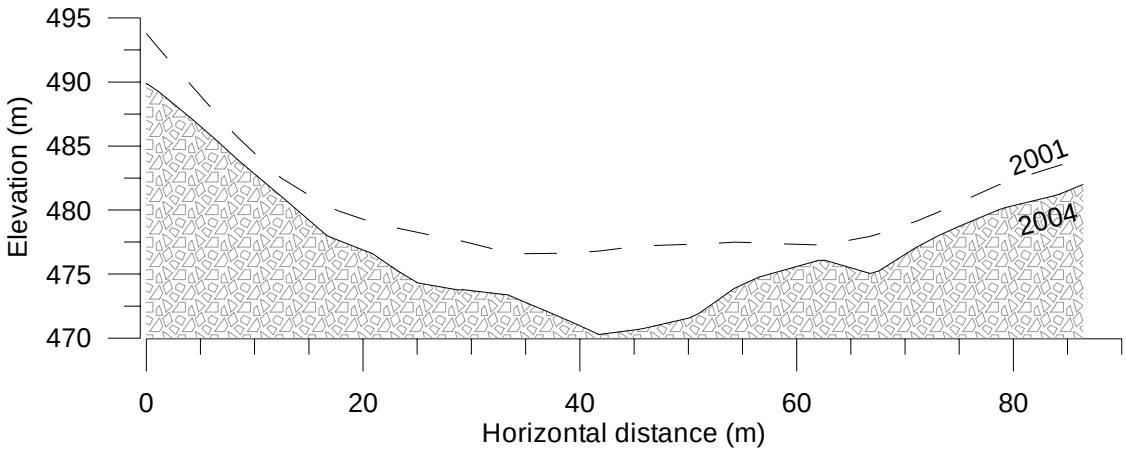

Appendix B

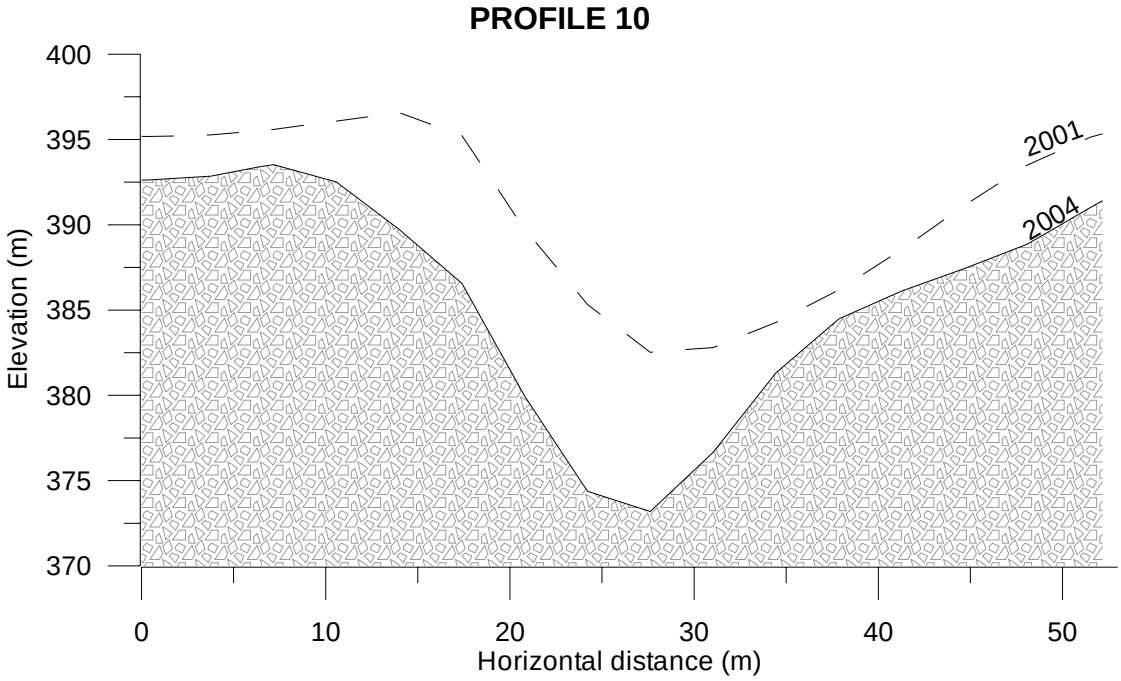
PROFILE 10
400
395
390
385
380
375
370
Elevation (m)
2001
2004
0
10
20
30
40
50
Horizontal distance (m)

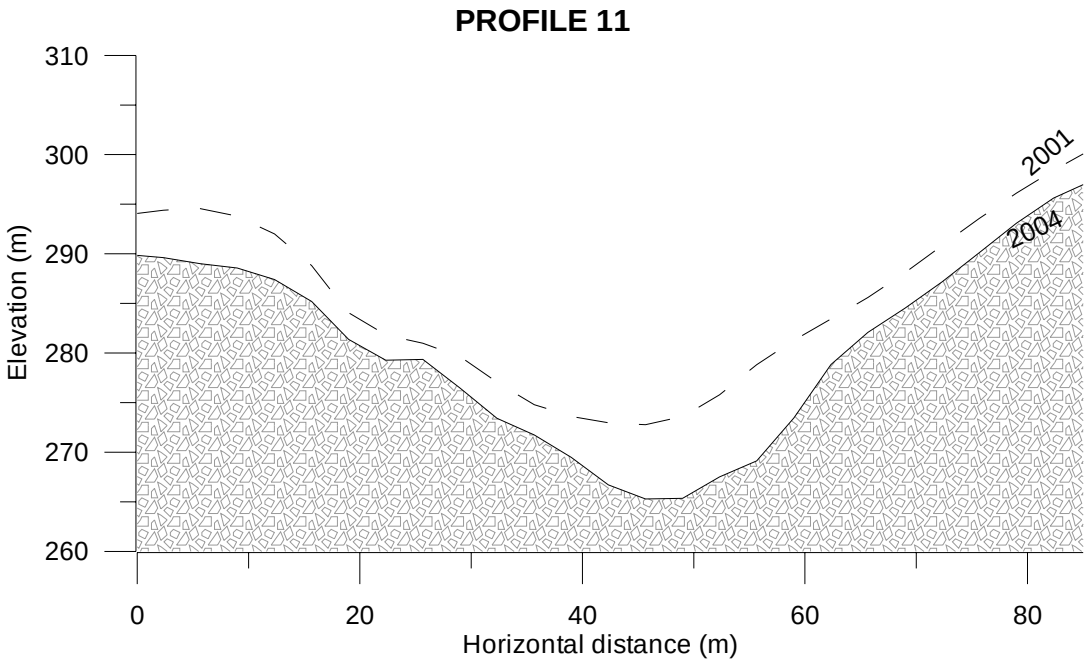
PROFILE 11
310
300
290
280
270
260
Elevation (m)
2001
2004
0
20
40
60
80
Horizontal distance (m)

Appendix B

PROFILE 12

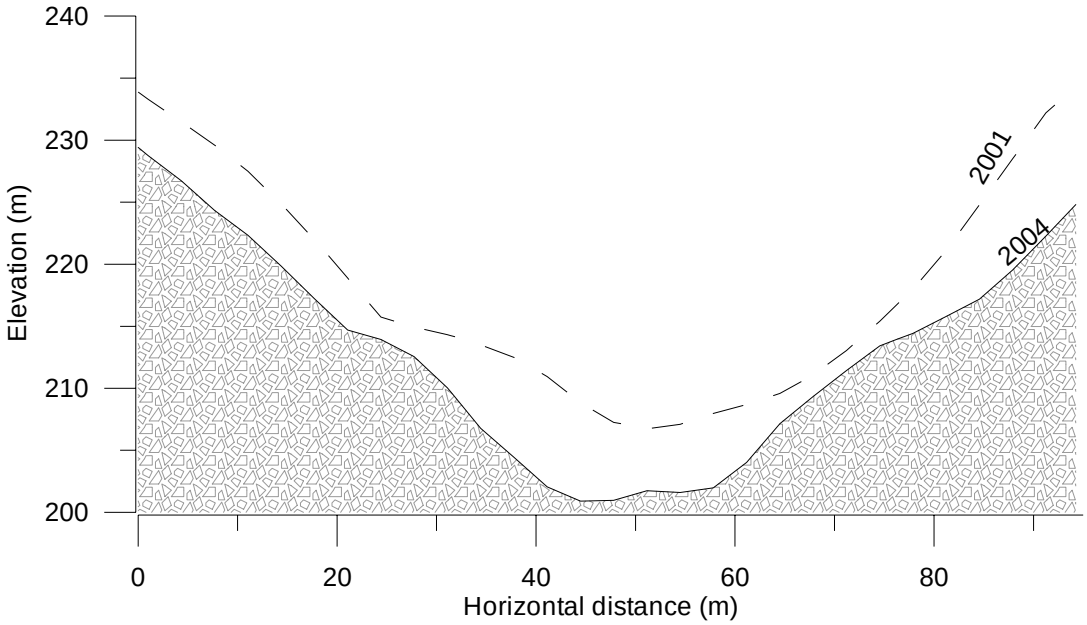

PROFILE 13

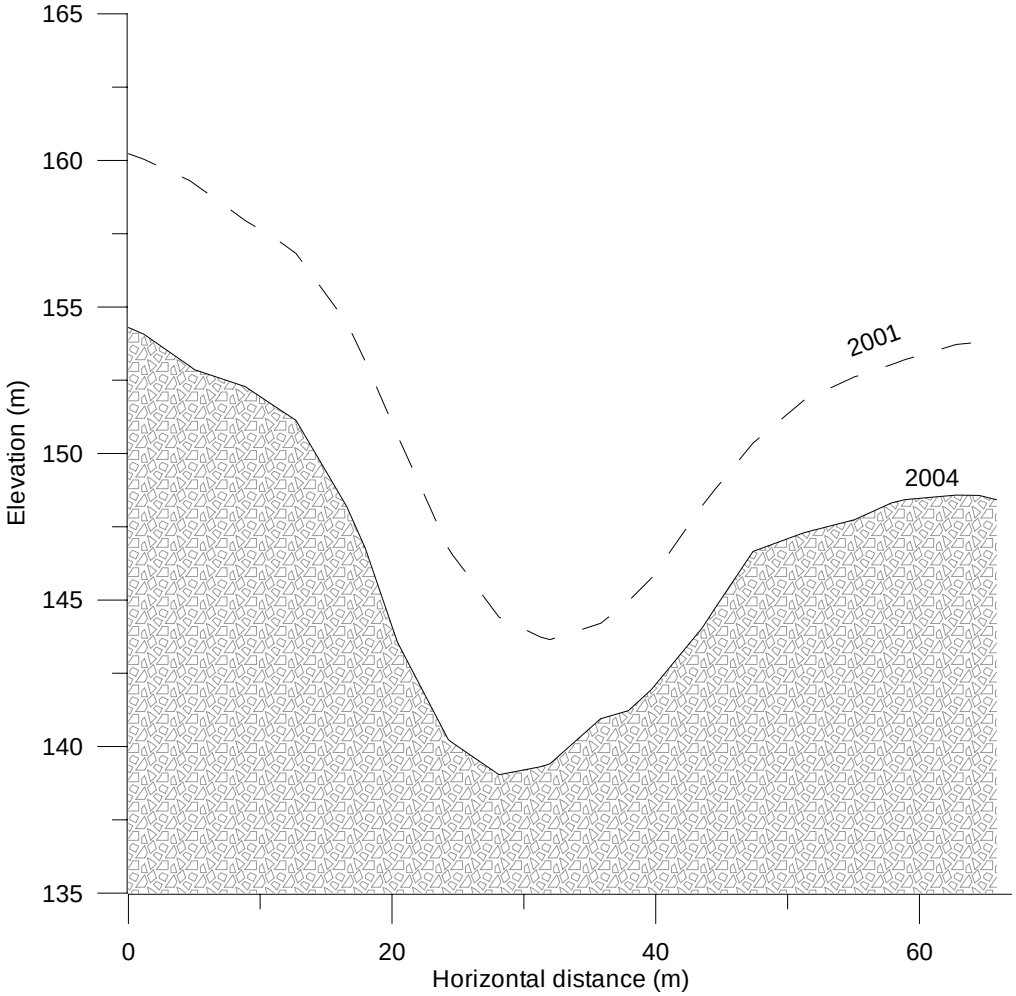

Appendix B

PROFILE 14

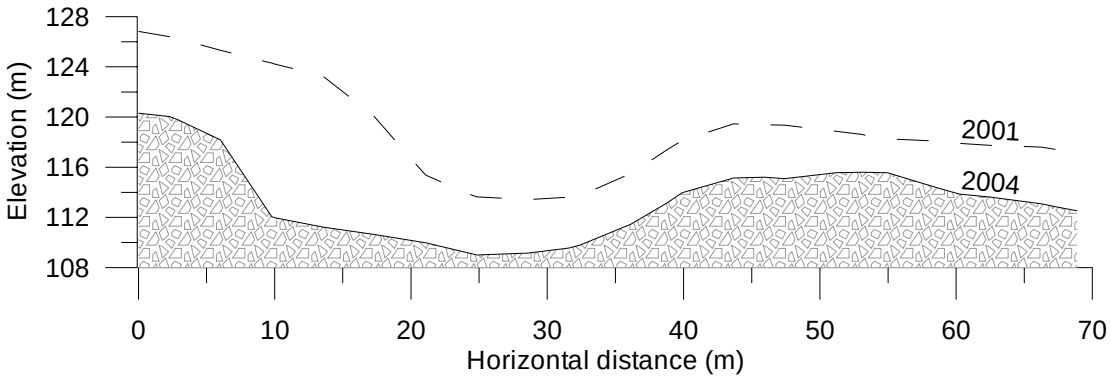

PROFILE 15

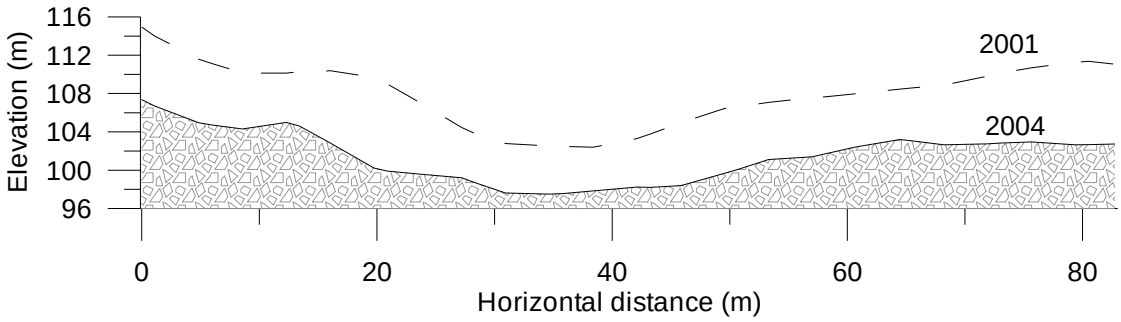

PROFILE 16

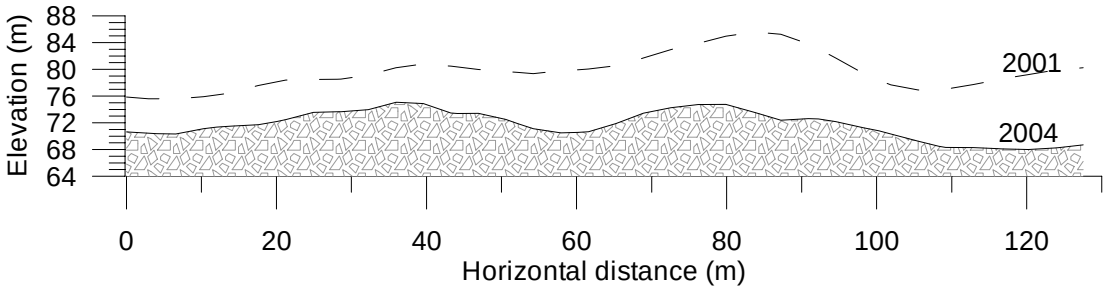

PROFILE 17

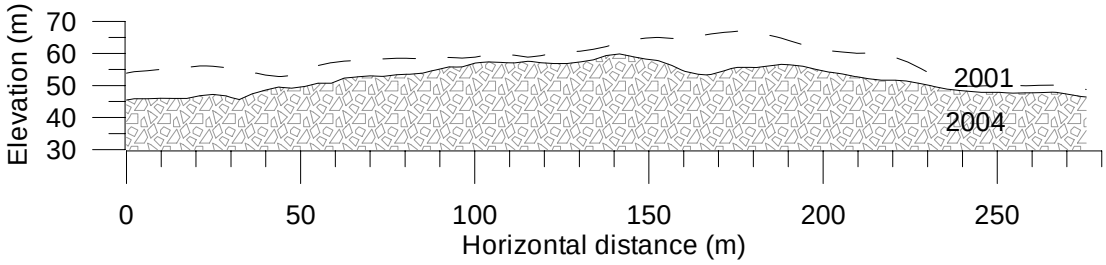

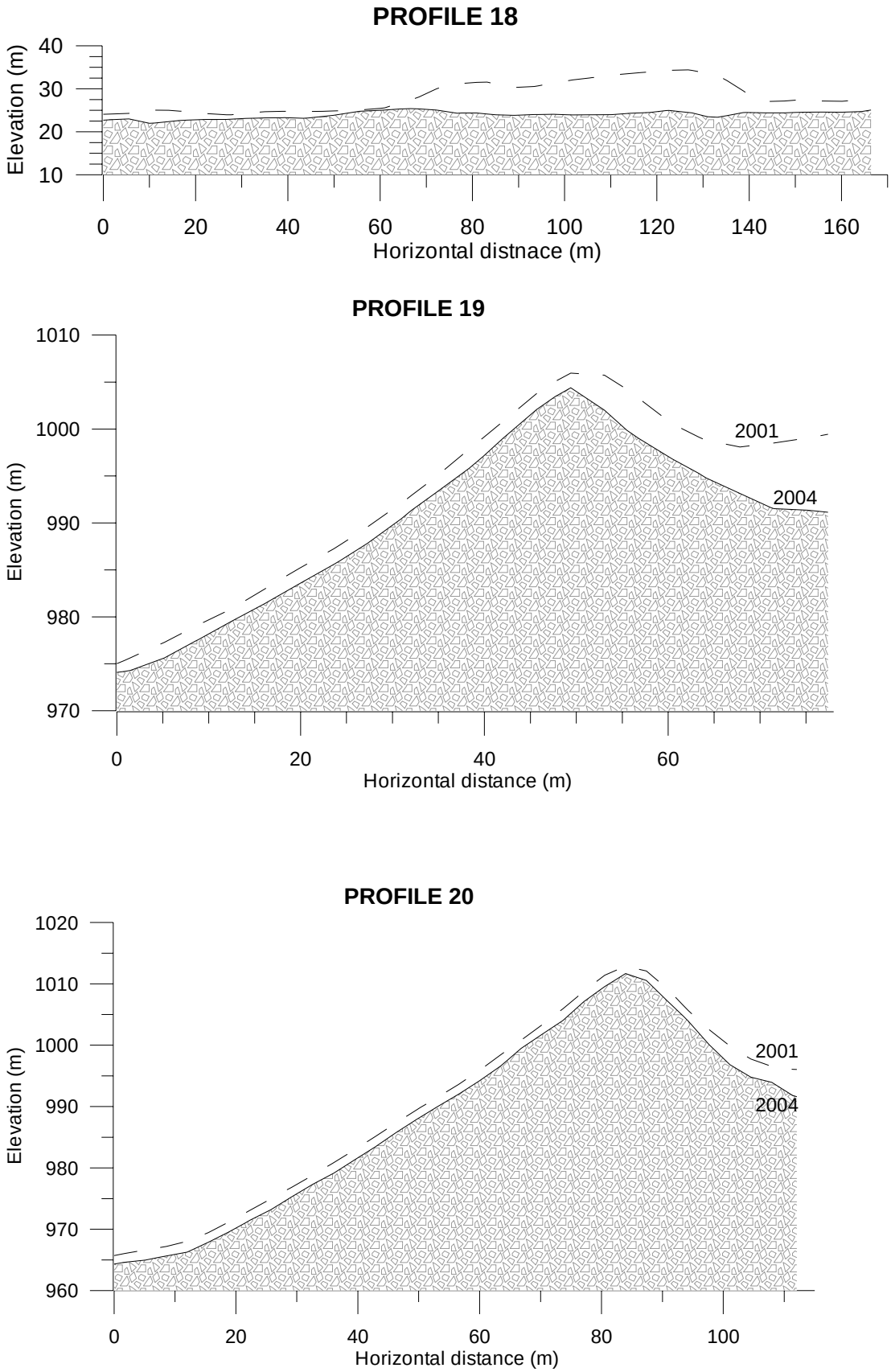

Figure B2-1 Illustrations of cross sections at intervals throughout debris flow track, showing pre- and post-flow terrain.

Appendix C
Water volume estimates

Scenarios of different water (and sediment) volumes

Used in the evaluation of water volume possibly involved in the 2004-event.

Table C-1 Different water volumes combined with different sediment volumes in the first and the last cross section of the track.

Scenario 1 50 000m^3 water	Time (s)	Area (m^2)	Sediment volume (m^3)	Velocity (m/s)
Cross section 1	2700	91,5	0	0,2
Cross section 15	2700	130	250000	0,9
Cross section 15	2700	130	450000	1,4
Scenario 2 100 000m^3 water	Time (s)	Area (m^2)	Sediment volume (m^3)	Velocity (m/s)
Cross section 1	2700	91,5	0	0,4
Cross section 15	2700	130	250000	1,0
Cross section 15	2700	130	450000	1,6
Scenario 3 200 000m^3 water	Time (s)	Area (m^2)	Sediment volume (m^3)	Velocity (m/s)
Cross section 1	2700	91,5	0	0,8
Cross section 15	2700	130	250000	1,3
Cross section 15	2700	130	450000	1,9
Scenario 4 300 000m^3 water	Time (s)	Area (m^2)	Sediment volume (m^3)	Velocity (m/s)
Cross section 1	2700	91,5	0	1,2
Cross section 15	2700	130	250000	1,6
Cross section 15	2700	130	450000	2,1
Scenario 5 400 000 m^3 water	Time (s)	Area (m^2)	Sediment volume (m^3)	Velocity (m/s)
Cross section 1	2700	91,5	0	1,6
Cross section 15	2700	130	250000	1,9
Cross section 15	2700	130	450000	2,4
Scenario 6 500 000 m^3 water	Time (s)	Area (m^2)	Sediment volume (m^3)	Velocity (m/s)
Cross section 1	2700	91,5	0	2,0
Cross section 15	2700	130	250000	2,1
Cross section 15	2700	130	450000	2,7

Appendix D

Sediment volume estimates

D1- Elevation change from 2001 to 2004

Showed as coloured contours

Section 1) Moraine scar:

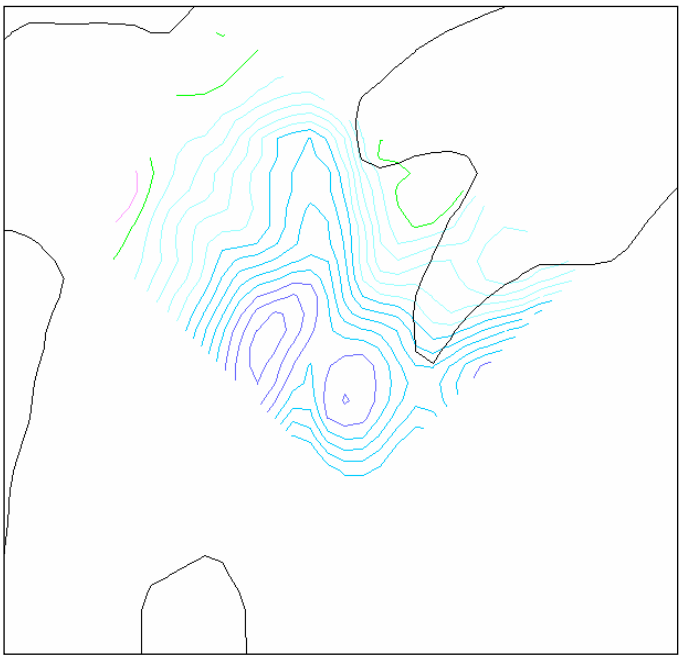

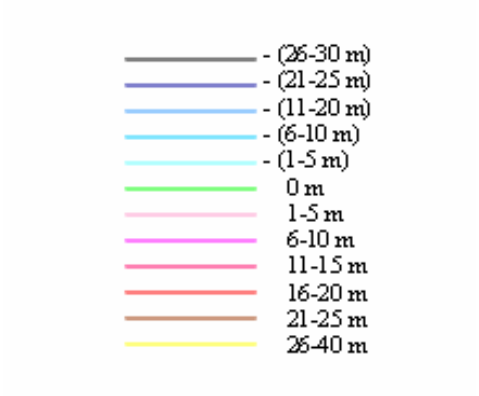

Legend

Figure D-1 Elevation change between aerial photo 2004 and aerial photo 2001. Section 1.

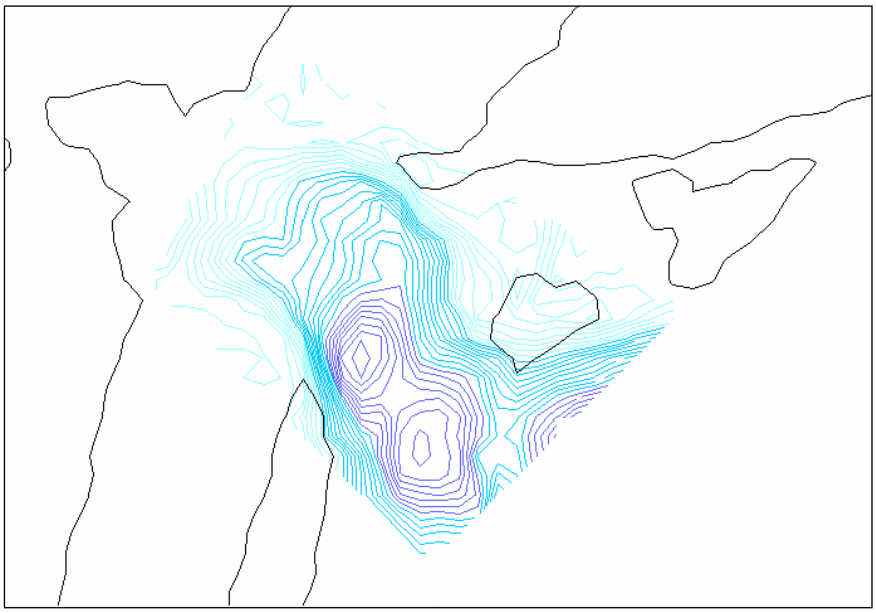

Figure D-2 Elevation change between laser 2004 and aerial photo 2001. Section 1.

Section 2) Flat area

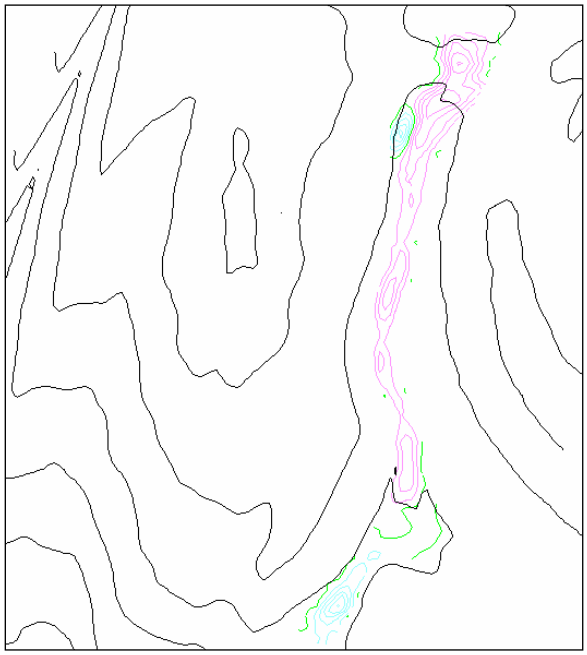

Figure D-3 Elevation change between aerial photo 2004 and aerial photo 2001. Section 2

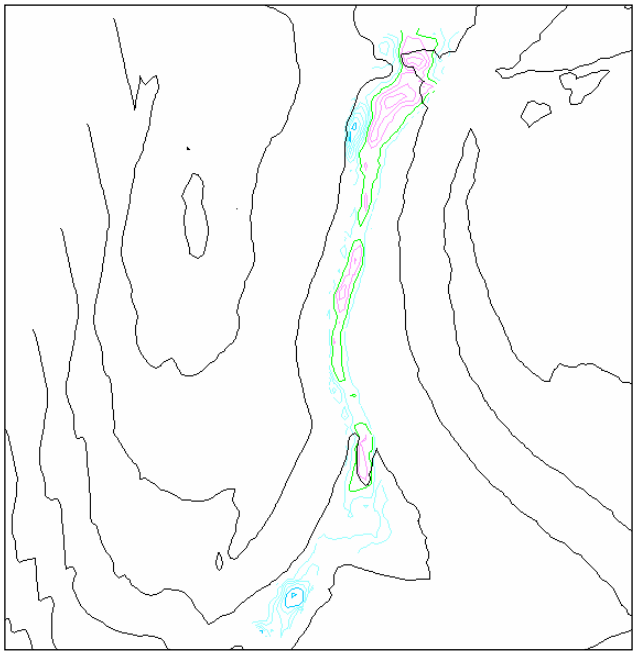

Figure D-4 Elevation change between aaser 2004 and aerial photo 2001. Section 2.

Section 3) Precipice:

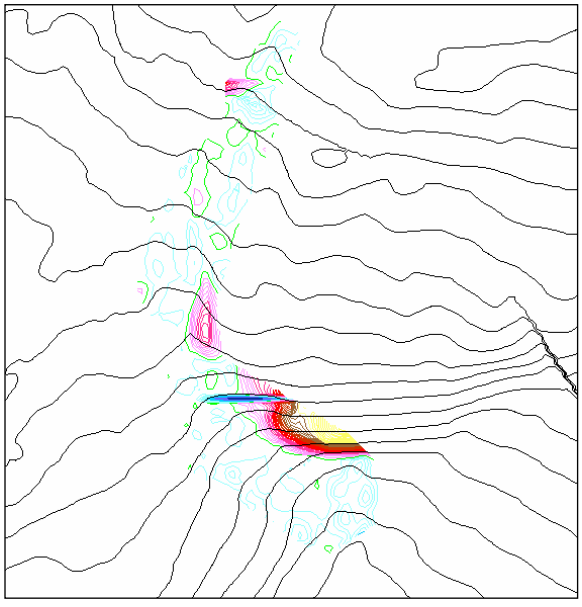

Figure D-5 Elevation change between aerial photo 2004 and aerial photo 2001. Section 3.

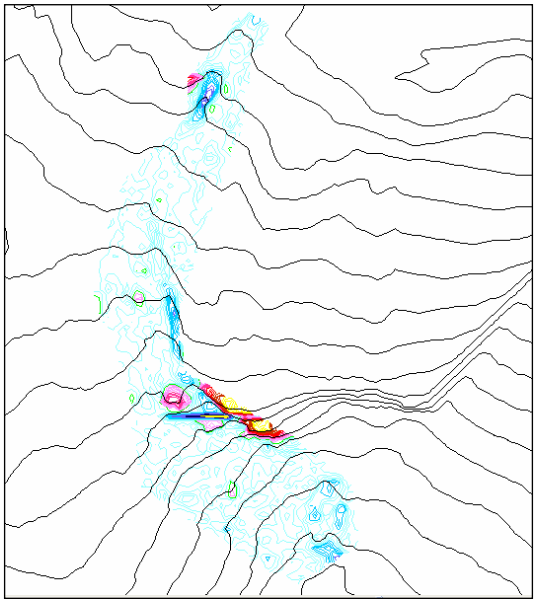

Figure D-6 Elevation change between laser 2004 and aerial photo 2001. Section 3.

Section 4) Beneath precipice

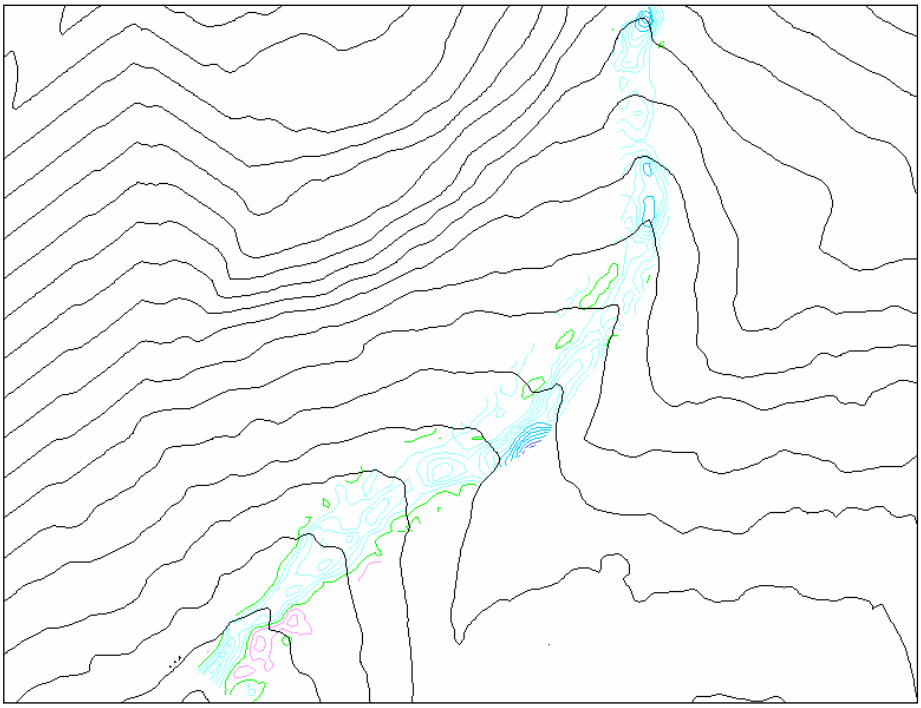

Figure D-7 Elevation change between aerial photo 2004 and aerial photo 2001. Section 4.

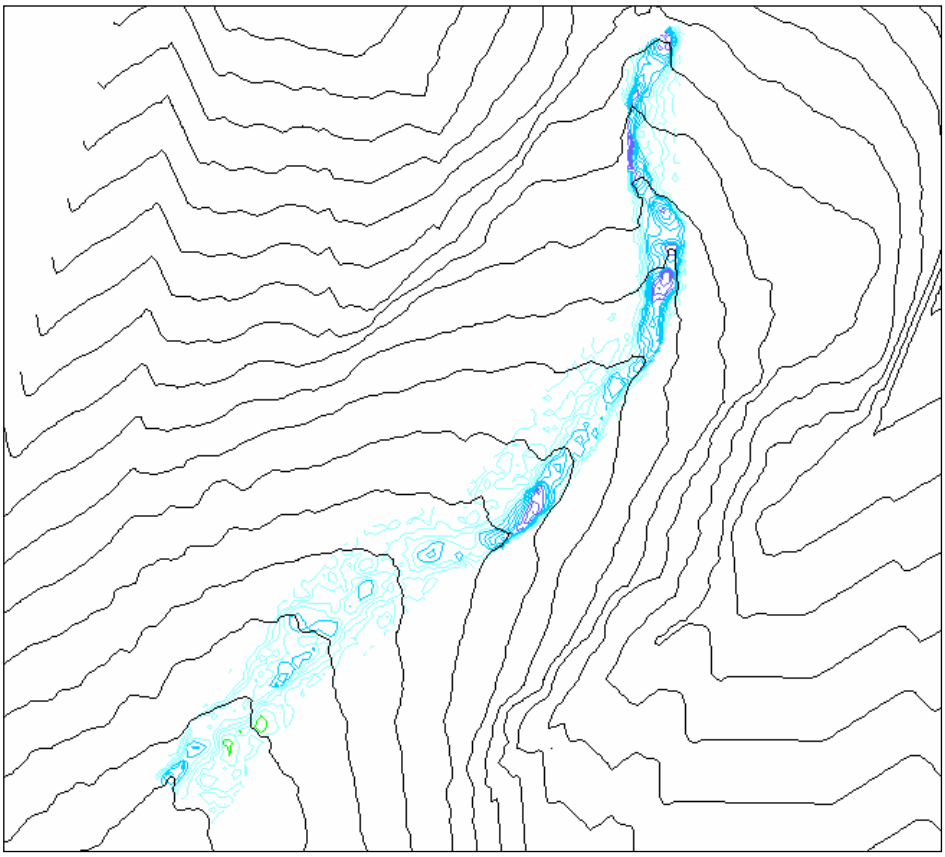

Figure D-8 Elevation change between laser 2004 and aerial photo 2001. Section 4.

Section 5) Tunga:

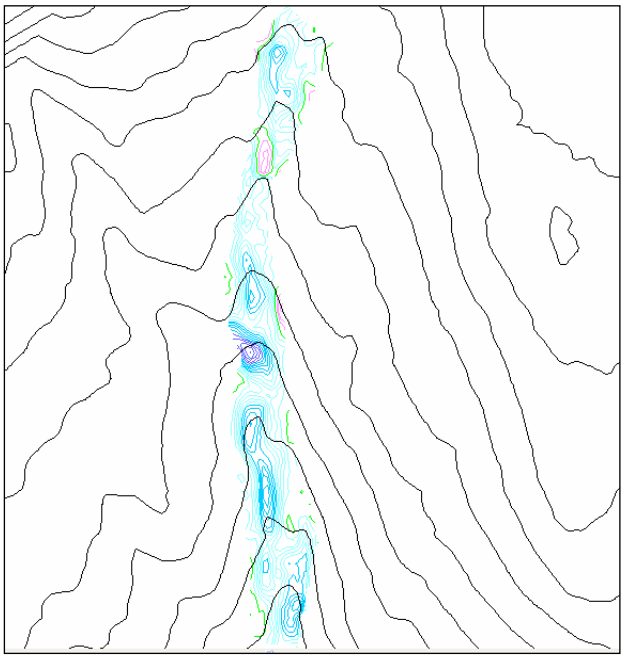

Figure D-9 Elevation change between aerial photo 2004 and aerial photo 2001. Section 5.

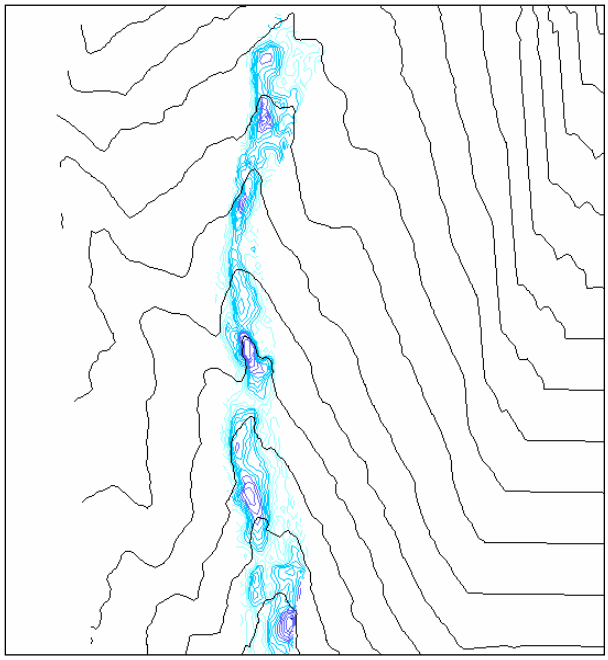

Figure D-10 Elevation change between laser 2004 and aerial photo 2001. Section 5.

Section 6) Tverrdalen:

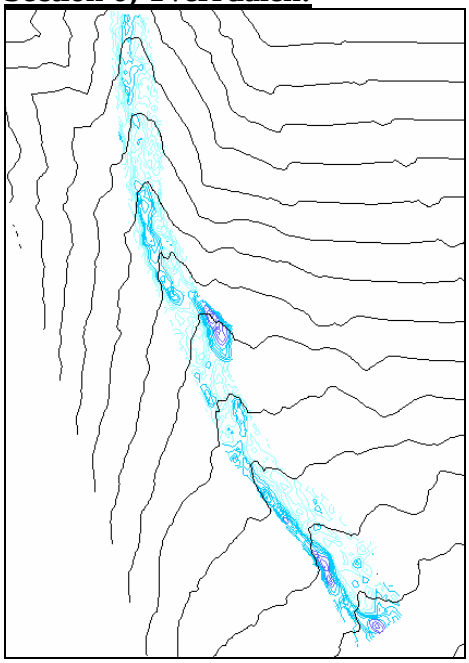

Figure D-11 elevation change between aerial photo and aerial photo 2001. Section 6.

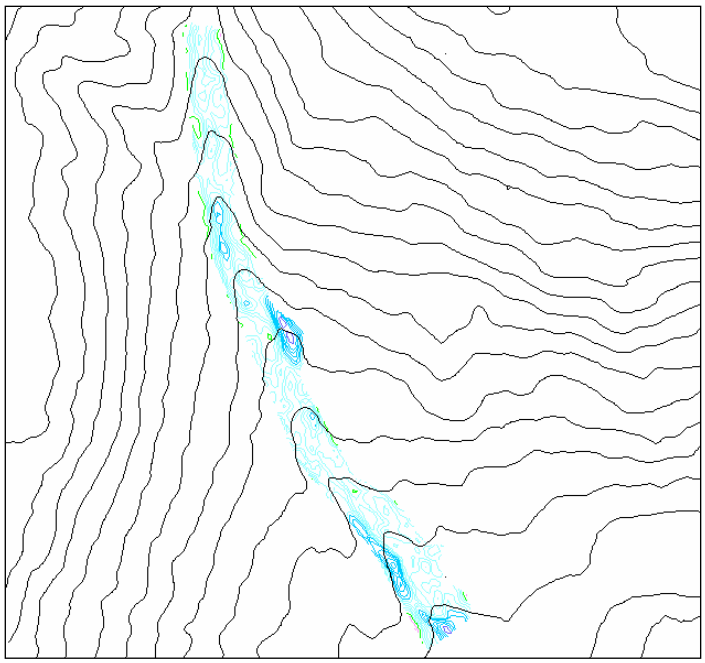

Figure D-12 Elevation change between laser 2004 and aerial photo 2001. Section 6.

Section 7) Fan area:

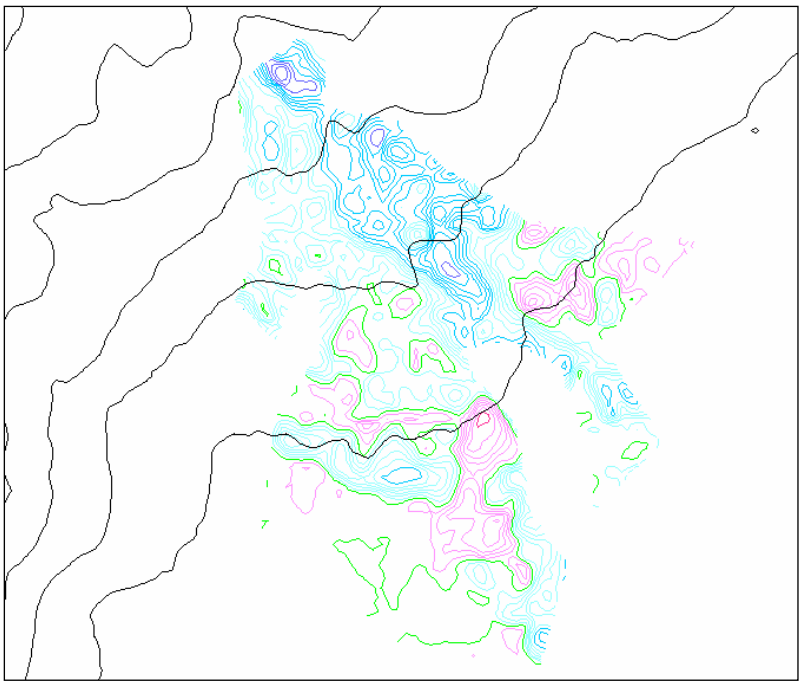

Figure D-13 Elevation change between aerial photo 2004 and aerial photo 2001. Section 7

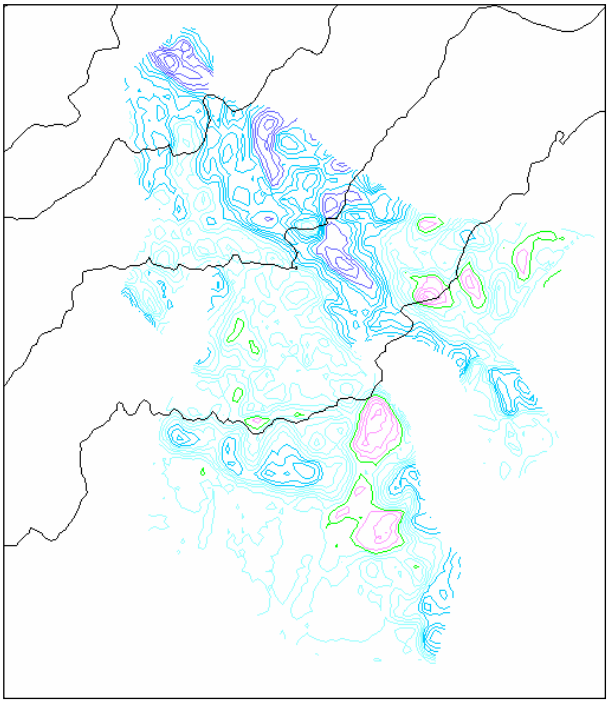

Figure D-14 Elevation change between laser 2004 and aerial photo 2001. Section 7.

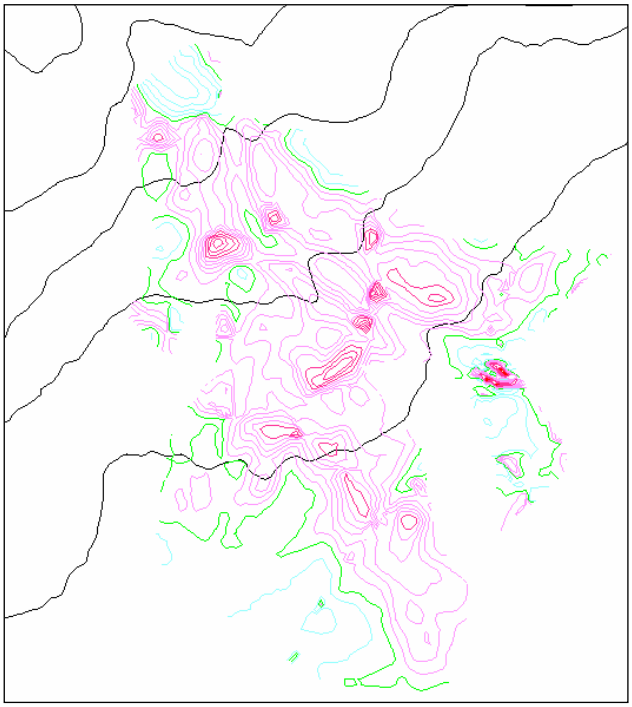

Figure D-15 Elevation change between aerial photo 2004 and economical map 1:5000. Section 7.

D2 – Grid volume computations

Generated from Surfer

1) AERIAL PHOTO generated grid 2004 minus aerial photo generated grid 2001

Section 1 Moraine scar

Grid Volume Computations

Wed Mar 02 11:51:54 2005

Upper Surface

Grid File Name:	C:\geodata\BLN\del5_04-01.grd
Grid Size:	1000 rows x 373 columns
X Minimum:	382100
X Maximum:	383340
X Spacing:	3.3333333333333
Y Minimum:	6814660
Y Maximum:	6817990
Y Spacing:	3.3333333333333
Z Minimum:	-13.622536042734
Z Maximum:	1.6938401841255

Lower Surface

Level Surface defined by Z = 0

Volumes

Z Scale Factor:	1

Total Volumes by:

Trapezoidal Rule:	-23040.619987584
Simpson's Rule:	-23031.377691285
Simpson's 3/8 Rule:	-23068.376144571

Cut & Fill Volumes

Positive Volume [Cut]:	124.46932230234
Negative Volume [Fill]:	23165.089309887
Net Volume [Cut-Fill]:	-23040.619987584

Areas

Planar Areas

Positive Planar Area [Cut]:	234.60064269777
Negative Planar Area [Fill]:	3659.8438017467
Blanked Planar Area:	4125305.5555556
Total Planar Area:	4129200

Surface Areas

Positive Surface Area [Cut]:	239.92442028364
Negative Surface Area [Fill]:	3993.8571091027

Section 2 Flat area

Grid Volume Computations

Wed Mar 02 11:52:32 2005

Upper Surface

Grid File Name:	C:\geodata\BLN\del7_04-01.grd
Grid Size:	1000 rows x 373 columns
X Minimum:	382100
X Maximum:	383340
X Spacing:	3.3333333333333
Y Minimum:	6814660
Y Maximum:	6817990
Y Spacing:	3.3333333333333
Z Minimum:	-5.194645664722
Z Maximum:	5.127811081045

Lower Surface
Level Surface defined by Z = 0

Volumes

Z Scale Factor:	1

Total Volumes by:

Trapezoidal Rule:	8526.1852803964
Simpson's Rule:	8577.9883413581
Simpson's 3/8 Rule:	8536.3132212506

Cut & Fill Volumes

Positive Volume [Cut]:	11598.171292613
Negative Volume [Fill]:	3071.9860122164
Net Volume [Cut-Fill]:	8526.1852803964

Areas
Planar Areas

Positive Planar Area [Cut]:	6911.0225056536
Negative Planar Area [Fill]:	2772.3108276797
Blanked Planar Area:	4119516.6666667
Total Planar Area:	4129200

Surface Areas

Positive Surface Area [Cut]:	7160.1934975717
Negative Surface Area [Fill]:	2880.7317650429

Section 3 Precipice

Grid Volume Computations

Wed Mar 02 11:51:32 2005

Upper Surface

Grid File Name:	C:\geodata\BLN\del4_04-01.grd
Grid Size:	1000 rows x 373 columns
X Minimum:	382100
X Maximum:	383340
X Spacing:	3.3333333333333
Y Minimum:	6814660

Y Maximum:	6817990
Y Spacing:	3.3333333333333
Z Minimum:	-24.042593456677
Z Maximum:	39.735525333542

Lower Surface
Level Surface defined by Z = 0

Volumes

Z Scale Factor:	1

Total Volumes by:

Trapezoidal Rule:	22925.611987949
Simpson's Rule:	24628.503310494
Simpson's 3/8 Rule:	24048.63142981

Cut & Fill Volumes

Positive Volume [Cut]:	50046.936797085
Negative Volume [Fill]:	27121.324809136
Net Volume [Cut-Fill]:	22925.611987949

Areas
Planar Areas

Positive Planar Area [Cut]:	6164.348188594
Negative Planar Area [Fill]:	21318.985144739
Blanked Planar Area:	4101716.6666667
Total Planar Area:	4129200

Surface Areas

Positive Surface Area [Cut]:	8644.7631255346
Negative Surface Area [Fill]:	23730.02369425

Section 4 Beneath precipice

Grid Volume Computations

Wed Mar 02 11:50:42 2005

Upper Surface

Grid File Name:	C:\geodata\BLN\del2_04-01.grd
Grid Size:	1000 rows x 373 columns
X Minimum:	382100
X Maximum:	383340
X Spacing:	3.3333333333333
Y Minimum:	6814660
Y Maximum:	6817990
Y Spacing:	3.3333333333333
Z Minimum:	-12.472552189756
Z Maximum:	2.5213887801567

Lower Surface
Level Surface defined by Z = 0

Volumes

Z Scale Factor:	1

Total Volumes by:

Trapezoidal Rule:	-48067.434458661
Simpson's Rule:	-48059.53778424
Simpson's 3/8 Rule:	-48128.42452532

Cut & Fill Volumes

Positive Volume [Cut]:	2863.9418417569
Negative Volume [Fill]:	50931.376300418
Net Volume [Cut-Fill]:	-48067.434458661

Areas
Planar Areas

Positive Planar Area [Cut]:	4063.1729142909
Negative Planar Area [Fill]:	22425.715974598
Blanked Planar Area:	4102711.1111111
Total Planar Area:	4129200

Surface Areas

Positive Surface Area [Cut]:	4132.4365747033
Negative Surface Area [Fill]:	23250.390041129

Section 5 Tunga

Grid Volume Computations

Wed Mar 02 11:52:12 2005

Upper Surface

Grid File Name:	C:\geodata\BLN\del6_04-01.grd
Grid Size:	1000 rows x 373 columns
X Minimum:	382100
X Maximum:	383340
X Spacing:	3.3333333333333
Y Minimum:	6814660
Y Maximum:	6817990
Y Spacing:	3.3333333333333
Z Minimum:	-15.046353728695
Z Maximum:	3.6416678861478

Lower Surface
Level Surface defined by Z = 0

Volumes

Z Scale Factor:	1

Total Volumes by:

Trapezoidal Rule:	-70157.184947588
Simpson's Rule:	-70049.769291291
Simpson's 3/8 Rule:	-69979.053019533

Cut & Fill Volumes

Positive Volume [Cut]:	1291.243555453
Negative Volume [Fill]:	71448.428503041
Net Volume [Cut-Fill]:	-70157.184947588

Areas
Planar Areas

Positive Planar Area [Cut]:	1323.1579033666
Negative Planar Area [Fill]:	18654.619874411
Blanked Planar Area:	4109222.2222222
Total Planar Area:	4129200

Surface Areas

Positive Surface Area [Cut]:	1396.4147000691
Negative Surface Area [Fill]:	20305.960905253

Section 6 Tverrdalen

Grid Volume Computations

Wed Mar 02 11:51:07 2005

Upper Surface

Grid File Name:	C:\geodata\BLN\del3_04-01.grd
Grid Size:	1000 rows x 373 columns
X Minimum:	382100
X Maximum:	383340
X Spacing:	3.3333333333333
Y Minimum:	6814660
Y Maximum:	6817990
Y Spacing:	3.3333333333333
Z Minimum:	-11.728902103986
Z Maximum:	2.0653015863519

Lower Surface
Level Surface defined by Z = 0

Volumes

Z Scale Factor:	1

Total Volumes by:

Trapezoidal Rule:	-103714.19169577
Simpson's Rule:	-103825.99025712
Simpson's 3/8 Rule:	-103714.97116161

Cut & Fill Volumes

Positive Volume [Cut]:	465.9367541456
Negative Volume [Fill]:	104180.12844992
Net Volume [Cut-Fill]:	-103714.19169577

Areas
Planar Areas

Positive Planar Area [Cut]:	719.04018503135
Negative Planar Area [Fill]:	31030.959814969
Blanked Planar Area:	4097450
Total Planar Area:	4129200

Surface Areas

Positive Surface Area [Cut]:	743.97914601519
Negative Surface Area [Fill]:	32847.787985577

Section 7 Fan

Grid Volume Computations Section 7 Fan

Wed Mar 02 11:46:46 2005

Upper Surface

Grid File Name:	C:\geodata\BLN\del1_04-01.grd
Grid Size:	1000 rows x 373 columns
X Minimum:	382100
X Maximum:	383340
X Spacing:	3.3333333333333
Y Minimum:	6814660
Y Maximum:	6817990
Y Spacing:	3.3333333333333
Z Minimum:	-13.913928492843
Z Maximum:	6.601791079104

Lower Surface
Level Surface defined by Z = 0

Volumes

Z Scale Factor:	1

Total Volumes by:
Trapezoidal Rule: -156284.03552152
Simpson's Rule: -156555.57537525
Simpson's 3/8 Rule: -156504.5820036

Cut & Fill Volumes
Positive Volume [Cut]: 28263.651010917
Negative Volume [Fill]: 184547.68653243
Net Volume [Cut-Fill]: -156284.03552152

Areas
Planar Areas
Positive Planar Area [Cut]: 23050.249204174
Negative Planar Area [Fill]: 49433.084129159
Blanked Planar Area: 4056716.6666667
Total Planar Area: 4129200

Surface Areas
Positive Surface Area [Cut]: 23725.14262855
Negative Surface Area [Fill]: 51808.479391347

2) LASER generated grid 2004 minus aerial photo generated grid 2001

Section 1 Moraine scar

Grid Volume Computations

Tue Mar 08 14:13:28 2005

Upper Surface
Grid File Name: C:\geodata\BLN\del5_laser-2001.grd
Grid Size: 1000 rows x 373 columns

X Minimum: 382100
X Maximum: 383340
X Spacing: 3.3333333333333

Y Minimum: 6814660
Y Maximum: 6817990
Y Spacing: 3.3333333333333

Z Minimum: -14.321922278021
Z Maximum: -0.10474884524331

Lower Surface
Level Surface defined by Z = 0

Volumes
Z Scale Factor: 1

Total Volumes by:
Trapezoidal Rule: -25777.938277528
Simpson's Rule: -25744.127694517
Simpson's 3/8 Rule: -25880.105985363

Cut & Fill Volumes
Positive Volume [Cut]: 0
Negative Volume [Fill]: 25777.938277528
Net Volume [Cut-Fill]: -25777.938277528

Areas

Planar Areas
Positive Planar Area [Cut]: 0
Negative Planar Area [Fill]: 3894.4444444444
Blanked Planar Area: 4125305.5555556
Total Planar Area: 4129200

Surface Areas
Positive Surface Area [Cut]: 0
Negative Surface Area [Fill]: 4392.9577909041

Section 2 Flat area

Grid Volume Computations

Tue Mar 08 14:21:51 2005

Upper Surface
Grid File Name:
C:\geodata\BLN\del7_laser-2001.grd
Grid Size: 1000 rows x 373 columns

Lower Surface
Level Surface defined by Z = 0

Volumes
Z Scale Factor: 1

Total Volumes by:
Trapezoidal Rule: -11334.400463597
Simpson's Rule: -11195.647403532
Simpson's 3/8 Rule: -11374.296362374

Cut & Fill Volumes
Positive Volume [Cut]: 3196.9007462097
Negative Volume [Fill]: 14531.301209807
Net Volume [Cut-Fill]: -11334.400463597

Areas
Planar Areas
Positive Planar Area [Cut]: 3077.0180951002
Negative Planar Area [Fill]: 6606.3152382331
Blanked Planar Area: 4119516.6666667
Total Planar Area: 4129200

Surface Areas
Positive Surface Area [Cut]: 3263.7773243266
Negative Surface Area [Fill]: 7022.368851044

X Minimum: 382100
X Maximum: 383340
X Spacing: 3.3333333333333

Y Minimum: 6814660
Y Maximum: 6817990
Y Spacing: 3.3333333333333

Z Minimum: -7.1414601919478
Z Maximum: 3.7210042633471

Section 3 Precipice

Grid Volume Computations

Tue Mar 08 14:06:05 2005

Upper Surface
Grid File Name:
C:\geodata\BLN\del4_laser-2001.grd
Grid Size: 1000 rows x 373 columns

X Minimum: 382100
X Maximum: 383340
X Spacing: 3.3333333333333

Y Minimum: 6814660
Y Maximum: 6817990
Y Spacing: 3.3333333333333

Z Minimum: -33.490694016405
Z Maximum: 29.855540278157

Lower Surface
Level Surface defined by Z = 0

Volumes
Z Scale Factor: 1

Total Volumes by:
Trapezoidal Rule: -62445.723499589
Simpson's Rule: -61102.825186629
Simpson's 3/8 Rule: -61664.587185912

Cut & Fill Volumes
Positive Volume [Cut]: 13825.44615675
Negative Volume [Fill]: 76271.169656339
Net Volume [Cut-Fill]: -62445.723499589

Areas
Planar Areas
Positive Planar Area [Cut]: 1421.5987847168
Negative Planar Area [Fill]: 26061.734548616
Blanked Planar Area: 4101716.6666667
Total Planar Area: 4129200

Surface Areas
Positive Surface Area [Cut]: 3644.678266211
Negative Surface Area [Fill]: 30704.327019055

Section 4 Beneath precipice

Grid Volume Computations

Tue Mar 08 14:00:16 2005

Upper Surface
Grid File Name:
C:\geodata\BLN\del2_laser-2001.grd
Grid Size: 1000 rows x 373 columns

X Minimum: 382100
X Maximum: 383340
X Spacing: 3.3333333333333

Y Minimum: 6814660
Y Maximum: 6817990
Y Spacing: 3.3333333333333

Z Minimum: -14.882675020411
Z Maximum: 0.77247450577914

Lower Surface
Level Surface defined by Z = 0

Volumes
Z Scale Factor: 1

Total Volumes by:
Trapezoidal Rule: -118875.20039108
Simpson's Rule: -118945.1591202
Simpson's 3/8 Rule: -118814.19690449

Cut & Fill Volumes
Positive Volume [Cut]: 20.222271765041
Negative Volume [Fill]: 118895.42266285
Net Volume [Cut-Fill]: -118875.20039108

Areas
Planar Areas
Positive Planar Area [Cut]: 79.08137955823
Negative Planar Area [Fill]: 26409.807509331
Blanked Planar Area: 4102711.1111111
Total Planar Area: 4129200

Surface Areas
Positive Surface Area [Cut]: 82.083901115784
Negative Surface Area [Fill]: 29156.846652193

Section 5 Tunga

Grid Volume Computations

Tue Mar 08 14:20:52 2005

Upper Surface
Grid File Name:
C:\geodata\BLN\del6_laser-2001.grd
Grid Size: 1000 rows x 373 columns

X Minimum: 382100
X Maximum: 383340
X Spacing: 3.3333333333333

Y Minimum: 6814660
Y Maximum: 6817990
Y Spacing: 3.3333333333333

Z Minimum: -16.249787571962
Z Maximum: -0.4496411248536

Lower Surface
Level Surface defined by Z = 0

Volumes
Z Scale Factor: 1

Total Volumes by:
Trapezoidal Rule: -130092.44202445
Simpson's Rule: -129689.85824893
Simpson's 3/8 Rule: -130268.70853772

Cut & Fill Volumes
Positive Volume [Cut]: 0
Negative Volume [Fill]: 130092.44202445
Net Volume [Cut-Fill]: -130092.44202445

Areas
Planar Areas
Positive Planar Area [Cut]: 0
Negative Planar Area [Fill]: 19977.777777778
Blanked Planar Area: 4109222.2222222
Total Planar Area: 4129200

Surface Areas
Positive Surface Area [Cut]: 0
Negative Surface Area [Fill]: 22927.896691037

Section 6 Tverrdalen

Grid Volume Computations

Tue Mar 08 14:00:46 2005

Upper Surface
Grid File Name:
C:\geodata\BLN\del3_laser-2001.grd
Grid Size: 1000 rows x 373 columns

X Minimum: 382100
X Maximum: 383340
X Spacing: 3.3333333333333

Y Minimum: 6814660
Y Maximum: 6817990
Y Spacing: 3.3333333333333

Z Minimum: -13.692993332252
Z Maximum: -0.66423129027669

Lower Surface
Level Surface defined by Z = 0

Volumes
Z Scale Factor: 1

Total Volumes by:
Trapezoidal Rule: -176947.70594778
Simpson's Rule: -177041.18451503
Simpson's 3/8 Rule: -177057.9945283

Cut & Fill Volumes
Positive Volume [Cut]: 0
Negative Volume [Fill]: 176947.70594778
Net Volume [Cut-Fill]: -176947.70594778

Areas
Planar Areas
Positive Planar Area [Cut]: 0
Negative Planar Area [Fill]: 31750
Blanked Planar Area: 4097450
Total Planar Area: 4129200

Surface Areas
Positive Surface Area [Cut]: 0
Negative Surface Area [Fill]: 34596.2399968

Section 7 Fan

Grid Volume Computations

Tue Mar 08 13:58:56 2005

Upper Surface
Grid File Name: C:\geodata\BLN\del1_laser-2001.grd
Grid Size: 1000 rows x 373 columns

X Minimum: 382100
X Maximum: 383340
X Spacing: 3.3333333333333

Y Minimum: 6814660
Y Maximum: 6817990
Y Spacing: 3.3333333333333

Z Minimum: -15.697561087415
Z Maximum: 4.4599154530773

Lower Surface
Level Surface defined by Z = 0

Volumes
Z Scale Factor: 1

Total Volumes by:
Trapezoidal Rule: -309974.9644005
Simpson's Rule: -310497.27731788
Simpson's 3/8 Rule: -310279.3445049

Cut & Fill Volumes
Positive Volume [Cut]: 4855.6665650563
Negative Volume [Fill]: 314830.63096556
Net Volume [Cut-Fill]: -309974.9644005

Areas
Planar Areas
Positive Planar Area [Cut]: 3926.0058594949
Negative Planar Area [Fill]: 68557.327473838
Blanked Planar Area: 4056716.6666667
Total Planar Area: 4129200

Surface Areas
Positive Surface Area [Cut]: 4153.4122533791
Negative Surface Area [Fill]: 72101.919668543

3) AERIAL PHOTO 2004 – economical map 1:5000
Section 7 Fan

Grid Volume Computations Section 7 Fan

Mon Mar 14 18:58:10 2005

Upper Surface

Grid File Name:	C:\geodata\BLN\Blanking files\del1_2004-oygard.grd
Grid Size:	1000 rows x 373 columns
X Minimum:	382100
X Maximum:	383340
X Spacing:	3.3333333333333
Y Minimum:	6814660
Y Maximum:	6817990
Y Spacing:	3.3333333333333
Z Minimum:	-4.6442870751037
Z Maximum:	13.630958241272

Lower Surface
Level Surface defined by Z = 0

Volumes

Z Scale Factor:	1

Total Volumes by:

Trapezoidal Rule:	105532.4371339
Simpson's Rule:	105108.77925305
Simpson's 3/8 Rule:	105573.08885247

Cut & Fill Volumes

Positive Volume [Cut]:	127120.39079521
Negative Volume [Fill]:	21587.953661304
Net Volume [Cut-Fill]:	105532.4371339

Areas
Planar Areas

Positive Planar Area [Cut]:	51581.959497219
Negative Planar Area [Fill]:	20901.373836115
Blanked Planar Area:	4056716.6666667
Total Planar Area:	4129200

Surface Areas

Positive Surface Area [Cut]:	54173.099548408
Negative Surface Area [Fill]:	21329.384258307

Appendix E

Gridding reports

Generation of grids from ascii-files

E1 - Aerial photo 2001

Mon Feb 28 17:03:34 2005
Elasped time for gridding: 2.39 seconds

Data Source

Source Data File Name:	C:\geodata\flybilder\1.txt
X Column:	A
Y Column:	B
Z Column:	C

Data Counts

Active Data:	143923
Original Data:	166189
Excluded Data:	0
Deleted Duplicates:	22266
Retained Duplicates:	22266
Artificial Data:	0
Superseded Data:	0

Univariate Statistics

	X	Y	Z
Minimum:	382099.618	6814659.852	20.074
25%-tile:	382489.618	6815259.851	36.927
Median:	382662.951	6815963.184	281.374
75%-tile:	382856.284	6817203.183	814.774
Maximum:	383339.617	6817993.182	1062.698
Midrange:	382719.6175	6816326.517	541.386
Range:	1239.999	3333.3300000001	1042.624
Interquartile Range:	366.66599999997	1943.3320000004	777.847
Median Abs. Deviation:	180	869.99900000077	252.245
Mean:	382677.65703957	6816190.8518609	408.16416132932
Trim Mean (10%):	382674.48774881	6816176.9704	395.15385561757
Standard Deviation:	246.06614547714	1017.533653465	379.19306606258
Variance:	60548.547949975	1035374.7359339	143787.38134994
Coef. of Variation:			0.92902097241367
Coef. of Skewness:			0.51421480598078

Inter-Variable Correlation

	X	Y	Z
X:	1.000	-0.205	-0.118
Y:		1.000	0.983
Z:			1.000

Inter-Variable Covariance

	X	Y	Z
X:	60548.547949975	-51295.610789026	-10997.512053628
Y:		1035374.7359339	379140.01070575
Z:			143787.38134994

Planar Regression: Z = AX+BY+C

Fitted Parameters

	A	B	C
Parameter Value:	0.13383117338135	0.37188285656179	-2585630.5600308

Standard Error:	0.00071369020343946	0.00017259072244388	1261.0167728621

Inter-Parameter Correlations

	A	B	C
A:	1.000	-0.205	-0.408
B:		1.000	0.977
C:			1.000

ANOVA Table

Source	df	Sum of Squares	Mean Square	F
Regression:	2	20080724101.859	10040362050.929	2.355E+006
Residual:	143920	613587184.16882	4263.3906626516	
Total:	143922	20694311286.028		

Coefficient of Multiple Determination (R^2): 0.97034995870662

Nearest Neighbor Statistics

	Separation	|Delta Z|
Minimum:	0.0009999992325902	0
25%-tile:	3.3329999996349	0.212
Median:	3.3329999996349	0.702
75%-tile:	3.3329999999842	1.475
Maximum:	3.3340000000317	69.241
Midrange:	1.6674999996321	34.6205
Range:	3.3330000007991	69.241
Interquartile Range:	3.492459654808E-010	1.263
Median Abs. Deviation:	0	0.564
Mean:	3.3182765700475	1.0260278690689
Trim Mean (10%):	3.3329999997272	0.88371592900541
Standard Deviation:	0.22100732959755	1.5453607401742
Variance:	0.04884423973584	2.3881398172719
Coef. of Variation:	0.066603046772074	1.5061586402879
Coef. of Skewness:	-14.943174132778	16.552595821589
Root Mean Square:	3.3256283068076	1.8549590306467
Mean Square:	11.05980363504	3.4408730053779

Complete Spatial Randomness

Lambda:	0.034820143546037
Clark and Evans:	1.2383911929997
Skellam:	348247.53000174

Exclusion Filtering

Exclusion Filter String:	Not In Use

Duplicate Filtering

Duplicate Points to Keep:	First
X Duplicate Tolerance:	0.00014
Y Duplicate Tolerance:	0.00039
Deleted Duplicates:	22266
Retained Duplicates:	22266
Artificial Data:	0

X	Y	Z	ID	Status
382186.28	6816419.8	383.576	83436	Retained
382186.28	6816419.8	382.992	108817	Deleted
382189.62	6816416.5	382.303	83356	Retained
382189.62	6816416.5	382.168	108756	Deleted

Appendix E

382189.62	6816419.8	383.074	83437	Retained
382189.62	6816419.8	383.432	108818	Deleted
382189.62	6816423.2	384.43	83517	Retained
382189.62	6816423.2	384.857	108884	Deleted
382189.62	6816426.5	385.509	83597	Retained
382189.62	6816426.5	387.097	108954	Deleted
382192.95	6816416.5	382.868	83357	Retained
382192.95	6816416.5	382.957	108757	Deleted
382192.95	6816419.8	384.182	83438	Retained
382192.95	6816419.8	384.997	108819	Deleted
382192.95	6816423.2	385.106	83518	Retained
382192.95	6816423.2	386.78	108885	Deleted
382192.95	6816426.5	386.672	83598	Retained
382192.95	6816426.5	389.203	108955	Deleted
382192.95	6816429.8	388.335	83677	Retained
382192.95	6816429.8	391.659	109029	Deleted
382192.95	6816433.2	390.387	83757	Retained
382192.95	6816433.2	394.41	109107	Deleted
382196.28	6816413.2	382.166	83277	Retained
382196.28	6816413.2	382.473	108700	Deleted
382196.28	6816416.5	384.163	83358	Retained
382196.28	6816416.5	384.193	108758	Deleted
382196.28	6816419.8	385.62	83439	Retained
382196.28	6816419.8	386.351	108820	Deleted
382196.28	6816423.2	387.019	83519	Retained
382196.28	6816423.2	388.659	108886	Deleted
382196.28	6816426.5	388.743	83599	Retained
382196.28	6816426.5	391.492	108956	Deleted
382196.28	6816429.8	390.693	83678	Retained
382196.28	6816429.8	394.015	109030	Deleted
382196.28	6816433.2	392.8	83758	Retained
382196.28	6816433.2	397.153	109108	Deleted
382196.28	6816436.5	395.203	83837	Retained
382196.28	6816436.5	399.377	109190	Deleted
382196.28	6816439.8	397.682	83916	Retained
382196.28	6816439.8	401.563	109276	Deleted
382199.62	6816413.2	384.306	83278	Retained
382199.62	6816413.2	384.209	108701	Deleted
382199.62	6816416.5	386.278	83359	Retained
382199.62	6816416.5	386.17	108759	Deleted
382199.62	6816419.8	388.432	83440	Retained
382199.62	6816419.8	388.093	108821	Deleted
382199.62	6816423.2	390.268	83520	Retained
382199.62	6816423.2	391.012	108887	Deleted
382199.62	6816426.5	392.264	83600	Retained
382199.62	6816426.5	393.503	108957	Deleted
382199.62	6816429.8	394.312	83679	Retained
382199.62	6816429.8	396.416	109031	Deleted
382199.62	6816433.2	396.454	83759	Retained
382199.62	6816433.2	399.287	109109	Deleted

382199.62	6816436.5	398.816	83838	Retained
382199.62	6816436.5	401.897	109191	Deleted
382199.62	6816439.8	401.35	83917	Retained
382199.62	6816439.8	404.193	109277	Deleted
382199.62	6816443.2	403.922	83995	Retained
382199.62	6816443.2	406.229	109367	Deleted
382202.95	6816409.8	386.502	83197	Retained
382202.95	6816409.8	384.656	108648	Deleted
382202.95	6816413.2	388.083	83279	Retained
382202.95	6816413.2	386.581	108702	Deleted
382202.95	6816416.5	389.661	83360	Retained
382202.95	6816416.5	388.746	108760	Deleted
382202.95	6816419.8	391.837	83441	Retained
382202.95	6816419.8	391.065	108822	Deleted
382202.95	6816423.2	394.174	83521	Retained
382202.95	6816423.2	393.45	108888	Deleted
382202.95	6816426.5	396.313	83601	Retained
382202.95	6816426.5	396.21	108958	Deleted
382202.95	6816429.8	398.367	83680	Retained
382202.95	6816429.8	398.953	109032	Deleted
382202.95	6816433.2	400.274	83760	Retained
382202.95	6816433.2	401.464	109110	Deleted
382202.95	6816436.5	402.42	83839	Retained
382202.95	6816436.5	404.199	109192	Deleted
382202.95	6816439.8	404.598	83918	Retained
382202.95	6816439.8	406.27	109278	Deleted
382202.95	6816443.2	406.787	83996	Retained
382202.95	6816443.2	408.223	109368	Deleted
382202.95	6816446.5	408.759	84073	Retained
382202.95	6816446.5	409.644	109462	Deleted
382202.95	6816449.8	410.245	84150	Retained
382202.95	6816449.8	410.483	109560	Deleted
382206.28	6816409.8	389.371	83198	Retained
382206.28	6816409.8	387.68	108649	Deleted
382206.28	6816413.2	391.047	83280	Retained
382206.28	6816413.2	389.867	108703	Deleted
382206.28	6816416.5	392.557	83361	Retained
382206.28	6816416.5	391.948	108761	Deleted
382206.28	6816419.8	394.888	83442	Retained
382206.28	6816419.8	394.365	108823	Deleted
382206.28	6816423.2	397.165	83522	Retained
382206.28	6816423.2	396.635	108889	Deleted
382206.28	6816426.5	399.254	83602	Retained
382206.28	6816426.5	399.239	108959	Deleted
382206.28	6816429.8	401.307	83681	Retained
382206.28	6816429.8	401.423	109033	Deleted

More ...

Breakline Filtering

Breakline Filtering: Not In Use

Appendix E

Gridding Rules

Gridding Method:	Triangulation with Linear Interpolation
Anisotropy Ratio:	1
Anisotropy Angle:	0

Output Grid

Grid File Name:	C:\geodata\flybilder\1.grd
Grid Size:	1000 rows x 373 columns
Total Nodes:	373000
Filled Nodes:	258962
Blanked Nodes:	114038

Grid Geometry

X Minimum:	382100
X Maximum:	383340
X Spacing:	3.3333333333333
Y Minimum:	6814660
Y Maximum:	6817990
Y Spacing:	3.3333333333333

Grid Statistics

Z Minimum:	20.159819294714
Z 25%-tile:	136.33052515263
Z Median:	382.75611578215
Z 75%-tile:	653.98848491381
Z Maximum:	1062.1982769148
Z Midrange:	541.17904810474
Z Range:	1042.0384576201
Z Interquartile Range:	517.65795976117
Z Median Abs. Deviation:	256.33262689478
Z Mean:	424.57086233518
Z Trim Mean (10%):	413.86272405126
Z Standard Deviation:	316.96838323507
Z Variance:	100468.95597065
Z Coef. of Variation:	0.74656179063188
Z Coef. of Skewness:	0.43919348815575
Z Root Mean Square:	529.83900678856
Z Mean Square:	280729.37311469

E2 - Aerial photo 2004

Mon Feb 28 17:07:24 2005
Elasped time for gridding: 4.28 seconds

Data Source

Source Data File Name:	C:\geodata\flybilder\4.txt
X Column:	A
Y Column:	B
Z Column:	C

Data Counts

Active Data:	254137
Original Data:	319464
Excluded Data:	0
Deleted Duplicates:	65327
Retained Duplicates:	65327
Artificial Data:	0
Superseded Data:	0

Univariate Statistics

	X	Y	Z
Minimum:	381866.285	6814666.519	20.112
25%-tile:	382422.951	6815656.518	207.614
Median:	382649.617	6816383.184	443.073
75%-tile:	382872.95	6817383.183	890.944
Maximum:	383586.283	6818283.182	1146.747
Midrange:	382726.284	6816474.8505	583.4295
Range:	1719.998	3616.6629999997	1126.635
Interquartile Range:	449.99900000001	1726.665	683.33
Median Abs. Deviation:	223.33300000004	846.66500000004	331.133
Mean:	382649.3014295	6816490.2583985	521.22701777388
Trim Mean (10%):	382647.39870378	6816489.5710823	517.59350503006
Standard Deviation:	331.10683613942	957.94572876683	357.72964068445
Variance:	109631.73693826	917660.01926261	127970.49582423
Coef. of Variation:			0.68632213696882
Coef. of Skewness:			0.19140447185483

Inter-Variable Correlation

	X	Y	Z
X:	1.000	0.378	0.364
Y:		1.000	0.984
Z:			1.000

Inter-Variable Covariance

	X	Y	Z
X:	109631.73693826	119853.37232484	43093.260209648
Y:		917660.01926261	337103.63041912
Z:			127970.49582423

Planar Regression: Z = AX+BY+C

Fitted Parameters

	A	B	C
Parameter Value:	-0.010044077519262	0.36814010955958	-2505058.8839297
Standard Error:	0.00042405971936356	0.00014659053156965	949.86564255272

Appendix E

Inter-Parameter Correlations

	A	B	C
A:	1.000	0.378	0.227
B:		1.000	0.987
C:			1.000

ANOVA Table

Source	df	Sum of Squares	Mean Square	F
Regression:	2	31428795776.588	15714397888.294	3.653E+006
Residual:	254134	1093242120.6954	4301.8333662375	
Total:	254136	32522037897.284		

Coefficient of Multiple Determination (R^2): 0.96638457515644

Nearest Neighbor Statistics

	Separation	|Delta Z|
Minimum:	0.0009999992325902	0
25%-tile:	3.3329999996349	0.364
Median:	3.3329999996349	0.86300000000006
75%-tile:	3.3329999999842	1.626
Maximum:	3.3340000000317	82.409
Midrange:	1.6674999996321	41.2045
Range:	3.3330000007991	82.409
Interquartile Range:	3.492459654808E-010	1.262
Median Abs. Deviation:	0	0.58599999999994
Mean:	3.3258943087087	1.1415874075794
Trim Mean (10%):	3.3329999997209	1.0231826691442
Standard Deviation:	0.15371177906636	1.4957159862722
Variance:	0.023627311023745	2.2371663115903
Coef. of Variation:	0.046216675816748	1.3102071522002
Coef. of Skewness:	-21.584475020201	22.952341911195
Root Mean Square:	3.3294444376982	1.8815919113172
Mean Square:	11.08520026372	3.5403881207341

Complete Spatial Randomness

Lambda:	0.040853748766393
Clark and Evans:	1.3444801558532
Skellam:	723141.39807708

Exclusion Filtering

Exclusion Filter String:	Not In Use

Duplicate Filtering

Duplicate Points to Keep:	First
X Duplicate Tolerance:	0.0002
Y Duplicate Tolerance:	0.00043
Deleted Duplicates:	65327
Retained Duplicates:	65327
Artificial Data:	0

X	Y	Z	ID	Status
382086.28	6816159.9	380.947	95749	Retained
382086.28	6816159.9	381.203	163694	Deleted
382086.28	6816163.2	381.377	95936	Retained
382086.28	6816163.2	381.419	163907	Deleted
382086.28	6816166.5	381.487	96123	Retained
382086.28	6816166.5	381.505	164119	Deleted

Appendix E

382086.28	6816169.8	381.47	96309	Retained
382086.28	6816169.8	381.559	164330	Deleted
382086.28	6816173.2	381.615	96495	Retained
382086.28	6816173.2	381.627	164541	Deleted
382086.28	6816176.5	381.752	96681	Retained
382086.28	6816176.5	381.96	164751	Deleted
382086.28	6816179.8	382.125	96867	Retained
382086.28	6816179.8	382.361	164960	Deleted
382086.28	6816183.2	382.232	97052	Retained
382086.28	6816183.2	382.666	165169	Deleted
382086.28	6816186.5	382.418	97238	Retained
382086.28	6816186.5	382.88	165377	Deleted
382086.28	6816189.8	382.599	97424	Retained
382086.28	6816189.8	383.146	165584	Deleted
382086.28	6816193.2	383.136	97610	Retained
382086.28	6816193.2	383.667	165791	Deleted
382089.62	6816153.2	379.271	95376	Retained
382089.62	6816153.2	379.496	163269	Deleted
382089.62	6816156.5	379.643	95563	Retained
382089.62	6816156.5	379.848	163482	Deleted
382089.62	6816159.9	380.162	95750	Retained
382089.62	6816159.9	380.331	163695	Deleted
382089.62	6816163.2	380.649	95937	Retained
382089.62	6816163.2	380.624	163908	Deleted
382089.62	6816166.5	380.527	96124	Retained
382089.62	6816166.5	380.496	164120	Deleted
382089.62	6816169.8	380.583	96310	Retained
382089.62	6816169.8	380.584	164331	Deleted
382089.62	6816173.2	380.703	96496	Retained
382089.62	6816173.2	380.782	164542	Deleted
382089.62	6816176.5	380.941	96682	Retained
382089.62	6816176.5	381.217	164752	Deleted
382089.62	6816179.8	381.168	96868	Retained
382089.62	6816179.8	381.593	164961	Deleted
382089.62	6816183.2	381.357	97053	Retained
382089.62	6816183.2	381.834	165170	Deleted
382089.62	6816186.5	381.5	97239	Retained
382089.62	6816186.5	382.044	165378	Deleted
382089.62	6816189.8	381.792	97425	Retained
382089.62	6816189.8	382.28	165585	Deleted
382089.62	6816193.2	382.288	97611	Retained
382089.62	6816193.2	382.758	165792	Deleted
382089.62	6816196.5	383.044	97797	Retained
382089.62	6816196.5	383.557	165997	Deleted
382089.62	6816199.8	383.832	97982	Retained
382089.62	6816199.8	384.346	166201	Deleted
382089.62	6816203.2	384.578	98167	Retained
382089.62	6816203.2	385.102	166405	Deleted
382089.62	6816206.5	385.304	98352	Retained
382089.62	6816206.5	385.916	166608	Deleted
382089.62	6816209.8	386.013	98537	Retained

382089.62	6816209.8	386.567	166811	Deleted
382089.62	6816213.2	386.728	98722	Retained
382089.62	6816213.2	387.257	167013	Deleted
382089.62	6816216.5	387.423	98907	Retained
382089.62	6816216.5	387.964	167214	Deleted
382089.62	6816219.8	388.13	99092	Retained
382089.62	6816219.8	388.624	167415	Deleted
382089.62	6816223.2	388.843	99277	Retained
382089.62	6816223.2	389.273	167615	Deleted
382089.62	6816226.5	389.576	99461	Retained
382089.62	6816226.5	389.891	167814	Deleted
382089.62	6816229.8	390.373	99645	Retained
382089.62	6816229.8	390.632	168013	Deleted
382089.62	6816233.2	391.115	99829	Retained
382089.62	6816233.2	391.367	168211	Deleted
382089.62	6816236.5	391.872	100013	Retained
382089.62	6816236.5	392.039	168408	Deleted
382092.95	6816146.5	377.934	95003	Retained
382092.95	6816146.5	377.994	162843	Deleted
382092.95	6816149.9	378.171	95190	Retained
382092.95	6816149.9	378.273	163056	Deleted
382092.95	6816153.2	378.551	95377	Retained
382092.95	6816153.2	378.743	163270	Deleted
382092.95	6816156.5	378.984	95564	Retained
382092.95	6816156.5	379.14	163483	Deleted
382092.95	6816159.9	379.505	95751	Retained
382092.95	6816159.9	379.582	163696	Deleted
382092.95	6816163.2	380.239	95938	Retained
382092.95	6816163.2	379.966	163909	Deleted
382092.95	6816166.5	379.863	96125	Retained
382092.95	6816166.5	379.836	164121	Deleted
382092.95	6816169.8	379.826	96311	Retained
382092.95	6816169.8	379.896	164332	Deleted
382092.95	6816173.2	379.902	96497	Retained
382092.95	6816173.2	380.09	164543	Deleted
382092.95	6816176.5	380.06	96683	Retained
382092.95	6816176.5	380.347	164753	Deleted
382092.95	6816179.8	380.278	96869	Retained
382092.95	6816179.8	380.674	164962	Deleted
382092.95	6816183.2	380.483	97054	Retained
382092.95	6816183.2	381.077	165171	Deleted
382092.95	6816186.5	380.705	97240	Retained
382092.95	6816186.5	381.281	165379	Deleted

More ...

Breakline Filtering

Breakline Filtering: Not In Use

Gridding Rules

Gridding Method: Triangulation with Linear Interpolation
Anisotropy Ratio: 1
Anisotropy Angle: 0

Appendix E

Output Grid

Grid File Name:	C:\geodata\flybilder\4.grd
Grid Size:	1000 rows x 373 columns
Total Nodes:	373000
Filled Nodes:	301380
Blanked Nodes:	71620

Grid Geometry

X Minimum:	382100
X Maximum:	383340
X Spacing:	3.3333333333333
Y Minimum:	6814660
Y Maximum:	6817990
Y Spacing:	3.3333333333333

Grid Statistics

Z Minimum:	20.157640111221
Z 25%-tile:	238.87994979498
Z Median:	469.00088362338
Z 75%-tile:	778.30199589778
Z Maximum:	1091.2145477548
Z Midrange:	555.68609393299
Z Range:	1071.0569076435
Z Interquartile Range:	539.42204610281
Z Median Abs. Deviation:	264.78705274751
Z Mean:	503.81371759017
Z Trim Mean (10%):	500.17718415413
Z Standard Deviation:	320.48336457827
Z Variance:	102709.58697141
Z Coef. of Variation:	0.63611480471631
Z Coef. of Skewness:	0.16956408408089
Z Root Mean Square:	597.10790398673
Z Mean Square:	356537.84900343

E3 - Laser 2004

Tue Mar 08 11:42:33 2005
Elasped time for gridding: 80.2 seconds

Data Source

Source Data File Name:	C:\geodata\laser\UTM-KDASC.txt
X Column:	A
Y Column:	B
Z Column:	C

Data Counts

Active Data:	3002033
Original Data:	3002073
Excluded Data:	0
Deleted Duplicates:	40
Retained Duplicates:	40
Artificial Data:	0
Superseded Data:	0

Univariate Statistics

	X	Y	Z
Minimum:	382154.29	6814765.92	20.03
25%-tile:	382766.21	6817355.62	888.57
Median:	383157.27	6818041.68	1102.23
75%-tile:	383531.83	6818647.49	1193.23
Maximum:	384039.02	6819375.81	1300.21
Midrange:	383096.655	6817070.865	660.12
Range:	1884.73	4609.8899999997	1280.18
Interquartile Range:	765.62	1291.8700000001	304.66
Median Abs. Deviation:	382.42999999999	632.84999999963	113.43
Mean:	383152.86001252	6817719.532954	909.98207293864
Trim Mean (10%):	383156.38725238	6817788.1918252	940.77711061502
Standard Deviation:	458.66760952131	1251.1753130911	410.05252833286
Variance:	210375.97602399	1565439.6640886	168143.07599217
Coef. of Variation:			0.45061605115875
Coef. of Skewness:			-1.3131517167397

Inter-Variable Correlation

	X	Y	Z
X:	1.000	0.693	0.674
Y:		1.000	0.976
Z:			1.000

Inter-Variable Covariance

	X	Y	Z
X:	210375.97602399	397497.4813115	126680.77281265
Y:		1565439.6640886	500937.26973612
Z:			168143.07599217

Planar Regression: Z = AX+BY+C

Fitted Parameters

	A	B	C
Parameter Value:	-0.0047547605544203	0.32133772041333	-2188058.6714678
Standard Error:	0.00015387405617685	5.6408629501807E-005	346.36134480256

Appendix E

Inter-Parameter Correlations

	A	B	C
A:	1.000	0.693	0.599
B:		1.000	0.992
C:			1.000

ANOVA Table

Source	df	Sum of Squares	Mean Square	F
Regression:	2	481427747146.18	240713873573.09	3.0957E+007
Residual:	3002030	23343315703.414	7775.8435803153	
Total:	3002032	504771062849.59		

Coefficient of Multiple Determination (R^2): 0.95375464755917

Nearest Neighbor Statistics

	Separation	|Delta Z|
Minimum:	0.0099999997764826	0
25%-tile:	0.39115214430591	0.050000000000182
Median:	0.57801384065422	0.14
75%-tile:	0.83186537367388	0.36000000000013
Maximum:	6.7000671630973	57.05
Midrange:	3.3550335814369	28.525
Range:	6.6900671633208	57.05
Interquartile Range:	0.44071322936797	0.30999999999995
Median Abs. Deviation:	0.21822732861669	0.11
Mean:	0.60110927438128	0.38875058335408
Trim Mean (10%):	0.59602506793952	0.24563168088591
Standard Deviation:	0.27413849536764	0.97492930362979
Variance:	0.075151914642432	0.95048714707607
Coef. of Variation:	0.45605434328027	2.5078529663371
Coef. of Skewness:	0.65042189941474	10.712072181549
Root Mean Square:	0.66066956520592	1.0495780881563
Mean Square:	0.43648427438938	1.1016141631378

Complete Spatial Randomness

Lambda:	0.34552204065862
Clark and Evans:	0.70667756238852
Skellam:	2844721.0597359

Exclusion Filtering

Exclusion Filter String:	Not In Use

Duplicate Filtering

Duplicate Points to Keep:	First
X Duplicate Tolerance:	0.00022
Y Duplicate Tolerance:	0.00054
Deleted Duplicates:	40
Retained Duplicates:	40
Artificial Data:	0

X	Y	Z	ID	Status
382977.57	6817765.4	1025.94	1648719	Retained
382977.57	6817765.4	1025.99	1799796	Deleted
383053.95	6818087.9	1081.09	2504845	Retained
383053.95	6818087.9	1080.74	2559402	Deleted

Appendix E

383056.23	6817585.5	987.25	1681033	Retained
383056.23	6817585.5	987.12	1765373	Deleted
383062.8	6818059.6	1068.38	2508999	Retained
383062.8	6818059.6	1068.39	2553047	Deleted
383071.17	6818210.4	1100.48	2483107	Retained
383071.17	6818210.4	1100.28	2590884	Deleted
383071.25	6818217.6	1105.05	2482035	Retained
383071.25	6818217.6	1105.03	2592697	Deleted
383096.63	6818219	1100.7	2481069	Retained
383096.63	6818219	1100.54	2593933	Deleted
383129.61	6817519.8	916.55	1590006	Retained
383129.61	6817519.8	914.9	1754927	Deleted
383161.92	6818624	1158.16	2418162	Retained
383161.92	6818624	1157.95	2696508	Deleted
383185.81	6818969	1229.4	2362959	Retained
383185.81	6818969	1229.39	2790117	Deleted
383198.6	6817839.2	1059.45	1610892	Retained
383198.6	6817839.2	1059.39	1824463	Deleted
383206.26	6818753.4	1183.92	2400041	Retained
383206.26	6818753.4	1184.13	2731907	Deleted
383214.04	6819031.9	1232.45	2350550	Retained
383214.04	6819031.9	1232.51	2807876	Deleted
383226.7	6817766.6	1045.09	1606467	Retained
383226.7	6817766.6	1045.23	1809571	Deleted
383228.15	6817721.3	1036.74	1603570	Retained
383228.15	6817721.3	1036.78	1800040	Deleted
383259.53	6817645.2	959.97	229499	Retained
383259.53	6817645.2	959.94	305298	Deleted
383316.78	6818397	1148.05	2275241	Retained
383316.78	6818397	1148.12	2644433	Deleted
383318.97	6818050.1	1100.56	2250020	Retained
383318.97	6818050.1	1100.59	2560232	Deleted
383347.14	6818687.6	1187.87	2298441	Retained
383347.14	6818687.6	1187.89	2721408	Deleted
383385.26	6818731.9	1193.88	2302659	Retained
383385.26	6818731.9	1193.9	2734068	Deleted
383408.81	6818746.1	1195.34	2304144	Retained
383408.81	6818746.1	1195.48	2738736	Deleted
383435.52	6818897.6	1208.41	2317705	Retained
383435.52	6818897.6	1208.42	2781590	Deleted
383447.61	6818706.1	1187.74	2301091	Retained
383447.61	6818706.1	1187.83	2730175	Deleted
383454.35	6819122	1225.25	2910994	Retained
383454.35	6819122	1225.47	2955865	Deleted
383529.33	6818187.1	1134	379736	Retained
383529.33	6818187.1	1134	621186	Deleted
383549.48	6817944.2	1087.36	333483	Retained
383549.48	6817944.2	1087.31	561038	Deleted
383562.38	6818043.5	1113.36	352826	Retained
383562.38	6818043.5	1112.89	585169	Deleted
383567.08	6818215.3	1138.15	386124	Retained

383567.08	6818215.3	1138.11	630820	Deleted
383573.38	6818537.4	1173.62	447503	Retained
383573.38	6818537.4	1173.59	716391	Deleted
383589.74	6818452.7	1162.42	432320	Retained
383589.74	6818452.7	1162.37	693867	Deleted
383596.39	6818394.2	1158.94	421228	Retained
383596.39	6818394.2	1158.82	678368	Deleted
383618.52	6818400.7	1158.94	423109	Retained
383618.52	6818400.7	1158.9	680917	Deleted
383631.27	6818731.8	1194.19	484158	Retained
383631.27	6818731.8	1194.16	770836	Deleted
383643	6818542.2	1176.46	449965	Retained
383643	6818542.2	1176.51	720540	Deleted
383682.44	6819136.8	1225.41	1077655	Retained
383682.44	6819136.8	1225.4	1143176	Deleted
383682.58	6819024.5	1218.02	537821	Retained
383682.58	6819024.5	1217.92	849008	Deleted
383729.94	6819339.1	1236.45	1112229	Retained
383729.94	6819339.1	1236.4	1185136	Deleted
383742.65	6817976.1	1206.93	575817	Retained
383742.65	6817976.1	1207.15	1039978	Deleted
383813.52	6818297.7	1147.06	661686	Retained
383813.52	6818297.7	1146.92	990502	Deleted
383873.88	6818521.2	1170.5	724182	Retained
383873.88	6818521.2	1170.54	938562	Deleted

Breakline Filtering

Breakline Filtering:	Not In Use

Gridding Rules

Gridding Method:	Triangulation with Linear Interpolation
Anisotropy Ratio:	1
Anisotropy Angle:	0

Output Grid

Grid File Name:	C:\geodata\laser\UTM-KDASC.grd
Grid Size:	1000 rows x 373 columns
Total Nodes:	373000
Filled Nodes:	277722
Blanked Nodes:	95278

Grid Geometry

X Minimum:	382100
X Maximum:	383340
X Spacing:	3.3333333333333
Y Minimum:	6814660
Y Maximum:	6817990
Y Spacing:	3.3333333333333

Grid Statistics

Z Minimum:	20.114760472913	Z Mean:	496.68480794195
Z 25%-tile:	219.79385729984	Z Trim Mean (10%):	492.31501696366
Z Median:	470.86468322257	Z Standard Deviation:	324.41048759275
Z 75%-tile:	758.5553760731	Z Variance:	105242.16446016
Z Maximum:	1092.4422907775	Z Coef. of Variation:	0.65315162132091
Z Midrange:	556.27852562519	Z Coef. of Skewness:	0.18468253027399
Z Range:	1072.3275303046		
Z Interquartile Range:	538.76151877326	Z Root Mean Square:	593.24359490895
Z Median Abs. Deviation:	266.63047803387	Z Mean Square:	351937.96290049

E4 - Economical map 1:5000 (Fan)

Mon Mar 14 18:36:52 2005
Elasped time for gridding: 1.86 seconds

Data Source

Source Data File Name:	C:\geodata\Oygard-kart\OEK-E89.txt
X Column:	A
Y Column:	B
Z Column:	C

Data Counts

Active Data:	76707
Original Data:	79621
Excluded Data:	0
Deleted Duplicates:	2914
Retained Duplicates:	1530
Artificial Data:	0
Superseded Data:	0

Univariate Statistics

	X	Y	Z
Minimum:	381342.01	6813336.041	9.12
25%-tile:	381929.067	6814287.63	125
Median:	382534.695	6814733.743	255
75%-tile:	383194.239	6815350.637	400
Maximum:	383876.285	6816241.028	1140
Midrange:	382609.1475	6814788.5345	574.56
Range:	2534.275	2904.9869999997	1130.88
Interquartile Range:	1265.172	1063.0070000002	275
Median Abs. Deviation:	631.342	511.53000000026	135
Mean:	382554.30140499	6814809.8324948	271.50023531099
Trim Mean (10%):	382553.71502405	6814804.9870506	265.69905775164
Standard Deviation:	695.26785284564	631.2999303966	170.29946876361
Variance:	483397.38720058	398539.60211875	29001.909061169
Coef. of Variation:			0.62725348495018
Coef. of Skewness:			0.49097788836272

Inter-Variable Correlation

	X	Y	Z
X:	1.000	-0.073	-0.095
Y:		1.000	0.006
Z:			1.000

Inter-Variable Covariance

	X	Y	Z
X:	483397.38720058	-32045.282029665	-11229.409626624
Y:		398539.60211875	673.91846860312
Z:			29001.909061169

Planar Regression: Z = AX+BY+C

Fitted Parameters

	A	B	C
Parameter Value:	-0.023097821758101	-0.00017678116877058	10312.401166979
Standard Error:	0.00088014295195934	0.0009693258918905	6638.8521625402

Appendix E

Inter-Parameter Correlations

	A	B	C
A:	1.000	-0.073	-0.123
B:		1.000	0.999
C:			1.000

ANOVA Table

Source	df	Sum of Squares	Mean Square	F
Regression:	2	19882939.273999	9941469.6369996	345.86
Residual:	76704	2204766499.0811	28743.826907085	
Total:	76706	2224649438.3551		

Coefficient of Multiple Determination (R^2): 0.0089375606471737

Nearest Neighbor Statistics

	Separation	|Delta Z|
Minimum:	0.0099999997764826	0
25%-tile:	2.6236127760968	0
Median:	3.9206730286925	5
75%-tile:	5.19859759987	5
Maximum:	126.9286856857	120
Midrange:	63.46934284274	60
Range:	126.91868568593	120
Interquartile Range:	2.5749848237732	5
Median Abs. Deviation:	1.2961620267987	0
Mean:	3.9996623533988	3.996999621938
Trim Mean (10%):	3.8626901998877	2.9905075539204
Standard Deviation:	2.5729348175874	6.9440379450329
Variance:	6.6199935755535	48.219662982057
Coef. of Variation:	0.64328800539899	1.7373126349374
Coef. of Skewness:	4.7736099490946	6.332033130152
Root Mean Square:	4.7557641359459	8.0122199769981
Mean Square:	22.617292516749	64.195668959808

Complete Spatial Randomness

Lambda:	0.010419264553358
Clark and Evans:	0.81652946011146
Skellam:	113577.56313328

Exclusion Filtering

Exclusion Filter String:	Not In Use

Duplicate Filtering

Duplicate Points to Keep:	First
X Duplicate Tolerance:	0.0003
Y Duplicate Tolerance:	0.00034
Deleted Duplicates:	2914
Retained Duplicates:	1530
Artificial Data:	0

X	Y	Z	ID	Status
381371.72	6814463.1	385	59032	Retained
381371.72	6814463.1	385	59135	Deleted
381383.4	6814462.5	380	58318	Retained
381383.4	6814462.5	380	58732	Deleted

Appendix E

381436.57	6815547	760	79261	Retained
381436.57	6815547	760	79297	Deleted
381440.18	6814460	375	57882	Retained
381440.18	6814460	375	58043	Deleted
381446.34	6814459.7	370	57487	Retained
381446.34	6814459.7	370	57520	Deleted
381455.18	6814459.3	365	56811	Retained
381455.18	6814459.3	365	56933	Deleted
381467.53	6814458.7	360	56081	Retained
381467.53	6814458.7	360	56167	Deleted
381478.88	6815375.9	740	79212	Retained
381478.88	6815375.9	740	79228	Deleted
381478.95	6814458.2	355	55281	Retained
381478.95	6814458.2	355	55644	Deleted
381496.48	6813427.8	19.51	710	Retained
381496.48	6813427.8	19.51	711	Deleted
381496.48	6813427.8	19.51	712	Deleted
381496.48	6813427.8	19.51	713	Deleted
381496.48	6813427.8	19.51	714	Deleted
381496.48	6813427.8	19.51	715	Deleted
381498.8	6813425.7	19.39	690	Retained
381498.8	6813425.7	19.39	691	Deleted
381498.8	6813425.7	19.39	693	Deleted
381498.8	6813425.7	19.39	694	Deleted
381498.8	6813425.7	19.39	695	Deleted
381498.8	6813425.7	19.39	696	Deleted
381521.05	6815689.3	680	79066	Retained
381521.05	6815689.3	680	79069	Deleted
381522.55	6814456.2	350	54953	Retained
381522.55	6814456.2	350	55080	Deleted
381533.28	6814455.8	345	54180	Retained
381533.28	6814455.8	345	54594	Deleted
381547.56	6814455.1	340	53703	Retained
381547.56	6814455.1	340	53710	Deleted
381581.42	6814453.6	335	52877	Retained
381581.42	6814453.6	335	52948	Deleted
381592.89	6813346.3	9.13	5	Retained
381592.89	6813346.3	9.13	6	Deleted
381604.37	6814452.5	330	52033	Retained
381604.37	6814452.5	330	52115	Deleted
381604.81	6813336	9.12	1	Retained
381604.81	6813336	9.12	2	Deleted
381604.81	6813336	9.12	3	Deleted
381624.49	6814451.6	325	51412	Retained
381624.49	6814451.6	325	51413	Deleted
381627.32	6815206.1	600	78608	Retained
381627.32	6815206.1	600	78719	Deleted
381634.56	6814451.2	320	50667	Retained
381634.56	6814451.2	320	51299	Deleted
381638.81	6814451	315	50096	Retained
381638.81	6814451	315	50562	Deleted
381639.38	6815450.7	600	78498	Retained
381639.38	6815450.7	600	78679	Deleted
381642.24	6814450.8	310	49817	Retained

381642.24	6814450.8	310	49907	Deleted
381644.77	6814450.7	305	48756	Retained
381644.77	6814450.7	305	48779	Deleted
381651.39	6815185	580	76931	Retained
381651.39	6815185	580	77070	Deleted
381664.22	6814449.8	300	48205	Retained
381664.22	6814449.8	300	48634	Deleted
381672.79	6815127	560	75631	Retained
381672.79	6815127	560	75662	Deleted
381693.9	6814448.5	295	47238	Retained
381693.9	6814448.5	295	47691	Deleted
381696.79	6813632	14.91	92	Retained
381696.79	6813632	14.91	93	Deleted
381703.22	6814448.1	290	46441	Retained
381703.22	6814448.1	290	46906	Deleted
381708.4	6814447.8	285	45971	Retained
381708.4	6814447.8	285	45998	Deleted
381713.55	6814447.6	280	44971	Retained
381713.55	6814447.6	280	45203	Deleted
381721.6	6814447.2	275	43980	Retained
381721.6	6814447.2	275	43981	Deleted
381728.72	6814446.9	270	43490	Retained
381728.72	6814446.9	270	43777	Deleted
381735.07	6814446.6	265	42810	Retained
381735.07	6814446.6	265	43026	Deleted
381739.47	6814446.4	260	41931	Retained
381739.47	6814446.4	260	42278	Deleted
381743.86	6814446.2	255	40928	Retained
381743.86	6814446.2	255	41419	Deleted
381748.01	6814446.1	250	40230	Retained
381748.01	6814446.1	250	40689	Deleted
381752.14	6814445.9	245	39635	Retained
381752.14	6814445.9	245	39636	Deleted
381759.09	6814445.6	240	38274	Retained
381759.09	6814445.6	240	38705	Deleted
381763.6	6814445.3	235	37644	Retained
381763.6	6814445.3	235	37753	Deleted
381769.08	6814445.1	230	37005	Retained
381769.08	6814445.1	230	37083	Deleted
381776.12	6814444.8	225	36191	Retained
381776.12	6814444.8	225	36511	Deleted
381776.89	6815160.7	505	71159	Retained

More ...

Breakline Filtering

Breakline Filtering: Not In Use

Gridding Rules

Gridding Method: Triangulation with Linear Interpolation
Anisotropy Ratio: 1
Anisotropy Angle: 0

Output Grid

Grid File Name: C:\geodata\Oygard-kart\OEK-E89_test2.grd

Appendix E

Grid Size:	1000 rows x 373 columns
Total Nodes:	373000
Filled Nodes:	162350
Blanked Nodes:	210650

Grid Geometry

X Minimum:	382100
X Maximum:	383340
X Spacing:	3.3333333333333
Y Minimum:	6814660
Y Maximum:	6817990
Y Spacing:	3.3333333333333

Grid Statistics

Z Minimum:	14.422229943157
Z 25%-tile:	29.95335920185
Z Median:	99.375458661279
Z 75%-tile:	217.71787750499
Z Maximum:	554.39100427432
Z Midrange:	284.40661710874
Z Range:	539.96877433116
Z Interquartile Range:	187.76451830314
Z Median Abs. Deviation:	73.075822990316
Z Mean:	133.23680957284
Z Trim Mean (10%):	125.35651725194
Z Standard Deviation:	110.92759806862
Z Variance:	12304.932013274
Z Coef. of Variation:	0.832559698962
Z Coef. of Skewness:	0.78672491700414
Z Root Mean Square:	173.36948819911
Z Mean Square:	30056.979438423

Appendix F

Dynamics of debris flows

F1 – Basic mechanics

When studying debris flow mechanics, we need some basic principles from soil mechanics. The Coulomb failure criterion is one of the most important ones:

$$\tau = \sigma' \tan\varphi' + c'$$

This is combined with Terzaghi's principle of effective stress:

$$\sigma' = \sigma - p$$

$$p = \rho g(h + z)$$

where:

τ = mean shear stress on the failure surface

φ' = angle of internal friction

c' = cohesion or intrinsic shear strength

σ = total normal stress

σ' = effective normal stress

p = pore fluid pressure

The c'-term could be recognised as a fixed *yield strength*. Some authors, like Iverson (2003), mean that a fixed yield strength would be valid only if all debris is liquefied. Field observations and experiments however, show variable pore pressure, liquefaction and strength. Iverson's view is explained by equations (6)-(8) showing the dependence of shear strength on pore pressure. He reports that unless $p \approx \sigma$ (liquefaction), the first component ($\sigma' \tan\varphi'$) of the strength often is much greater than the cohesion component (c' = yield strength). Pore fluid pressure carries some of the stress, and *liquefaction* occurs when the effective stress reduces to zero, due to elevation of pore pressure or reduction of total stress.

F2 - Dynamical models

Further description of the models briefly described in Section 10.5.1.

1) Rheological models

τ for a Newtonian fluid:

$$\tau_{xy} = \mu\left(\frac{\partial u}{\partial y} + \frac{\partial v}{\partial x}\right)$$

→ all viscous terms ($\frac{\partial \tau_{xx}}{\partial x} + \frac{\partial \tau_{xy}}{\partial y} + \frac{\partial \tau_{xz}}{\partial z}$) in eq. (10) become $\mu\left[\frac{\partial^2 u}{\partial x^2} + \frac{\partial^2 u}{\partial y^2} + \frac{\partial^2 u}{\partial z^2}\right]$

→ $\rho\left(\frac{\partial u}{\partial t} + u\frac{\partial u}{\partial x} + v\frac{\partial u}{\partial y} + w\frac{\partial u}{\partial z}\right) = -\rho g_x - \frac{\partial P}{\partial x} + \mu\left[\frac{\partial^2 u}{\partial x^2} + \frac{\partial^2 u}{\partial y^2} + \frac{\partial^2 u}{\partial z^2}\right]$

Similar equations apply for the other directions.

2) Hungr and Iverson models

The forces acting on a debris flow are:
Inertial force = Gravity – Friction – Earth pressure (- Drag force)
Mass · Acceleration = Force
This is shown in the general equation of Iverson et al. (1997):

$$\boxed{\frac{1}{g}\frac{du}{dt} = \sin\beta - \cos\beta\tan\varphi + \frac{p(H)}{\gamma_t H}\tan\varphi}$$

where
H = depth of the flow
p(H) = pore pressure at depth H
u = downslope velocity

This equation can be expanded to account for evolving shape of the debris flow. An important aspect of a debris flow is the effect of pore pressure distribution, which has a crucial role in the mobility of the mass (Iverson et al, 1997), and must be considered in a dynamical model. Hungr tries to satisfy that in his model (2000). Based on the St Venant equation, he describes the forces on a debris flow as follows:

$$\rho H w \Delta x\left(\frac{\partial u}{\partial t} + \beta\frac{\partial u}{\partial x}\right) = \rho g H w \Delta x \sin\beta - T w \Delta x - \frac{dp}{dx} w \Delta x$$

This equation appears to differ slightly from the other ones, because also the mass of the body is included, and H (depth), w (width) and Δx (length downslope) are the dimensions of an average slice of the flow. β is a momentum averaging factor. The right hand side illustrates

the sum of the driving and the resisting forces, as described by the Coulomb rule. The earth pressure force Hungr gives as:

$$\frac{dp}{dx} = -\rho g H \frac{dH}{dx} \cos\beta$$

The resisting stress consists of both frictional (T_f) and viscous (T_v) components:
$T = T_f + T_v$

Concentration of large clasts decreases from maximum at tip, to zero at end. This means that the frictional component of the flow resistance varies linearly from a maximum at x = 0 to zero at the end (x = L) (Hungr, 2000):

$$T_f = \rho g H \cos\beta \left(1 - x\frac{r_u}{L}\right) \tan\varphi$$

where
r_u = pore pressure ratio
L = distance
With this equation Hungr meant to illustrate that the flow is liquefied at the end of boulder accumulation (x = L) and frictional stresses disappear, while the viscous component of resisting stress grows in this area:

$$T_v = \frac{3u\mu}{H} \times \frac{x}{L}$$

where
u = mean velocity of surge

Iverson (1997 b) suggests a hydraulic model based on Coulomb mixture theory using depth averaging and summing the two-phase flow equations. The resulting model is suggested to handle both varying pore pressure and varying mode of deformation. Whether the material is locally extending or compressing can influence the longitudinal normal force in the debris flow. This theory intends to model the variation from a granular frictional surge in the head, to a Newtonian fluid surge in the tail:

$$\frac{\partial u}{\partial t} + u\frac{\partial u}{\partial x} = g\left[\sin\beta - \left(\cos\beta - \frac{p_{bed}}{\rho g h}\right)\tan\varphi_{bed}\right] - u_f\left(m+2\right)\frac{\mu}{\rho}\frac{u}{h^2} - k_{a/p}\left[g\cos\beta\frac{\partial H}{\partial x} - \frac{1}{\rho}\frac{\partial p_{bed}}{\partial x}\right] - \frac{1}{\rho}\frac{\partial p_{bed}}{\partial x}$$

where
H = flow depth, normal to bed
u = velocity, depth averaged
x = downslope distance, parallel to bed,
t = time
p_{bed} = pore fluid pressure at base of flow

φ_{bed} = friction angle of debris on bed
v_f = fluid volume fraction
μ = viscosity
m = describes vertical velocity profile
$k_{a/p}$ = lateral grain-pressure coefficient, a 0 active, p = passive

$$k_{a/p} = 2\frac{1 \mp \left[1 - \cos^2 \varphi_{\text{int}} \left(1 + \tan^2 \varphi_{bed}\right)\right]^{1/2}}{\cos^2 \varphi_{\text{int}}} - 1$$

where
φ_{int} = internal friction angle of the granular solids
- in the $\mp$ is used for k_a, (active, as in an extending case)
+ in the $\mp$ is used for k_p, (passive, as in a compressing case).

The first right hand side term of eq. (25) represents the gravitational driving force and the Coulomb frictional resistance. The second term is the resistance due to shearing of viscous fluid, and the third term illustrates the longitudinal (earth pressure) force due to flow depth- and pore pressure distributions. According to Iverson (1997b) this third term distinguishes these equations from the ones using Bingham rheology for example.

These equations show that if $p_{bed} = \rho g h \cos\beta$, pore pressure = weight of overlying material, liquefaction occurs, and Coulomb bed friction vanishes. Complete liquefaction also reduces the third term to a term describing lateral forces in a viscous fluid. If $p_{bed} = 0$, the material behaves like a Coulomb solid. In this case the longitudinal normal force depends strongly on whether the sediment is extending ($\partial u/\partial x \succ 0$) or compressing ($\partial u/\partial x \prec 0$).

Iverson (1997) concludes that the coarse grained heads dominate the flow resistance, and that the rheology of the finer slurry does not have a significant influence on the dynamics. Bagnold has also said that the coefficient of solid to solid friction is virtually the same for a sheared dispersion of granular solids as for the same material in continuous contact (Iverson, 2003).

F3 – Velocity estimation based on ballistic stones

Derivation of equation (11.10).

$$x = \frac{d}{\cos\beta} \quad or \quad x = \sqrt{2d}$$

$$Acceleration: \frac{dy^2}{dt^2} = -g$$

$$v_y = v_0 - gt \quad \rightarrow \quad y = v_0 t - \frac{1}{2} gt \quad \rightarrow \quad t = \frac{2v_{0y}}{g}$$

$$x = v_{0x} t \qquad \rightarrow \quad t = \frac{x}{v_{0x}}$$

$$y = \frac{v_{0y} x}{v_{ox}} - \frac{1}{2} g \frac{x^2}{{v_0}^2 x}$$

$$x = \frac{2v_{0x} v_{0y}}{g} = \frac{2{v_0}^2 \cos\beta \sin\beta}{g} = \frac{{v_0}^2}{g}$$

$$v_0 = \sqrt{xg}$$

$$\boxed{v_0 = \sqrt{g \cdot d / \cos\beta}}$$